# MODIFICATION OF HIGH SURFACE AREA ELECTRODES
FOR THE ELECTROCATALYTIC REDUCTION OF CO$_2$

RODNEY D.L. SMITH
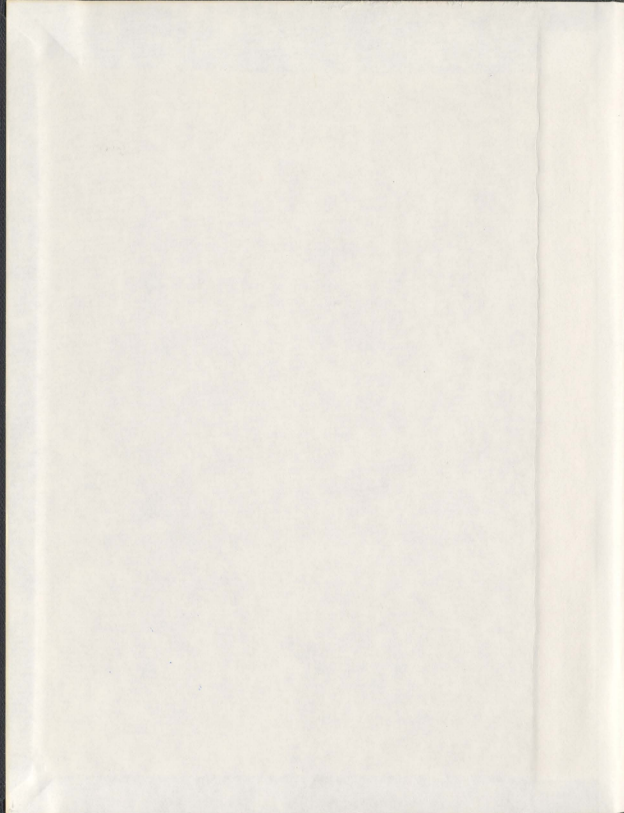
001311

Modification of high surface area electrodes

for the electrocatalytic reduction of CO_2

by

Rodney D. L. Smith

B.Sc. (Honours), University of Manitoba

Winnipeg, Manitoba 2007

A thesis submitted to the School of Graduate Studies in partial

fulfillment of the requirements for the degree of

Doctor of Philosophy

Department of Chemistry

Memorial University of Newfoundland

St. John's, Newfoundland

February 13, 2012

Abstract

Vulcan XC72 was modified with 9,10-anthraquinone (AQ) and polypyridyl ruthenium complexes using three approaches. Techniques employed include spontaneous diazonium coupling reaction, benzimidazole forming reaction, and formation of benzimidazole-based polymers on the carbon surface.

Following the spontaneous diazonium coupling reaction for immobilization of AQ, a surface coverage limit far below that expected for a close-packed monolayer was observed. Varying reaction conditions and pretreatments to the carbon surface failed to increase the surface coverage beyond this limit. The limit was found to include both covalently bound and physisorbed AQ. It was found that washing the modified carbon with benzene was necessary to remove all physisorbed AQ. Upon removal of physisorbed material, differences in surface coverage values for covalently bound AQ were observed to vary, depending on reaction conditions and surface pretreatments. An azo- linkage between the immobilized species and the carbon surface was observed using cyclic voltammetry. X-ray photoelectron spectroscopy (XPS) and cyclic voltammetry results indicate approximately 10% of immobilized molecules are bound through an azo- linkage.

A novel approach that coupled aryl diazonium molecules to surface bound carboxylic acid functionality, producing a benzimidazole linkage, was devel-

oped and explored using AQ. Two unique forms of AQ were observed following the reaction procedure. XPS results indicated that one was the desired, benzimidazole-linked form, while the other was likely bound through an amine linkage. The ability to immobilize polymeric systems on carbon surfaces using this technique was examined through sequential reactions. Following successful sequential immobilizations, a one-pot reaction was then employed to immobilize benzimidazole-based polymers containing bidentate coordination sites on the carbon surface.

The immobilization of polypyridyl ruthenium complexes was performed using all three approaches. Poor voltammetric behavior was observed for carbon powders modified using any of the three techniques. However, thermogravimetric analysis, XPS and elemental analysis indicated the presence of significant amounts of ruthenium in modified samples. Evidence of ruthenium ligands in the modified material was observed, suggesting polymerization of ruthenium complexes is responsible for the poor electrochemistry.

The polybenzimidazole-based polymers used in this study were found to be active redox catalysts for the reduction of CO_2. Product analysis indicated that none of the common CO_2 reduction products are formed.

Acknowledgements

I thank my friends and family for their support throughout my education. I am forever thankful to my parents, who are responsible for the sense of curios-

ity and confidence (and impulsiveness) that lead to and drove me through my education. To my fiancee Rebecca, I say thank you for your love and patience, and for holding on through the ups and downs. Also for your help in editing my thesis.

I express my deepest appreciation to my supervisor, Dr. Peter G. Pickup. His guidance, patience and insight have been instrumental over the course of my studies.

Contents

List of Tables

List of Figures

List of Schemes

List of Abbreviations

AAQ	1-Amino-9,10-anthraquinone
AFM	Atomic force microscopy
APCI	Atmospheric pressure chemical ionization
AQ	9,10-Anthraquinone
ATR	Attenuated total reflectance
BPDC	2,2′-bipyridine-4,4′-dicarboxylic acid
BPPG	Basal plane pyrolytic graphite
bpy	2,2′-Bipyridine
CFP	Carbon fiber paper
CME	Chemically modified electrode
DAAQ	1,2-Diaminoanthraquinone
DAB	3,3′-Diaminobenzidine
DEA	*N,N*-Diethylaniline
DHBA	Dihydroxybenzoic acid
DMA	*N,N*-Dimethylacetamide
DMF	Dimethylformamide
EA	Elemental analysis
EDG	Electron donating group
EWG	Electron withdrawing group
FT-IR	Fourier-transform infrared spectroscopy
FWHM	Full-width at half-mass
GC	Glassy carbon
HOPG	Highly-oriented pyrolytic graphite
ISCT	Inner-sphere charge transfer
ITO	Indium-doped tin oxide

LB	Langmuir-Blodgett film
LS	Langmuir-Schaefer film
MALDI	Matrix-assisted laser desorption/ionization
MLCT	Metal to ligand charge transfer
MS	Mass spectrometry
NAB	4-(4′- nitrophenylazo)benzene
NMR	Nuclear magnetic resonance
NP	Nitrophenyl
OSCT	Outer-sphere charge transfer
pbt	2-(2′-pyridyl)benzothiazole
PDA	1,2-Phenylenediamine
phenNH2	5-amino-1,10-phenanthroline
PPA	Polyphosphoric acid
PPF	Pyrolyzed photoresist
PTFE	Polytetrafluoroethylene
PVP	Polyvinylpyridine
SAM	Self-assembled monolayer
SCE	Saturated calomel electrode
SHE	Standard hydrogen electrode
SIMS	Secondary ion mass spectrometry
TGA	Thermogravimetric analysis
TMOS	Tetramethyl orthosilicate
TOF	Time of flight
TPP	Tetraphenylporphyrin
vibpy	Vinylbipyridine
XPS	X-ray photoelectron spectroscopy
XRF	X-ray fluorescence spectroscopy

List of Symbols

C   Capacitance

C_{Ru} Corrected ruthenium concentration (XRF)

C_s Specific capacitance

$E_{1/2}$ Half-wave potential

ΔE_p Peak separation

F   Faraday constant

i   Current

i_{cc} Charging current

I_{Ru} Measured signal intensity (Ru, XRF)

m   Mass

MW   Molecular weight

N   Moles of species present

n   Electrons involved in reduction/oxidation

Q   Charge

R   Gas constant

SA   Surface area

S_s Specific surface area

t   Time

T   Temperature

v Scan rate

Γ Surface coverage

Introduction

1.1   Introduction

The search for a sustainable source of energy has become a popular topic of research. An intriguing area of this field is the recycling of carbon dioxide. The chemical [1] and electrochemical [2, 3] conversion of CO_2 to higher energy, higher value chemicals has been examined in several recent reviews. Further, it has been proposed that efficient reduction of CO_2 to methanol makes a "methanol economy" feasible [4]. In such an economy, it is envisaged that CO_2 would take the place of fossil fuels as a global carbon source.

The electrochemical reduction of CO_2 has been, and continues to be, extensively studied. Lead and mercury have been shown to act as "inert" electrodes towards CO_2 [3]. In this case "inert" refers to the lack of specific interactions between CO_2 and the electrode surface. This results in observed electrochemical reduction of CO_2 at its thermodynamic redox potential. Under standard aqueous conditions, the one electron reduction of CO_2 occurs at -1.90 V *vs.* the standard hydrogen electrode (SHE) [2, 3]. At an "inert" electrode, this reduction process converts linear CO_2 to a bent $CO_2^{\cdot-}$ species. If the reduction is performed under aqueous conditions, using a lead or mercury electrode, formate is the only observed product [3]. When the reduction is performed using aprotic solvents, carbon monoxide, formate and oxalate are observed [3].

Electrocatalysis can be used to lower the electrochemical potential required to drive the process, alter the product distribution, or even introduce new products. In the traditional sense, electrocatalysis refers to the situation where interactions occur between the electrode surface and the species being reduced (or oxidized). Bard has recently compared electron transfer processes at an electrode surface to homogeneous outer-sphere charge transfer (OSCT) and inner-

sphere charge transfer (ISCT) reactions [5]. In OSCT, an electron transfer occurs between two species that possess no bonding interactions. The analogous process at the electrode surface is the situation where neither the reactant or product interact with the electrode surface, resulting in a simple electron transfer. An example is the one electron reduction of CO_2 using a mercury electrode, where the mercury surface is observed to be "inert". In ISCT, an electron transfer occurs between two compounds that are joined by a bridging moiety. This bridging moiety alters the electronic nature of the species involved, effectively altering the mechanism, kinetics and thermodynamics of the reaction. The presence of interactions between either the reactant or product and the electrode surface induces a similar situation in electrochemistry, known as electrocatalysis.

An excellent example of the effects of electrocatalysis was observed in a study on the variation of electrode material for the reduction of CO_2 under aqueous conditions [6]. In the study, different metals were shown to alter the electrochemical potential required to reduce CO_2. The identity of the metal was also shown to affect the product distribution. Most metals favored production of either carbon monoxide or formate. The potentials required for metals that favored formate production were comparable to those necessary for CO_2 reduction at a mercury or lead electrode. This indicates that these metals exhibit poor electrocatalytic activity towards reduction of CO_2. The potentials required for metals that favored carbon monoxide production were less negative than those necessary when using lead or mercury electrodes. The less extreme potential requirements, and observation of a new product, indicates that these metals are active electrocatalysts for CO_2 reduction. In other words, CO_2 undergoes chemical interactions with the electrode surface. Unique among the metals examined

3

in the study, reduction of CO_2 at a copper electrode was found to produce hydrocarbons such as methane and ethene. The unique behavior of copper was first reported by Hori *et al.* in 1985 [7]. A review regarding the electrocatalytic reduction of CO_2 at copper electrodes has been published [8].

The electrochemical reduction of CO_2 at glassy carbon electrodes has been studied [9]. Reduction was found to be possible at -1.50 V vs. Ag/Ag^+, the reduction was found to be extremely sluggish. Modification of the glassy carbon surface by electrochemical oxidation was found to shift the CO_2 reduction peak to less negative potentials, but long electrolysis periods were still required to observe any CO_2 reduction products. Consistent with this observation, activated carbon fiber electrodes were observed to be poor electrodes for the electrochemical reduction of CO_2 [10].

The observation of unique behavior, such as that observed during reduction of CO_2 at a copper electrode, indicates that electrocatalysis (in the traditional sense) of CO_2 reduction is a promising area of research. However, this form of electrocatalysis has proven to be very difficult to make meaningful progress in. Although much work has been performed, no mechanistic rationale has been found to relate chemical concepts with observed reactivity [3]. The difficulty in establishing electrocatalytic reaction mechanisms makes it difficult to predict new materials that may be active [5]. This complicates the search for new catalytic materials, making trial and error the predominant method of exploration.

An alternate form of electrochemical catalysis, which is often also referred to as electrocatalysis, is more descriptively known as redox catalysis. Redox catalysis relies on the presence of a molecule that acts as a chemical catalyst. Mechanisms of redox catalysis can be easier to deduce than traditional electrocatalysis. These mechanisms are often described using E and C, where E stands

4

for a simple electron transfer and C stands for a chemical transformation. For example, an EC mechanism for a reduction is a simple electron transfer from the electrode to the catalyst (or substrate), followed by reaction of the reduced form of the catalyst (or substrate) with the substrate (or catalyst). Such catalytic reactions rely on interactions between a catalyst and a substrate, where both species are typically solvated.

Aside from the ability to more easily deduce a mechanism, redox catalysis also benefits from the ability to tune the electronic and steric properties of the catalyst. For example, small changes in the ligand environment of a coordination compound can significantly alter its behavior. As a result, the study of reduction of CO_2 by redox catalysis has received a lot of attention. Much research has been performed in this area using transition metal complexes; many of these complexes are discussed in a recent review [3]. Although electrocatalytically active coordination compounds containing abundant transition metals have been reported, for example iron porphyrins [11–13] or a recently reported copper dimer compound [14], more research has focussed on rare metals. Specifically, polypyridyl ruthenium and polypyridyl rhenium compounds have received much attention [3].

Major drawbacks accompanying the use of rare materials as catalysts include the associated cost and supply concerns for commercialization of a viable technology. It is therefore important to minimize the amount of material utilized. Redox catalysis is typically studied by cyclic voltammetry, small scale electrolyses and rotating disk electrode voltammetry on a homogeneous solution containing the catalyst and the substrate [3]. While useful for characterization purposes, such solution based approaches represent an ineffective use of material for electrochemically driven reactions. In an electrochemically driven reaction

5

only a small layer of the solution near the electrode surface is involved in the reaction. Any catalyst outside of the small layer is inactive, and therefore unnecessary. Use of homogeneous reaction conditions also necessitates the need to separate the catalyst from the products.

An effective approach for overcoming these drawbacks is immobilization of the catalyst species on the electrode surface. Once modified with a molecular species, electrodes are known as chemically modified electrodes (CMEs). In regards to redox catalysis, CMEs make it possible to establish a high concentration of catalyst near the electrode surface (active catalyst) while minimizing the amount of inactive catalyst. As an added benefit, the catalyst may be recovered by simple removal of the CME from the reaction vessel.

Research on CMEs is a mature field, and a large variety of methods have been developed for CME preparation. At the simplest level, CMEs can be separated into two categories: those with chemical species covalently bound to the electrode surface, a process known as chemisorption, and those with chemical species non-covalently bound to the electrode surface, known as physisorption. Each of these two categories can themselves be broken up into a large number of categories. A survey of methods reported in the literature for immobilization of compounds on electrode surfaces is given in the following sections. Specific examples pertaining to immobilization of transition metal complexes, and to CO_2 redox catalysis are presented where possible.

1.2 Non-Covalent Chemically Modified Electrodes

1.2.1 Langmuir-Blodgett Films

Langmuir-Blodgett (LB) and Langmuir-Schaefer (LS) films have long been used to deposit monolayers of amphiphilic organic molecules on solid surfaces. The LB technique has also been explored for immobilization of transition metal complexes on solid surfaces, but the use of transition metals poses some technical problems. For organic molecules, an LB film is typically formed using amphiphilic molecules. A thin layer of the amphiphilic molecule is carefully placed on the surface of a liquid, known as the subphase (typically H_2O). The molecules orient themselves in the lowest energy fashion: with the hydrophilic end facing the water layer, and the hydrophobic tail facing away. Dipping a solid material, frequently a glass slide, through the thin layer and into the subphase, followed by removal of the glass slide results in physisorption of a monolayer of material on the solid surface.

Attempts to directly mimic this process with transition metal compounds have produced mixed results. An LB film was reported to be successfully formed on a glass slide using a polypyridyl ruthenium compound in which a bipyridine ligand was modified with two nonadecane (C_{19}) alkyl tails [15]. Similar attempts at immobilization of nickel (II) tetraazacyclotetradecane complexes ([Ni(cyclam)]$^{2+}$) were reported to produce unstable monolayers on glassy carbon (GC) and indium-tin oxide (ITO) electrodes [16]. In this case, the cyclam ligand was modified with one or two pentadecane (C_{15}) groups. Films produced in this case were observed to be lost upon removal of the electrode from the subphase.

Various approaches have been attempted to expand the ability to immobilize transition metal complexes in the form of LB or LS films. One such approach relied on electrostatic attraction between *tris*-(2,2'-bipyridine)ruthenium (II) ([Ru(bpy)$_3$]$^{2+}$) and Nafion, a commercial, sulfonated fluoropolymer [17]. A solution containing Nafion and [Ru(bpy)$_3$]$^{2+}$ was found to be suitable for LS film generation when using a 0.1 M NaCl(aq) subphase. Cyclic voltammetry on LS films generated on an ITO surface this way indicated a growth of ruthenium content following multiple dip-coats, indicating that formation of multilayers does not inhibit electrochemical activity. Further, the catalytic oxidation of tripropylamine by the ruthenium present in these electrodes reveals that Nafion does not interfere with the catalytic capability of the transition metal complex.

Another approach involved the incorporation of a [Ru(bpy)$_3$]$^{2+}$ moiety into an acrylic polymer [18]. In this study, copolymerization of 2-(4-(4'-methyl-2,2'-bipyridyl))ethyl acrylate with either *N-tert*-pentylacrylamide or *N*-dodecyl-acrylamide was followed by refluxing the polymer in a solution of Ru(bpy)$_2$Cl$_2$ (Figure 1.1). The resulting copolymer formed suitable films for LB film generation when placed on the surface of water. Using spectroelectrochemical techniques, the amount of ruthenium present in LB films deposited on ITO this way, using either copolymer, was shown to increase linearly with the number of dip-coats. However, cyclic voltammetry only showed a linear increase for the copolymer prepared from *N-tert*-pentylacrylamide. Cyclic voltammetry on the copolymer prepared from *N*-dodecylacrylamide suggested the amount of ruthenium present remained unchanged following multiple dip-coats. The reason behind the difference lies in charge transfer mechanisms and highlights a potential difficulty in designing CMEs.
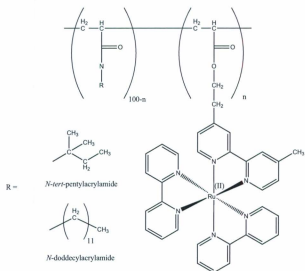
Figure 1.1: Copolymer used by Taniguchi *et al.* [18] to deposit LB films with [Ru(bpy)$_3$]$^{2+}$ moieties on ITO.

Electron transfer between the electrode surface and an electroactive species can only occur over very short distances. In the case of a CME modified with a monolayer of electroactive species, each and every molecule present is capable of being reduced (or oxidized) by the electrode. In CMEs modified with multiple layers of electroactive species, such as the copolymer case [18], a significant portion of the electroactive species is located too far from the electrode surface to be directly reduced. However, in many cases complete reduction of the electroactive species can still be achieved, as was observed for one CME in the copolymer case. This is because mechanisms exist which allow diffusion of the electron from the electrode surface outwards into the multilayer [19]. In the case of the CME created with the *N*-dodecylacrylamide copolymer the long alkyl chain acted as a barrier between neighboring ruthenium complexes, effectively eliminating electron diffusion [18].

9

1.2.2 Polymer Confinement

The importance of charge transport considerations in regard to the use of electroactive species confined in polymeric materials was covered in a 2006 review by Yagi and Kaneko [19]. In the article, two modes of charge transport are highlighted: physical displacement and charge hopping. Physical displacement involves simple diffusion of the redox species through the polymer, while charge hopping involves electron transfer from one redox species to the next [19].

Redox catalysis by CMEs prepared by confinement of transition metal complexes in polymer matrices [19, 20] and electron diffusion through such materials [19] has been the focus of several reviews. Commonly used techniques in this field include the use of ion-exchange polymers, such as Nafion [16, 17, 21], or coordinating polymers, such as poly(4-vinylpyridine) (PVP) [22] (Figure 1.2). In this way, the attractive forces of electrostatic binding or coordinative bonding are employed to inhibit leaching of the transition metal complex into solution. Within this field, various approaches have been used to produce CMEs with a polymer layer. In the case of ion-exchange polymers, the production of a LB film based on Nafion and $[Ru(bpy)_3]^{2+}$ has already been discussed [17].

Two other techniques are commonly used for confining electroactive species in polymers. The first involves the application of a film of the polymer to the electrode surface, accomplished by techniques such as drop-coating or spin-coating. This is followed by immersion of the electrode in a solution containing the desired transition metal complex. On soaking, the transition metal complex ion-exchanges (or diffuses in the case of coordinating polymers) into the polymer layer, establishing the desired CME [16, 21]. The second method is similar, but the two steps are combined into one. In this case a solution con-

poly(4-vinylpyridine)

Nafion
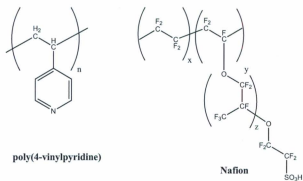
Figure 1.2: Chemical structure of two polymers commonly used for immobilization of transition metals in CMEs prepared by polymer confinement.

taining the polymer and the desired transition metal complex is applied to the electrode surface, eliminating the need for a separate impregnation step [22]. The confinement of transition metal complexes in polymeric materials contains significant overlap with other techniques discussed here and therefore is not discussed in detail.

The redox catalysis of carbon dioxide reduction has been examined using many of these non-covalent approaches to CME preparation. Solutions of many different metal phthalocyanines are known to be active redox catalysts for the reduction of carbon dioxide [3]. The only observed reduction product is typically CO, which is produced in competition with H_2 production (H^+ reduction). The polymer confinement method was used to immobilize a cobalt phthalocyanine in a layer of PVP on a pyrolytic graphite electrode [22]. When used in CO_2 purged aqueous solutions the CME was observed to improve the product selectivity, increasing the selectivity towards CO and decreasing it towards H_2. The catalyst turnover number was also observed to increase, and catalysis became possible at a slightly less negative potential (-1.0 V *vs.* SCE). Repeat electrolyses

with a single CME also revealed that the PVP matrix increased the stability of the electrode compared to a CME prepared without PVP.

1.2.3 Composite Materials

Related to CMEs based on polymer confinement are a series of composite materials. A family of materials known as sol-gels has become important and widespread in electrochemistry, particularly in the field of electrochemical sensors. The broad use of sol-gels in electrochemistry has been well documented [23–25]. These materials are prepared by the polymerization of inorganic alkoxides such as tetramethyl orthosilicate (TMOS) [26]. The highly cross-linked network of inorganic oxides is capable of confining or covalently binding electroactive species while simultaneously allowing diffusion of small molecules. A potential drawback of this method is the possibility of restricted electron transfer to the electrode surface [26]. Cyclic voltammetry revealed that electron transfer for $[Ru(bpy)_3]^{2+}$ immobilized in a silicate based sol-gel was inhibited. The porous nature of the sol-gel allowed diffusion of the ruthenium complex, but at a slow rate [26].

Another family of composite materials consists of a binding agent (*i.e.* a polymer), a conducting material and the desired electroactive species. This approach is very similar to simple confinement of electroactive species in a polymer matrix; a concept introduced earlier. However, several benefits may be introduced by this approach. For example, addition of carbon nanotubes to a Nafion film was found to offer improved current response (compared to a simple Nafion membrane) for a CME used as a Eu^{3+} detector [27]. The improvement was attributed to improved electron diffusion through the modified

12

layer, due to the conducting properties of carbon nanotubes. This technique is commonly used in supercapacitor research, where high surface area carbon powders are held together by polymeric binding agents. The capacitive behavior of these composite materials can be further enhanced by addition of an electroactive molecule such as 1,2-naphthaquinone [28].

Finally, carbon paste electrodes are a family of composite electrodes that have been used to generate functional CMEs. For preparation of a carbon paste electrode a thick paste is made by mixing a wax (*e.g.* paraffin wax) with a conducting carbon powder (*e.g.* graphite powder, activated carbon, carbon black, etc.). A specialized CME can be created by incorporation of the desired electroactive species into the mixture. An example of this approach is the mixture of ferrocene carboxylic acid, graphite powder and paraffin wax to generate a CME designed for quantitative measurement of ascorbic acid [29].

1.2.4   Self-Assembled Monolayers

The formation of self-assembled monolayers (SAMs) has also commonly been used in the preparation of CMEs. The self-assembly of a $[Ni(cyclam)]^{2+}$ species was accomplished by introduction of pyridine substituents on the cyclam ligand [16] (complex shown in Figure 1.3). The study showed that formation of a SAM of the nickel complex on a thin mercury film electrode was possible. Further, it was reported that the resulting CME was more robust than analagous LB films, allowing the CME to be transferred between solutions without loss of functionalization.

Formation of SAMs often capitalizes on the attractive forces between sulfur and gold. Introduction of a thiol moiety to the species to be immobilized results

R = H, R' = $C_{16}H_{33}$

R = R' = $C_{16}C_{33}$

R = H, R' = pyridine
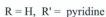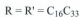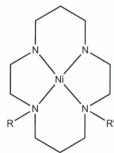
Figure 1.3: Structure of [Ni(cyclam)]$^{2+}$ complexes used by Kaden and coworkers for CME preparation by the LB and SAM approaches [16].

in efficient tethering of the species to gold surfaces. This technique has been used to immobilized [Ru(NH$_3$)$_5$(pyr)]$^{2+}$ (pyr = pyridine) groups on the surface of gold electrodes [30]. Results of this report indicated that electron transfer kinetics in such systems are highly dependant on the length of alkyl chain used to immobilize the electroactive species to the electrode surface. A two order of magnitude increase in electron transfer rate was observed upon decreasing the alkyl chain from C_{15} to C_{11}, highlighting the importance of minimizing the distance between the immobilized species and the electrode surface.

The catalytic reduction of CO$_2$ by a series of [Ni(cyclam)]$^{2+}$ complexes was examined using a variety of CME preparation techniques [16]. Discussed earlier, the authors prepared CMEs using an ion-exchange polymer (*i.e.* Nafion), LB films, and SAMs. It was found that, of the three approaches, SAMs offered the best electron transfer kinetics while Nafion films offered greater stability. The activity of LB films were found to be highly dependant on the orientation of the

14

monolayer, which was controlled by changing substituent groups. Removal of electrodes with LB films prepared this way from the Langmuir-Blodgett trough resulted in loss of the LB film, indicating very weak stability. No kinetic data or product analysis was performed, but catalysis occurred at a potential of *ca.* -1.3 V *vs.* SCE.

1.2.5 Electropolymerization

The final method for non-covalent CME preparation to be discussed here is electropolymerization. Due to the excellent chemical and electrochemical properties of polypyridyl ruthenium complexes, they were fundamental in early development of this technique with regard to transition metal containing polymers [31–33]. Electropolymerization of polypyridyl ruthenium complexes was initially performed reductively, utilizing a vinylbipyridine ligand (vibpy) [31]. The mechanism of polymerization was shown to be radical polymerization of the radical-anion formed upon reduction of the vibpy ligand [32]. The technique was quickly expanded to include oxidative polymerization, utilizing aminopyridine based ligands [33]. Pyridine based ligands used in the initial discovery are depicted in Figure 1.4.

CMEs prepared by electropolymerization of *bis*-vinylterpyridine complexes of Co(II), Fe(II), Ru(II) and Os(II) on glassy carbon electrodes have also been examined [34]. CMEs prepared by reductive electropolymerization of all complexes were found to catalytically reduce CO_2. The Cr and Co complexes were found to be active at the least extreme potentials, -0.86 and -0.87 V *vs.* SSCE, respectively. All other polymers were found to catalytically reduce CO_2 between -1.1 and -1.2 V. Product analysis following electrolysis indicated that formalde-

4-vinyl-4'-methyl-2,2'-bipyridine

4-vinylpyridine

5-aminophenanthroline

3-aminopyridine
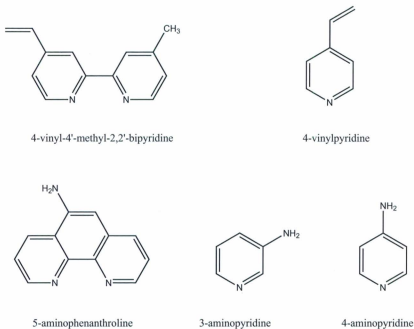
4-aminopyridine

Figure 1.4: Pyridyl ligands employed in the initial studies on the electrochemical polymerization of metal complexes on electrode surfaces. Vinylpyridine ligands (top) were used for reductive polymerization, aminopyridine ligands (bottom) were used for oxidative electropolymerization [31–33].

hyde was the only product formed, with no formic acid or CO being detected (only Co, Fe and Cr complexes were examined). The Faradaic efficiency was found to be highly dependant on the metal center. The Faradaic efficiencies reported were 28% (Fe), 39% (Co), and 87% (Cr).

As a final example of non-covalent CMEs for redox catalysis of CO_2: an interesting ruthenium polymer, based on a Ru(0)-Ru(0) backbone, was prepared by electropolymerization and studied for catalytic CO_2 reduction [35–39]. Ruthenium complexes of the general formula *trans*-(Cl)-$[Ru(L)(CO)_2(Cl)_2]$ or *trans*-(CH_3CN)-$[Ru(L)(CO)_2(CH_3CN)_2]^{2+}$, where L is a bidentate, bipyridine based
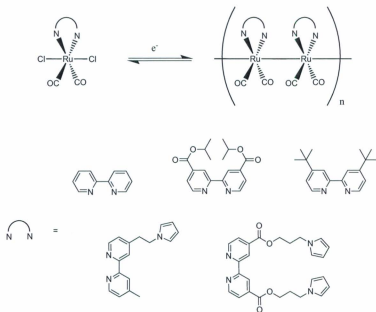
Figure 1.5: Structure of metal-metal bonded ruthenium polymers studied by Deronzier and coworkers [37]. A selection of bipyridyl ligands containing electron withdrawing groups and electron donating groups are shown.

ligand, were found to deposit a dark blue colored film on electrodes when examined reductively [35]. These films were attributed to a polymer of the general structure $[Ru(L)(CO)_2]_n$, where Ru(0)-Ru(0) bonds formed the polymer backbone. Shortly after this discovery, the polymer formed by electropolymerization of $[Ru(bpy)(CO)_2Cl_2]$ on a carbon electrode was found to be an active redox catalyst for CO_2 reduction [36]. Electrolyses performed with these CMEs were reported to quantitatively produce CO [36]. The electropolymerization technique was expanded to include a selection of bipyridine based ligands, including bipyridine substituted with electron donating groups (EDGs), electron withdrawing groups (EWGs), and electropolymerizable pyrrole groups [37]. It

was found that, under aqueous conditions, CO was the only observed product for polymers based on EDG substituted ligands. Use of EWG substituted ligands altered the reactivity, producing formate as the primary product, along with small amounts of CO. For polymers substituted with pyrrole side-chains, electrochemical generation of polypyrrole was observed to increase the stability of the polymer films [37]. Altering the properties of the linker between the bipyridine ligand and the pyrrole side-chain were found to allow control of product identity while allowing for increased stability by electropolymerization of the pyrrole groups. For example, a simple alkyl chain (EDG) linker was observed to produce solely CO, while an an alkyl-ester (EWG) linker was found to produce formate ions as the major product [39].

1.3 Covalent Chemically Modified Electrodes

Preparation of CMEs is also possible through covalent tethering of the desired species. This field may be roughly classified into two categories: modification through electrochemically initiated reactions and modification by chemically initiated reactions.

1.3.1 Chemically Initiated Modifications

The covalent modification of electrodes through chemically induced reactions generally relies on reactions between the incoming species and surface functionality located on the electrode surface. The first report of successful modification of electrode surfaces was accomplished via silane chemistry designed to target hydroxy surface functionality [40]. In this case, modification of antimony-

doped tin oxide (SnO_2) electrodes was accomplished by reaction with alkyltri-alkoxysilanes, or alkyltrichlorosilanes. Halogen-silicon (*e.g.* Cl-Si) and alkoxy-silicon (*e.g.* CH_3CH_2O-Si) bonds react with nucleophilic sites, such as surface hydroxy groups (Sn-OH), covalently immobilizing the silicon atom to the surface. A polymerization reaction also occurs between trialkoxysilanes, resulting in a polysiloxane covalently bound to the surface. The C-Si bond attaching the alkyl group to the polysiloxane is more stable, which allowed the immobilization of desired functionality on the SnO_2 surface. Alkyl groups studied included nitrogen moieties such as pyridine and ethylenediamine [40], chosen for their ability to coordinate to transition metals. The polysiloxane approach for modifying surfaces expanded to include a wide variety of electrode materials, including metal oxides such as TiO_2 and PtO [41], and carbonaceous materials such as carbon blacks [42] and boron-doped diamond [43]. Carbon black was chosen for use in the present work, as will be discussed in Section 1.5. Therefore, attention here is focussed on the covalent modification of graphitic carbons.

Two recent reviews highlight successful modification techniques for covalent modification of carbon nanotubes [44, 45]. Two general approaches are outlined in both reviews. The first is a two step reaction, where installation of functional groups on the carbon surface (*e.g.* carboxylate groups by oxidation of the surface) is followed by modification of the functional groups using the appropriate chemistry (*e.g.* esterification or amidification). The second technique relies on direct reaction between reactive species, such as radicals, and the carbon surface. The most successful and adaptable modification technique appears to be the spontaneous reaction of diazonium ions with carbon surfaces. This particular reaction is applicable to a wide range of carbonaceous materials, and is

believed to generate C-C bonds. This makes it a powerful technique for immobilization of a wide range of species. This approach was chosen for use in the present work and is discussed in detail in Section 1.4.
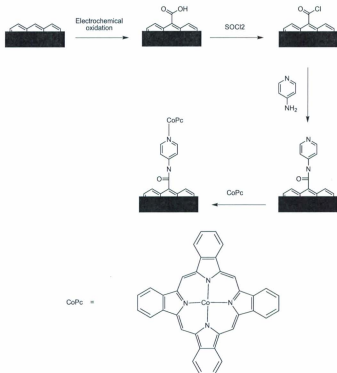
Figure 1.6: Modification process used to covalently immobilize porphyrin complexes on carbon surfaces. Example shown depicts the immobilization of cobalt(II) phthalocyanine [46, 47].

Reports of covalent immobilization of transition metal complexes on electrode surfaces have been published. For example, immobilization of cobalt(II) porphyrin complexes on glassy carbon electrodes was accomplished in a multistep procedure [46]. The steps involved are shown in Figure 1.6. They were: (i) oxidation of the carbon surface, (ii) conversion of carboxylic acid groups to

acid chlorides by treatment with $SOCl_2$, (iii) reaction of the acid chloride modified carbon with 4-aminopyridine, and finally (iv) complexation of Co with the surface-bound pyridine group. This approach was expanded to include a variety of similar metal complexes, and explored for a redox catalysis of carbon dioxide reduction [47]. Although good electrochemical behavior was observed using such systems, the obvious drawback is the lengthy modification procedure.

1.3.2 Electrochemically Initiated Modifications

A much more popular approach for covalent modification of carbon surfaces is known as electrografting. The general strategy behind electrografting is the formation of a reactive species by electron transfer. This field of research has received attention in recent years, and a comprehensive review has been recently published [48]. Two forms of electrografting exist: oxidatively induced reactions and reductively induced reactions. The most studied oxidatively induced reactions are initiated by oxidation of amines or carboxylates, followed by reaction of the oxidized species with the carbon surface. Reductively, the primary starting materials are commonly vinyls or aryl diazonium ions [48].

Oxidative electrografting of amines was first accomplished on carbon surfaces in 1990 [49]. It was then shown that primary amines were much more effectively bound to carbon surfaces than secondary amines, and little to no bonding was observed for tertiary amines [50]. In the initial discovery of this technique, it was observed that when diamines were used, both nitrogen groups were bound to the surface [49]. To circumvent this potential problem, one of the amines was protected before oxidative electrografting [51, 52]. Removal of

the protecting group allows further chemistry to be carried out with the amine, such as formation of an amide linkage [51, 52]. Oxidative electrografting of aminopyridine has been used to immobilize CoTPP (cobalt (II) tetraphenyl-porhyrin) [53] and polypyridyl osmium and ruthenium complexes [54].

Successful immobilization of CoTPP on glassy carbon electrodes was examined with a series of voltammetric experiments [53]. It was found that modification of the glassy carbon surface by oxidative electrografting of aminopyridine resulted in a CME with enough CoTPP to constitute 100 monolayers. The authors suggested that a monolayer was bound and that the additional CoTPP was physisorbed (non-covalent attachment). This hypothesis was supported by the observation that rinsing the electrode resulted in a significant decrease in the amount of CoTPP detected voltammetrically. The CMEs were found to actively catalyze the reduction of CO_2 at potentials of -1.0 V *vs.* SCE, producing CO and H_2 (H^+ reduction) as the reduction products. It was also found that removal of physisorbed CoTPP resulted in improved electrocatalysis. The faradaic efficiency for CO production increased from 31% before rinsing the electrode to 63% following heavy rinsing.

The immobilization of polypyridyl ruthenium and osmium complexes on glassy carbon electrodes was examined using two approaches [54]. The first was the oxidative electrografting of aminopyridine, followed by reaction with $M(bpy)_2Cl_2$ (M = Ru(II) or Os(II)). The second approach was the direct oxidative electrografting of $[M(bpy)_2(Cl)(NH_2pyr)]^+$, where NH_2pyr is 4-aminopyridine. Both approaches were found to be successful, producing surface coverages of 3.8×10^{-10} and 1.7×10^{-10} mol cm^{-2}, respectively. These values suggest approximately four and two monolayers, respectively. The authors note that when accounting for surface roughness, the surface coverages are approximately 0.4

and 0.2 monolayers. It was suggested that the difference between the two techniques was due to steric considerations. It was suggested that the role of sterics was minimized in the indirect grafting method, as it involved elevated temperatures to coordinate the transition metal complexes to the immobilized pyridine groups.
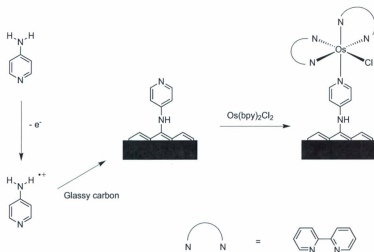
Figure 1.7: Modification process used by Aramata *et al.* to covalently immobilize polypyridyl osmium and ruthenium complexes on carbon surfaces [54]. Example shown depicts the two step, indirect immobilization of $[Os(bpy)_2(Cl)(pyr)]^{2+}$ on a glassy carbon electrode.

Oxidative electrografting of carbon surfaces was expanded to include covalent immobilization of substituted aromatic molecules on glassy carbon by a process similar to the Kolbe reaction [55] (Scheme 1.1). Oxidation of arylacetates resulted in oxidative decarboxylation of the acetate, producing an aryl radical. This aryl radical is then free to react with the carbon surface. It was shown, by atomic force microscopy (AFM) depth-profiling, that the reaction proceeded rapidly [56]. During controlled potential electrolysis, no change in film thick-

ness was observed upon increasing the reaction time from 30 s to 300 s. However, the thickness of layers deposited by this technique were found to increase with applied potential: from approximately 3-4 nm thick for 100 mV beyond the required oxidation potential to 18 nm thick for 800 mV beyond [56]. It was found that both alkylacetates and arylacetates could be covalently immobilized on glassy carbon at mild potentials by employing ferrocene as a redox mediator [57]. The oxidative electrografting of 4'-methyl-(2,2'-bipyridine)-4-acetic acid was reported as a successful method for immobilization of polypyridyl ruthenium complexes [58].
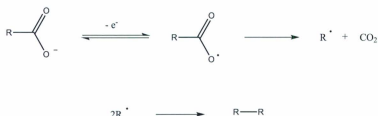
Scheme 1.1: Reaction mechanism of the Kolbe reaction.

The electrochemically initiated reaction between diazonium ions and electrode surfaces is a technique that has received far more interest in recent years. This particular reaction is believed to generate C-C bonds, making it a powerful modification method. This approach is discussed in detail in Section 1.4.

1.4   CME Preparation Using Diazonium Ions

Over the last two decades, aryl diazonium ions have become extremely popular reagents for the preparation of covalent CMEs. Discovery of the ability to modify carbon surfaces using aryl diazonium ions was first reported in 1992 by

Delamar *et al.* [59]. In the initial report, it was shown that reductive cycling of a glassy carbon electrode in a solution of 4-nitrophenyl diazonium tetrafluoroborate resulted in covalent immobilization of nitrobenzene on the electrode surface [59]. Since the initial report, the surfaces modified by electrochemical one electron reduction of aryl diazonium ions to aryl radicals and N_2 has since spread to other electrode materials, such as: semiconductors [60, 61], carbon nanotubes[62] and metals, including Co, Ni, Cu, Zn, Pt and Au [63].

Shortly after the report of electrochemically induced modifications, the spontaneous reaction of aryl diazonium ions with graphitic materials was patented by Cabot Corporation [64]. The finding that aryl diazonium ions spontaneously react with carbon materials was an important one, as it greatly simplifies the modification process for application on a much larger scale. It has also been shown that the spontaneous modification technique is not limited to carbonaceous materials, but also extends to metals such as Fe, Cu and Ni[65].

Although the two modification techniques are very similar to one another, they differ in that there is application of an external driving force during the electrochemically induced reaction. Therefore, the reaction kinetics and mechanism may be expected to be different between the two techniques. Research performed on each of the two techniques is examined in Sections 1.4.2 and 1.4.3. Use of diazonium chemistry to immobilize transition metal complexes is examined in Section 1.4.4.

Modification of carbon surfaces by diazonium chemistry has seen a lot of research over the past two decades. Comprehensive reviews have been recently published that cover the current state of research in regards to reductive electrografting of diazonium ions to carbon surfaces [48] and the spontaneous grafting of diazonium ions to carbon surfaces [66]. Therefore, the following sections

present a more general overview, focussing on topics that are important in regards to CME design.

1.4.1 Characterization of Carbon Based CMEs

Before delving into the differences between the electrochemical and spontaneous modifications, it is worthwhile to introduce the instrumental techniques that have been used to study CMEs prepared using both procedures. Directly proving the existence of a C-C bond between the aromatic carbon surface and the aromatic modifying material is an incredibly difficult, likely impossible, task. However, several different approaches have yielded indirect evidence of a C-C bond. This section briefly introduces these instrumental analyses.

Vibrational spectroscopy has been used to prove the presence of functional groups in modified carbon materials following modification by aryl diazonium ions. Surface Raman spectroscopy was used by the McCreery group to show the presence of -NO_2 functionality on GC and HOPG that had been modified with 4-nitrobenzene using the electrochemically initiated procedure [67]. Infrared reflectance absorbance spectroscopy was similarly used by the McDermott group to show the presence of diethylaniline immobilized on glassy carbon electrodes [68].

X-Ray photoelectron spectroscopy (XPS) has been widely used in modification studies both to show the existence of a wide variety of modifying species on carbon surfaces [67, 69–72] and to quantify the surface coverage [67, 70, 71]. It is noteworthy that Yu *et al.* also used XPS results to suggest that up to 35% of nitrogen observed in nitrobenzene modified glassy carbon is due to an azo-linkage between nitrobenzene and the glassy carbon surface, indicating that

approximately 27% of immobilized molecules are not immobilized by a C-C bond [72]. The azo- moieties were found to be electrochemically inactive, which agrees with an earlier study where 4-(4-nitrophenylazo)benzenediazonium was used to modify pyrolyzed photoresist films [73]. This is an important finding as observation of an N 1s signal at lower binding energy is often observed, but is consistently assigned to NO_2 groups which had been reduced during the XPS experiment [65]. Such assignments have been based on the failure to observe electrochemistry of the azo- linkage (-N=N-).

Cyclic voltammetry is another commonly used technique for examining modified electrodes. Two general techniques have been used. The first is the immobilization of electroactive molecules such as 4-nitrobenzene [59, 67, 69]. Nitrobenzene can be electrochemically reduced by a 2 electron EC mechanism to a nitrosylphenyl moiety, which in turn exhibits a reversible 2 electron reduction [74]. It has been reported that all immobilized molecules are not electroactive following electrografting of aryl diazonium ions on pyrolyzed photoresists [72, 73]. The second technique involves immobilizing non-electroactive species and monitoring the electrochemistry of a solvated species with reversible electrochemistry.

Electrochemical blocking effects of immobilized films have been explored using potassium ferricyanide ($K_3Fe(CN)_6$) under aqueous conditions following immobilization of diethylaniline on highly-ordered pyrolytic graphite [75] and glassy carbon [68]. In both cases, an increase in the cyclic voltammetric peak separation was observed. The separation increased from an original value of 78 mV to 115 mV after two electrochemical modification cycles, and to 230 mV after 30 minutes of electrochemical cycling. This is indicative of a large decrease in electron transfer kinetics, as would be caused by inhibited mass transfer to

the electrode surface.

Atomic force microscopy has also been used in several ways. It has been used to follow the nucleation and growth of polymers on the surface of basal-plane HOPG electrodes following electrochemically initiated modification [75]. It has also been used as a tool to measure the thickness of layers formed on the surface following electrochemically driven modification [73, 76, 77].

Thermogravimetric analysis has been used to analyze the thermal stability of carbon powders modified by spontaneous reaction with aryl diazonium ions [78]. Results indicated a very strongly bound layer, suggesting covalent immobilization.

Mass spectrometry has also been used to examine carbons modified by diazonium grafting [79, 80]. Specifically, time-of-flight secondary-ion mass spectrometry (SIMS-TOF) has been used to show the presence of oligomeric structures on the surface following modification, as well as provide mechanistic insight on the modification mechanism.

1.4.2 Electrochemically Initiated Grafting

Important considerations for choosing a modification technique for CME preparation include the stability of the linkage, whether a monolayer or a multilayer forms, whether the modifying layer is uniform, and whether all the immobilized material is electroactive. Some key papers addressing these issues are highlighted in this section, with specific regard to the reductive electrografting of aryl diazonium ions on carbon surfaces.

It is widely accepted that the electrografting of diazonium ions results in a C-C linkage between the incoming aryl diazonium molecule and the carbon

surface. The original publication of the technique attributed the covalent modification to a one electron reduction of the aryl diazonium to N_2 and an aryl radical [59], based on previously reported electrochemistry of aryl diazonium ions. The aryl radical was believed to be the reactive species that bound to the carbon surface. Although this mechanism is favored by most publications, the true situation appears to be a combination of several competing reactions.

The first indication of the existence of an azo-bridge in CMEs prepared by electrografting aryl diazonium ions came form XPS results, where a signal was observed at *ca.* 400 eV. Preliminary studies focussed on the immobilization of nitrobenzene on carbon surfaces. The presence of this unexpected peak was attributed to a background signal due to nitrogen functionality on the carbon surface [67], contamination [81], or from reduction of the nitro group during XPS acquisition [65]. A subsequent report studied the electrografting of 4-carboxyphenyl groups. The report showed that the GC used possessed no nitrogen content prior to functionalization, and that immobilization of the 4-carboxyphenyl group resulted in an XPS signal at 400 eV. These results indicated that although reduction of nitro groups during XPS acquisition may be occurring, azo-linkages were definitely being formed during the reaction [82]. It was suggested that diazonium ions were binding adjacent to phenol or naphthol groups on the carbon surface, as shown in Figure 1.8 [82]. Further evidence of azo- linkages arises in a time-of-flight secondary ion mass spectrometry (SIMS-TOF) study [80]. In their study, Doppelt *et al.* observed mass fragments that correspond to monomeric fragments containing an N_2 group, and dimeric fragments bound by an azo- linkage.

It should be noted that although there is strong evidence of azo- linkages forming, they appear to be electrochemically inactive when incorporated into
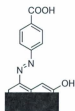
Figure 1.8: Structure proposed by Saby *et al.* to explain the presence of N 1s signals observed in XPS spectra following electrografting of carboxyphenyl groups on the surface of glassy carbon [82].

immobilized films by electrografting [72, 73].

A further possibility is highlighted in a SIMS-TOF study of electrografted diazonium ions on glassy carbon [79]. In this report, mass fragments were observed that corresponded to monomer and dimer fragments that possessed an extra oxygen. Such an observation suggests that the modification also occurs through some form of oxygen functionality, such as an ether or ester linkage. Such a mechanism has been suggested for the spontaneous grafting procedure (discussed in Section 1.4.3), and therefore may also occur during the electrochemically initiated reaction.

The topic of monolayers and multilayers produced by the electrografting of diazonium ions can be rather confusing. This is partially due to the large number of different substrates modified using the approach. For example, the modification of a metallic electrode, such as copper, behaves differently than carbon electrodes, which behave differently than semiconductor electrodes. Even within the confines of carbon electrodes the topic can be confusing as each type of carbon has a different structure, and therefore can be expected to react differently. For example, as is discussed further in Section 1.5, glassy carbon electrodes possess a high degree of edge-plane carbon, while HOPG electrodes

can be made with basal-plane carbon being the dominant form. A significant amount of research has been carried out using GC electrodes, HOPG electrodes and pyrolyzed photoresist films (PPF); the multilayer versus monolayer issue with respect to these substrates is discussed in the next few paragraphs.

Many early reports suggested that monolayer coverages were obtained by electrografting of diazonium ions [59, 67, 82]. However, subsequent studies have challenged this concept and suggested that film thickness is highly dependant on a multitude of factors. These factors are known to include the identity of the aryl diazonium species [77], the electrochemical potential used for grafting [83], the total current passed [76, 84], and the reaction medium [73, 77].

Due to growth in evidence of multilayer production, it is generally accepted that multilayer formation can occur. The observation of oligomers on the surface of GC on examination with SIMS-TOF [79], and numerous publications employing AFM to show thick films upon electrografting [68, 73, 75–77] have left little doubt that multilayers can form. The structure of such multilayers is believed to be a polyphenylene-type polymer, such as that shown in Figure 1.9 [68, 75].

The identity of the diazonium species has been shown to affect the thickness of films formed. An AFM study indicated that immobilization of 4-(4′-nitrophenylazo)benzene (NAB) resulted in thinner films than electrografting of nitrophenyl (NP) groups under identical conditions [77]. The aryl diazonium ions used to immobilize these moieties are shown in Figure 1.10. The authors suggested that this behavior was related to the fact that NAB films exhibited greater electrochemical blocking tendency than NP films.

It has been shown that thinner films that exhibit greater electrochemical blocking are obtained when the modification was performed using aqueous solu-

31
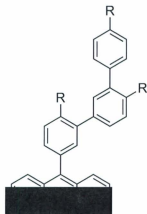
Figure 1.9: Template proposed for polymer films deposited upon electrografting of aryl diazonium species to the electrode surfaces. Where R represents substituents from the aryl diazonium ion (*e.g.* R = NO$_2$ for 4-nitrobenzene diazonium).

tions, as opposed to acetonitrile solutions [77]. In this study, NP and NAB groups were immobilized on PPF surfaces.

The electrochemical potential used to achieve electrografting has been shown to be an important parameter [83]. The results of a study that examined the amount of material deposited on a GC electrode at various potentials, with all other parameters constant, indicated that increasing the overpotential resulted in a significant increase in amount of material deposited.

It has been observed that deposition of films that correspond to monolayer thickness is possible, if suitable conditions are applied [76, 84]. These conditions generally employ solutions with low concentrations of the diazonium ion and short periods of electrografting. Conditions that have been found suitable for PPF electrodes are 1 mM solutions of the appropriate diazonium species, and two electrochemical cycles at a scan rate of 200 mV s^{-1} [76].

4-(4'-nitrophenylazo)benzenediazonium   4-nitrobenzenediazonium
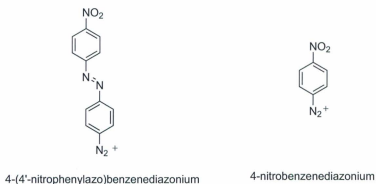
Figure 1.10: Aryl diazonium ions used to immobilize 4-nitrophenyl and 4-(4'-nitrophenylazo)benzene groups on electrode surfaces.

The ability to form a close-packed monolayer has been questioned [77, 83]. In studying the role of electrochemical potential on the thickness of grafted films, Downard observed that, for films deposited using low overpotentials, the surface coverage of the film was slightly less than what was expected for a monolayer [83]. Through a comparison of results from cyclic voltammetry and AFM, it was suggested that a monolayer of NP groups immobilized on a PPF electrode had a surface coverage of approximately 2.5×10^{-10} mol cm^{-2} [77]. This value is approximately 20% of the density expected for a close-packed monolayer, suggesting that the film possessed a loosely packed structure.

To understand the structure of films deposited by electrografting of diazonium ions, an informative study was performed using HOPG electrodes [75]. The study employed AFM to examine the deposition of diethylaniline (DEA) groups on the surface of HOPG by reductive diazonium electrografting. The results clearly showed significant binding of thick DEA films at the edge-plane regions of HOPG, while the basal-plane regions exhibited scattered clumps of deposited film. The preference of edge-plane sites over basal-plane sites was

attributed to the higher reactivity of edge-plane sites than basal-plane sites, which had been previously observed [69]. The presence of apparently polymeric clumps on the basal-plane was attributed to initial reaction of the reagent with defect-sites. Once immobilized, this site acted as a "nucleus" for further polymerization.

A final consideration is the electrochemical activity of films immobilized using this approach. It has recently been shown that it is not possible to electrochemically reduce all electroactive species present in deposited films [72]. XPS was used to quantify the amount of nitro- groups present in NP films on GC and PPF following either chemical (using Na_2S) or electrochemical reduction. It was observed that, for all of three different solvent systems, a significant amount of nitro- groups remained unreacted following electrochemical reduction.

A literature search revealed no reports on electrografting of aryl diazonium ions on carbon blacks. This is likely due to the experimental difficulties that would accompany the use of electrode material that is in powder form. The modification of "bucky paper" electrodes by electrografting of aryl diazonium ions has been studied [62]. Such electrodes are prepared by filtration of a carbon nanotube suspension.

1.4.3 Spontaneous Grafting Reaction

Although the spontaneous reaction between aryl diazonium ions and carbon blacks was patented by Cabot Corporation in 1996 [64], it wasn't until 2001 that the academic community began using the technique [62, 85]. In 2001 [62], James Tour and coworkers reported that simply exposing carbon nanotubes to a solution of aryl diazonium ions (prepared *in-situ*, dichlorobenzene solution)

resulted in carbon nanotubes that were similar to those modified by electro-grafting of aryl diazonium ions [85]. The modification technique has expanded to include modification of GC electrodes [65, 79] and PPF electrodes [86]. In recent years, a series of studies have examined the modification of carbon blacks in closer detail [71, 78]. Care must be taken in directly comparing literature results, as it has been shown that both the nature of the substrate and the diazonium ion affect the thickness and structure of deposited films [87].

One of the initial reports on the spontaneous modification of GC surfaces by aryl diazonium ions compared the SIMS-TOF results obtained for a modified surface with those of a similar electrode modified by electrografting [79]. Results showed that modification had proceeded, but to a smaller extent than the electrografted sample. Further, the intensity of signal for oligomers (dimers, trimers, tetramers) observed following the electrografting reaction was significantly reduced for the surface modified by spontaneous grafting.

The affect of reaction time and diazonium ion concentration on the thickness of the film deposited on GC (and Fe) was examined [65]. It was observed that, for GC electrodes, the surface coverage of immobilized NP groups tripled as the the reaction time was increased from 1 min to 60 min. Similarly, increasing the concentration of the diazonium ion from 0.1 mM to 10 mM resulted in a four-fold increase in surface coverage.

In contrast to the results obtained for the modification of GC surfaces, it was found that diazonium ion concentration and reaction time had no affect on the thickness of films spontaneously deposited on a carbon black (Vulcan XC72) [71]. In the study, the amount of NP groups deposited on the surface of Vulcan XC72 was measured by XPS. It was observed that neither an increase in reaction time from 1 h to 12 h, or a 10 fold increase in diazonium ion concentration

resulted in increased surface coverages. The study also found that a maximum surface coverage was consistently obtained during the modification process. Alterations to the modification procedure, designed to increase the surface coverage of NP groups, were unsuccessful. The authors attributed the surface coverage limit to saturation of the limited reactive sites (edge-plane and defects in the basal-plane). These results suggest that modification of carbon blacks does not result in polymerization on the surface, and that formation of a complete monolayer may not be feasible (due to basal-plane content).

The discrepancies in results between carbon black [71] and GC [65] are likely due to the the nature of the substrates being modified. As mentioned earlier, it has been shown that the substrate can have a significant influence on the outcome of the spontaneous grafting reaction [87].

The exact reaction mechanism and type of linkage formed during the spontaneous grafting remains unclear. Several reaction mechanisms have been proposed in the literature and are given in Scheme 1.2. Results obtained following variation of the substrate material suggest that the reaction mechanism is similar to the electrografting mechanism [87]. Such a mechanism would involve the transfer of an electron from the carbon surface to the diazonium ion, producing the same reactive aryl radical as is believed to be formed during electrografting.

While this process is likely occurring, several other proposed reaction mechanisms appear in the literature. Similar to results obtained following the electrografting of diazonium ions, XPS has frequently revealed a peak near 400 eV [65, 71, 78, 87]. It has been suggested that this peak is due to azo- linkages to the carbon surface, which likely originate from reaction of the diazonium ion *ortho* to phenolic surface functionality, producing structures such as that shown in Figure 1.8 [78].
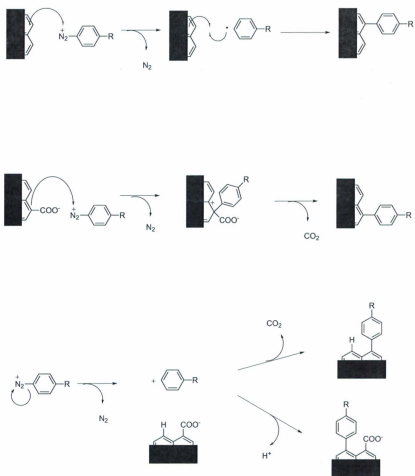
Scheme 1.2: Proposed mechanisms for the spontaneous grafting of aryl diazonium ions on carbon surfaces. The aryl radical mechanism (top) [85], concerted decarboxylation mechanism (middle) [71] and aryl carbocation mechanisms (bottom) [88] and their sources are discussed in the text.

A concerted dediazoniation reaction has also been suggested [71]. This suggestion was based on the observation that nearly identical surface compositions were observed following spontaneous modification of untreated Vulcan XC72 and chemically oxidized Vulcan XC72. Such an outcome would require the loss of carboxylic acid surface functionality (shown by XPS to be added during chemical oxidation), which the authors suggested could occur as depicted in Scheme 1.2.

During the development of a chemically driven grafting process, which is discussed shortly, Compton and coworkers observed the presence of two electrochemical processes in cyclic voltammograms following spontaneous grafting of anthraquinone on graphite powder [88]. This led the authors to propose two competing mechanisms. In the absence of a reducing agent, the authors suggested that rather than spontaneous reduction and homolytic cleavage of the N_2 moiety from the aryl diazonium ion, heterolytic decomposition occurred under aqueous conditions. Such a process would result in an aryl cation being the reactive species, rather than an aryl radical. They proposed that this aryl cation could then react with the carbon surface in two separate ways: (i) direct reaction with the carbon surface, releasing a terminal hydrogen as H^+, or (ii) reaction with surface carboxylates, resulting in an ester linkage to the surface. The presence of two distinct redox processes was not observed for the spontaneous modification of glassy carbon surfaces [65]. This suggests that such a mechanism may be specific to graphite powder, which once again highlights the care that must be taken when comparing results between different substrates.

As a final consideration, the accessibility of surface area to the reactive species has been examined [71, 89]. It has been shown, through N_2 adsorption experiments, that the covalent immobilization of aryl groups via diazonium chem-

istry results in a decrease of measurable surface area. A phenomenon termed constriction was used to explain these observations. Immobilization of aryl groups on the surface of the carbon surface was shown to decrease the amount of surface area present due to pores with a diameter of 20 Å or less.

1.4.4 Immobilization of Transition Metal Complexes on Carbon Surfaces

At the onset of the current project, examples of transition metal complexes immobilized on carbon surfaces through diazonium chemistry were sparse. Over the course of the current work, several publications from other research groups reported the successful immobilization of transition metal complexes on carbon surfaces through diazonium chemistry. A literature search revealed no reports on the modification of carbon blacks with transition metal complexes using diazonium chemistry.

Belanger and coworkers have used diazonium chemistry to prepare ionic films on glassy carbon surfaces. The ionic films were used to electrostatically immobilize transition metal complexes on the surface [90]. Chemical reduction of the transition metal ions was then used to produce metallic deposits on the electrode surface. Electrografting of the appropriate diazonium ion was used to covalently immobilize 4-diethylaniline and 4-sulfonate phenyl groups on the surface. This was followed by exposure of the CME to an aqueous solution of the appropriate pH containing the desired transition metal, and then by chemical reduction.

The first reports of polypyridyl transition metal complexes being immobilized on carbon surfaces through diazonium chemistry appeared in 2008 [91].

In this report polypyridyl ruthenium complexes were electrografted directly onto GC electrodes and carbon nanotubes. The authors noted evidence of polymerization on the surfaces. Potentiostatic electrolysis indicated film thicknesses suggesting up to 343 monolayers being formed. Diazonium ions were prepared in-situ, and it was found that a phenyl spacer placed between the pyridyl ligand and the amine group was necessary to accomplish modification using this approach. For example, it was found that a complex containing 4-amino-2,2′-bipyridine as a ligand could not be electrografted, but a complex containing 4-(4′-aminophenyl)-2,2′-bipyridine as a ligand could be.

A two-step modification procedure has been used to successfully immobilize polypyridyl osmium complexes on glassy carbon [92], based on a procedure previously reported for modification of gold surfaces [93]. This modification procedure was initiated by electrografting of benzoic acid groups on the surface of glassy carbon. An amide linkage was then formed between the CME and polypyridyl osmium complexes containing a 4-(aminomethyl)pyridine ligand. CMEs prepared this way were found to be quite stable: a decrease in surface coverage of only 5% was observed over a period of 30 days.

The first report of spontaneous grafting of pyridine-based functionality was recently published [94]. In this report, the spontaneous reaction between 3-aminopyridine, 6-aminoquinoline and 5-aminophenanthroline with glassy carbon was accomplished in acetonitrile solution. CMEs prepared this way were then treated with a solution of $RuCl_3$, which resulted in the immobilization of ruthenium on the surface, as indicated by XPS. The authors suggested this method could be used to immobilize polypyridyl ruthenium complexes on the surface.

1.5 Solid Supports

Due to their highly conjugated structure, graphitic carbon materials are capable of electronic conduction, enabling their use as electrode materials. Although all graphitic materials are not identical, they are composed of similar structural elements. The basic structural elements of graphitic materials are referred to as the (i) basal-plane and (ii) the edge-plane. These structural elements are drawn in Figure 1.11. The basal-plane of graphitic carbons primarily consists of a series of sp^2 hybridized carbon atoms bound to three neighboring carbon atoms. Defects in the basal-plane are known to occur, where sp^3 hybridized carbons take the place of sp^2 hybridized carbons. The edge-plane of graphitic carbons corresponds to the edges of basal-plane segments, where sp, sp^2 and sp^3 hybridized carbons exist. A large variety of functional groups can exist on the edge-plane, such as ethers, lactones, and hydroxyl groups. The type and amount of functional groups present is related to the preparation and handling of the material.

Highly-oriented pyrolytic graphite (HOPG) is a form of graphitic carbon frequently used for electrochemistry. According to the IUPAC definition, HOPG is a synthetic form of graphite, where the angle between the layers is less than 1 degree [95]. This form of carbon is primarily basal-plane graphite. Preparation of a fresh graphite surface can be accomplished by simply applying adhesive tape to the surface. Removal of the adhesive tape pulls the top layer of graphite from the electrode surface, resulting in exposure of a clean graphite surface.

Glassy carbon (GC) is commonly used in modern electrochemistry. Also known as vitreous carbon or glass-like carbon, this form of carbon is named for its glass-like appearance [95]. This form of carbon is considered to possess
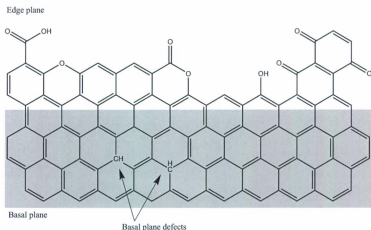
Figure 1.11: Representation of the structural elements of graphitic carbons. Shown are the basal plane (bottom, shaded), defects in the basal plane, edge plane (top) and examples of functional groups potentially present on the edge plane surface.

a high degree of edge-plane graphite [69].

Pyrolyzed photoresist films (PPF) are films of graphitic carbon deposited on flat (silicon) surfaces. To prepare the films, a photoresist is spin-coated on a silicon wafer. The film is dried, then pyrolyzed, producing a thin, conductive carbon film [77].

Carbon black, the type of carbon chosen for the present study, is a form of carbon synthesized by the thermal decomposition or incomplete combustion of carbon-hydrogen materials [95]. There exist a large number of carbon blacks, each synthesized under varying reaction conditions. The synthetic procedure affects multiple properties of the carbon black, including specific surface area, functional groups, particle size and pore size. Further, it has been shown that post-synthesis treatments such as ultrasonication can affect these properties [96, 97].

Carbon blacks were chosen for this study due to their low cost, high surface area, excellent stability, and range of functional groups present. Vulcan XC72 was the specific carbon black chosen, due to its use in previous studies [71, 78]. As discussed in the previous section, the nature of the substrate can have significant effects on the grafting mechanism. The use of this particular carbon simplifies comparison of results with previous literature reports [71, 78].

1.6 Objectives

The aspirations of the current project are to create CME materials for use in gas diffusion electrodes. The gas diffusion electrodes, in turn, would be used to accomplish the electrocatalytic reduction of gaseous CO_2. Immobilization of polypyridyl ruthenium complexes presents a suitable target, as they are known to be chemically stable, and with appropriate ligand design can catalyze the reduction of CO_2.

A large electroactive surface area would maximize the efficiency of a gas diffusion electrode. Therefore, the work reported here has focussed on modification of a high surface area carbon black. Specifically, Vulcan XC72 was chosen for this work for reasons introduced in Section 1.5.

While it has been shown that the entire film is not electroactive following electrografting of diazonium ions, the same has not been shown for the spontaneous grafting of carbon blacks. Considering that much thinner layers are deposited using the spontaneous grafting, it is anticipated that the entire layer should be electroactive. As cyclic voltammetry presents one of the simplest, fastest methods of analyzing CMEs, it would be useful to investigate it as a means to quantify surface coverages.

The goals of this project are as follows:

i. Perform an electrochemical study on Vulcan XC72 modified by spontaneous diazonium grafting of a simple, electroactive organic molecule to test the ability of cyclic voltammetry to act as an accurate quantitative tool.

ii. Immobilize polypyridyl ruthenium complexes on Vulcan XC72 using spontaneous diazonium grafting chemistry.

iii. Attempt to maximize the amount of polypyridyl ruthenium complex immobilized on the carbon surface.

iv. Examine whether prepared materials are active redox catalysts for CO_2 reduction.

Experimental

2.1 Instrumentation

Electrochemical experiments were performed using a Hokuto-Denko HA301 potentiostat with a HB111 waveform generator. All potentials are reported against a saturated calomel reference electrode (SCE), which was measured to be -0.40 V *vs.* the ferrocene redox couple.

X-ray photoelectron spectroscopy (XPS) measurements were performed by Sergei Rudenja or Kevin McEleney, members of Prof. Michael Freund's research group. Spectra were acquired using a Kratos Axis Ultra, equipped with a delay line detector. The acquired spectra were filtered with 5 point quadratic Savitsky-Golay algorithm. Curve fitting was performed by Rodney Smith using *XPSPeak 4.1* software. All spectra were calibrated to 284.5 eV for the main C1s peak. To fit the data the full-width at half-mass was restricted to certain values, dependant on the element being examined. Peaks in the C 1s region were restricted to 1.2 eV, those in the N 1s region were restricted to 1.4 eV, and those in the O 1s region were restricted to 1.6 eV.

UV-visible-near infrared spectroscopy (UV-vis) was performed with a Varian Cary 6000i UV-Vis-NIR spectrophotometer. Solutions were examined in quartz cuvettes with a 1 cm path length. The dual-beam spectrophotometer used a cuvette containing the appropriate solvent for background correction.

Nuclear magnetic resonance spectroscopy (NMR) was performed using three different instruments. A Bruker Avance III was used for 300 MHz acquisitions, a Bruker Avance 500 was used for 500 MHz acquisitions, and a Bruker Avance 600 was used for 600 MHz acquisitions. Spectra were analyzed using the *MestRe Nova* software package.

Fourier-Transform infrared spectroscopy (FTIR) was performed on a Bruker

Alpha-T spectrophotometer. An attenuated total reflectance stand (ATR) with a diamond lens was employed. Background scans were performed with the ATR stand empty. Data was analyzed using the *OPUS 6.5* software package.

Infrared spectra were predicted using *Gaussian '09*. The appropriate polymer fragment was optimized using the B3LYP density functional method and the 3-21G basis set. Frequency calculations were then performed, and the data plotted using *GaussView 5.0*. Frequencies were scaled by a factor of 0.965 [98].

Thermogravimetric analysis (TGA) was performed using a TA Instruments Q500. The dynamic, high resolution scan option was used. With this option, the instrument automatically varied scan rate between 1 and 50 °C min^{-1} dependant on the rate of mass loss. Thermal scans were performed under an air atmosphere. Data was analyzed using TA Instruments' *Universal Analysis* software package.

X-ray fluorescence spectroscopy (XRF) was performed using a PANalytical MiniPal4. Data was analyzed using the MiniPal4 software package.

Elemental analyses (EA) were performed by Canadian Microanalytical Services Ltd., 207-8116 Alexander Road, Delta, B.C., V4G 1G7. Analyses consisted of carbon, hydrogen, nitrogen and sulfur analysis. Experimental data was fitted using *Excel Solver* software [99]. Free-standing polymer data was fitted by varying the number of water molecules per monomer unit. Ruthenium modified polymer data was fitted by varying the number of water molecules and monomer units of the polymer per ruthenium complex.

Mass spectrometry (MS) was performed using an Agilent Systems 1100 series LCMSD (G1946 Quadrupole) instrument equipped with an atmospheric pressure chemical ionization source (APCI-MS) or an Applied Biosystems 4800

instrument MALDI-TOF/TOF mass spectrometer and a 355 nm laser. APCI-MS was performed using *ca.* 0.2 mM solutions in acetonitrile. A 50 μL sample injection and 20 V ionization voltage were used with a scan range up to 1000 m/z. MALDI-ToF samples were prepared by mixing 1 mL of a solution of the sample (1 mg mL^{-1}) with 5 mL of a matrix solution. The matrix solution was prepared by dissolution of 10 mg dihydroxybenzoic acid (DHBA) in 1 mL acetonitrile. A 1μL aliquot was spotted on the MALDI sample plate.

2.2 Chemicals

Vulcan XC72 was obtained from Cabot Corporation. The carbon powder was ground to a fine powder using a mortar and pestle before use. Unmodified Toray TGPH-090 carbon fiber paper was used.

Chemicals used include: hypophosphorous acid (J. T. Baker Chemicals), *ortho*-phosphoric acid (85%, Anachemia), 1-aminoanthraquinone (Sigma-Aldrich), phosphorous pentoxide (EMD Chemicals), Fast Red AL (Acros), Azure A (Sigma-Aldrich), sodium nitrite (Fisher Scientific), anthraquinone (Sigma-Aldrich), 1,2-diaminoanthraquinone (Sigma-Aldrich), 3,3'-diaminobenzidine (Sigma-Aldrich), 2,5-pyridinedicarboxylic acid (Sigma-Aldrich), picolinic acid (Sigma-Aldrich), aminothiophenol (Sigma-Aldrich), 2,2'-bipyridine-4,4'-dicarboxylic acid (Sigma-Aldrich), formic acid (90%, J. T. Baker Chemicals), formaldehyde solution (36.5–30.0%, Anachemica), 1,2-phenylenediamine (Sigma-Aldrich) and anthraquinone-2-carboxylic acid (Sigma-Aldrich). Ruthenium(III) chloride ($RuCl_3$) was obtained from Precious Metals Online, P.O. Box 8053, Monash University LPO, Melbourne, VIC 3168, Australia. 5,6-Diaminophenanthroline was obtained from Prof. Brian MacLean (St. Francis Xavier University).

Industrial grade nitrogen from Air Liquide was used. Bone-dry grade CO_2 was used for electrocatalysis experiments (Air Liquide).

Polyphosphoric acid (PPA) was freshly prepared before each use. For preparation of PPA, P_2O_5 (*ca.* 19 g) and H_3PO_4 (*ca.* 10 g) were combined under an N_2 atmosphere. The mixture was then mechanically stirred overnight at 110 °C. Due to the viscosity of PPA, all reactions involving PPA required mechanical stirring.

2-(2-Pyridyl)benzothiazole (pbt) was synthesized using a previously published route [100]. Picolinic acid (1.09 g, 8.9 mmol) and aminothiophenol (1.24 g, 9.9 mmol) were added to *ca.* 30 g of PPA. The mixture was mechanically stirred at 110 °C for 22 h, 140 °C for 17 h, and 180 °C for 25 h. The mixture was then stirred in 900 mL of water. The mixture was filtered to remove a grey solid from a pale yellow solution. The grey solid was suspended in hot methanol. Filtration of the hot mixture yielded a pink-orange solution. Evaporation of the methanol produced 1.232 g of a yellow solid. ^1H NMR confirmed the yellow solid to be pbt. Neutralization of the aqueous solution by addition of NaOH resulted in precipitation of 0.110 g of a yellow solid. The solid was confirmed to be pbt. ^1H NMR (500 MHz, CDCl$_3$), δ /ppm. 8.72 (d, J = 4.8 Hz,1 H), 8.41 (d, J = 7.9 Hz, 1 H), 8.12 (d, J = 8.2 Hz, 1 H), 7.99 (d, J = 8.0 Hz, 1 H), 7.88 (t, J = 7.6 Hz, 1 H), 7.54 (t, J = 7.7 Hz, 1H), 7.40-7.47 (m, 2 H).

Cis-bis(2,2'-bipyridine) dichlororuthenium(II) (Ru(bpy)$_2$Cl$_2$) was prepared as follows. A 50 mL portion of dimethylformamide (DMF) was purged with N_2 for 10 min. A solution of RuCl$_3$ (1.75 g, 6.7 mmol), 2,2'-bipyridine (2.5 g, 16 mmol) and LiCl (2.2 g, 51 mmol) in DMF was refluxed for overnight. The solution volume was reduced to *ca.* 10 mL under reduced pressure. Acetone (200 mL) was added to the flask, which was then refrigerated overnight. A dark

precipitate was collected by vacuum filtration and rinsed with H_2O until the eluent ran clear. The dark solid was then redissolved in 150 mL of refluxing 50% EtOH. Lithium chloride (11.4 g) was added slowly, with stirring. The solution volume was reduced to *ca.* 50 mL under reduced pressure and refrigerated overnight. The dark precipitate was once again collected by vacuum filtration and washed with H_2O. After vacuum drying, a total of 2.07 g (4.3 mmol, 64% yield) of product was obtained. Purity of the sample was verified by cyclic voltammetry ($E^{1/2}$ = +0.37 V *vs.* SCE in CH_3CN containing 0.1 M NEt_4BF_4, Pt electrode). APCI-MS on a CH_3CN solution of the product yielded an envelope of peaks, with an *m/z* centered at 489.9. The isotopic pattern of this set of peaks matched that expected for $[Ru(bpy)_2(CH_3CN)(Cl)]^+$, which has an expected *m/z* of 489.9. Also present were much weaker sets of peaks with *m/z* values of 448.9 ($[Ru(bpy)_2Cl]^+$) and of 934.8 ($[(bpy)_2(Cl)Ru\text{-}Cl\text{-}Ru(bpy)_2(Cl)]^+$).

Cis-bis(2-(2-pyridyl)benzothiazole) dichlororuthenium(II) ($Ru(pbt)_2Cl_2$) was prepared based on the synthesis of $Ru(bpy)_2Cl_2$. A 30 mL portion of DMF was purged with N_2. A solution of pbt (0.48 g, 2.3 mmol), $RuCl_3$ (0.30 g, 1.1 mmol) and LiCl (0.40 g, 9.4 mmol) was refluxed overnight. The volume of the blue solution was reduced to *ca.* 5 mL under reduced pressure. A 40 mL portion of acetone was added to the flask, which was then refrigerated overnight. The dark solid was collected by vacuum filtration. The product was then washed with acetone (*ca.* 100 mL) and H_2O. This procedure yielded 0.25 g (0.41 mmol, 35% yield) of product. Cyclic voltammetry (Pt electrode, 0.1 M NEt_4BF_4 in CH_3CN) on the product revealed a reversible process with an $E_{1/2}$ value of 0.43 V vs. SCE and an irreversible oxidation with a peak potential of 1.10 V vs. SCE. The 0.43 V peaks are attributed to the Ru(III)/Ru(II) redox process. The irreversible 1.10 V peak is believed to be oxidation of pbt ligands. APCI-MS on a CH_3CN

solution of the product yielded an envelope of peaks with an m/z centered at 601.9. The isotopic pattern matches that expected for $[Ru(pbt)_2(CH_3CN)(Cl)]^+$ (predicted m/z = 601.98).

Synthesis of $[Ru(bpy)_2(phenNH_2)](PF_6)_2$ was performed as follows. A solution of $Ru(bpy)_2Cl_2$ (0.402 g, 0.83 mmol) and 5-amino-1,10-phenanthroline (NH_2phen, 0.221 g, 1.1 mmol) in 40 mL of 75% EtOH was made. The red-purple solution was purged with N_2, then refluxed under N_2 atmosphere overnight. Over this period the solution changed to a yellow-orange color. The solution was removed under reduced pressure, leaving an orange residue. The residue was dissolved in H_2O and a solution of 0.99 g (5.3 mmol) of KPF_6 in H_2O was added. The orange precipitate was collected by vacuum filtration. After drying under vacuum, a total of 617 mg was collected (0.66 mmol, 83% yield). Cyclic voltammetry (Pt electrode, 0.1 M NEt_4BF_4 in CH_3CN) revealed a quasi-reversible redox process with an approximate $E_{1/2}$ of 1.32 V vs. SCE. The anodic peak possessed a shoulder on the low potential side, due to irreversible oxidation of the pbt ligands. MALDI-ToF MS yielded three large peak envelopes (> 30% relative intensity) and two small peak envelopes (<15% relative intensity). The m/z of the large envelopes were centered at 567.0 ($[Ru(bpy)_2(DHBA)]^+$), 606.0 ($[Ru(bpy)(NH_2phen)(DHBA)]^+$) and 754.0 ($[Ru(bpy)_2(NH_2phen)](PF_6)^+$). The m/z of the small peak envelopes were centered at 625.1 and 924.1. The identity of these peaks is unknown.

All other chemicals used were ACS grade or better and used without purification, unless otherwise stated.

2.3 Techniques

In this work, the surface coverage (Γ) of electroactive species on the carbon surface was used to compare various modification attempts. Two methods were employed and compared to each other for estimation of surface coverage values. Both methods relied on cyclic voltammetry to quantify the electroactive species, but employed different methods for determination of the amount of Vulcan XC72.

The amount of an electroactive species present on an electrode can be determined through integration of its voltammetric peak. Equation 2.3.1 yields the moles of the species present (N), where Q is the charge under the voltammetric peak, n is the number of electrons in the process and F is Faraday's constant. Determination of the area under voltammetric curves was achieved using *EC-Lab V9.40* software with subtraction of the background charging current.

$$N = \frac{Q}{nF} \tag{2.3.1}$$

In Method 1, the amount of Vulcan XC72 present on the electrode surface was estimated through comparison of the observed capacitance (C) with literature values for the specific capacitance of Vulcan XC72 (C_s). Incorporation of literature values for specific surface area (S_s) can be used to convert the mass of Vulcan XC72 into surface area (SA), as shown in equation 2.3.2. For anthraquinone modified carbons, the observed capacitance was estimated from the cyclic voltammogram at +0.1 V vs. SCE. The values used for C_s and S_s were 12.6 F g^{-1} and 131 m^2 g^{-1}, respectively [101].

$$SA = \frac{CS_s}{C_s} \tag{2.3.2}$$

Combination of the above two equations yields equation 2.3.3, which produces an estimated surface coverage of the electroactive species in mol cm^{-2}.

$$\Gamma = \frac{QC_s}{nFS_sC} \tag{2.3.3}$$

The major benefit of this method is fast data acquisition. However, the accuracy is highly dependant on the values of C_s and S_s. Significant variation in these values is observed in the literature. For example, S_s varies from 131 m^2 g^{-1} [101] to 223 m^2 g^{-1}[71] for unmodified Vulcan XC72. Due to the possibility of a significant error, Γ values were determined with an alternate method for comparison.

In Method 2, the mass of modified carbon powder deposited on the electrode surface was measured directly. The same procedure for electrode preparation was followed, but electrodes were allowed to air dry overnight to ensure complete solvent evaporation. The mass of carbon powder on each electrode was taken as the difference in mass of the electrode before and after deposition of the carbon powder. Similar to the first method, integration of the oxidation peak allowed determination of the moles of electroactive species present. Surface coverages calculated using this method are reported as moles of electroactive species per gram of modified carbon powder. While perhaps not as descriptive a unit as mol cm^{-2}, this approach has the benefit of eliminating error due to uncertainty in C_s and S_s. Division of the mol g^{-1} value by S_s (cm^2 g^{-1}) can be used to draw a comparison between the two methods. The overall process required for this is represented in equation 2.3.4, where m is the mass of modified

powder on the electrode.

$$\Gamma = \frac{Q}{nFmS_s} \qquad (2.3.4)$$

Immobilization of 9,10-Anthraquinone on Vulcan XC72 Through Spontaneous Diazonium Reaction

3.1 Introduction

Parts of this chapter have been published in a peer-reviewed journal [102].

Modification of carbonaceous materials has been an active area of research in recent years. Perhaps one of the most significant discoveries has been the reaction of aryl diazonium ions with carbon surfaces, resulting in the immobilization of aryl groups [59, 64]. Due to difficulty in proving covalent C-C bonding on carbon-based surfaces, most research in the past two decades has focussed on providing indirect evidence of covalent attachment of the organic molecules to the carbon surfaces. With the growing body of information suggesting a covalent bond, researchers have begun moving away from basic research on these systems and towards applied research.

At the commencement of this project, application-based research remained focussed on immobilization of organic molecules for various purposes, such as immobilization of organic compounds for the controlled release of chemicals [103]. The diazonium technique had not been utilized to immobilize transition-metal complexes. As such, immobilization of pyridine-based molecules through the reaction of their diazonium ions was identified as an attractive approach to immobilize metal complexes on carbon surfaces.

Two distinct techniques have been developed to react aryl diazonium ions with conducting surfaces; electrochemically induced reactions [59] and spontaneous chemical reactions [64]. The spontaneous chemical reaction path was chosen for this project for several reasons:

i. Use of electrochemically induced reactions has focussed primarily on flat carbon surfaces such as glassy carbon.

ii. Spontaneous reactions between dissolved diazonium ions and carbon surfaces would be much easier to scale-up than the electrochemically induced reactions.

iii. Electrochemically induced reactions have been shown to produce multilayered films of organic molecules on carbon surfaces [71, 73, 77], with a portion being electrochemically inactive [73].

iv. The spontaneous reaction has been shown to produce sub-monolayers on high surface area carbons [71].

Due to its capability of rapidly providing qualitative and quantitative information, cyclic voltammetry was employed as the primary technique for examination of the modified carbon powders. Cyclic voltammetry is frequently employed in studies on carbon surfaces modified via spontaneous or electrochemically driven diazonium reactions. It has been used as both a qualitative and quantitative tool. Qualitatively, it has been most widely used to confirm the presence of various electroactive species on electrode surfaces such as glassy carbon (GC) [59, 67–69, 71], highly-oriented pyrolytic graphite (HOPG) [69, 75], basal-plane pyrolytic graphite (BPPG) [103] and graphite powder [88, 103]. It has also been used in conjunction with solution-phase redox couples such as $[Fe(CN)_6]^{3-/4-}$ [68, 75] and $[Ru(NH_3)_6]^{3+/2+}$ [68, 70, 82] to study charge transfer blocking effects. Such studies have been used to indirectly confirm the presence of non-electroactive species such as N,N-diethylaniline immobilized on a carbon surface [68, 75], as well as provide mechanistic information pertaining to the diazonium reaction [68, 75]. Quantitative studies utilizing cyclic voltammetry have been employed in carbon modification studies, but primarily for flat carbon surfaces such GC [59, 67, 69, 104] and HOPG [69].

Compton and coworkers have used cyclic voltammetry to quantify the surface coverage of nitrobenzene and anthraquinone on glassy carbon powder and synthetic graphite powder [88]. In their study, the low surface area carbon powders were modified using the spontaneous diazonium reaction. The modified powders were then abrasively immobilized on HOPG electrodes by gently rubbing the HOPG electrode on a filter paper containing the modified powder. The amounts of anthraquinone or nitrobenzene were determined through integration of the voltammograms, but no mention was made on determination of the surface area of the carbon powder.

The goals of this research were to explore the ability of cyclic voltammetry to be used as a quantitative tool for modified carbon powders, and to test whether cyclic voltammetry could reveal new information regarding the reaction between carbon powders and diazonium ions. The approach used was based on a recent publication that studied the immobilization of 4-nitrobenzene on high surface area carbon materials [71]. This study by Toupin and Belanger utilized elemental analysis and XPS to determine the amount of nitrogen present in the modified materials. As carbon blacks possess a negligible amount of nitrogen functionality, the amount of nitrobenzene present corresponds directly to the amount of nitrogen found. By performing a similar study, quantification using cyclic voltammetry can be compared to an independent quantification technique. A simple organic molecule, 9,10-anthraquinone (herein referred to as anthraquinone), was chosen for immobilization on Vulcan XC72 using the spontaneous diazonium reaction. Anthraquinone was chosen for use in the study due to its excellent electrochemical behavior and its commercial availability as a diazonium salt (Fast Red AL salt). Under aqueous conditions anthraquinone exhibits a stable, reversible two electron reduction to the corresponding diol (see

Scheme 3.3). Various pretreatment processes were used here, based on those of Belanger and Toupin [71], and are depicted in Scheme 3.1. Also studied were the effect of several acids, reaction time, the effect of sequential exposure to diazonium ions and the role of physisorption versus chemisorption.
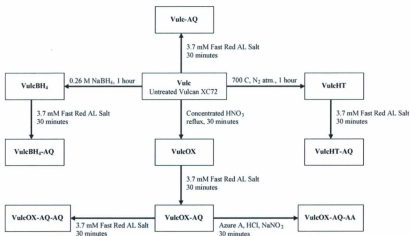
Scheme 3.1: Reaction pathway design for the anthraquinone diazonium study.

3.2 Results and Discussion

3.2.1 The Effect of Carbon Surface Pretreatments

Following the strategies of Belanger and Toupin [71], samples of Vulcan XC72 were either chemically oxidized by refluxing in concentrated HNO_3 (VulcOX) or treated by heating at 700 °C under an inert atmosphere (VulcHT). These treatments result in an increase and decrease, respectively, of oxygen functionality on the carbon surface, primarily in the form of carboxylic acid groups [71]. The carboxylic acid groups on the surface can be envisioned to play several roles

59

in the modification process. Their presence may have a harmful effect through constriction [71], where less of the carbon surface area would be accessible for reaction with the diazonium ions. This would result in a surface coverage lower than a theoretical monolayer. However, their presence may also aid in driving the reaction to completion [71]. For the reaction to proceed the diazonium ion must lose $N_2(g)$, leaving a positive charge on the incoming species or the modified carbon surface. It is conceivable that as the reaction proceeds, positive charge builds up on the extensively conjugated carbon support. Such a buildup of charge would decrease the ability of the carbon material to further react with the incoming positive diazonium ions. Based on XPS results, the presence of carboxylic acid groups on the surface has been suggested to provide a reaction pathway for the release of positive charge [71]. In the mechanism proposed by Toupin and Belanger, illustrated in Scheme 3.2, covalent binding of the incoming species induces decarboxylation of the surface acid groups, yielding CO_2 and releasing the positive charge as H^+.
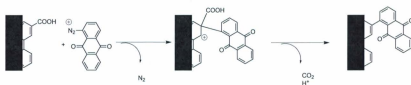
Scheme 3.2: Decarboxylation mechanism proposed by Belanger and Toupin. Reaction scheme adapted to the anthraquinone diazonium reaction employed here.

An additional pretreatment was also tried; suspension of the carbon powder in an aqueous solution of a chemical reducing agent, $NaBH_4$ (VulcBH$_4$). The purpose of this pretreatment was to provide a secondary probe of whether a buildup of positive charge could be responsible for lower than expected surface coverages.

All diazonium coupling reactions in this section were performed using 5% HCl in an ice bath, as described in Section 3.4.4. Following the grafting procedure, the modified carbon powder yielded the voltammogram seen in Figure 3.1. Two reversible electrochemical processes can be seen in the first scan of the voltammogram (solid line): the minor process, peaks (i) and (ii), showed an $E_{1/2}$ of 0.29 V vs. SCE while the major process, peaks (iii) and (iv), exhibits an $E_{1/2}$ of -0.14 V. When cycled between 0 and +0.6 V peaks (i) and (ii) were found to be stable and reversible (not shown). However, when the cathodic window was extended to -0.4 V, these peaks were completely eliminated (dashed line in Figure 3.1). This behavior suggests that the species responsible for the minor process is eliminated upon reduction of the anthraquinone moiety. Peaks (i) and (ii) are believed to be due to a two electron, two proton conversion between a hydrazo- and an azo- linkage, depicted in Scheme 3.3.

A literature search did not reveal any electrochemical evidence of an azo-linkage being formed during the spontaneous diazonium reaction. However, the existence of an azo- linkage has been observed between several different aromatic species and various carbonaceous substrates using non-electrochemical techniques. These techniques, including XPS [78, 105], SIMS-TOF [79, 80] and IR spectroscopy [80], have provided evidence of an azo- linkage being formed. For the electrochemically induced reaction, the azo- linkage was also observed using XPS [72], IR spectroscopy and SIMS-TOF [80]. The Downard group, which commonly uses the electrochemically induced form of the reaction, has reported evidence that immobilization of nitrobenzene on pyrolyzed photoresist films results in azo- linkages [72]. A detailed study of the modification of pyrolyzed photoresist films with 4-nitroazobenzene was reported by the Downard group [73]. In their study, the azo- linkages of 4-nitroazobenzene were
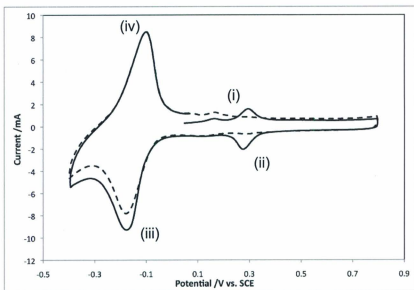
Figure 3.1: Cyclic voltammogram obtained from Vulcan XC72 that was modified by suspension in a solution of Fast Red AL salt for 1 h. The initial cycle (solid) and steady state obtained for subsequent cycles (dashed) are displayed. Performed in 1.0 M H_2SO_4 at 100 mV s^{-1}, with the modified carbon deposited on a carbon fiber paper electrode.
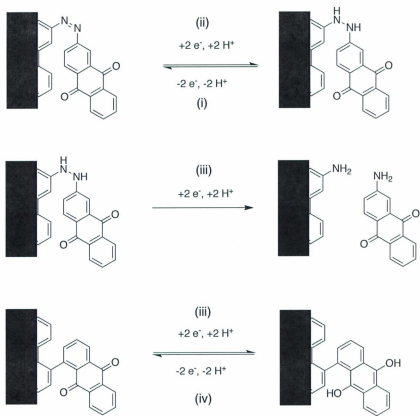
Scheme 3.3: Assignment of electrochemical processes observed in Figure 3.1

found to be electrochemically active when in solution, but films immobilized on the carbon surface were found to be electrochemically inactive. The suggested explanation for this observation was inhibition of electrolyte diffusion due to the compact nature of the films produced by the electrochemically induced form of the reaction. The materials modified during this thesis work appear to result in much less compact, sub-monolayer structures. Therefore restricted electrolyte diffusion is unlikely to be an issue.

Assignments for the electrochemical peaks observed in Figure 3.1 are depicted in Scheme 3.3. Support of the assignment of the minor electrochemical process to an azo- linkage comes from research on the immobilization of azo-containing organic molecules [103]. Upon immobilization of 2,5-dimethoxy-4-[4-(nitrophenyl) azo]benzene on graphite powder using the spontaneous diazonium reaction it was observed that the azo- linkage undergoes a reversible two electron reduction to a hydrazo- bridge at approximately -0.1 V vs. SCE. Under acidic conditions (pH = 1) this hydrazo- bridge was found to be reductively cleaved during a second two electron reduction between -0.3 and -0.4 V, resulting in two amines.

XPS was performed on untreated Vulcan XC72, Vulcan XC72 modified using the spontaneous diazonium coupling, and a Vulcan XC72 with 1-amino-9,10-anthraquinone adsorbed to the surface (4.4.2). Curve-fitting of the spectra was performed as described in Chapter 2. The curve-fitted XPS spectra are included in Appendix A; the peaks observed are listed in Table 3.1. The O 1s core-level spectrum for untreated Vulcan XC72 was fitted with two peaks, 533.1 eV and 533.0 eV. These peaks are similar to those observed by Toupin and Belanger for unmodified Vulcan XC72 [71]. The peaks were attributed to C-O and C=O functionality, respectively, on the carbon surface by Toupin and Belanger, and are

similarly assigned here. The sample modified using the diazonium coupling was fitted with the same two peaks, as well as a much larger peak with a binding energy of 531.6 eV. The location of O 1s peak growth is similar to that observed upon modification of glassy carbon with anthraquinone [104, 106], and is therefore attributed to the carbonyl groups of anthraquinone. Anthraquinone adsorbed on the surface similarly revealed three emission peaks, attributed to C-O surface functionality (531.1 eV), C=O surface functionality (533.0 eV) and the oxygen of anthraquinone (531.5 eV).

Table 3.1: Peak locations and peak areas obtained by curve-fitting N 1s and O 1s core-level spectra of untreated Vulcan XC72 and Vulcan XC72 that was modified by suspension in an acidic aqueous solution of Fast Red AL salt for 1 h.

Sample	Binding Energy (eV)[a]			
	N 1s	O 1s		
Unmodified	none	531.1 (178)		533.0 (213)
AQ modified	400.3 (206)	531.1 (874)	531.6 (1915)	533.0 (871)
AAQ adsorbed	399.1 (287)	531.1 (696)	531.5 (714)	533.0 (618)

[a] peak areas are given in brackets (counts per second)

The N 1s core-level spectrum for untreated Vulcan XC72 revealed no peaks, adsorbed 1-aminoanthraquinone showed a single peak at 399.1 eV, and the anthraquinone diazonium modified sample showed a single peak at 400.3 eV. The presence of a peak at this location has often been observed following modification of various surfaces using the diazonium reaction. Several studies regarding the nature of this peak have been performed recently [72, 78, 105]. Using three separate approaches, the three research groups have convincingly attributed the presence of this peak to indicate that an azo- linkage forms. This provides further support to the assignment of the minor electrochemical process observed in Figure 3.1 to an azo- linkage.

Qualitatively, the behavior observed for VulcHT (Figure 3.2) and VulcBH$_4$ (Figure 3.3) following modification with anthraquinone under identical conditions was comparable to that for untreated Vulcan XC72. The voltammogram for VulcOX (Figure 3.4) modified under the same conditions contains increased current between 0 V and +0.5 V vs. SCE due to an increase in oxygen functionality on the surface. The location of this increased background current complicates identification of an azo- linkage in this sample. However, judging by the lack of current decrease following the first cycle, it appears as though the peaks attributed to an azo- linkage were not present.

The surface coverage of anthraquinone was estimated using both quantification methods presented in Section 2.3. Results are presented in Table 3.2. Measurements were made for each sample using four separate electrodes, error values given are standard deviations between the four electrodes. Method 1 used the literature value for specific capacitance (C_s) to estimate the amount of Vulcan XC72 present and Method 2 used the known mass. A value of 131 m^2 g^{-1} was used to convert Method 2 values from mol g^{-1} to mol cm^{-2} [101].

Table 3.2: Comparison of anthraquinone surface coverages for carbon powders modified by suspension in an acidic aqueous solution of Fast Red AL salt for 1 h.

| | Γ_{AQ} [a, b] | | |
| | Method 1 | Method 2 | |
Carbon Support	(x 10^{-11} mol cm^{-2})	(x10^{-5} mol g^{-1})	(x10^{-11} mol cm^{-2})
Vulc	3.7 ± 0.1	8.7 ± 1.5	6.6 ± 1.1
Vulc [c]	-	0.81 ± 0.07	0.62 ± 0.05
VulcOX	2.2 ± 0.1	8.6 ± 0.3	6.5 ± 0.2
VulcHT	2.6 ± 0.2	5.5 ± 0.3	4.1 ± 0.2
VulcBH$_4$	5.8 ± 0.3	10.3 ± 1.4	7.9 ± 1.1

[a] Surface area of Vulcan XC72 taken to be 131 m^2 g^{-1}
[b] standard deviation based on four separate electrodes
[c] Calculated for azo- linkage, peak (i) in Figure 3.1
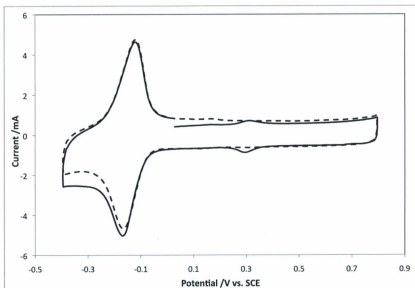
Figure 3.2: Cyclic voltammogram obtained from heat treated Vulcan XC72 (VulcHT) that was modified by suspension of the treated carbon in an acidic aqueous solution of Fast Red AL salt for 1 h. The initial (solid) and second cycle (dashed) are displayed. Performed in 1.0 M H_2SO_4 at 100 mV s^{-1}, with the modified carbon deposited on a carbon fiber paper electrode.
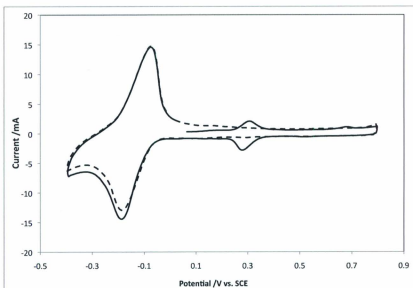
Figure 3.3: Cyclic voltammogram obtained from NaBH$_4$(aq) treated Vulcan XC72 (VulcBH$_4$) that was modified by suspension of the treated carbon in an acidic aqueous solution of Fast Red AL salt for 1 h. The initial (solid) and second cycle (dashed) are displayed. Performed in 1.0 M H$_2$SO$_4$ at 100 mV s^{-1}, with the modified carbon deposited on a carbon fiber paper electrode.
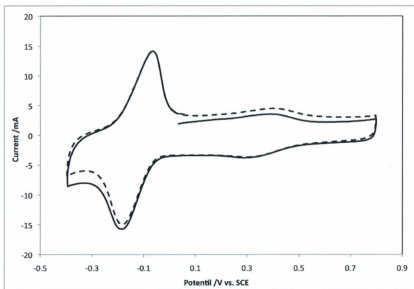
Figure 3.4: Cyclic voltammogram obtained from chemically oxidized Vulcan XC72 (VulcOX) that was modified by suspension of the treated carbon in an acidic aqueous solution of Fast Red AL salt for 1 h. The initial (solid) and second cycle (dashed) are displayed. Performed in 1.0 M H_2SO_4 at 100 mV s^{-1}, with the modified carbon deposited on a carbon fiber paper electrode.

As can be seen, quantification using Method 2 indicates a significantly higher surface coverage in all four cases. The most extreme discrepancy is that for Vulcan XC72 which was chemically oxidized by HNO_3, in which Method 1 suggests a coverage that is one-third of that indicated by Method 2. Considering that S_s was held constant between methods, the values used for C_s in Method 1 must be wrong. To verify this, values for C_s were estimated for each of the Vulcan XC72 samples, both before and after modification with anthraquinone. C_s values were estimated using equation 3.2.1 in conjuction with cyclic voltammograms from electrodes prepared with a known mass of modified carbon. Where i_{cc} is the charging current at +0.1 V vs. SCE (A), v is the scan rate (V s^{-1}) and m is the mass of carbon powder on the electrode (g). The results are presented in Table 3.3.

$$C_s = \frac{i_{cc}}{vm} \qquad (3.2.1)$$

Table 3.3: Experimentally obtained C_s values for carbon powders modified by suspension in an acidic aqueous solution of Fast Red AL salt for 1 h. Measurements taken at 0.1 V vs. SCE at a scan rate of 100 mV s^{-1}.

Carbon Support	C_s (F g^{-1})	
	Before Modification	After Modification
Vulc	10.6 ± 2.4	25.8 ± 3.2
VulcOX	41.4 ± 1.7	38.8 ± 1.3
VulcHT	18.9 ± 1.7	21.8 ± 1.4
VulcBH$_4$	18.3 ± 1.2	18.2 ± 2.3

The experimentally obtained value for untreated Vulcan XC72 was in agreement with the literature value used in Method 1 [101]. However, upon immobilization of anthraquinone the value was found to double to 25.8 F g^{-1}. As a result, Method 1 overestimates the amount of carbon present, resulting in a Γ_{AQ} value that is half of the true value. It was also found that C_s varies signif-

icantly between the different pretreated samples, with the chemically oxidized Vulcan XC72 yielding a C_s four times larger than for the untreated sample. Interestingly, it was observed that for all but the untreated Vulcan XC72, C_s was found to be unchanged upon immobilization of anthraquinone. Although more accurate, Method 2 is expected to slightly underestimate surface coverages. The mass of modified powder includes not only Vulcan XC72 present, but also the anthraquinone groups bound to the surface. The amount of Vulcan XC72 will therefore be slightly overestimated using this technique. However, an anthraquinone surface coverage of 1.0×10^{-4} mol g^{-1} translates into 21 mg of anthraquinone per gram of modified material. This equates to approximately a 2% error in mass.

Considering these results it is advisable that for quantification purposes on high surface area carbons the amount of carbon present be determined by mass. This allows representation of Γ in terms of mol g^{-1}, units that eliminate uncertainty due to variability in S_g and C_s. The value can be readily converted to mol cm^{-2} for comparison to other literature techniques (equation 2.3.4).

Quantification of the minor voltammetric peak at 0.29 V vs. SCE, assigned earlier to an azo- linkage between anthraquinone and the carbon surface, reveals that approximately 8% of the immobilized material was bound by an azo-linkage rather than a carbon-carbon bond. A similar value, 10.6%, is obtained through a quantitive comparison of the peak areas of the N 1s peak attributed to an azo- linkage and the O 1s peak attributed to the anthraquinone carbonyl groups (Table 3.1). This value is much lower than that observed by the Downard group [72]; however a meaningful comparison is difficult to draw due to the differences in techniques, diazonium ions used and substrates being modified.

The highest surface coverage obtained for anthraquinone was obtained by using the untreated Vulcan XC72, which yielded a coverage of 1.0×10^{-4} mol g^{-1}. If one assumes an accessible surface area equivalent to that for nitrobenzene modified Vulcan XC72 [71], this translates to 8.3×10^{-11} mol cm^{-2}. Taking a specific surface area of 131 m^2 g^{-1} for Vulcan XC72, this value is approximately 22% of the theoretical close-packed monolayer coverage for anthraquinone. However, taking a specific surface area of 223 m^2 g^{-1}, approximately 13% of a monolayer is calculated. The variation in specific surface area measurements of Vulcan XC72 in the literature makes it difficult to assign relative error upon converting surface coverage units to mol cm^{-2}.

3.2.2 The Effect of Acids and Reaction Time

Variation of acids in the reaction mixture was explored as an attempt to increase the surface coverage beyond the maximum observed value of 1.0×10^{-4} mol g^{-1}. Diazonium ions are reactive species susceptible to attack by nucleophiles such as hydroxide [107]. To probe whether rapid decomposition of the diazonium ion results in a lower than expected surface coverages, the reaction solution was acidified by addition of hydrochloric acid. Addition of hypophosphorous acid (H_3PO_2) was also attempted, as it has been suggested [74] and studied [71, 88] as a chemical reducing agent for driving the reaction.

As can be seen in Table 3.4, it seems that addition of acid slightly decreased surface coverages. This indicates that aqueous decomposition of the diazonium ions is likely not a significant problem. Cyclic voltammetry on Vulcan XC72 modified in the presence of HCl (Figure 3.5) yielded voltammograms identical in structure to those modified without added acid. However, voltammograms
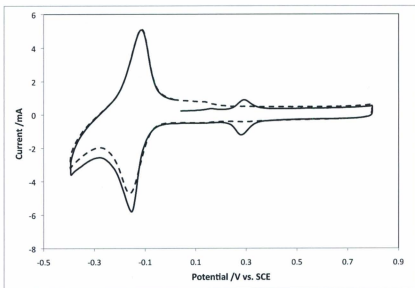
Figure 3.5: Cyclic voltammogram obtained from Vulcan XC72 modified with anthraquinone in the presence of HCl. First cycle (solid line) and steady state observed for subsequent cycles (dashed line) portrayed. Performed in 1.0 M H_2SO_4 at 100 mV s^{-1} with modified carbon adsorbed to a carbon fiber paper electrode.
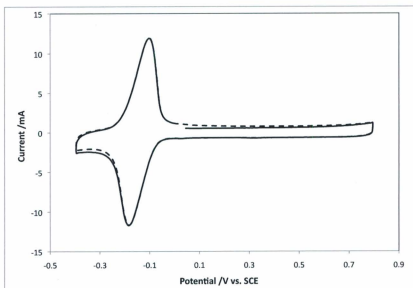
Figure 3.6: Cyclic voltammogram obtained from Vulcan XC72 modified with anthraquinone in the presence of H_3PO_2. First cycle (solid line) and steady state observed for subsequent cycles (dashed line) portrayed. Performed in 1.0 M H_2SO_4 at 100 mV s^{-1} with modified carbon adsorbed to a carbon fiber paper electrode

for samples modified in the presence of H_3PO_2 (Figure 3.6) lacked the set of peaks with $E_{1/2}$ of 0.29 V. This indicates that no azo- linkages were formed between anthraquinone and the carbon surface. To achieve a total elimination of azo- linkages the diazonium ions must be reduced by H_3PO_2 much more rapidly than the carbon surface can reduce them, lending some weight to the argument for using H_3PO_2.

Table 3.4: Anthraquinone surface coverages for untreated Vulcan XC72 modified by suspension of the untreated carbon powder in an aqueous solution of Fast Red AL salt, containing no acid, hydrochloric acid, or hypophosphorous acid, for 1 h.

	Γ_{AQ}	
Acid Used	x 10^{-5} mol g^{-1}	x 10^{-11} mol cm^{-2} [a]
none	10.2 ± 0.1	7.6 ± 0.6
HCl	8.7 ± 1.5	6.7 ± 1.1
H_3PO_2	8.5 ± 1.0	6.5 ± 0.7

[a] calculated assuming S_s = 131 m^2 g^{-1}

To test the effects of reaction time, the reaction was carried out for 10, 30 and 60 min. Reactions were performed in an ice bath with no acid added. The surface coverages obtained are shown in Figure 3.7, with error bars representing the standard deviation between four separate electrodes. No surface coverage variation was observed throughout the reaction times attempted, suggesting that the reaction proceeds to completion within 10 minutes. These results can be compared to those of a study performed using the spontaneous diazonium reaction to modify glassy carbon electrodes [65]. In their study, Adenier *et al.* found that the surface coverage of nitrobenzene grafted to glassy carbon nearly tripled, from 2.0 x 10^{-9} mol cm^{-2} after one minute to 5.8 x 10^{-9} mol cm^{-2} after 60 minutes of reaction time. The surface coverage was observed to double between six minutes and 60 minutes of reaction time, from 2.8 x 10^{-9} to 5.8 x 10^{-9} mol cm^{-2}. However, a meaningful comparison between results is difficult due
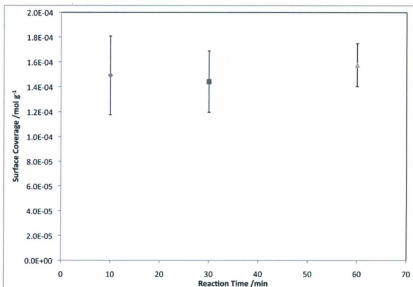
Figure 3.7: Anthraquinone surface coverage upon variation of reaction time for Vulcan XC72 exposed to a neutral solution of Fast Red AL in an ice bath for the given time. Error bars represent the standard deviation between four electrodes.

to differences in substrate and diazonium reagent.

3.2.3 The Role of Physisorption

Variation of reaction temperature, surface pretreatments, reaction time, solution pH and incorporation of a chemical reducing agent all resulted in insignificant changes in the surface coverages of anthraquinone obtained by the spontaneous coupling of Fast Red AL salt with Vulcan XC72. The maximum attainable surface coverage appears to be *ca.* 1.5×10^{-4} mol g^{-1}, obtained for the untreated carbon. This coverage translates to approximately 13% of a monolayer if one assumes 223 m^2 g^{-1} [71], or 22% of a monolayer if one assumes a similar degree of constriction as is observed upon immobilization of nitrobenzene on Vulcan XC72 (121 m^2 g^{-1}) [71].

As a final attempt to increase surface coverages, a modified carbon powder sample (VulcOX-AQ) was exposed to a solution of Fast Red AL salt a second time (VulcOX-AQ-AQ). A comparison of voltammograms, normalized by background current, is given in Figure 3.9. A surprising result was observed: the surface coverage seemed to have decreased. In an attempt to develop a clearer understanding of this behavior a second electrochemically active organic molecule, Azure A (shown in Figure 3.8), was employed.
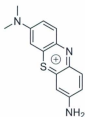
Figure 3.8: Structure of Azure A.

Azure A was chosen for several reasons:

i. Azure A exhibits reversible electrochemical activity at a potential well separated from anthraquinone

ii. Azure A possesses an aryl amine, which is necessary for synthesis of the diazonium reagent

iii. Azure A is a comparable size to anthraquinone

Reacting Azure A diazonium ions with VulcOX-AQ (VulcOX-AQ-AA) resulted in a significant decrease in the anthraquinone surface coverage (Figure 3.9). It is highly unlikely that the spontaneous diazonium reaction would result in breaking of a covalent carbon-carbon bond between the carbon surface and anthraquinone. Therefore these results suggest that a significant portion of the anthraquinone immobilized by the initial spontaneous diazonium reaction was only physisorbed to the surface. An aromatic species such as anthraquinone would be expected to exhibit significant π-π interactions with a carbonaceous material such as Vulcan XC72. It was therefore hypothesized that a significant amount of anthraquinone was strongly physisorbed rather than covalently bound.

The results of a simple experiment designed to test the physisorption hypothesis are presented in Table 3.5. Vulcan XC72 (50 mg) was suspended in 25 mL of a 5 mM solution of unsubstituted anthraquinone in acetone:MeOH (1:1). Following simple rinsing of the modified powder with MeOH, H_2O and acetone, cyclic voltammetry revealed that a significant amount of anthraquinone was present. This material was then cleaned using ultrasonication in the same solvents. The cyclic voltammetry results indicated that approximately 70 % of
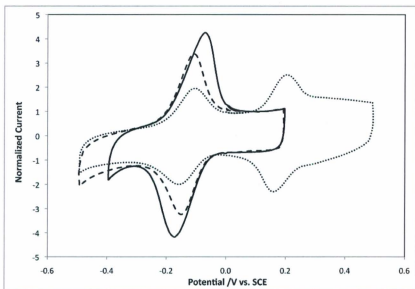
Figure 3.9: Cyclic voltammetry following sequential treatments of oxidized Vulcan XC72: VulcOX-AQ (solid line), VulcOX-AQ-AQ (dashed line) and VulcOX-AQ-AA (dotted line) are portrayed. Performed in 1.0 M H_2SO_4 at 100 mV s^{-1} with modified carbon adsorbed to a carbon fiber paper electrode. Charging currents are normalized at +0.1 V vs. SCE for comparison purposes.

the adsorbed anthraquinone was removed by these ultrasonication treatments, Table 3.5. However, a surface coverage of 3.8×10^{-5} mol g^{-1} was still observed after using these procedures. This is a significant amount of anthraquinone that remains adsorbed, especially if one considers that 1.5×10^{-4} mol g^{-1} seems to be the maximum coverage attainable by spontaneous diazonium coupling. As mentioned, strong π-π stacking interactions are believed to be responsible for this hard to remove material. It was hypothesized that an aromatic solvent should be capable of removing a greater portion of the adsorbed anthraquinone through interference with π-π stacking interactions. Following this logic, Vulcan XC72 with adsorbed anthraquinone was suspended in stirred benzene for 15 min, then air dried. Cyclic voltammetry revealed that this washing procedure resulted in near quantitative removal of adsorbed anthraquinone, as seen in Figure 3.10. It is noteworthy that the only literature report found that employed benzene (or any aromatic solvent) for washing was the original report of the electrochemically induced diazonium reaction for the modification of glassy carbon electrodes by (4-nitrophenyl)diazonium ions [59].

Table 3.5: Efficacy of adsorbed anthraquinone removal following washing procedures.

Washing Procedure	Γ_{AQ} x 10^{-5} mol g^{-1}	Removal %
Rinsed[a]	13.2 ± 0.7	(reference value)
Ultrasonicated[b]	3.8 ± 0.8	71
Benzene rinse[c]	-	> 99

[a] using each of MeOH, H$_2$O and acetone
[b] in each of MeOH, H$_2$O and acetone for 30 min
[c] soaked in stirred benzene for 15 minutes

Following these findings, samples prepared by diazonium coupling and described in Sections 3.2.1 and 3.2.2 were exposed to the benzene washing procedure. The results are summarized in Table 3.6. Multiple washes were per-
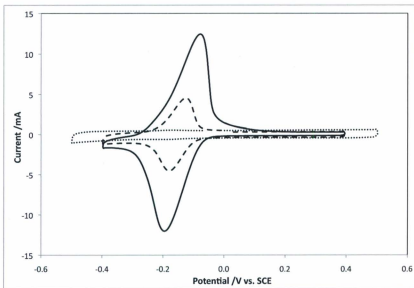
Figure 3.10: Cyclic voltammetry performed on Vulcan XC72 with unsubstituted anthraquinone adsorbed on the surface following various washing procedures. Rinsing with MeOH, acetone and H_2O (solid line), ultrasonication in MeOH (dashed line), and soaking in benzene (dotted line) were employed. Cyclic voltammetry performed in 1.0 M H_2SO_4 at 100 mV s^{-1} with modified Vulcan XC72 depostied on a carbon fiber paper electrode.

formed using clean benzene for each wash to test whether more material could be removed. In all cases, an insignificant change in surface coverage was observed beyond the first wash. Results obtained employing this washing treatment reveal a much different scenario than was observed for modified carbons that had not been washed with benzene. Pretreatments were found to play a significant role in the amount of covalently bound material, with chemically oxidized Vulcan XC72 producing the largest amount of covalently bound anthraquinone and heat treated Vulcan XC72 producing the smallest amount. Additionally, H_3PO_2 was found to play a larger role than was indicated earlier, yielding the lowest surface coverage of covalently bound anthraquinone of all samples. Washing sequentially modified samples (VulcOX-AQ-AA) with benzene was found to completely remove the Azure A, Figure 3.11, indicating that maximum covalent surface coverage of anthraquinone appears to be obtained during the initial reaction.

Table 3.6: Anthraquinone surface coverages for carbon powders described in Section 3.2.1 (Vulcan XC72 pretreatments) and Section 3.2.2 (variation of acid used) following a 15 min soak in stirred benzene.

Carbon support	Γ_{AQ} (x 10^{-5} mol g^{-1})		
or acid used	Total	Covalently bound (%)	Adsorbed (%)
Vulc (HCl)	8.7 ± 1.5	3.9 (45)	4.8 (55)
VulcOX	8.6 ± 0.3	6.6 (76)	2.1 (24)
VulcHT	5.5 ± 0.3	1.7 (31)	3.8 (69)
VulcBH$_4$	10.3 ± 1.4	3.7 (36)	6.6 (64)
no acid	10.2 ± 0.3	5.3 (52)	4.9 (48)
H_3PO_2	8.5 ± 1.0	1.5 (18)	7.5 (82)

The findings here are important as they indicate that commonly used washing procedures reported in the literature for flat carbon surfaces [59, 67, 82, 83] appear to be inadequate for removal of adsorbed anthraquinone from high surface area carbons. Literature reports on spontaneous diazonium coupling of various
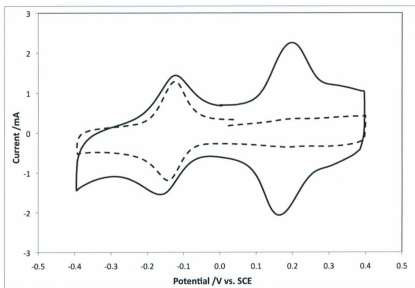
Figure 3.11: Cyclic voltammetry on Vulcan XC72 sequentially modified by the spontaneous diazonium reactions (VulcOX-AQ-AA) before (solid line) and after (dashed line) washing with benzene. Performed in 1.0 M H_2SO_4 at 100 mV s^{-1} with modified carbon deposited on carbon fiber paper electrodes.

83

organic compounds, such as anthraquinone [74, 88], nitrobenzene [71, 74, 78, 88], 2,5-dimethoxy-4-[4-(nitrophenyl)azo]benzene [103], benzene and azobenzene [78], to carbon powders have employed simple rinsing of the modified material with a variety of non-aromatic solvents. It is possible that the results obtained here are specific to anthraquinone and Vulcan XC72. However, it highlights the importance of attempting a variety of washing procedures for different systems.

While total surface coverages are important, the amount of anthraquinone covalently bound relative to the total amount present on the carbon surface is more informative. A comparison of oxidized carbon (76% covalently bound) to untreated carbon (45%) suggests that introduction of carboxylic acid groups to the carbon surface increases the ability to form a covalent bond. A possible explanation for this observation was introduced in Section 3.2.1, in which a decarboxylation pathway is made available for relief of positive charge buildup [71], graphically depicted in Scheme 3.2. An alternative explanation, which likely plays a parallel role, examines the type of carbon surfaces exposed (basal plane vs. edges). Allongue *et al.* studied the modification of both HOPG, a carbon surface that is primarily basal plane, and glassy carbon, which possesses a greater degree of edge planes, using the electrochemically induced diazonium reaction [69]. It was found that the reaction proceeded much faster on glassy carbon electrodes than HOPG. This observation was attributed to the nature of the two carbon materials, with glassy carbon possessing more edge sites and defects in the basal plane. HOPG, which is primarily basal plane, was still found to react, but at a much slower rate. Chemical oxidation of the carbon material creates carboxylic acid groups on the carbon surface, which in turn cause defects on the basal planes of Vulcan XC72. Increasing the number of these reactive defect

sites would result in an increased surface coverage for covalently bound material. The increase in defects would simultaneously reduce the ability of Vulcan XC72 to adsorb aromatic molecules, as cluttering of the basal plane surface with carboxylic acid groups would interfere with π-π stacking.

The reverse argument of that used for the oxidized carbon may be used to explain the results obtained for heat treated and chemically reduced carbon. In each of these cases only approximately 30% of material on the electrode was found to be covalently bound. Heat treatment reduces the amount of oxygen functionality on the carbon surface [71]. This would reduce the ability of the material to relieve a positive charge buildup using the mechanism discussed in the last paragraph. It would also decrease the amount of cluttering on the carbon surface, presenting more of the flat, aromatic basal plane surface that would be ideal for π-π stacking.

Introduction of HCl to the reaction mixture appears to have had a negligible effect on covalently bound anthraquinone, yielding 52% covalently bound. This number is comparable to the 45% obtained for untreated Vulcan XC72 using no added acid. However, use of H_3PO_2 resulted in a large decrease in covalently bound anthraquinone. Although initial testing indicated that the presence of H_3PO_2 yielded comparable anthraquinone coverages to the other methods (Section 3.2.2), results obtained after washing the modified carbon with benzene indicate that over 80% of the immobilized material was adsorbed to the carbon. These results are not all that surprising, considering that H_3PO_2 is known to reduce arenediazonium ions by replacing the $-N_2^+$ moiety with a simple -H [108–110]. Using aqueous H_3PO_2 to reduce several different diazonium ions, Kornblum *et al.* reported reaction yields of 65-81% in just 10 min [110]. It is therefore logical to expect that this protodediazoniation reaction is in direct
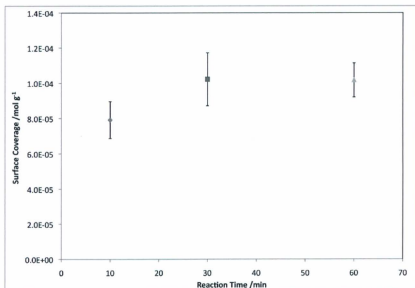
Figure 3.12: Effect of reaction time on covalently bound anthraquinone upon variation of reaction time. Vulcan XC72 was suspended in a neutral solution of Fast Red AL in an ice bath for the given time, then washed with benzene. Error bars represent the standard deviation between four electrodes.

competition with the surface immobilization reaction. Given the results obtained here, it appears that the dediazoniation reaction proceeds at a faster rate than surface immobilization. The resulting unsubstituted anthraquinone then adsorbs to the surface of the Vulcan XC72. These results also explain the lack of electrochemistry due to the azo- linkage in Figure 3.6, as the anthraquinone diazonium ions are reduced in solution, before coming into contact with the carbon surface.

The effect of reaction time on covalently bound anthraquinone was explored by exposing electrodes used to generate Figure 3.7 to the benzene washing procedure. The resultant anthraquinone surface coverages given in Figure 3.12, with the error bars representing standard deviation between four electrodes. Although the overall surface coverage remained constant over this time frame, it appears as though the degree of covalently bound material did not. The covalently bound surface coverage was observed to increase slightly, from 0.8×10^{-5} to 1.0×10^{-4} mol g^{-1}, between 10 and 30 minutes. The surface coverage then remained constant between 30 and 60 minutes.

3.2.4 Accessible Surface Area

Maximum observed coverages can be combined with theoretical monolayer density to obtain an estimate of the limits of accessible surface area caused by constriction. Using the van der Waals surface of anthracene as the approximate size of anthraquinone (11.65 Åx 7.44 Åx 3.88 Å) [111], the surface area of flat-lying anthraquinone can be estimated to be 87 Å^2 per molecule. This translates to a theoretical monolayer surface coverage 1.9×10^{-10} mol cm^{-2}. If anthraquinone were perpendicular to the carbon surface, as it would be if co-

valently bound, the theoretical monolayer surface coverage would be 3.7×10^{-10} mol cm^{-2}. Dividing the observed total surface coverage limit (1.5×10^{-4} mol g^{-1}) by each of these theoretical values, the accessible surface area can be predicted to be in the range of 40 - 79 m^2 g^{-1}.

Using two different N$_2$ adsorption isotherm techniques, Toupin and Belanger measured a surface area of 52-76 m^2 g^{-1} for Vulcan XC72 that had been chemically oxidized [71]. The pore size distribution for Vulcan XC72 was calculated. Toupin and Belanger reported that over half of the surface area of Vulcan XC72 is due to pores with a diameter less than 15 - 20 Å[71]. Therefore, it seems reasonable to attribute that the overall surface coverage limit ("Total" column in Table 3.6) to constriction, where anthraquinone is able to access only *ca.* 40 - 79 m^2 g^{-1} of the Vulcan XC72 surface area.

3.3 Conclusions

Surface coverages of anthraquinone immobilized on Vulcan XC72 by a spontaneous diazonium reaction were estimated using cyclic voltammetry. It was shown that, when determined voltammetrically, the ideal way of representing the surface coverage of electroactive species immobilized on high surface area carbons is in terms of moles of immobilized species per gram of modified carbon powder. This approach eliminates the potentially large error due to uncertainty in the surface area and variation in specific capacitance upon modification of the carbon surface.

The maximum surface coverage of anthraquinone on Vulcan XC72 appears to be limited in two unique ways. The overall limit appears to be approximately 1.5×10^{-4} mol g^{-1}. This value appears to be the total amount of anthraquinone

that can be immobilized on the surface, through both physisorption and covalent coupling. This limit was not significantly affected by pretreatments of the carbon surface or variations in reaction conditions attempted. Considering the work by Belanger and Toupin, the likely cause for this overall limit is limited surface area that is accessible to anthraquinone [71]. Using cyclic voltammetry and x-ray photoelectron spectroscopy, it was shown that approximately 8-10% of the total anthraquinone immobilized on the surface is anchored through an azo- linkage.

The second limitation observed was that for covalently bound anthraquinone. This limit was observed by washing modified carbons with benzene, which successfully removed strongly adsorbed anthraquinone. The limit was found to vary depending on the surface pretreatments and reaction conditions employed. This limit may be due to the amount of available reactive sites, namely the amount of edge-plane portions and defects in the basal plane of Vulcan XC72 [69]. This assignment is supported by the observed increase in covalently bound material upon introduction of defects (chemical oxidation), the decrease in covalently bound material upon removal of defects (heat treatment) and the ability to completely remove Azure A from the carbon surface when it was used in a secondary reaction. Kinetics may also play an important role. Differences between the rate of the spontaneous reaction and the rate of physisorption may also play an important role in this observed limitation.

Reaction conditions were found to play a minimal role in total anthraquinone immobilized, but a significant role in the covalent binding of anthraquinone, with H_3PO_2 producing the lowest covalent surface coverage. The total surface area of Vulcan XC72 that is accessible to anthraquinone is estimated to be 40 - 79 m^2 g^{-1}.

3.4   Experimental

Information regarding instrumentation and chemicals can be found in Chapter 2.

3.4.1   Chemical Oxidation of Vulcan XC72

To prepare oxidized Vulcan XC72, abbreviated here as VulcOX, Vulcan XC72 was first crushed to a fine powder with a mortar and pestle. The carbon powder was added to a round bottom flask containing 50 mL of conc. HNO_3. The suspension was refluxed for 30 min. During reflux, evolution of a brown gas (NO_2) was observed. The suspension was allowed to cool to room temperature and vacuum filtered using a porous glass crucible. The black powder was washed with H_2O, collected and dried overnight under vacuum at 40 ºC.

3.4.2   Heat Treatment of Vulcan XC72

Vulcan XC72 was heated under inert atmosphere in an attempt to reduce the oxygen content on the surface. The final product is labelled VulcHT. Vulcan XC72 (5.78 g) was crushed to a fine powder using a mortar and pestle. The powder was placed in a quartz tube, which was then placed into a tube furnace. The quartz tube was purged with N_2 at a flow rate of 50 mL min^{-1}. The tube furnace was heated from room temperature to 700 ºC at a rate of 10 ºC min^{-1}. The temperature was held constant at 700 ºC for 2 h, after which the apparatus was allowed to cool to room temperature while maintaining the N_2 atmosphere.

3.4.3 Chemical Reduction of Vulcan XC72

The attempted chemical reduction of Vulcan XC72 was carried out immediately prior to modification as described in Section 3.4.4.

3.4.4 Spontaneous Diazonium Grafting of Anthraquinone on Pretreated Vulcan XC72 Samples

Spontaneous reaction between the anthraquinone diazonium ion and each of Vulc, VulcOX, VulcHT and VulcBH$_4$ was typically executed using the following procedure. Approximately 50 mL of H$_2$O and 5 mL conc. HCl were added to a round bottom flask and purged with N$_2$ for 10 min. Addition of HCl was substituted with 5 mL of a 0.26 M solution NaBH$_4$ for VulcBH$_4$ modification. A 50 mg portion of the appropriate carbon black, ground to a fine powder using a mortar and pestle, was added to the round bottom flask. Ultrasonication of the suspension was used to disperse the carbon. The suspension was cooled in an ice bath. At this point in the the VulcBH$_4$ modification, the suspension was allowed to stir for 1 h. Fast Red AL salt (50 mg, 0.18 mmol) was added to the suspension giving a diazonium ion concentration of *ca.* 3.3 mM. The mixture was stirred for 1 hour. The carbon powder was collected by vacuum filtration over a porous glass frit and washed successively with ethanol, acetone and H$_2$O. The powder was dried overnight, under vacuum at 40 °C.

3.4.5 Spontaneous Diazonium Grafting of Anthraquinone on Vulcan XC72, Variation of Acid

Modification of Vulcan XC72 in the presence of HCl is described in Section 3.4.4. Modifications with no added acid, and with H_3PO_2 added were carried out following a similar procedure, with the following changes. For the modification with no added acid, the addition of 5 mL of HCl was omitted. For the modification using H_3PO_2, addition of 5 mL of HCl was replaced by addition of H_3PO_2.

3.4.6 Adsorption of 1-Amino-9,10-Anthraquinone to the Surface of Vulcan XC72

A round bottom flask was filled with Vulcan XC72 (50 mg), 10 mL of 4 M HCl and 1-amino-9,10-anthraquinone (50 mg, 0.22 mmol). The mixture was sonicated to disperse the carbon powder, then heated to reflux overnight. The suspension was then cooled, vacuum filtered and rinsed with three 30 mL aliquots of ethanol, acetone and water.

3.4.7 Spontaneous Diazonium Grafting of Anthraquinone on Vulcan XC72, Variation of Reaction Time

Modification was carried out as described in Section 3.4.4, with the exception of HCl addition. Reactions were carried out under neutral aqueous conditions. The modification was performed three times, with the reaction time being 10, 30 and 60 min.

3.4.8 Sequential Reactions for Spontaneous Diazonium Modification of Vulcan XC72

The procedure for synthesis of VulcOX-AQ was described in Section 3.4.4.

VulcOX-AQ-AQ was made using the following procedure. VulcOX-AQ (50 mg) was exposed to a solution of anthraquinone-1-diazonium chloride solution a second time, yielding VulcOX-AQ-AQ. A round bottom flask was filled with 20 mL of H_2O, 2 mL of conc. HCl and 50 mg of VulcOX-AQ. The powder was dispersed using ultrasonication, and the suspension cooled in an ice bath. Fast red AL salt (37 mg, 0.14 mmol) was added, giving a diazonium ion concentration of 6.2 mM. The mixture was stirred in an ice bath for 1 h. The powder was collected by vacuum filtration over a glass frit and washed with H_2O, acetone and methanol. The powder was then dried overnight, under vacuum at 40 °C.

VulcOX-AQ-AA was made using a similar procedure. A round bottom flask was filled with 25 mg of VulcOX-AQ, 10 mL of H_2O and 1 mL of conc. HCl. The carbon powder was dispersed by ultrasonication. Azure A (30 mg, 0.10 mmol) was added to the suspension, giving a concentration of 9.3 mM. The mixture was cooled in an ice bath. Two 0.5 mL aliquots of a 0.36 M aqueous solution of $NaNO_2$ were then added, staggered by 15 min. The mixture was stirred in an ice bath for a total of 1 h. The powder was then collected by vacuum filtration and washed with H_2O, acetone and ethanol. The powder was then dried overnight, under vacuum at 40 °C.

3.4.9 Adsorption of Unsubstituted Anthraquinone to Vulcan XC72

Unsubstituted anthraquinone (26.9 mg, 0.13 mmol) was dissolved in 25 mL of a 1:1 mixture of acetone and methanol. Vulcan XC72 (50 mg) was crushed to a fine powder, added to the solution, and dispersed by ultrasonication. The mixture was stirred overnight at room temperature. The carbon powder was collected by vacuum filtration and washed with H_2O, methanol and acetone. Following this, the sample was divided in two portions and subjected to the washing procedures described in Section 3.4.10.

3.4.10 Washing Procedures for Removal of Anthraquinone Physisorbed to Vulcan XC72

Vulcan XC72 with adsorbed anthraquinone was subjected to two additional washing procedures. One portion of the powder was sonicated in *ca.* 10 mL of methanol for 30 min. The carbon powder was then collected by vacuum filtration and rinsed with methanol, H_2O and acetone. The second portion was dispersed in methanol by ultrasonication. An aliquot of the suspension was applied to a strip of carbon fiber paper. The carbon fiber paper was then soaked in a vial containing *ca.* 10 mL of benzene for 15 min.

Following the excellent results of the benzene washing procedure, each of the samples from Sections 3.4.4, 3.4.5, 3.4.7 and 3.4.8 were subjected to the same method of washing.

Development of a Novel Benzimidazole Linkage. Immobilization of Polybenzimidazoles on Vulcan XC72

4.1 Introduction

Parts of this chapter have been published in a peer-reviewed journal [112].

The attraction of utilizing a high surface area carbon powder as an electrode support is the possibility of immobilizing a large amount of transition metal complexes on the surface while maintaining good conductivity. However, the results of Chapter 3 suggest that covalent immobilization of a complete monolayer on these materials may not be possible. A limited surface coverage was observed when modifications of the carbon surface were attempted using the spontaneous diazonium coupling. This is thought to be due to either limited accessibility of the carbon surface, a phenomenon known as constriction [71], or the fact that the basal-plane of graphitic materials is less reactive towards the diazonium ion than the edge-plane and defects in the basal-plane [69].

Whether the surface coverage limitation is due to either of these effects, or a combination of both, the spontaneous diazonium coupling technique was not deemed to be an ideal approach to accomplish the goals of this project. As such, a new approach was designed.

It was thought that a more successful approach would maximize the role of reactive sites known to be present on the surface. Further, the reactive sites should be known to be accessible to incoming molecules. It is known that treatment of carbon powders with nitric acid results in an increase of carboxylic acid groups on the surface [71]. The ability to easily add carboxylic acid groups to the carbon surface identifies them as a desirable functional group. The ability to use a chemical reagent to produce them also indicates that the carboxylic acid groups on the surface should be accessible to incoming molecules. Based on this rationale, a novel approach was designed to maximize modification of the

surface by targeting carboxylic acid functionality.

The newly designed approach relied on the cyclization reaction between aryl-diamines and carboxylic acids, which results in the formation of a benzimidazole linkage. Such a reaction has been reported in the literature using a variety of approaches. In the first technique, known as "melt polymerization", the reactants are heated to high temperatures (*ca.* 300-400 °C) in the absence of solvent [113]. A second approach relies on acid catalysis. Several methods exist for this approach. One method, the Phillips benzimidazole synthesis, involves heating a solution of an *ortho*-arylamine and a carboxylic acid in 4 M HCl(aq) [114]. An alternative method employs an anhydrous acid, typically polyphosphoric acid (PPA), to drive the reaction. While commonly used in recent years for synthesis of benzimidazole based polymers (polybenzimidazoles) [115], this approach has also been used for synthesis of more simple, benzimidazole containing compounds [116]. In regards to polybenzimidazole synthesis, the PPA technique has been utilized with temperatures ranging from 120 to 200 °C [117, 118]. More recent literature has examined the use of less extreme reaction conditions, such as employing microwave irradiation [119], and the reaction of aryldiamines with aldehydes using air [120] or I_2 [121] as an oxidant.

The acid catalyzed approach was chosen for this project because it (i) requires lower temperatures, (ii) has been more widely documented, and (iii) allows the use of a solvent, allowing for better mixing. Scheme 4.1 depicts the anticipated reaction between a mixture of 2,2′-bipyridine-4,4′-dicarboxylic acid, 3,3′-diaminobenzidine and Vulcan XC72 in PPA. It was envisaged that one end of 3,3′-diaminobenzidine would react with a carboxylic acid group on the surface of Vulcan XC72, resulting in a C-C bond between the resulting benzimidazole
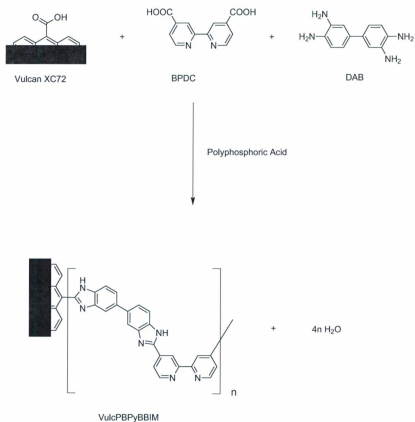
Scheme 4.1: Proposed reaction for covalent immobilization of a benzimidazole-based coordinating polymer on the surface of Vulcan XC72. The reaction between the surface of Vulcan XC72 (simplified) with 3,3'-diaminobenzidine (DAB) and 2,2'-bipyridine-4,4'-dicarboxylic acid (BPDC) is shown.

and the carbon surface. The aryldiamine on the opposite end of the immobilized molecule would then be free to react with 2,2'-bipyridine-4,4'-dicarboxylic acid. Continuation of the reaction should result in a coordinating polymer immobilized on the surface of Vulcan XC72. This simple approach could be utilized to convert a single reaction site on the carbon surface to a surface bound coordination polymer, capable of binding multiple transition metal complexes.

The inclusion of bipyridyl moieties in polymers to impart the ability to bind transition metal complexes is the topic of a recent review [122]. Such an approach has been especially successful for synthesis of ruthenium containing polymers, due to the fact that polypyridyl ruthenium complexes are known for their stability. The polymer formed from combination of 3,3'-diaminobenzidine and 2,2'-bipyridine-4,4'-dicarboxylic acid, shown in Scheme 4.1, was therefore deemed to be an excellent system to study. The polymer was synthesized as described in 4.4.5, and is abbreviated here as PBPyBBIM. When synthesized in the presence of Vulcan XC72 (Section 4.4.6), the product is abbreviated as VulcPBPyBBIM.

Also examined in this work is the immobilization of a polymer synthesized by the reaction between 3,3'-diaminobenzidine and 2,5-pyridine dicarboxylic acid. This polymer has been previously studied [123] and is abbreviated here as PPyBBIM. When synthesized in the presence of Vulcan XC72 (Section 4.4.6), the material is abbreviated as VulcPPyBBIM.

It is difficult to determine how to experimentally confirm successful covalent immobilization of a polybenzimidazole on the surface of a carbon powder. While techniques such as IR spectroscopy and XPS could be used to confirm the presence of the polymer, there is no clear way to confirm the covalent immobilization. The benzimidazole group formed between the polymer and the

carbon surface would be expected to exhibit indistinguishable behavior from the benzimidazole groups throughout the polymer. Therefore, it was deemed necessary to begin with examination of a less complex system.

The reaction was initially investigated by the reaction of 1,2-diaminoanthraquinone (DAAQ) with Vulcan XC72, portrayed in Scheme 4.2. The electroactivity of anthraquinone allowed for rapid determination of the presence of anthraquinone on the surface using cyclic voltammetry. Confirmation of covalent immobilization of anthraquinone was carried out by XPS spectroscopy.
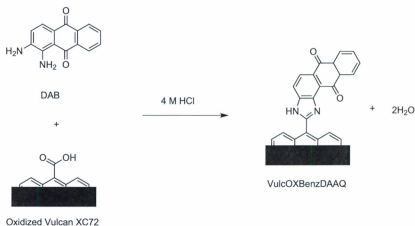
Scheme 4.2: Proposed reaction for immobilization of 1,2-diaminoanthraquinone (DAAQ) on the surface of Vulcan XC72 by acid catalyzed benzimidazole fomation.
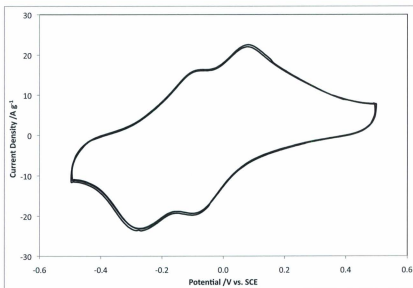
Figure 4.1: Cyclic voltammogram obtained for VulcOX-DAAQ(PPA). Cyclic voltammetry performed in 1.0 M H_2SO_4 at 100 mV s^{-1}, with the modified carbon deposited on a carbon fiber paper electrode. The first two cycles are shown.

4.2 Results and Discussion

4.2.1 Immobilization of 1,2-Diaminoanthraquinone on Vulcan XC72

The reaction between DAAQ and chemically oxidized Vulcan XC72 in the presence of PPA was performed as described in Section 4.4.1. A cyclic voltammogram acquired on the modified powder (VulcOX-DAAQ(PPA)) is presented in Figure 4.1. The modified powder exhibited electrochemical activity in the region expected for anthraquinone. However, two sets of peaks were unexpectedly observed. The two peak sets possessed $E_{1/2}$ values of -0.004 and -0.189 V vs. SCE and ΔE_p values of 170 and 167 mV, respectively. For comparison, the immobilization of anthraquinone by spontaneous diazonium coupling yielded a single, reversible peak with an $E_{1/2}$ value of -0.14 V and a ΔE_p of 69 mV.

The anticipated electrochemical behavior following immobilization of an electroactive species on an electrode surface is a single set of redox peaks with a ΔE_p value of 0 mV [124]. The observation of two distinct peak sets and a large ΔE_p value for each set suggests that the reaction does not proceed exactly as expected.

A large ΔE_p value indicates one of two situations. The first is slow electron transfer kinetics, the second is the presence of an uncompensated cell resistance [124]. Anthraquinone has shown no sign of poor electron transfer kinetics in either the adsorbed or surface-bound form (Chapter 3). Therefore, uncompensated cell resistance is the likely cause of this behavior.

The effect of uncompensated cell resistance is expressed mathematically in equation 4.2.1 [124]. The equation states that the electrochemical potential at

the electrode surface ($E_{electrode}$) is equal to the electrochemical potential applied by the potentiostat ($E_{applied}$) minus the product of the current (i) and uncompensated cell resistance (R_u).

$$E_{electrode} = E_{applied} - iR_u \qquad (4.2.1)$$

The observable effect of uncompensated resistance is a widening of the voltammogram, where redox peaks are pulled farther apart. The effect is enhanced with larger currents. The voltammogram obtained for VulcOX-DAAQ(PPA) possessed a sloped baseline; additional behavior indicative of uncompensated cell resistance.

The use of such highly acidic conditions and presence of multiple functional groups may be expected to induce unwanted chemical reactions in the system. One such reaction may be the intermolecular reaction of an arylamine of one DAAQ molecule with a ketone of another, shown in Scheme 4.3. Such a reaction has been reported, using 9,10-anthraquinone derivatives and primary alkylamines [125].
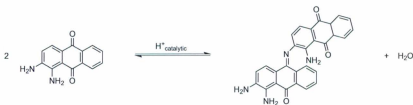
Scheme 4.3: Possible intermolecular reaction for 1,2-diaminoanthraquinone.

This style of reaction is known to proceed via acid catalysis, with the corresponding Schiff base and H_2O being the products. The equilibrium in this style of reaction generally favors the amine and ketone [126], necessitating removal

of H_2O to drive the reaction forward. One of the reasons that PPA is widely used in the synthesis of polybenzimidazoles is the fact that it is very reactive towards H_2O. This allows it to drive the reaction forward by consuming H_2O produced during the reaction [115]. By a similar rationale, the presence of PPA may be expected to drive the imine forming reaction in Scheme 4.3 towards the Schiff base product. This in turn indicates that the combination of Vulcan XC72 and DAAQ in PPA may result in deposition of an anthraquinone based polymer on the carbon surface.

It has been shown that when depositing polymers on an electrode surface the ionic resistance of the system increases with the thickness of the polymer film [127]. The presence of an anthraquinone containing polymer on the surface would introduce ionic resistance to the system, a form of uncompensated resistance. This may explain the large ΔE_p values and sloped baseline in the voltammogram. The combination of a feasible polymerization mechanism and electrochemical behavior suggesting the presence of a polymer suggests that the use of PPA is most likely producing an anthraquinone based polymer on the surface. However, it is impossible to say whether the polymer is covalently bound or physisorbed.

The presence of such a polymer raises the possibility that one of the two sets of redox peaks may be due to imine functionality, which is known to be electrochemically active [128]. Redox potentials of imine groups are typically observed at more negative redox potentials, around -0.6 to -1.0 V vs. SCE. They are also known to be highly unstable when electrochemically examined in aqueous conditions [128]. Therefore, it is unlikely that either of the two sets of redox peaks are due to imine functionality.

Following these results, alternative reaction conditions were employed. Con-
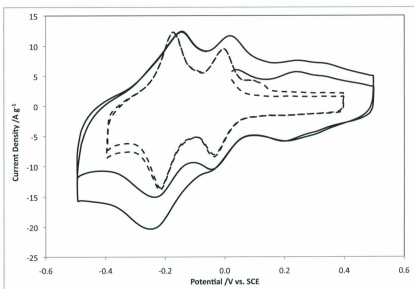
Figure 4.2: Cyclic voltammograms obtained for VulcDAAQ(HCl) (dashed line) and VulcOX-DAAQ(HCl) (solid line) deposited on carbon fiber paper electrodes. Cyclic voltammetry performed in 1.0 M H_2SO_4 at 100 mV s^{-1}. The first two cycles are shown for each sample.

sidering the nature of the unwanted side-reaction, the use of aqueous conditions should minimize the risk of imine formation. The Phillips benzimidazole reaction was employed. Described in 4.4.1, the procedure involved heating a suspension of Vulcan XC72 in a solution of DAAQ in 4 M HCl(aq) [114]. The reaction was carried out using both pristine Vulcan XC72 (VulcDAAQ-(HCl)) and chemically oxidized Vulcan XC72 (VulcOX-DAAQ(HCl)). The cyclic voltammogram obtained for the two samples are compared in Figure 4.2.

Modification of VulcOX using the new approach produced a voltammogram containing three sets of reversible redox peaks. The subtle peaks present in the 0.1 V to 0.4 V range are also observed for unmodified VulcOX. These peaks are due to quinone species on the carbon surface, known to be present following oxidation of carbon surfaces [129]. A reversible peak set is observed with an $E_{1/2}$ of -0.029 V and ΔE_p of 29 mV. A second set of reversible peaks is observed with an $E_{1/2}$ of -0.190 V and ΔE_p of 86 mV. While almost identical in location to the peaks observed for VulcOX-DAAQ(PPA), the ΔE_p values of both peak sets are much closer to the expected value of 0 mV. Peak current densities were approximately half of those observed for the sample modified using PPA. A significant decrease in current for the most negative cathodic peak was observed between the first and second cycle. This interesting behavior is discussed later in this section.

Two sets of peaks were observed in the voltammogram of Vulc-DAAQ(HCl). These peaks possessed $E_{1/2}$ values of -0.020 and -0.197 V and ΔE_p values of 26 and 41 mV, respectively. The peaks were much sharper than those observed for VulcOX using either PPA or 4 M HCl, and the lower ΔE_p values indicate lower resistance and good electron transfer kinetics. Peak current densities for VulcDAAQ(HCl) were comparable to those of VulcOX-DAAQ(HCl). Cyclic

voltammetry data for the three modified carbon samples is summarized in Table 4.1.

Table 4.1: Cyclic voltammetry data for carbon powders reacted with 1,2-diaminoanthraquinone in the presence of acid.

Sample	$E_{p,a}$ V	$E_{p,c}$ V	ΔE_p mV	$E_{1/2}$ V	Γ (x 10^{-4} mol g^{-1})
VulcOX-DAAQ(PPA)	+0.080	-0.088	170	-0.004	-
	-0.102	-0.269	167	-0.189	
VulcOX-DAAAQ(HCl)	-0.014	-0.043	29	-0.029	1.5 ± 0.3
	-0.147	-0.233	86	-0.190	
Vulc-DAAQ(HCl)	-0.007	-0.033	26	-0.020	0.81 ± 0.05
	-0.176	-0.217	41	-0.197	

Potentials given *vs.* SCE

As in Chapter 3, anthraquinone surface coverages were measured by cyclic voltammetry on electrodes with a known mass of modified powder. Due to peak overlap, the surface coverages were calculated using the anodic peak of both peak sets. Reported values are based on four electrodes of each sample and are included in Table 4.1. Vulc-DAAQ(HCl) was observed to have an anthraquinone surface coverage of 8.1 x $10^{-5} \pm 0.5$ x 10^{-5} mol g^{-1}. The surface coverage of anthraquinone on VulcOX-DAAQ(HCl) was observed to be significantly higher; 1.5 x $10^{-4} \pm 0.3$ x 10^{-4} g mol^{-1}. These surface coverage values are comparable to those obtained for Vulcan XC72 modified using the spontaneous diazonium reaction. However, it is important to remember that values obtained for the benzimidazole technique include total surface coverage, which was split between two forms of anthraquinone.

The persistence of both sets of reversible redox peaks following the use of acidic aqueous reaction conditions indicates that neither peak is due to imine functionality. To probe whether the electrochemical activity was due to nitrogen functionality rather than anthraquinone, the modification procedure was

executed using 1,2-phenylenediamine (PDA) in place of DAAQ, as described in Section 4.4.3. Cyclic voltammetry was performed on the resulting material, labelled VulcOX-PDA. The voltammogram, included in Appendix D, exhibited a reversible set of peaks with an $E_{1/2}$ of -0.147 V vs. SCE. A small set of peaks produced a shoulder on the negative side of both peaks. The low current density observed and the location of the electrochemical activity for the peaks in VulcOX-PDA, as compared to the two reversible electrochemical processes observed for DAAQ modified carbon samples, indicates that nitrogen is not responsible for either of the electrochemical processes observed in DAAQ modified samples.

The location of the peak sets suggests that two distinct forms of anthraquinone are present. In Chapter 3 it was observed that adsorbed anthraquinone exhibited electrochemical behavior that was indistinguishable from the covalently bound form. This suggests that the two forms observed here must be significantly different from one another to result in such a peak separation. Successful immobilization through a benzimidazole linkage would result in an aromatic ring fused to anthraquinone, which would likely result in a noticeable peak shift compared to unreacted DAAQ, or DAAQ bound through a single nitrogen amide linkage.

To test for the presence of an amide linkage between the carbon surface and DAAQ, Vulc-DAAQ(HCl) was refluxed in 1 M NaOH(aq) for 70 min. The cyclic voltammogram, shown in Appendix D, was found to remain unchanged following this treatment. From this, it is highly unlikely that DAAQ is bound through an amide linkage.

The redox potential of DAAQ adsorbed to Vulcan XC72 was determined by soaking a carbon fiber paper electrode coated with Vulcan XC72 in a methanolic

solution of DAAQ (*ca.* 4 mM) for 5 min. The electrode was air dried, then examined using cyclic voltammetry. The voltammogram, shown in Appendix D, revealed an $E_{1/2}$ of -0.180 V and a ΔE_p of 84 mV. The similarity in peak locations suggests that the more negative of the two peak sets in the modified carbon powder may be due to adsorbed DAAQ.

A significant decrease in peak current was observed between the first and second cycles for the most negative cathodic peak in the voltammogram of VulcOX-DAAQ(HCl), Figure 4.2. This led us to examine the electrochemical stability of the anthraquinone modified powders. A carbon fiber paper electrode with Vulc-DAAQ(HCl) deposited on its surface was electrochemically cycled for three hours at 100 mV s^{-1} in 1 M H_2SO_4(aq). Shown in Figure 4.3, the -0.020 V peak set was found to be very stable, while the -0.197 V set was found to be almost quantitatively eliminated. Elimination of the more negative peak set also revealed a small set of peaks with an $E_{1/2}$ of *ca.* -0.09 V. Similar instability towards electrochemical cycling was observed for VulcOX-DAAQ(HCl). The voltammograms obtained before and after 3 h of electrochemical cycling are shown in Appendix D.

Anthraquinone is known to be an electrochemically stable, reversible electrochemical system. For the present reaction system it is difficult to envisage formation of any functional group that would produce such strong, reversible electrochemistry as is observed. Based on the stability and location of the two electrochemical processes, the electrochemistry can be attributed to forms of anthraquinone that are strongly (-0.020 V) and weakly (-0.197 V) bound to the surface. Voltammetric results do not give any indication of the type of linkage. Aside from the desired benzimidazole linkage, it is possible that a reaction analogous to that proposed by Buttry *et al.* results in covalent modification of

109
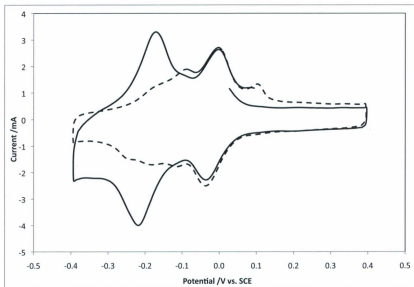
Figure 4.3: Cyclic voltammogram obtained for Vulc-DAAQ(HCl) before (solid line) and after (dashed line) 3 hours of electrochemical cycling. Cyclic voltammetry performed in 1.0 M H_2SO_4 at 100 mV s^{-1}.

the carbon surface with DAAQ through a 2° amine linkage [106]. It is unlikely, however, that either of the covalent linkages would be so easily cleaved as observed for the -0.197 V set of peaks. It is therefore reasonable to assign the most negative set of peaks to adsorbed, unreacted DAAQ.

X-ray photoelectron spectroscopy was used to examine the spectral regions corresponding to N 1s and O 1s emissions for both Vulc and VulcOX modified with DAAQ using the Phillips benzimidazole reaction. The raw data for each sample was adjusted, and curve fitting was performed as described in Chapter 2. The curve-fitted XPS spectra are included in Appendix A; the curve-fitting results are tabulated in Table 4.2. Also presented for comparison are (i) Vulc, (ii) VulcOX, (iii) VulcAQ formed using the spontaneous diazonium reaction (Chapter 3), and (iv) 1-amino-9,10-anthraquinone adsorbed on the surface of Vulcan XC72 (Vulc-AAQ, Section 4.4.2).

As expected, the N 1s region of both Vulc and VulcOX revealed no nitrogen presence in the samples. The O 1s section of Vulc could be fitted with two peaks, centered at 531.1 and 533.0 eV. The O 1s section of Vulc has previously been fitted with two peaks by Toupin and Belanger: at 531.9 and 533.6 eV [71]. In their work, these peaks were attributed to C-O and C=O groups on the carbon surface. The 531.1 and 533.0 eV peaks observed here are therefore attributed to C-O and C=O functionality, respectively.

It should be highlighted that the use of two peaks to model the O 1s region of a carbon is a simplification meant for modelling purposes. In reality many different forms of oxygen exist on the carbon surface. Much effort has been made at accurate quantification of the various functional groups [96, 97, 130]. Each of the various functional groups would be expected to exhibit slightly different O 1s binding energies, painting a much more complex picture than

Table 4.2: X-ray photoelectron spectroscopy data for modified carbon powders.

| | Binding Energy /eV[a] | | | |
Sample	N 1s	Identity	O 1s	Identity
Vulc			531.1 (178)	C-O
			533.0 (213)	C=O
VulcOX			531.1 (1787)	C-O
			532.2 (2052)	
			533.0 (1789)	C=O
			533.9 (1404)	
VulcAQ (diazonium)	400.2 (206)	azo-bridge	531.1 (874)	C-O
			531.6 (1915)	AQ
			533.0 (871)	C=O
			535.7 (234)	
Vulc -AAQ[b]	399.1 (287)	arylamine	531.1 (696)	C-O
			531.5 (618)	AQ
			533.0 (714)	C=O
Vulc-DAAQ(HCl)	399.1 (178)	benz[c]	531.0 (611)	C-O
	399.1 (464)	arylamine	531.5 (841)	AQ
	400.6 (173)	benz	533.0 (573)	C=O
VulcOX-DAAQ(HCl)	399.0 (732)	arylamine	531.1 (2481)	C-O
	399.1 (498)	benz	531.5 (3173)	AQ
	400.6 (509)	benz	532.2 (1914)	
			533.0 (573)	C=O
			533.9 (3134)	

[a] Values in brackets represent signal intentsity in counts per second.
[b] 1-amino-9,10-anthraquinone
[c] benzimidazole

portrayed here. However, the simplified modelling employed here makes it possible to detect changes in the spectrum upon modification.

The O 1s region of VulcOX could not be properly curve-fitted with two peaks. To obtain a good fit, the intensities of the two peaks observed in Vulc were held at a 1:1 ratio. Additional peaks were then added until a good fit was obtained. It was found that two additional peaks were required, at 532.2 and 533.9 eV. The fitted spectra is included in Appendix A.

In Chapter 3 the N 1s region of VulcAQ, modified using the spontaneous diazonium coupling, was shown to exhibit a single peak at 400.2 eV. This signal was attributed to an azo-bridge between anthraquinone and the carbon surface. The O 1s region revealed four peaks, attributed to C-O surface functionality (531.1 eV), the carbonyl of anthraquinone (531.6 eV), C=O surface functionality (533.0 eV) and a weak satellite peak (535.7 eV). A single peak was observed in the N 1s region for Vulc-AAQ. Located at 399.1 eV, this peak is attributed to the arylamine of the adsorbed anthraquinone species. The O 1s region for this sample could be fitted with the expected peaks: C-O surface functionality (531.6 eV), anthraquinone C=O (531.5 eV) and C=O surface functionality (533.0 eV).

The O 1s region of Vulc-DAAQ(HCl) was successfully fitted with the two peaks expected for C-O and C=O surface functionality, as well as the 531.5 eV peak due to anthraquinone. The spectrum of VulcOX-DAAQ(HCl) was fitted with the four peaks found for VulcOX, as well as a strong emission at 531.5 eV. This data further confirms the presence of anthraquinone on the surface for both modified samples.

The N 1s region for Vulc-DAAQ(HCl) could be successfully curve-fitted using two peaks. The curve-fit included peaks at 399.1 and 400.6 eV, with relative

intensities of *ca.* 4:1. However, VulcOX-DAAQ(HCl) required three peaks to properly curve-fit the data: at 399.0, 399.1 and 400.6 eV. These peaks had relative intensities of 3:2:2.

Version 3.5 of the NIST XPS database indicates that the N 1s emission of benzimidazole rings falls in the range of 397.6 to 400.4 eV [131]. Database entries indicate that it is possible to observe either a single emission, or separate emissions for the two nitrogens. For VulcOX-DAAQ(HCl), three peaks were required to obtain a proper curve-fit. Based on this, and the electrochemical behavior of the sample, the peaks can therefore be assigned as follows. Based on the 1:1 relative intensities, the emission peaks at 399.1 and 400.6 eV are assigned to nitrogens of a benzimidazole ring. Based on the similarity in location to that observed for adsorbed 1-aminoanthraquinone, the 399.0 eV peak is attributed to unreacted arylamine groups. Considering this, a reasonable curve-fit for Vulc-DAAQ(HCl) would include splitting the 399.1 eV peak into two distinct species as presented in Table 4.2. The peaks for Vulc-DAAQ(HCl) are similarly assigned as two benzimidazole nitrogens (399.1 and 400.6 eV), and an arylamine nitrogen at 399.1 eV.

In their work, Buttry *et al.* found strong adhesion of 2-aminoanthraquinone to the surface of carbon fibers [106]. They proposed that amines undergo nucleophilic attack on alkene groups located on the surface of carbon powders. Using XPS, they report N 1s binding energies of 399.6 eV for their modified carbon fibers. While the possibility of such a reaction occurring in this work cannot be completely eliminated, the combination of XPS results and electrochemical behavior found here suggests that the present system results in two forms of anthraquinone on the carbon surface: (i) anthraquinone covalently immobilized through the desired benzimidazole linkage, and (ii) unreacted DAAQ adsorbed

to the carbon surface.

4.2.2 Immobilization of Secondary Molecules Using Benzimidazole Linkages

Having evidence suggesting successful immobilization of anthraquinone on a carbon surface through the desired benzimidazole linkage, we set out to test whether a surface immobilized species could be utilized to perform sequential reactions. Shown in Scheme 4.4, the chosen approach was a two step reaction. In the first step, 1,2-diaminobenzidine was first reacted with Vulcan XC72 in the presence of 4 M HCl(aq) to produce a modified powder labelled Vulc-DAB. This modified powder was then exposed to anthraquinone-2-carboxylic acid under similar conditions, producing Vulc-DAB-AQ. The modification procedures are given in Section 4.4.4.

Cyclic voltammetry on both Vulc-DAB and Vulc-DAB-AQ, Figure 4.4, produced excellent results. The voltammogram of Vulc-DAB exhibited a single reversible set of peaks with an $E_{1/2}$ of -0.144 V. The similarity in location to the peak set observed for Vulc-PDA, as well as that revealed for Vulc-DAAQ upon cycling, suggests that this peak set is due to nitrogen based functionality. The small size of this peak set relative to that for anthraquinone in Vulc-DAAQ, as well as in Figure 4.4, indicates that it is not due to the benzimidazole group.

The main feature of the voltammogram obtained on Vulc-DAB-AQ is a reversible set of peaks with an $E_{1/2}$ of -0.072 V. The location of the peak set is in the region expected for anthraquinone species, and cyclic voltammetry indicates a surface coverage of $1.2 \times 10^{-4} \pm 0.2 \times 10^{-4}$ mol g^{-1}. Both peaks of this set exhibit a shoulder on the more negative side, likely due to the species respon-
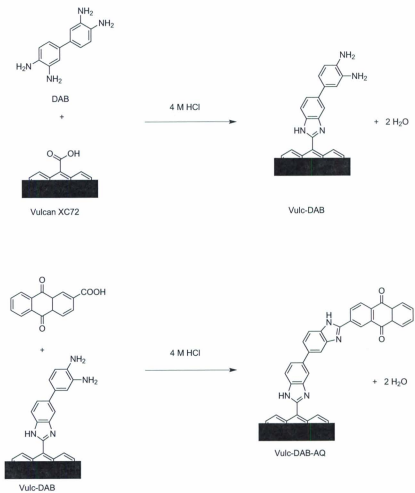
Scheme 4.4: Proposed reaction for immobilization of anthraquinone on the surface of Vulcan XC72 through sequential reactions of (DAB) and anthraquinone-2-carboxylic acid.
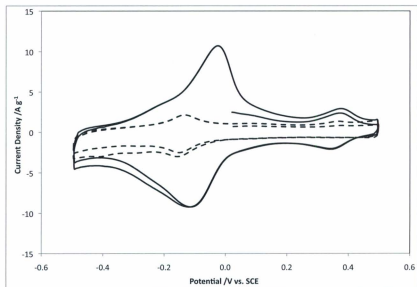
Figure 4.4: Cyclic voltammograms obtained for Vulc-DAB and Vulc-DAB-AQ
deposited on carbon fiber paper. Cyclic voltammetry performed in
1.0 M H$_2$SO$_4$ at 100 mV s^{-1}.

sible for the -0.144 V peaks observed in Vulc-DAB. A small, reversible peak set with an $E_{1/2}$ of 0.358 V is also present. This set of peaks exhibits a current density similar to the peaks observed in Vulc-DAB, suggesting that they may result from similar processes. These peaks may indicate the presence of stable intermediates of the benzimidazole formation.

X-ray photoelectron spectroscopy was once again employed to probe the nature of the linkage. Curve-fitting results from the N 1s and O 1s regions of the XPS spectra are summarized in Table 4.3. Spectra of the O 1s region for both samples are included in Appendix A. It was possible to curve-fit the O 1s region of Vulc-DAB with two peaks; at 531.6 and 533.0 eV. When compared to the XPS results for unmodified Vulcan XC72, it can be seen that the peak attributable to C-O functionality on the carbon surface is shifted slightly, from 531.1 eV (Vulc) to 531.6 eV (Vulc-DAB). It was also observed that the approximate ratio between the 531.6 and 533.0 eV peaks is 1:2 for Vulc-DAB, where it was approximately 1:1 for the 531.1 and 533.0 eV peaks of Vulc.

Table 4.3: X-ray photoelectron spectroscopy data for sequentially modified carbon powders.

	Binding Energy /eV[a]			
Sample	N 1s	Identity[b]	O 1s	Identity
Vulc-DAB	398.7 (99)	benz1	531.6 (382)	C-O
	399.4 (233)	arylamine	533.0 (602)	C=O
	400.4 (108)	benz1		
Vulc-DAB-AQ	398.7 (820)	benz1	531.6 (1164)	C-O
	399.2 (820)	benz2	531.6 (2976)	AQ
	400.4 (810)	benz1	533.0 (1829)	C=O
	400.7 (780)	benz2		

[a]Values in brackets represent signal intentsity in counts per second
[b]benz1 = benzimidazole between DAB and Vulcan XC72
benz2 = benzimidazole between DAB and AQ

The O 1s region of Vulc-DAB-AQ can also be curve-fitted with two peaks. The peaks observed were in identical locations to those of Vulc-DAB, but the ratio of intensities reversed, producing a ratio of approximately 2:1 for the 531.6 and 533.0 eV peaks. Anthraquinone was earlier found to possess an O 1s binding energy of 531.5 - 531.6 eV. The increase in signal intensity can therefore be attributed to the presence of anthraquinone on the surface. Such an assignment is corroborated by cyclic voltammetry results.

The curve-fitted spectra corresponding to the N 1s region of Vulc-DAB and Vulc-DAB-AQ are given in Figure 4.5. For Vulc-DAB, the region was successfully fitted with three peaks. Located at 398.7, 399.4 and 400.4 eV, an intensity ratio of 1:2:1 was observed. Based on the relative peak intensities and the N 1s binding energy of 399.1 eV for the arylamine of 1-aminoanthraquinone adsorbed to the carbon surface, the 399.4 eV peak observed here is attributed to unreacted arylamine groups. The remaining two peaks, 398.7 and 400.4 eV, are therefore attributed to the two nitrogens of the desired benzimidazole linkage between the carbon surface and the diaminobenzidine molecule.

The N 1s region of Vulc-DAB-AQ was observed to broaden and develop into what appears to be two peaks. However, the data could not be curve-fitted with two peaks while maintaining a FWHM of 1.4 eV for the peaks. To obtain an appropriate curve-fitting of the data, the assumption was made that the peaks attributed to benzimidazole nitrogens in Vulc-DAB would be present in Vulc-DAB-AQ. Based on this assumption, the 398.7 and 400.4 eV peaks were held at a 1:1 ratio served as the starting point. Additional peaks were then added individually and the curve-fit was optimized while maintaining the 1:1 intensity ratio between the 398.7 and 400.4 eV peaks. It was found that addition of two peaks was necessary to fit the data. The peaks were located at 399.2 and
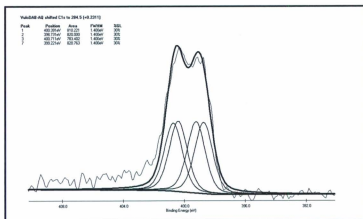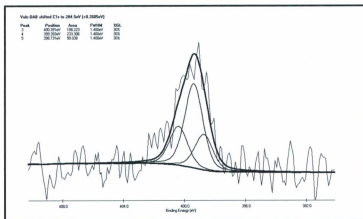
Figure 4.5: XPS spectrum (N 1s region) obtained for Vulcan XC72 modified sequentially by reaction with 1,2-diaminobenzidine (top), then anthraquinone-2-carboxylic acid (bottom) in 4 M HCl(aq).

400.7 eV and possessed an intensity ratio of approximately 1:1. In this curve fitting, the relative intensity of all four peaks were approximately equal. Based on the known presence of anthraquinone, the disappearance of the XPS peak attributed to arylamine nitrogens, the appearance of two peaks in the region known for benzimidazoles [131], and the relative intensity of the new peaks, the 399.2 and 400.7 eV peaks are attributed to nitrogens of a benzimidazole linkage formed between the terminal end of surface-bound 1,2-diaminobenzidine and the incoming anthraquinone-2-carboxylic acid.

Combination of cyclic voltammetry and XPS results for Vulc-DAB and Vulc-DAB-AQ suggests that the series of reactions proceeded as desired. However, the interpretation of XPS results offers no explanation for the presence of the 0.358 V redox process observed in the voltammogram of Vulc-DAB-AQ. It also does not offer any clue to the identity of the species responsible for the redox process located at -0.144 V in Vulc-DAB, which also seemed to be present as a shoulder on the anthraquinone peaks in the voltammogram of Vulc-DAB-AQ. Based on its appearance following exposure to 1,2-diaminobenzidine, the species responsible for the -0.144 V peak is likely nitrogen-based. The appearance of a set of peaks at 0.358 V, with comparable current densities to the -0.144 V peaks, following reaction with anthraquinone-2-carboxylic acid suggests a similar species; perhaps a stable reaction intermediate. Inability to ascertain the source of these redox processes made it impossible to include them in the XPS data analysis. However, both of these unexplained redox processes exhibit very small current densities compared to anthraquinone. The surface coverage of the species responsible for these unknown processes are therefore low compared to that of anthraquinone. Ignoring their presence during XPS data analysis would not be expected to introduce significant error.

4.2.3 Immobilization of Polybenzimidazoles on Vulcan XC72

As discussed in Section 4.1, it is very difficult to confirm covalent binding of a polymer to the surface of Vulcan XC72. However, the results of Sections 4.2.2 and 4.2.1 suggest that immobilization of aryldiamines on the surface of Vulcan XC72 through benzimidazole linkages is feasible. Based on these results, it is assumed that synthesis of polybenzimidazoles in the presence of Vulcan XC72 results in immobilization of the polymer on the carbon surface.

The procedure used for synthesis of the two polymers is based on the acid catalyzed reaction using PPA. The procedures used for synthesis of the polymers is described (i) in the absence of Vulcan XC72 in Section 4.4.5, and (ii) in the presence of Vulcan XC72 in Section 4.4.6. The materials resulting from polymer synthesis in the presence of Vulcan XC72 are labelled VulcPPyBBIM and VulcPBPyBBIM.

Polybenzimidazoles are known for poor solubility, primarily due to their rigid polymer backbone and strong interchain hydrogen bonding [132]. Both PPyB-BIM and PBPyBBIM, synthesized as described in Section 4.4.5, were found to be sparingly soluble in dimethylacetamide (DMA) and moderately soluble in concentrated H_2SO_4. Dissolution of PPyBBIM in DMA produced a pale yellow solution, while use of H_2SO_4 produced a dark yellow-orange solution. Dissolution of PBPyBBIM in DMA yielded a yellow-orange solution, and H_2SO_4 produced a dark orange solution.

UV-visible spectra of each of the two polymers dissolved in DMA are shown in Figure 4.6. The solution of PPyBBIM was observed to possess a single absorbance, located at 401 nm. This location is identical to that previously reported and attributed to a π-π^* transition [100, 133]. The solution of PBPyBBIM
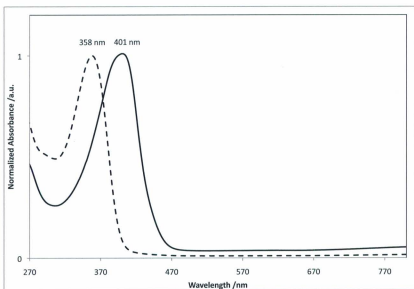
Figure 4.6: Normalized UV-vis spectra on solutions of PPyBBIM (solid line) and PBPyBBIM (dashed line) in dimethylacetamide.

was also observed to possess a single absorbance. The absorbance was located at 358 nm and is similarly attributed to a π-π^* transition.

A mixture of CF_3CO_2D and D_2O was previously utilized to acquire a ^1H NMR spectrum for PPyBBIM [100, 133]. Polymers synthesized here were found to be insoluble in this mixture, possibly indicating longer polymer chain lengths. However, solubility of both polymers in H_2SO_4 allowed the acquisition of ^1H NMR using D_2SO_4 as the solvent. Using a solution of 4,4-dimethyl-4-silapentane-1-sulfonic acid in D_2SO_4, the shift of D_2SO_4 was determined to be 10.82 pm . This shift was used as a reference point for spectra of the polymer solutions.

The ^1H NMR obtained for PPyBBIM is included in Appendix C. Chemical shifts observed were slightly different than those previously reported [100, 133], likely due to the use of a different solvent system. However, the spectrum obtained is consistent with the expected structure of the polymer.

Six major peaks were observed for PBPyBBIM in D_2SO_4 when ^1H NMR was performed at 25 °C, all of which appeared to be broad singlets. Upon increasing the temperature, four peaks became well-resolved doublets. These peaks fit the shift and splitting pattern expected for the polymer. Homonuclear correlation spectroscopy was performed; the spectrum is included in Appendix C. Assignment of the peaks is given along with the spectrum in Figure 4.7. Minor peaks were also observed in the spectrum. These integrate as approximately 0.1 H compared to the major peaks and exhibit a splitting pattern similar to the major peaks. These minor peaks are believed to be due to the terminal portions of the polymer, suggesting average chain lengths of approximately 20 monomer units.

In an attempt to confirm the presence of polymer on the surface of Vulcan XC72, infrared spectroscopy was performed using an attenuated total reflectance

124
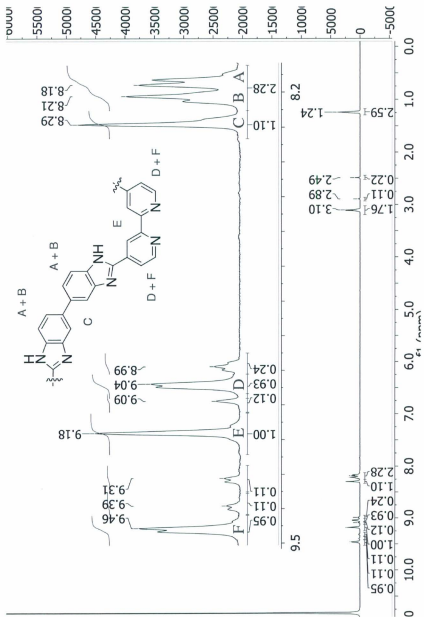
Figure 4.7: ^{1}H NMR spectrum obtained for PBPyBBIM dissolved in D_2SO_4. Spectrum was acquired at 80 °C to enhance spectral resolution.

Figure 4.8: Infrared transmittance spectra obtained for PPyBBIM (bottom, blue line), VulcPPyBBIM (bottom, red line), PBPyBBIM (top, blue line) and VulcPBPyBBIM (top, red line).
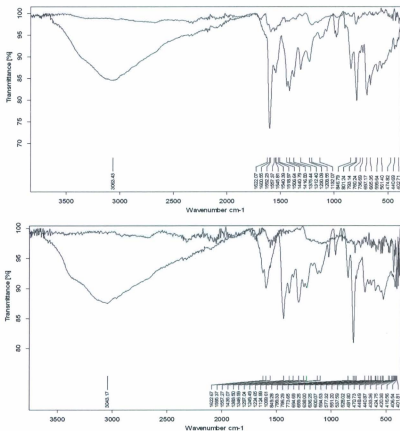
stand. Infrared transmittance spectra for PPyBBIM and PBPyBBIM are given in Figure 4.8. The IR spectrum for PPyBBIM has been previously reported [100], and the spectrum obtained here is in good agreement. However, no IR spectrum was available for comparison with PBPyBBIM. Computational calculations were employed to predict the absorbance spectrum for a representative fragment of PBPyBBIM. Optimization and frequency calculations were performed using the B3LYP hybrid functional and 3-21G basis set. The fragment modelled represents 1.5 units of the polymer chain. The structure used and the predicted spectrum are given in Figure 4.9. Absorbance energies were scaled by 0.965 [98]. Although predicted absorbance energies show slight deviation from experimentally obtained values, the predicted spectrum shows reasonable agreement with the experimental spectrum. Based on similarities in absorbance envelopes, two of the strongest absorbances observed experimentally (1600 and 1506 cm^{-1}) can be reasonably matched with computed vibrations due to asymmetric (1564 cm^{-1}) and symmetric (1390 cm^{-1}) wagging of the bipyridine ring, respectively. Being strong absorbances, these vibrations prove useful in identification of PBPyBBIM on carbon surfaces.

Due to the strong absorbance of electromagnetic radiation by Vulcan XC72, the raw spectra for polymers synthesized in the presence of the carbon powder exhibited strong absorbance throughout the 400 - 4000 cm^{-1} window. The raw data for these samples was therefore modified using the Opus software suite (Version 6.5). Data was modified by (i) baseline correction, and (ii) 25 point smoothing (Savitzky-Golay algorithm). Infrared spectra of VulcPPyB-BIM and VulcPBPyBBIM are shown alongside their freestanding counterparts in Figure 4.8. Both samples possessed very poor spectral resolution due to the intense absorption of light by the carbon support. For VulcPBPyBBIM, only
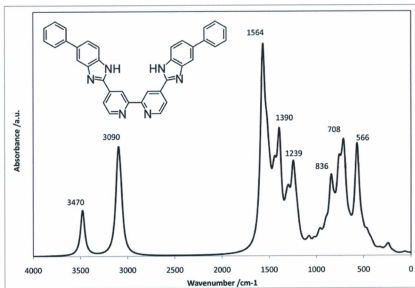
Figure 4.9: Predicted infrared absorbance spectra for a representative fragment of PBPyBBIM. Calculations performed using B3LYP/3-21G and scaled as described in text.

the asymmetric bipyridine wag is clearly visible, at 1592 cm^{-1}. Other vibrations appear to be present but are impossible to assign. Due to poor resolution, the spectrum obtained for VulcPPyBBIM reveals no absorbance bands conclusively indicative of PPyBBIM.

Attempts were made to obtain ^{1}H NMR spectra on VulcPPyBBIM and VulcPBPyBBIM using solid state, magic angle spinning. These attempts yielded no legible spectra, likely due to Vulcan XC72's ability to hold electric charge.

Although analytical techniques failed to confirm the presence on polymers on the carbon surface, more rudimentary tests suggest that immobilization of the polymer was successful. Addition of VulcPBPyBBIM and VulcPPyBBIM to conc. H$_2$SO$_4$ produced stable, cloudy solutions. These solutions were similarly colored to H$_2$SO$_4$ solutions of PBPyBBIM and PPyBBIM. In contrast, suspension of Vulcan XC72 in conc. H$_2$SO$_4$ results in the powder rapidly settling out. Observation of a stable, cloudy solution is reminiscent of the behavior of modified single-walled carbon nanotubes, which have been reported to become "soluble" in organic solvents following modification with alkyl chains [134]. Here, immobilization of polymer material on the carbon surface may be inducing a similar type of behavior. Were the polymer chains free-standing and separate from the carbon support, one would expected unmodified Vulcan XC72 to settle out of suspension. Similar tests using DMA resulted in slight discoloration of the solution, but the carbon powder rapidly settled out of solution.

4.3   Conclusions

The apparent surface coverage limit described in Chapter 3 prompted the development of a novel approach for modification of Vulcan XC72. Immobi-

lization of a pyridine (or bipyridine) containing polymer using benzimidazole chemistry was identified as a possible approach. Immobilization of a polymer on Vulcan XC72 would produce a complex system that would be difficult to study. Therefore, a study was carried out to determine the feasibility of the approach using a simpler system. Anthraquinone was once again utilized for testing purposes. Targeting the carboxylic acid groups on the surface of Vulcan XC72, reaction of 1,2-diamino-9,10-anthraquinone with the carbon surface was executed using common benzimidazole forming conditions (heating in polyphosphoric acid). Evidence of unwanted side reactions prompted the use of less extreme conditions associated with the Phillips benzimidazole synthesis. Combination of XPS and CV results suggest that the benzimidazole forming condensation reaction proceeds when Vulcan XC72 is heated in a solution of 1,2-diamino-9,10-anthraquinone in 4 M HCl(aq).

Reaction of 1,2-diamino-9,10-anthraquinone with Vulcan XC72 produced two forms of anthraquinone under these conditions. The first form is believed to be the desired form, where anthraquinone is bound to the carbon surface through a benzimidazole ring. This form exhibited reversible behavior when studied with CV, with the electrochemical peaks centered at -0.020 V vs. SCE. The second form exhibited voltammetric peaks at -0.180 V which are unstable to electrochemical cycling. This form is believed to be physisorbed 1,2-diamino-9,10-anthraquinone. However, it is possible that the species is bound to the surface through an amine linkage [106]. These assignments were supported by XPS results.

The model system study was expanded to involve a series of reactions. The reaction of 3,3'-diaminobenzidine with Vulcan XC72 was followed by reaction of the modified powder with anthraquinone-2-carboxylic acid. The sequential

reaction to produce a chain of two benzimidazole linkages was performed to confirm the ability to build a polymer on the carbon surface. Once again, XPS and CV results suggest the modification proceeded as desired.

Two coordinating polymers were synthesized and characterized by ^{1}H NMR, IR spectroscopy and UV-vis spectroscopy. The polymers were then synthesized in the presence of Vulcan XC72. Characterization of the modified carbon powders produced only weak evidence towards the presence of polymers on the carbon surface. Although the polymers are certainly present in the material, it is uncertain whether the polymers were successfully bound to the surface.

4.4 Experimental

Information regarding instrumentation and chemicals can be found in Chapter 2.

4.4.1 Immobilization of 1,2-diaminoanthraquinone on Vulcan XC72

Using Polyphosphoric acid (PPA). Approximately 25 g of PPA was prepared in a round bottom flask under N_2 atmosphere as described in Chapter 2. The flask was heated to 100 °C, then *ca.* 50 mg of VulcOX (see Section 3.4.1) and *ca.* 50 mg (0.2 mmol) of 1,2-diaminoanthraquinone were added. The mixture was mechanically stirred at 150 °C for 24 h, then poured into a beaker containing 250 mL of water. The mixture was stirred for 10 min before the modified carbon powder was collected by vacuum filtration. Rinsing the modified powder with both ethanol or methanol resulted in red discoloration of the solvents.

The powder was rinsed repeatedly until discoloration ceased. The powder was then ultrasonicated in methanol for 30 min then collected by vacuum filtration. Further rinsing with methanol did not result in a color change. Carbon powder modified by this method is referred to as VulcOX-DAAQ(PPA).

Using 4 M HCl(aq). The following procedure was carried out using both untreated Vulcan XC72 and VulcOX (see Section 3.4.1). A 50 mg portion of Vulc(OX) and 50 mg(0.2 mmol) of 1,2-diaminoanthraquinone were ultrasonicated in 20 mL of 4 M HCl(aq). The suspension was refluxed with stirring overnight. The suspension was cooled to room temperature and the modified powder was collected by vacuum filtration. The modified powder was rinsed successively with ethanol, acetone and water. Carbon powders modified by this method are referred to as Vulc-DAAQ(HCl) and VulcOX-DAAQ(HCl).

4.4.2 Adsorption of 1-Amino-9,10-anthraquinone

Vulcan XC72 (*ca.* 50 mg) was dispersed in 10 mL of 4 M HCl(aq) by ultrasonication. A *ca.* 50 mg portion (0.22 mmol) of 1-amino-9,10-anthraquinone (AAQ) was added to 10 mL of EtOH and the two mixtures were combined. The mixture was heated to reflux to fully dissolve the AAQ, and stirred overnight. The carbon powder was vacuum filtered while hot and rinsed successively with acetone and water. The modified carbon powder is labelled Vulc-AAQ.

4.4.3 Reaction of 1,2-Phenylenediamine with Vulcan XC72

Approximately 50 mg of chemically oxidized Vulcan XC72 and 50.2 mg (4.6 mmol) of 1,2-phenylenediamine were ultrasonicated in 10 mL of 4 M HCl(aq). The mixture was refluxed with stirring overnight. The suspension was cooled

to room temperature and the modified carbon was collected by vacuum filtration. The modified powder was washed by ultrasonication in 15 mL of methanol for 15 min. The powder was once again collected by vacuum filtration and rinsed with methanol.

4.4.4 Reaction of 3,3'-Diaminobenzidine and Anthraquinone-2-carboxylic Acid with Vulcan XC72

Reaction of 3,3'-Diaminobenzidine. Approximately 50 mg of Vulcan XC72 and 54.6 mg (0.24 mmol) of 3,3'-diaminobenzidine were ultrasonicated in 10 mL of 4 M HCl(aq). The suspension was then heated at reflux for 24 h. The mixture was cooled to room temperature and collected by vacuum filtration. The resulting powder was washed with two 30 mL portions of water to remove excess acid. The powder was then sonicated in methanol, collected by vacuum filtration and washed sequentially with methanol and water. The modified powder is labeled Vulc-DAB.

Reaction of Anthraquinone-2-carboxylic Acid. Approximately 25 mg of Vulc-DAB and 30 mg (0.12 mmol) of anthraquinone-2-carboxylic acid were ultrasonicated in 10 mL of 4 M HCl(aq). The suspension was refluxed overnight (*ca.* 21 h). The suspension was cooled and collected by vacuum filtration. The modified powder was washed sequentially with water, methanol and acetonitrile. The powder was then ultrasonicated in methanol, collected by vacuum filtration and washed with methanol and water. The modified powder is labeled Vulc-DAB-AQ.

4.4.5 Synthesis of Free-Standing Polymers

Procedures are based on previously reported procedure for synthesis of poly([6, 6'-bibenzimidazole-2,2;-diyl]-2,5-pyridine) [133].

Poly([6,6'-bibenzimidazole-2,2';-diyl]-2,5-pyridine). Approximately 30 g of PPA was prepared under an N_2 atmosphere as described in Chapter 2. The flask was opened and filled with 2,5-pyridinedicarboxylic acid (0.82 g, 4.9 mmol) and 3,3'-diaminobenzidine (1.04 g, 4.9 mmol). The mixture was stirred at 120 °C for 8 h. An additional 5 g of P_2O_5 was added to ensure consumption of H_2O produced during the reaction, and the mixture was stirred for an additional 15 h. The mixture was then stirred for 36 h at 160 °C, and 50 h at 180 °C. The mixture was cooled and poured into 200 mL of H_2O. The suspension was stirred for 72 h, with the H_2O being changed twice. A mass of 2.494 g (134% yield) was obtained following vacuum filtration and oven drying. To remove the phosphate groups responsible for the excess mass, the rust-colored solid was suspended in 1 M NaOH(aq) for 24 h. The dark solid was collected by vacuum filtration and rinsed three times with 30 mL of H_2O. The sample was dried at 60 °C under vacuum, resulting in 1.430 g of a burgundy colored solid (77% yield). The solid is labelled PPyBBIM. Elemental analysis: Predicted for $C_{19}H_{11}N_5 \cdot 6.31H_2O$: C 53.95; H 5.63; N 16.56; O 23.87. Found: C 54.05; H 4.11; N 15.73. ^{1}H NMR (500 MHz, D_2SO_4), δ /ppm: 9.51 (2.3 H), 9.30 (1 H), 8.84 (0.7 H), 8.05 (5.5 H).

A low hydrogen content was reported in the previous synthesis of PPyB-BIM and was attributed to residual phosphates present in the material [133]. However, in the current work, the poor EA data fit is believed to be due to contaminant metal ions. As is discussed in Chapter 5, several transition met-

als were found to be present in PPyBBIM and PBPyBBIM, primarily copper, iron and zinc. The hypothesis is supported by the fact that a better EA data fit was obtained for polymers following reaction with polypyridyl ruthenium complexes (Section 5.4.4). Displacement of the majority of transition metal ions by polypyridyl ruthenium complexes allows for better modelling of the polymer system, resulting in better data fits.

Poly([6,6′- bibenzimidazole-2,2′-diyl]-4,4′-(2,2′-bipyridine). Approximately 30 g of PPA was prepared under an N_2 atmosphere as described in Chapter 2. The flask was then filled with 3,3′-diaminobenzidine (302 mg, 1.4 mmol) and 2,2′-bipyridine-4,4′-dicarboxylic acid (341 mg, 1.4 mmol). The mixture was stirred at 120 °C for 20 h before an additional 5.0 g of P_2O_5 was added. The mixture was then stirred at 160 °C for 54 h, then 180 °C for 16 h. The mixture was transferred to a beaker containing 200 mL of 0.2 M NaOH (aq) and stirred for 24 h. The solid was collected by vacuum filtration and dried at 60 °C under vacuum. A dark solid weighing 912 mg (141% yield) was obtained. The solid was ground to a brown powder. A 570 mg portion of the powder was suspended in 100 mL of 1 M NaOH(aq) for 24 h. Vacuum filtration and drying resulted in 318 mg of a dark orange solid (*ca.* 94% yield). The dark orange solid is labelled PBPyBBIM. Elemental analysis: Predicted for $C_{24}H_{14}N_6 \cdot 6H_2O$: C 58.29; H 5.30; N 16.99; O 19.41. Found: C 58.43, H 4.41; N 16.17. The poor EA data fit is once again attributed to the presence of metal ions in the polymer. ^1H NMR was performed on PBPyBBIM at 80 °C to enhance spectral resolution. ^1H NMR (600 MHz, D_2SO_4), δ/ppm. Major peaks: 8.17 (d, J = 8.95 Hz, 1 H), 8.22 (d, J = 8.61 Hz, 1 H), 8.29 (s, 1 H), 9.04 (d, J = 5.4 Hz, 1 H), 9.18 (s, 1 H), 9.46 (d, J = 5.75 Hz, 1 H). Minor peaks: 8.15 (s, 0.1 H), 8.98 (d, J = 6.08 Hz, 0.1 H), 8.99 (d, J = 6.00 Hz, 0.1 H), 9.09 (s, 0.1 H), 9.32 (d, J = 6.00 Hz, 0.1 H), 9.40 (d, J = 5.56

Hz, 0.1 H).

4.4.6 Immobilization of Polymers on Vulcan XC72

Syntheses based on previously reported synthesis of poly([6,6'-bibenzimidazole-2,2'-diyl]-2,5-pyridine) [133].

Poly([6,6'-bibenzimidazole-2,2';-diyl]-2,5-pyridine) on Vulcan XC72. Approximately 30 g of PPA was prepared in a round bottom flask under an N_2 atmosphere as described in Chapter 2. Approximately 200 mg of chemically oxidized Vulcan XC72 was crushed to a fine powder and added to the flask. Portions of 3,3'-diaminobenzidine (308 mg, 1.44 mmol) and 2,5-pyridinedicarboxylic acid (240 mg, 1.44 mmol) were then added to the flask. The mixture was stirred under N_2 atmosphere at 120 °C for 6 h, then an additional 5.1 g of P_2O_5 was added to the flask and the temperature was increased to 160 °C. After stirring for *ca.* 72 h the mixture was heated to 180 °C and stirred for a final 7 h. The viscous mixture was allowed to cool and transferred into a beaker containing 300 mL of water. The suspension was stirred for 24 h, then diluted to 800 mL of water and stirred for another 72 h. A black solid was collected by vacuum filtration and dried in vacuum at 60 °C. A total of 995 mg of black solid was collected and is labelled VulcPPyBBIM.

Poly([6,6'- bibenzimidazole-2,2'-diyl]-4,4'-(2,2'-bipyridine) on Vulcan XC72. Approximately 30 g of PPA was prepared under an N_2 atmosphere as described in Chapter 2. Portions of chemically oxidized Vulcan XC72 (200 mg), 2,2'-bipyridine-4,4'-dicarboxylic acid (339 mg, 1.39 mmol) and 3,3'-diaminobenzidine (299 mg, 1.40 mmol) were added to the flask. The mixture was stirred under N_2 atmosphere at 120 °C for 11 h. An extra 5.0 g of P_2O_5 was added to the flask

and the mixture was stirred at 160 °C for 24 h, then 180 °C for 54 h. The hot, viscous liquid was then poured into 1 L of 2 M NaOH(aq) and stirred for 42 h. Vacuum filtration followed by drying at 60 °C under vacuum yielded 1.187 g of black powder. Suspension of the powder in 80 mL of H_2O produced a basic suspension. The suspension was acidified by addition of conc. HCl. Vacuum filtration and drying yielded 0.650 g of black solid. The black powder is labelled VulcPBPyBBIM.

Immobilization of Ruthenium Complexes on Vulcan XC72

5.1 Introduction

Chapters 3 and 4 explored three different techniques for the modification of carbon powders with organic molecules. In these chapters the spontaneous diazonium reaction, the Phillips benzimidazole synthesis, and the polybenzimidazole synthesis were examined for their ability to immobilize organic molecules on high surface area carbon powders. In this chapter, the ability of these techniques to immobilize transition metal catalysts is explored.

Vulcan XC72 was once again utilized as the carbon support. Surface modifications focused on immobilization of ruthenium complexes through surface bound, bidentate ligands. For the spontaneous diazonium reaction and benzimidazole synthesis this involved immobilization of a polypyridyl ruthenium complex by covalent immobilization of a 1,10-phenanthroline ligand. For polymeric systems, the monomer units of both PBPyBBIM and PPyBBIM are expected to act as bidentate ligands. Therefore, polypyridyl ruthenium complexes were directly reacted with VulcPPyBBIM and VulcPBPyBBIM.

Two ruthenium complexes were used for modification of carbon powders. These included *cis*-bis(2,2′-bipyridine) dichlororuthenium(II) (Ru(bpy)$_2$Cl$_2$) and *cis*-bis(2-(2-pyridyl)benzothiazole) dichlororuthenium(II) (Ru(pbt)$_2$Cl$_2$). The first complex was used in initial experiments as a model complex. The second complex was used to examine the ability to immobilize complexes that can electrocatalytically reduce CO$_2$ [135].

Due to the commercial availability of 5-amino-1,10-phenanthroline (phenNH$_2$, **1** in Scheme 5.1) and the fact that phenanthroline has been widely studied as a ligand in ruthenium complexes, phenNH$_2$ was chosen as the anchoring ligand for the diazonium portion of this study. The aryl amine in phenNH$_2$ is nec-

essary for synthesis of a diazonium ion. Two routes for immobilization of the metal complex were envisioned in such a system. Both routes should yield $[Ru(L)_2(phen)]^{2+}$ covalently anchored to Vulcan XC72 through the phenanthroline ligand and are depicted in Scheme 5.1.

In the direct route, $[Ru(bpy)_2(phenNH_2)]^{2+}$ was first synthesized. The amine located on the phenanthroline ligand was then converted to a diazonium ion using an aqueous solution containing $NaNO_2$ and HCl. Introduction of Vulcan XC72 was expected to result in the spontaneous reaction between the complex and the carbon surface. In the indirect route, $phenNH_2$ was first converted to a diazonium ion. The ion was then allowed to react with the carbon surface. The appropriate precursor ruthenium complex was then reacted with the surface immobilized phenanthroline.

Immobilization of ruthenium complexes on the surface using a benzimidazole linkage was examined using only an indirect approach. Reaction of 5,6-diamino-1,10-phenanthroline with Vulcan XC72 was carried out, then followed by reaction of the modified powder with $Ru(L)_2Cl_2$, where L is 2,2'-bipyridine (bpy) or 2-(2'-pyridyl)benzothiazole (pbt).

Both VulcPPyBBIM and VulcPBPyBBIM were examined for their ability to bind ruthenium complexes. For comparison purposes, the freestanding polymers were also examined.

Ruthenium (II) complexes containing six pyridine-based ligands normally exhibit one reversible oxidation and several reversible reductions. The oxidation wave is due to a Ru(III)/Ru(II) redox process, while the reductions are ligand localized. The electrochemical potentials of Ru(III)/Ru(II) processes have been shown to vary predictably based on the nature of the ligands [136]. For example, in acetonitrile solution the standard potential of $Ru(bpy)_2Cl_2$, which pos-
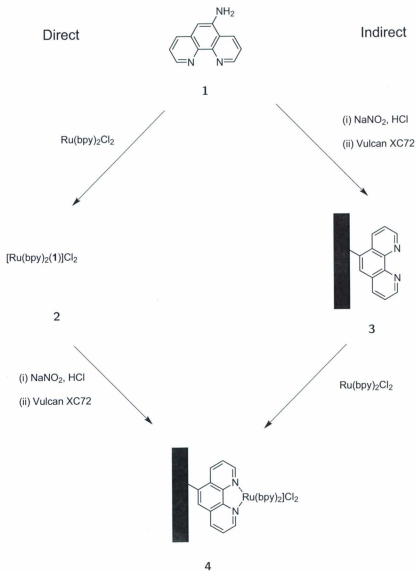
Scheme 5.1: Proposed direct immobilization and indirect immobilization of a ruthenium complex on Vulcan XC72 using diazonium reactions.
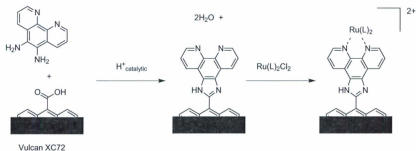
Scheme 5.2: Proposed immobilization of ruthenium complexes (L = bpy or pbt) on Vulcan XC72 using a benzimidazole linkage.

sesses four bonds to π-electron withdrawing pyridine groups and two bonds to electron donating chloride, is found around 0.58 V vs. NHE. Replacement of the two chloride ligands with a phenanthroline ligand, $[Ru(bpy)_2(phen)]^{2+}$, shifts the standard potential to approximately 1.55 V vs. NHE [136].

This predictable variability of the Ru(III)/Ru(II) redox couple makes it attractive for monitoring the modification of carbonaceous materials. Reaction of $Ru(bpy)_2Cl_2$ with a surface immobilized phenanthroline ligand, or coordinating polymer, would produce ruthenium coordinated to six pyridine-based ligands. Covalent attachment of the phenanthroline ligand to the carbon surface may be expected to alter it's electronic nature. However, substitution of phenanthroline has been shown to affect only small changes on the standard potential for Ru(III)/Ru(II) [136]. Therefore, the surface immobilized complex would be expected to possess an oxidation potential near 1.5 V vs. NHE (*ca.* 1.26 V vs. SCE). If the incoming ruthenium complex were simply adsorbed, it would possess four pyridine-based ligands and two chlorides, giving it an oxidation potential nearly 1 V less positive. Monitoring the Ru(III)/Ru(II) process rather than the ligand reductions also simplifies quantification of the immobilized complex, as it eliminates the possibility of interference due to overlap

142

between multiple processes.

Where possible, voltammetric quantification of samples was carried out as described in Chapter 3. The charge under the one electron Ru(III)/Ru(II) oxidation peak was used. Surface coverages are given in the same mol g^{-1} unit used for anthraquinone in Chapter 3.

The presence of ruthenium on the modified carbon powders allowed for their characterization by several other instrumental techniques. Namely, x-ray fluorescence spectroscopy (XRF) and thermogravimetric analsis (TGA) were employed. XRF was used to confirm the presence of ruthenium in the modified carbon powders. Both TGA and XRF were used for quantification.

When excited by x-rays, ruthenium exhibits 5 fluorescence emissions: 2.56 (Lα_1), 2.68 (Lβ_1), 19.28 (Kα_1), 21.65 (Kβ_1), and 22.07 (Kβ_2) keV. The most intense emissions are the Kα_1 and Kβ_1 lines. The presence of emissions at these locations is indicative of the presence of ruthenium in a sample.

Table 5.1: Mixing ratios used for creation of XRF calibration standards.

	Mass Used (mg)		Concentration
Standard No.	1.0% Ru mixture^a	Vulcan XC72	% Ru
1	0	200	0
2	19.5	179.3	0.10
3	40.0	159.6	0.20
4	57.8	139.9	0.30
5	81.8	119.5	0.41

^{a} created by mixing 5.4 mg of RuCl$_3 \cdot$ 3 H$_2$O with 205.3 mg Vulcan XC72

In this work, ruthenium was quantified through a calibration curve created using the Kα_1 and Kβ_1 emissions. Calibration standards were created by a two step process. First, 5.4 mg of RuCl$_3 \cdot$ 3 H$_2$O, which is 38.7% Ru, was mixed with 205.3 mg of Vulcan XC72 to give a powder with a concentration of 1.0% Ru (wt/wt). Portions of the resulting ruthenium mixture were then mixed with

Vulcan XC72 according to Table 5.1 to obtain samples with the desired concentration of ruthenium, ranging from 0 to 0.41% Ru. The linear calibration curve created using these five standards exhibited an R^2 value of 0.93. As the x-axis of the calibration curve is mass percent of 200 mg standards, samples examined must be weighed and the raw data corrected for mass differences using equation 5.1.1. Where C_{Ru} is the corrected concentration of ruthenium (% mass), I_{Ru} is the ruthenium concentration according to the calibration curve (% mass), and m is the mass of the sample in mg.

$$C_{Ru} = \frac{200 I_{Ru}}{m} \tag{5.1.1}$$

To test the accuracy of the calibration curve, a 5.9 mg sample of $Ru(bpy)_2Cl_2$ was analyzed. The ruthenium complex has a theoretical ruthenium concentration of 20.87%. The calibration curve indicated an average I_{Ru} value of 0.627% ruthenium. Using these values with equation 5.1.1, a C_{Ru} value of 21.3% was obtained. The close agreement between experimental and theoretical values suggests that the approach utilized provides an accurate measurement of ruthenium concentration.

When analyzing the ruthenium modified carbon powders, the surface coverage of ruthenium was calculated using equation 5.1.2. The corrected concentration of ruthenium was multiplied by the sample mass to obtain the mass of ruthenium present. Dividing the mass of ruthenium by the molecular weight of ruthenium, 101.07 g mol^{-1}, yields the moles of ruthenium present. This can be converted to the surface coverage of ruthenium, in mols g^{-1}, by dividing by the mass of Vulcan XC72 (m_{Vulc}). The mass of Vulcan XC72 present is estimated by subtraction of the mass of ruthenium complex present (bridging ligand in-
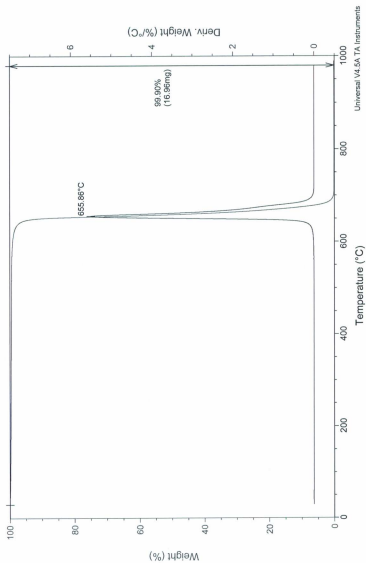
Figure 5.1: Thermogram obtained from a dynamic, high-resolution TGA scan on 16.97 mg of untreated Vulcan XC72 under an air atmosphere.
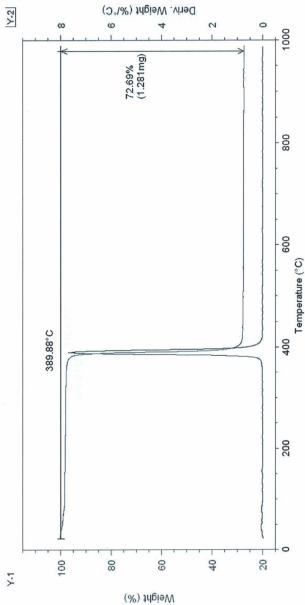
Figure 5.2: Thermogram obtained from a dynamic, high-resolution TGA scan on 1.76 mg of Ru(bpy)$_2$Cl$_2$. TGA performed under an air atmosphere.

cluded) from the total sample mass.

$$\Gamma_{Ru} = \frac{C_{Ru}m}{MW_{Ru}m_{Vulc}} \tag{5.1.2}$$

To obtain quantitative information, thermogravimetric analysis was performed in an air atmosphere. A dynamic, high-resolution scan was utilized in which the ramp rate automatically varied between 1 and 50 °C min^{-1}, dependant on the rate of mass change.

The thermogram obtained for a 16.97 mg portion of untreated Vulcan XC72 is given in Figure 5.1, and that for a 1.76 mg sample of Ru(bpy)$_2$Cl$_2$ is shown in Figure 5.2. A single mass loss event was observed for Vulcan XC72, in which a total of 16.96 mg, or 99.9%, of the sample was lost. The mass loss event showed a peak mass loss at 647 °C. This mass loss event is attributed to the combustion of the carbon black. The fact that only 0.1% of the original mass remained following the scan indicates that nearly complete combustion of Vulcan XC72 occurs. A single mass loss event was also observed for Ru(bpy)$_2$Cl$_2$, at 390 °C. A 27.3% residual mass was observed, the residue obtained was a fine black powder with a blue sheen. The theoretical residual mass for the decomposition of Ru(bpy)$_2$Cl$_2$ to RuO$_2$ is 27.5%, obtained by dividing the molecular weight of RuO$_2$ by that for Ru(bpy)$_2$Cl$_2$.

From these results, it can be inferred that any residual mass in a ruthenium modified sample is due to the presence of ruthenium oxide, RuO$_2$. The molecular weight of RuO$_2$, 133.07 g mol^{-1}, can be used to convert the residual mass into the moles of ruthenium present. The mass of ruthenium complex present on the surface can then be calculated. Subtraction of the mass of ruthenium complex from the total mass yields the mass of Vulcan XC72. Dividing the

moles of ruthenium present by the mass of Vulcan XC72 yields the ruthenium surface coverage in mol g^{-1}, the same units used for voltammetric and XRF quantifications.

5.2 Results and Discussion

5.2.1 Electrochemistry

Indirect modifications of Vulcan XC72 with $[Ru(L)_2(phen)]^{2+}$ using the spontaneous diazonium reaction were carried out following the procedure described in Section 5.4.1, where L is bpy or pbt. Abbreviations for specific samples are included in the experimental descriptions. Cyclic voltammetry on ruthenium modified powders consistently produced poor electrochemical behavior.

A cyclic voltammogram acquired for VulcPhenRu(bpy)$_2$ deposited on glassy carbon, focused on the Ru(III)/Ru(II) process, is depicted in Figure 5.3. The initial cycle on this modified carbon seems to exhibit a single oxidation peak at 1.47 V vs. SCE with no corresponding reduction on the reverse scan. Subsequent cycles exhibited no redox activity at this potential, but revealed small reversible peaks with $E_{1/2}$ of 1.32 V. This behavior may be explained using the results of the anthraquinone study on the role of physisorption (Section 3.2.4). The anthraquinone study showed that a significant portion of the diazonium reagent was adsorbed onto the carbon surface rather than being covalently bound. Assuming that 9,10-phenanthroline similarly adsorbs, reaction of Ru(bpy)$_2$Cl$_2$ with the physisorbed ligand may yield $[Ru(bpy)_2(L')]^{2+}$, where L' is the phenanthroline based ligand that was adsorbed onto the carbon surface. The apparent irreversibility may then be explained by the desorption of the
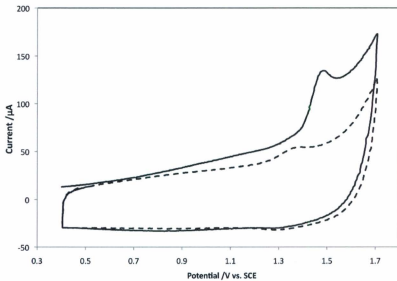
Figure 5.3: Cyclic voltammogram of VulcPhenRu(bpy)$_2$. The solid line is the first cycle, the dashed line is the second cycle. Cyclic voltammetry performed in CH$_3$CN containing 0.1 M NEt$_4$BF$_4$ at 100 mV s^{-1} with modified carbon deposited on a glassy carbon working electrode.

ruthenium complex upon oxidation. The small reversible peaks are tentatively assigned to the covalently immobilized complex. The small difference in half-wave potentials can be explained by differences in the electronic structure between the covalently immobilized phenanthroline ligand and the physisorbed ligand.

Ruthenium complexes with sulfur containing ligands such as pbt have been shown to exhibit electrocatalytic activity towards the reduction of CO_2 [135]. As such, immobilization of $[Ru(pbt)_2(phen)]^{2+}$ on the carbon surface would satisfy the goal of immobilizing an electrocatalytic complex on high surface area carbon. A cyclic voltammogram for VulcPhenRu(pbt)$_2$ deposited on carbon fiber paper is presented in Figure 5.4. The modified carbon exhibited an increase in anodic current above +0.5 V and an increase in cathodic current below -1.0 V. However, on reverse scans there was no mirrored increase in current. No clear peaks are observed in the voltammogram, only a broad increase in current. A cyclic voltammogram of VulcPhenRu(bpy)$_2$ deposited on carbon fiber paper revealed similar behavior to that observed on glassy carbon. An anodic current increase was observed with an onset of *ca.* +1.0 V vs. SCE. On the reverse scan, a cathodic peak is clearly visible at +1.29 V. These currents are attributable to the Ru(III)/Ru(II) process that was observed for the modified powder deposited on glassy carbon. On the negative scan, a current onset of -1.23 V initiates what appears to be a series of reduction peaks, attributable to the ligand based reductions of the polypyridyl ruthenium complex. The reverse scan produced anodic current that was similar in magnitude, suggesting reversible behavior.

The direct reaction between $[Ru(bpy)_2(phenNH_2)]^{2+}$ and Vulcan XC72 was attempted by *in-situ* diazonium ion generation . The effect of reaction temperature was examined. Conversion of the arylamine to a diazonium ion would
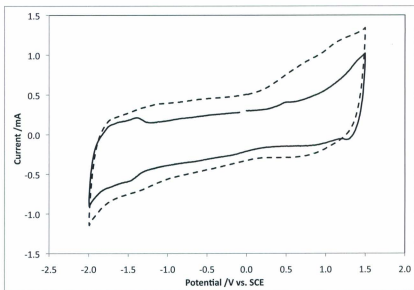
Figure 5.4: Cyclic voltammograms for VulcPhenRu(bpy)$_2$ (solid line) and VulcPhenRu(pbt)$_2$ (dashed line). Cyclic voltammetry performed in CH$_3$CN containing 0.1 M NEt$_4$BF$_4$ at 100 mV s^{-1} with modified carbon deposited on a carbon fiber paper electrode.

result in three positive charges on the complex. As such, the diazonium ion would be expected to be much less stable than Fast Red AL salt. The reaction was performed at room temperature and in an ice bath to determine if this had any affect on the spontaneous reaction. The effect of an increase or decrease of oxygen functionality on the surface of Vulcan XC72 was also explored. Experimental procedures are given in Section 5.4.1.

Vulcan XC72 was pretreated using the methods described in Sections 3.4.1 and 3.4.2. Heat treatment under an inert atmosphere was used to decrease the oxygen content of the carbon powder; chemical oxidation by refluxing in concentrated HNO_3 was used to increase the oxygen content. Surface coverages were estimated as described in Chapter 3, where surface coverage was calculated for electrodes containing a known mass of modified carbon powder. Surface coverage results as estimated by cyclic voltammetry are given in Table 5.2.

Table 5.2: Surface coverages for direct immobilization of $[Ru(bpy)_2(phen)]^{2+}$ on Vulcan XC72 as determined by cyclic voltammetry.

| | Γ_{Ru} | |
Sample	(x 10^{-6} mol g^{-1})	(x 10^{-12} mol cm^{-2})[a]
VulcRu(rt)	2.7 ± 0.9	2.1
VulcOX-Ru	7.8 ± 0.6	5.9
VulcHT-Ru	3.1 ± 1.8	2.3

[a] calculated assuming 131 m^2 g^{-1}

No difference in surface coverage was observed between untreated and heat treated Vulcan XC72. Cyclic voltammetric measurements indicated a ruthenium surface coverage of approximately 3.1 x 10^{-6} g mol^{-1}. Using a specific surface area of 131 m^2 g^{-1} for Vulcan XC72 [101], this translates to a coverage of 2.3 x 10^{-12} mol cm^{-2}. Chemically oxidized Vulcan XC72 was observed to produce a surface coverage of 7.8 x 10^{-6} mol g^{-1}, which is approximately 5.9 x 10^{-12} mol cm^{-2}.

Using a molecular radius of 7.1 Å, Abruña *et al.* estimated a monolayer of polypyridyl ruthenium complexes to be on the order of 8×10^{-11} mol cm^{-2} [137]. Although the observed surface coverage for chemically oxidized Vulcan XC72 is almost triple the value observed for the other two samples, it is less than 10% of a theoretical monolayer. Considering the role of constriction, and the results of Chapter 3, this seems to be a reasonable value.

Aryldiazonium ions are very reactive species which are prone to decomposition in the presence of nucleophiles such as hydroxide ions [107]. Reduced temperatures and acidic conditions are capable of stabilizing diazonium ions. The direct reaction, which requires acidic conditions, was performed at room temperature and in an ice bath to probe whether rapid decomposition of the diazonium ions may be responsible for the low surface coverages. Comparison of voltammograms, Figure 5.5, reveals subtle differences between the modified materials depending on whether the reaction was performed at room temperature or in an ice bath.

When employing an ice bath, the modified materials were found to exhibit a single, reversible electrochemical process with an $E_{1/2}$ of 1.32 V vs. SCE. The peaks exhibited a ΔE_p of 20 mV at a scan rate of 100 mV s^{-1}, which decreased to 10 mV at 50 mV s^{-1}. This behavior approaches the 0 mV that is indicative of a surface immobilized species [124], and suggests that the observed peaks were due to the desired modified carbon. In addition, the peak locations are identical to those assigned to the Ru(III)/Ru(II) redox couple in VulcPhenRu(bpy)$_2$ obtained by the indirect spontaneous diazonium reaction.

When the reaction was performed at room temperature, a second reversible electrochemical process was observed with an $E_{1/2}$ of 1.09 V vs. SCE. The major process remains that which is attributed to the Ru(III)/Ru(II) process. Interest-
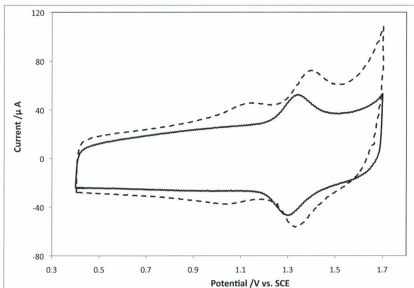
Figure 5.5: Cyclic voltammograms obtained for VulcRu (solid line) and Vul-cRu(rt) (dashed line). Cyclic voltammetry performed in CH₃CN containing 0.1 M NEt₄BF₄ at 100 mV s⁻¹ with the modified carbon deposited on a glassy carbon working electrode.

ingly, this minor peak was stable to electrochemical cycling and gave a ΔE_p of 60 mV at 100 mV s^{-1}. This suggests that it is due to a diffusion limited, reversible process [124]. The nature of this minor process is not yet understood, but the results suggest that a second reaction pathway exists for the spontaneous diazonium reaction between ruthenium complexes and Vulcan XC72 when performed at room temperature. The major process observed in the voltammogram possessed a half-wave potential of 1.36 V. The region in which the peak was observed indicates that this process is due to the Ru(III)/Ru(II) redox process. However, this process was located 40 mV more positive than was observed for the sample modified using an ice bath.

The shift in peak location suggests that a slightly different form of the ruthenium complex was immobilized on the surface when the reaction was performed at room temperature. A possibility is that polymerization of the diazonium containing complex is occurring, resulting in a metallopolymer immobilized on the surface. Formation of a metallopolymer on the surface would explain the observed shift in half-wave potential. Although sub-monolayer surface coverages are expected when using the spontaneous diazonium reaction ([71], Chapter 3), a number of recent publications have reported evidence suggesting that the spontaneous diazonium reaction can result in polymerization on the surface of carbon materials [138, 139].

The benzimidazole approach for immobilization of phenanthroline on Vulcan XC72 and the subsequent reaction with Ru(bpy)$_2$Cl$_2$, or Ru(pbt)$_2$Cl$_2$, was accomplished as described in Section 5.4.2. Carbon powders modified using this technique exhibited peculiar electrochemical behavior. Cyclic voltammograms for VulcBenzRu(bpy)$_2$ and VulcBenzRu(pbt)$_2$, shown in Figure 5.6, exhibited small, poorly defined electrochemical peaks. The half-wave potentials

observed for the modified powders are compared to selected polypyridyl ruthenium complexes in Table 5.3.

Table 5.3: Half-wave potentials for VulcBenzRu(pbt)$_2$, VulcBenzRu(bpy)$_2$ and selected polypyridyl ruthenium complexes.

Sample	Half-wave Potential /V vs. SCE			
VulcBenzRu(bpy)$_2$		-1.26^d	-1.68^d	
[Ru(bpy)$_2$(phenNH$_2$)](PF$_6$)$_2$^{e}	1.34^b	-1.36	-1.55	-1.80
VulcBenzRu(pbt)$_2$	0.2 - 1.2^c	-1.08	-1.27	-1.73^d
[Ru(bpy)(pbt)$_2$](PF$_6$)$_2$^{e}	1.40	-1.06	-1.27	-1.73
Ru(pbt)$_2$Cl$_2$^{e}	0.43		-1.36	-1.50

^{a} broad, shapeless reduction with -1.30 V onset. Two weak oxidation peaks observed
^{b} oxidation peak potential given, reverse reduction peak distorted by broad reduction current
^{c} broad, irreversible oxidation
^{d} reduction current doesn't form a peak, potential of oxidation peak given
^{e} obtained from solution of complex in acetonitrile containing 0.1 M NEt$_4$BF$_4$

The 0 to 1.5 V region for VulcBenzRu(bpy)$_2$ exhibited no electrochemical peaks, although the expected Ru(III)/Ru(II) process should reside here. In the same region, VulcBenzRu(pbt)$_2$ exhibited a broad oxidative current with no corresponding reduction current. This behavior resembles that of the carbon powders modified using the diazonium method deposited on carbon fiber paper, where oxidation currents in this region were followed by little or no reduction current.

The 0 to -2.0 V region revealed several processes for both carbon powders modified using the benzimidazole approach. A comparison of VulcBenzRu(pbt)$_2$ with the electrochemical behavior of acetonitrile solutions of Ru(pbt)$_2$Cl$_2$ and [Ru(bpy)(pbt)$_2$](PF$_6$)$_2$ suggests that the desired complex may be present on the surface. Two redox processes were observed in this region for Ru(pbt)$_2$Cl$_2$, with half-wave potentials of -1.36 and -1.50 V vs. SCE. Replacing the two chloride
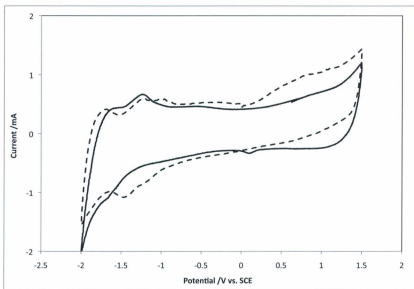
Figure 5.6: Cyclic voltammograms of VulcBenzRu(bpy)$_2$ (solid line) and VulcBenzRu(pbt)$_2$ (dashed line). Cyclic voltammetry performed in CH$_3$CN containing 0.1 M NEt$_4$BF$_4$ at 100 mV s^{-1} with modified carbon deposited on a carbon fiber paper electrode.

ligands with a bipyridine ligand resulted in three sets of peaks: -1.06, -1.27 and -1.73 V. Two sets of peaks were observed for VulcBenzRu(pbt)$_2$, with estimated half-wave potentials of *ca.* -1.08 and -1.27 V. A sharp reduction current increase is observed at the edge of the scan window that induces an oxidative peak at -1.73 V. These electrochemical processes occur at potentials very similar to the ligand-based reductions of [Ru(bpy)(pbt)$_2$](PF$_6$)$_2$. This suggests that although a Ru(III)/Ru(II) peak is not observed, the desired complex may in fact be present on the surface.

It is more difficult to compare the 0 to -2.0 V region for VulcBenzRu(bpy)$_2$ with solvated complexes. The modified carbon powder exhibited a shapeless current increase with an onset of *ca.* -1.20 V. Two oxidation peaks are then observed in the reverse scan, with peak potentials of -1.26 and -1.68 V. Cyclic voltammetry on an acetonitrile solution of Ru(bpy)$_2$(phenNH$_2$)](PF$_6$)$_2$ revealed electrochemical processes at 1.34, -1.36, -1.55 and -1.80 V. While the oxidation peaks observed for VulcBenzRu(bpy)$_2$ (-1.26 and -1.68 V) match reasonably to the -1.36 and -1.55 V processes of [Ru(bpy)$_2$(phenNH$_2$)](PF$_6$)$_2$, the voltammogram does not show enough definition to draw any conclusions. Due to the absence of clear Ru(III)/Ru(II) redox peaks, quantification using cyclic voltammetry could not be performed.

As described in Section 5.4.3, modification of VulcPPyBBIM with Ru(bpy)$_2$Cl$_2$ was carried out using two different solvents. Initially, 75% EtOH was employed. Dimethylformamide (DMF) was subsequently used in order to achieve a higher reaction temperature. Voltammograms for both samples, given in Figure 5.7, showed no substantial differences from one another.

Both voltammograms exhibited an irreversible oxidation peak located at 1.0 V. This is in the region expected for a ruthenium complex with six pyridine-
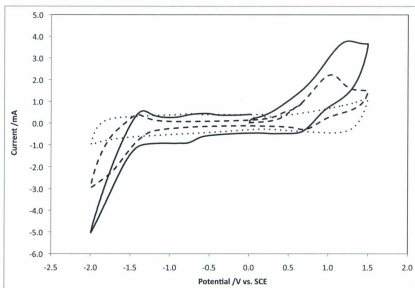
Figure 5.7: Cyclic voltammograms for VulcPPyBBIM-Ru(bpy)$_2$. Voltammograms shown for modification performed in 75% EtOH (solid line) and DMF (dashed line). Also included is a voltammogram of unmodified Vulcan XC72 (dotted line). Cyclic voltammetry performed in CH$_3$CN containing 0.1 M NEt$_4$BF$_4$ at 100 mV s^{-1} with modified carbon deposited on a carbon fiber paper electrode.

based ligands. The reverse scan does not include a corresponding reduction. Continuing the reduction scan, a current increase was observed with an onset of -1.3 V for the sample modified in 75% EtOH, and -1.2 V for that modified in DMF. These reduction currents are followed by a significantly smaller oxidation peak at -1.38 (EtOH) and -1.46 V (DMF) on the reverse scan.

Reaction of VulcPBPyBBIM with both Ru(bpy)$_2$Cl$_2$ and Ru(pbt)$_2$Cl$_2$ produced voltammograms with characteristics comparable to ruthenium-modified Vul-cPPyBBIM. Shown in Figure 5.8, both voltammograms exhibited an oxidation current with an onset of *ca.* 1.0 V. The irreversible oxidation peak was not as sharp as observed for ruthenium-modified VulcPPyBBIM. Irreversible reduction currents were observed with an onset of -0.5 V for VulcPBPyBBIM-Ru(bpy)$_2$ and -0.9 V for VulcPBPyBBIM-Ru(pbt)$_2$. Both VulcPBPyBBIM-Ru(bpy)$_2$ and VulcPBPyBBIM-Ru(pbt)$_2$ were observed to exhibit greater uncompensated resistance than the ruthenium-modified VulcPPyBBIM samples, as evidenced by the sloped baselines. The PBPyBBIM powders did not exhibit any oxidation current in the -1 to -2 V region.

It is interesting that the use of a polybenzimidazole resulted in an oxidation peak in the location expected for oxidation of a ruthenium complex, but lacks the expected electrochemical behavior in the -1 to -2 V region while the use of a single benzimidazole linkage produces the opposite behavior: the expected ligand redox behavior in the -1 to -2 V region and no ruthenium oxidation peaks.

In an attempt to gain insight into this unusual electrochemical behavior, a sample of free-standing PPyBBIM was reacted with Ru(bpy)$_2$Cl$_2$ using a similar procedure (Section 5.4.4). A cyclic voltammogram obtained from a film of the polymer deposited on carbon fiber paper is included and discussed in more detail in Chapter 6. The voltammogram showed a shapeless, irreversible
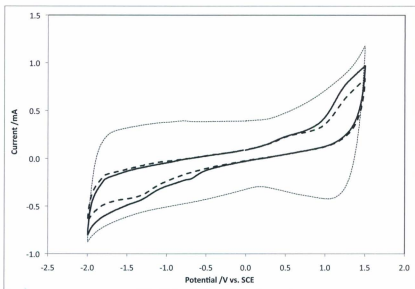
Figure 5.8: Cyclic voltammograms for VulcPBPyBBIM-Ru(bpy)$_2$ (solid line), VulcPBPyBBIM-Ru(pbt)$_2$ (dashed line) and unmodified Vulcan XC72 (dotted line). Cyclic voltammetry performed in CH$_3$CN containing 0.1 M NEt$_4$BF$_4$ at 100 mV s^{-1} with modified carbon deposited on a carbon fiber paper electrode.
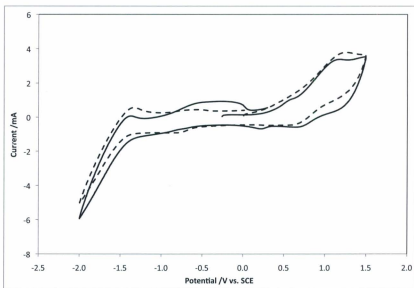
Figure 5.9: Cyclic voltammograms for a 3:1 physical mixture of PPyBBIM-Ru(bpy)$_2$ and Vulcan XC72 (solid line), and one for VulcPPyBBIM-Ru(bpy)$_2$ (dashed line). Cyclic voltammetry performed in CH$_3$CN containing 0.1 M NEt$_4$BF$_4$ at 100 mV s^{-1} with modified carbon deposited on a carbon fiber paper electrode.

reduction current with an onset of -1.0 V. Interestingly, it was found that simply mixing the free-standing, modified polymer with Vulcan XC72 (3 polymer : 1 Vulc, wt/wt) altered the electrochemical behavior. Shown in Figure 5.9, it was observed that physically mixing Vulcan XC72 with the modified polymer produced a voltammogram nearly identical to that of VulcPPyBBIM-Ru(bpy)$_2$. The irreversible nature of the Ru(III)/Ru(II) process exhibited by all of the polymer modified powders precludes the use of cyclic voltammetry for quantitative information.

5.2.2   Examination of Modified Carbons Using XRF and TGA

Although cyclic voltammetry could not be used to quantify ruthenium on the surface of all modified carbon powders, the presence of ruthenium provides a handle for other analytical techniques. Introduced in Section 5.1, both XRF and TGA were used in an attempt to quantify ruthenium immobilized on the surface. The techniques were used to examine two of the diazonium modified carbon samples (VulcRu(rt) and VulcPhenRu(pbt)$_2$), the two benzimidazole modified carbon samples (VulcBenzRu(bpy)$_2$ and VulcBenzRu(pbt)$_2$), and the three polymer modified carbon samples (VulcPPyBBIM-Ru(bpy)$_2$, VulcPBPyBBIM-Ru(bpy)$_2$ and VulcPBPyBBIM-Ru(pbt)$_2$).

Thermogravimetric analysis was employed to quantify ruthenium in each of the modified powders. To achieve this, the temperature was increased from room temperature to 1000 °C under an air atmosphere. Under such conditions all elements present in the modified powders, with the exception of ruthenium, would be expected to be oxidized to gaseous products. Oxidation of ruthenium in the sample would lead to formation of RuO$_2$, a solid. The residue

present upon completion of the TGA scan can therefore be used to determine the amount of ruthenium present in the sample. Unless otherwise noted, all temperatures given in this section refer to the peak observed in the differential thermogram.

In Section 5.1, unmodified Vulcan XC72 was shown to undergo combustion at 648 °C. Here, two carbon powders modified using the diazonium approach were observed to have no mass loss events at this temperature. Figure 5.10 shows the thermogram and differential thermogram (dm/dT) obtained for VulcRu(rt). The thermogram for VulcPhenRu(pbt)$_2$ is included in Appendix B. Both modified powders exhibited two significant mass loss events, with mass loss being complete by 650 °C. The differential TGA trace indicates that the first mass loss event occurred at 461 °C for the VulcRu(rt) and 429 °C for the VulcPhenRu(pbt)$_2$. The first mass loss event was much sharper, and resulted in a smaller mass loss than the second event for both samples. The second mass loss event occurred at 561 °C for VulcRu(rt) and 552 °C for VulcPhenRu(pbt)$_2$. This mass loss event proceeded more slowly than the first event, as indicated by the broad shape of the differential TGA trace, and resulted in a larger mass loss. A fine, dark powder with a blue sheen was observed following completion of the TGA scan to 1000 °C. A TGA scan on Ru(bpy)$_2$Cl$_2$ (Section 5.1) revealed a single, sharp mass loss event at 390 °C. The residual mass confirmed the identity of the dark residue to be RuO$_2$.

Due to the rapid nature of the mass loss, and the small degree of mass loss compared to the second thermal event, it is believed that the first mass loss event is due to decomposition of ruthenium in the sample. Further, the mass loss during the event suggests the presence of the desired ruthenium complex. The TGA scan on VulcRu(rt) was performed on 4.827 mg of modified powder.
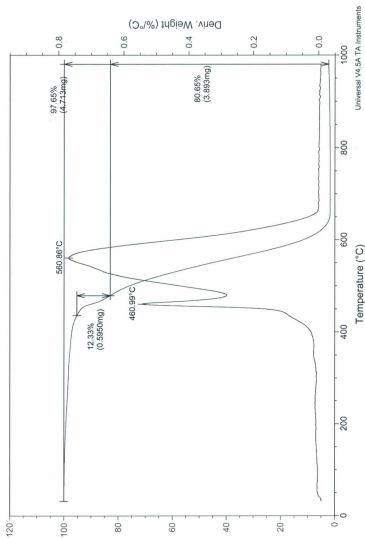
Figure 5.10: Thermogram obtained from a dynamic, high-resolution TGA scan on 4.83 mg of VulcRu(rt). TGA performed under air atmosphere.

A total of 0.114 mg of residue was observed following the TGA scan, or 0.857 mmol of RuO_2. Multiplication of the moles of ruthenium atoms present with the molecular weight of $[Ru(bpy)_2(phen)]Cl_2$ indicates that the modified powder should contain 0.569 mg of ruthenium complex. The experimentally observed mass loss for the first process, 0.595 mg, is very close to the theoretical value. Similarly, the TGA scan on VulcPhenRu(pbt)$_2$ indicates that 0.537 mg of $Ru(phen)(pbt)_2]Cl_2$ should be present in the modified powder. Experimentally, a loss of 0.593 mg was observed.

The second thermal event is attributed to the combustion of the carbon support. It is interesting to note that the presence of ruthenium in the sample appears to have a catalytic affect on combustion of the carbon powder, allowing it to proceed approximately 100 °C lower than observed for unmodified Vulcan XC72 (Figure 5.1).

Carbon powders modified using the benzimidazole approach produced similar results. Included in Figure 5.11 are the thermogram and differential thermogram for VulcBenzRu(bpy)$_2$. Those for VulcBenzRu(pbt)$_2$ are presented in Appendix B. TGA traces for both VulcBenzRu(bpy)$_2$ and VulcBenzRu(pbt)$_2$ also possessed two thermal processes: a small, sharp mass loss followed by a large, broad mass loss. As shown in Table 5.4, mass losses were observed in similar locations as observed for the samples modified using the diazonium approach.

Thermograms obtained for three polymer modified samples exhibited three mass loss processes each, listed in Table 5.4. The thermogram for VulcPBPyBBIM-Ru(bpy)$_2$ is shown in Figure 5.12, thermograms for the other two samples are included in Appendix B. For all three samples the first mass loss is below 100 °C and is attributed to liberation of adsorbed H_2O. The second mass loss for all samples is in a similar location to that attributed to oxidation of ruthenium in

166
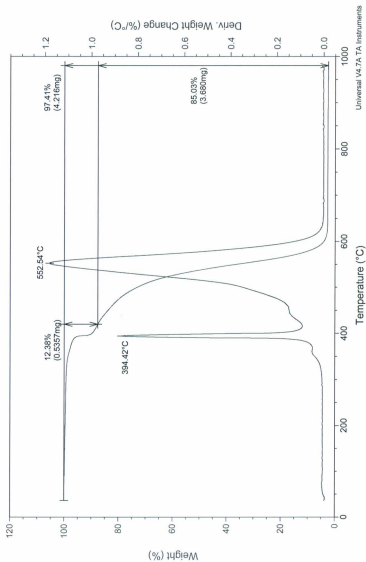
Figure 5.11: Thermogram obtained from a dynamic, high-resolution TGA scan on 4.33 mg of VulcBenzRu(bpy)$_2$. TGA performed under air atmosphere.
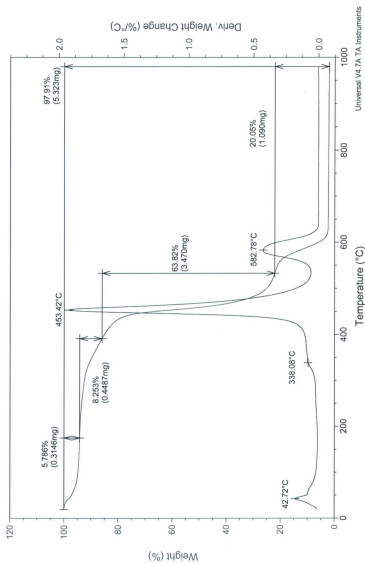
Figure 5.12: Thermogram obtained from a dynamic, high-resolution TGA scan on 5.44 mg of VulcPBPyBBIM-Ru(bpy)₂. TGA performed under air atmosphere.

Table 5.4: Temperature of observed mass loss processes for ruthenium modified carbon powders.

Sample	$T_1{}^a$	$T_2{}^a$	$T_3{}^a$	Residue
		°C		mass %
VulcRu(rt)		462	561	2.4
VulcPhenRu(pbt)$_2$		429	552	2.6
VulcBenzPhenRu(bpy)$_2$		394	553	2.6
VulcBenzPhenRu(pbt)$_2$		433	560	1.2
VulcPPyBBIM-Ru(bpy)$_2$	45	404	567	5.1
VulcPBPyBBIM-Ru(bpy)$_2$	43	453	583	2.1
VulcPBPyBBIM-Ru(pbt)$_2$	41	442	561	2.4

each of the previous samples. The third mass loss falls in the region attributed to combustion of Vulcan XC72 in the previous samples. In VulcPBPyBBIM-Ru(bpy)$_2$ and VulcPBPyBBIM-Ru(pbt)$_2$, the mass loss around 450 °C was observed to be the major process in the thermogram, contributing to mass loss of 63.8 and 63.7%, respectively. The mass loss attributed to combustion of Vulcan XC72 only contributed 20.0 and 19.5% for these two samples. This is quite different than the results observed for VulcPPyBBIM-Ru(bpy)$_2$. For this sample, a mass loss of 21.0% was observed at 403 °C, and 61.8% can be attributed to combustion of Vulcan XC72.

In an attempt to gain insight into the differences between carbons modified by the two types of polymers, TGA was performed on the free-standing polymers as well as polymer modified carbon powders (prior to exposure to ruthenium). The thermograms for PPyBBIM, PBPyBBIM, VulcPBPyBBIM and VulcPPyBBIM, are shown in Appendix B. The results suggest that the amount of polymer present varied between VulcPPyBBIM and VulcPBPyBBIM.

PPyBBIM was observed to lose 11.7% of it's mass under 100 °C. PBPyBBIM was observed to lose 13.0% in this same region. Polybenzimidazoles are known to be hygroscopic, allowing these mass losses to be assigned to liberation of ad-

sorbed H_2O. Both polymers then underwent a two step decomposition. A large mass loss was observed at 535.0 °C for PPyBBIM and 543.9 °C for PBPyBBIM. A smaller mass loss was then observed at 784.6 °C for PPyBBIM and 587.1 °C for PBPyBBIM. It should be noted that neither polymer underwent 100% mass loss. Residue of 4.8% and 7.8% were observed for PPyBBIM and PBPyBBIM, respectively. However, no solid residue was visible on the sample holder for either sample.

VulcPPyBBIM was observed to undergo a 19.7% mass loss between 400 and 550 °C. This was followed by a 69.1% mass loss at 639 °C. Based on the thermogram of PPyBBIM, the mass loss between 400 and 550 °C can be attributed to oxidation of the polymer. The location of the second mass loss allows assignment to the combustion of Vulcan XC72. Subtracting H_2O from the total mass, it can be estimated that $ca.$ 22% of the mass of VulcPPyBBIM is due to PPyBBIM. A 3.3% mass residue was present on completion of the scan on VulcPPyBBIM.

In contrast, VulcPBPyBBIM showed much different behavior. A 6.2% mass loss was observed below 100 °C, attributable to H_2O adsorbed to the polymer. The 400 to 650 °C region revealed a sharp mass loss near 500 °C. The differential thermogram revealed a separate process, as evidenced by a shoulder centered around 575 °C. The total mass loss for this region was 65.3%. A final mass loss event was observed at 733.2 °C, which resulted in a mass loss of 15.8%. The mass loss in the 400 to 650 °C region is consistent with that observed for PBPyBBIM, and is therefore attributed to oxidation of the polymer. The mass loss attributed to H_2O liberation is approximately one-tenth the mass of the polymer, which is also consistent with the results obtained for PBPyB-BIM. Therefore the mass loss at 733.2 °C must be due to combustion of Vulcan XC72. Subtracting the mass of H_2O from the total mass, the mass loss due to

PBPyBBIM (400-650 °C region) represents *ca.* 70% of the total mass. A 2.5% mass residue was present on completion of the scan on VulcPBPyBBIM.

Thermogravimetric analysis was also performed on three ruthenium modified, free-standing polymers: PPyBBIM-Ru(bpy)$_2$, PBPyBBIM-Ru(bpy)$_2$ and PBPyBBIM-Ru(pbt)$_2$. These polymers were prepared as described in Section 5.4.4. The thermogram for PBPyBBIM-Ru(bpy)$_2$ is presented in Figure 5.13. Thermograms for the other samples are included in Appendix B. Under 100 °C all three samples resulted in a mass loss of approximately 10%, consistent with the amount of H$_2$O adsorbed in PPyBBIM and PBPyBBIM. All three samples then exhibited a single, very sharp mass loss event. This event was located at *ca.* 420 °C for both PBPyBBIM samples and produced a mass loss of approximately 83%. For PPyBBIM-Ru(bpy)$_2$, a mass loss of 75.1% was observed at 404.9 °C. On completion of the scan, a dark powder was visually observed. The differences between the thermograms for unmodified and ruthenium-modified polymers suggest that RuO$_2$ catalyzes the oxidation of the polymer.

Results from TGA on carbon powders modified using each of the three approaches indicate that ruthenium was present in each of the samples. As mentioned in Section 5.1, the assumption that all mass residue is due to RuO$_2$ allows the quantification of ruthenium in the sample. The observation of near quantitative mass loss for Vulcan XC72 suggests that the assumption is valid for samples modified using the spontaneous diazonium reaction and Phillips benzimidazole synthesis. The significant residue observed for VulcPPyBBIM and VulcPBPyBBIM may invalidate the assumption for powders modified using the polybenzimidazole approach. However, the observation that RuO$_2$ catalyzes oxidation of the polymer may induce complete loss of the polymer, and therefore makes the assumption valid. The data for powders modified using
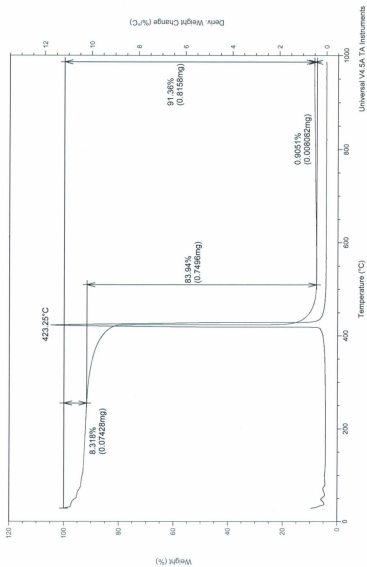
Figure 5.13: Thermogram obtained from a dynamic, high-resolution TGA scan on 0.89 mg of PBPyBBIM-Ru(bpy)$_2$. TGA performed under air atmosphere.

all three approaches was analyzed under the assumption that the final residue was completely due to RuO$_2$. Comparison of results from TGA and XRF will reveal the validity of this assumption.

Surface coverages of polypyridyl ruthenium complexes were calculated as described in Section 5.1 and are presented in Table 5.5. Residual mass percentages are the uncorrected, experimentally observed values. Surface coverage values are given in moles of ruthenium complex per gram of Vulcan XC72, and moles of ruthenium per square centimeter of surface area. Surface area was calculated assuming a specific surface area of 131 m^2 g^{-1} for Vulcan XC72 [101].

Table 5.5: Surface coverages of ruthenium complexes on Vulcan XC72 as determined by TGA.

Sample	$C_{Ru}{}^{a}$ (mass %)	Γ_{Ru} (x 10^{-4} mol g^{-1})	Γ_{Ru} (x 10^{-10} mol cm^{-2})^{b}
VulcRu(rt)	1.8	2.0	1.5
VulcPhenRu(pbt)$_2$	2.0	2.3	1.8
VulcBenzPhenRu(bpy)$_2$	2.0	2.3	1.7
VulcBenzPhenRu(pbt)$_2$	0.9	1.0	0.7
VulcPPyBBIM-Ru(bpy)$_2$	3.9	6.1	4.6
VulcPBPyBBIM-Ru(bpy)$_2$	1.6	6.1	4.6
VulcPBPyBBIM-Ru(pbt)$_2$	1.8	7.0	5.4

^{a} calculated assuming mass residue is pure RuO$_2$
^{b} calculated assuming 131 m^2 g^{-1}

For samples modified using the spontaneous diazonium reaction or the Phillips benzimidazole reaction, calculation of the mass of Vulcan XC72 was straightforward. The mass of Vulcan XC72 was obtained by subtraction of the mass of ruthenium complex from the total mass. The mass of ruthenium complex present was estimated by multiplication of the moles of RuO$_2$, calculated from residue, by the molecular weight of the complex in question, including the bridging phenanthroline ligand. For samples modified using the polybenzimidazole approach, calculations were more complex. The moles of ruthenium

were first calculated from the residual mass. The mass of the precursor ruthenium complex (i.e. Ru(bpy)$_2$Cl$_2$ or Ru(pbt)$_2$Cl$_2$) was then subtracted from the total mass, yielding the combined mass of Vulcan XC72, polymer and adsorbed H$_2$O. The mass of H$_2$O was then subtracted, taken to be the mass loss below 100 °C, leaving the mass of Vulcan XC72 and polymer. The mass of Vulcan XC72 was obtained by multiplying this value by the percentage of mass believed to be due to Vulcan XC72. Based on the thermograms and earlier discussion, the percentage of mass believed to be due to Vulcan XC72 are 78% for VulcPPyB-BIM and 30% for VulcPBPyBBIM.

Reliance on an unproven assumption for quantification of ruthenium in the modified powders using TGA introduced an unknown amount of uncertainty in the results. It is therefore important to compare the results obtained with results of an alternate technique. X-ray fluorescence spectroscopy is a fundamentally different analytical technique, making it an excellent choice .

The XRF emission spectra for VulcRu(rt) and VulcPBPyBBIM-Ru(pbt)$_2$ are given in Figure 5.14. The XRF spectra exhibited strong emission lines at 19.2 and 21.6 keV, as did all other ruthenium modified powders examined. These emission lines correspond to the K$_{\alpha 1}$ and K$_{\beta 1}$ emissions that are characteristic of ruthenium, confirming the presence of ruthenium atoms in all seven modified powders. A calibration curve was prepared as described in Section 5.1. Linear regression of the calibration curve revealed an R^2 value of 0.93. The calibration curve was successful at accurately determining the amount of ruthenium present in Ru(bpy)$_2$Cl$_2$. Quantitative results obtained using the calibration curve are presented for the seven modified polymers in Table 5.6. The amount of Vulcan XC72 present in each modified powder was estimated with the same method used for TGA results.
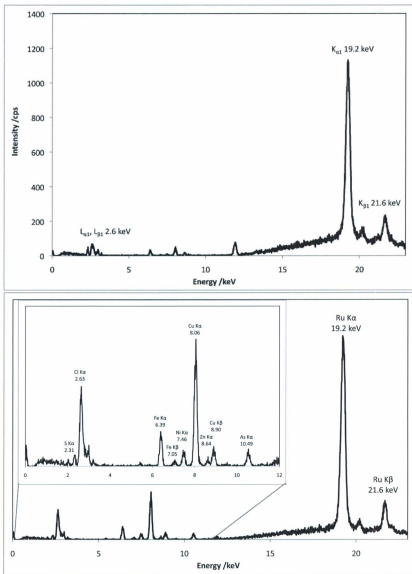
Figure 5.14: X-ray fluorescence spectra for VulcRu(rt) (top) and VulcPBPyBBIM-Ru(pbt)$_2$ (bottom). Characteristic ruthenium emission lines are labelled.

Table 5.6: Surfaces coverage of ruthenium complexes on Vulcan XC72 as determined by XRF spectroscopy.

Sample	C_{Ru} (mass %)	Γ_{Ru} (x 10^{-4} mol g^{-1})	Γ_{Ru} (x 10^{-10} mol cm^{-2})^a
VulcRu(rt)	1.2	1.2	0.9
VulcPhenRu(pbt)$_2$	1.8	2.0	1.6
VulcBenzRu(bpy)$_2$	2.3	2.7	2.1
VulcBenzRu(pbt)$_2$	1.1	1.2	0.9
VulcPPyBBIM-Ru(bpy)$_2$	2.3	3.7	2.8
VulcPBPyBBIM-Ru(bpy)$_2$	1.6	6.5	5.0
VulcPBPyBBIM-Ru(pbt)$_2$	2.3	9.8	7.5

^{a} calculated assuming 131 m^2 g^{-1}

Although distilled H_2O was used in all steps, XRF spectra revealed the presence of metal impurities in the modified powders. Besides the ruthenium emissions, powders modified using the spontaneous diazonium reaction and the Phillips benzimidazole synthesis exhibited K_α emissions of bromine (11.90), copper (8.07 keV), iron (6.36 keV) and chlorine (2.60 keV). Powders modified with polybenzimidazoles exhibited emissions for arsenic (10.49 keV), zinc (8.64 keV), copper (8.09 keV), nickel (7.46 keV), iron (6.39 keV) and chlorine (2.63 keV). Modified powders that were reacted with Ru(pbt)$_2$Cl$_2$ exhibited emissions at 2.30 keV, attributable to sulfur K_α emission. Considering that coordinating ligands (or polymers) are being immobilized on the surface, the modified powders must be binding trace amounts of the elements from the water used to wash them. The presence of arsenic in polymer modified samples must originate from the polyphosphoric acid; likely an impurity in *ortho*-phosphoric acid.

To further test the agreement between XRF and TGA for quantification of ruthenium in samples, the amount of ruthenium present in ruthenium modified polymers was examined. Each of the three modified polymers prepared as

described in Section 5.4.4 were examined. Commercial elemental analyses (EA) were obtained and XRF was performed on these samples, and the results compared to TGA results. Information regarding EA acquisition and data fitting is given in Chapter 2.1.

Although it was difficult to produce a good fit of the EA data for unmodified polymer samples (Chapter 4), good fits of the EA data were obtained for ruthenium modified polymers. Data fitting for PBPyBBIM-Ru(bpy)$_2$ suggested a ratio of 1 Ru(bpy)$_2$Cl$_2$: 1.49 PBPyBBIM monomer units: 4.63 H$_2$O molecules. This fit resulted in predicted CHN values within 0.16% of the experimentally obtained values. The predicted structure contains a ruthenium content of 8.9% (wt/wt). The data for PPyBBIM-Ru(bpy)$_2$ also produced an excellent fit. A ratio of 1 Ru(bpy)$_2$Cl$_2$: 1.46 PPyBBIM monomer units: 5.48 H$_2$O molecules resulted in a difference of less than 0.10% between the predicted and experimentally obtained CHN values. The predicted structure contains a ruthenium content of 9.8% (wt/wt). The data for PBPyBBIM-Ru(pbt)$_2$ was more difficult to model. The best fit of the data produced differences as high as 0.60% between measured and predicted elemental composition. However, a significant sulfur content (3.38%) was measured in PBPyBBIM-Ru(pbt)$_2$, indicating that the pbt ligand must be present in the material. In turn, this suggests that the polymer is acting as a coordinating ligand for polypyridyl ruthenium complexes, proving the viability of using the polymers to immobilize ruthenium on carbon surfaces.

The amount of ruthenium is presented in Table 5.7, expressed in the mass percent of ruthenium, as determined by the three analytical methods. Values given represent the mass of ruthenium present divided by the total mass of sample examined.

For all three samples, the three techniques yielded a fairly large spread in

Table 5.7: Ruthenium content (wt/wt) in polypyridyl ruthenium modified co-ordination polymers.

Sample	EA	XRF	TGA
PPyBBIM-Ru(bpy)$_2$	9.8%	7.4%	9.3%
PBPyBBIM-Ru(bpy)$_2$	8.9%	4.0%	6.6%
PBPyBBIM-Ru(pbt)$_2$	5.3%	3.5%	5.3%

results. Absolute differences of 1.8 to 4.9% were observed. EA consistently suggested the highest amount of ruthenium. TGA results consistently suggested a larger amount of ruthenium than XRF results, which is also the general trend in the data obtained for surface coverage of ruthenium in modified powders (Table 5.5 and Table 5.6). Elemental analysis consistently produced results closer to those acquired by TGA. It therefore seems that although both XRF and TGA may underestimate the amount of ruthenium in the sample, with TGA likely closer to the true value.

Taking the surface coverage values as indicated by TGA (Table 5.5), a ruthenium surface coverage range of 1.0×10^{-4} mol g^{-1} (VulcBenzPhenRu(pbt)$_2$) to 2.3 $\times 10^{-4}$ mol g^{-1} (VulcPhenRu(pbt)$_2$ and VulcBenzPhenRu(bpy)$_2$) was observed. These values are comparable to the highest surface coverages measured for immobilization of anthraquinone in Chapter 3 (ca. 1.5×10^{-4} mol g^{-1}). Modification using the polybenzimidazole method resulted in higher ruthenium surface coverages, ranging from 6.1×10^{-4} to 7.0×10^{-4} mol g^{-1}.

Assuming a specific surface area of 131 m^2 g^{-1} for Vulcan XC72, these values translate to a surface coverage range of 0.7×10^{-10} to 1.8×10^{-10} mol cm^{-2}. If the surface area of Vulcan XC72 is taken to be 232 m^2 g^{-1} [71], the surface coverage range decreases to 0.4×10^{-10} to 1.0×10^{-10} mol cm^{-2}. These value are close to the theoretical surface coverage for a monolayer of polypyridyl ruthenium complexes on a flat surface: 8×10^{-11} mol cm^{-2} [137]. The results therefore suggest

that there is enough ruthenium present in the material to constitute between 0.5 and 2.25 monolayers of polypyridyl ruthenium complexes. For the polymer modified samples, a ruthenium surface coverage range of 2.6 x 10^{-10} to 5.4 x 10^{-10} mol g^{-1} was obtained.

The results for the spontaneous diazonium reaction and the Phillips benzimidazole synthesis contradict the results obtained in Chapter 3, as well as the results of Toupin and Belanger [71]. Based on Toupin and Belanger's work and the electrochemical results of Chapter 3, it was estimated that constriction limits the accessible surface area of Vulcan XC72 to approximately 27-55 m^2 g^{-1} for anthraquinone. Being larger than anthraquinone, polypyridyl ruthenium complexes would be expected to be excluded from a larger amount of this surface area. Such restricted access to surface area would indicate several layers of ruthenium complexes in these modified carbons. Decomposition of the complexes to RuO$_2$ under the reaction conditions employed is unlikely. The results therefore support the idea that polymerization of the ruthenium complexes occurred on the carbon surface, as was suggested by cyclic voltammetry results (Figure 5.5).

5.2.3 Check for Adsorption of Ruthenium

Following results of the previous section, attempts were made to remove noncovalently bound material from the surface. Experiments focussed on VulcRu(rt). It was found that soaking 36.3 mg of the modified powder in acetonitrile resulted in discoloration of the solvent. This behavior was not previously observed, although cyclic voltammetry was carried out on the modified powder using acetonitrile based electrolyte solutions. It is possible that failure to

observe discoloration during cyclic voltammetry was due to the small amount of modified carbon present during the electrochemical experiments, typically around 0.3 mg. Discoloration of solvent would be difficult to detect when using such a small amount of modified carbon powder.

The modified carbon powder was successively washed with acetonitrile; it was observed that only the first aliquot of acetonitrile changed color. The acetonitrile washings were decanted and combined in a 50 mL volumetric flask. The modified carbon powder was dried at 95 °C and reweighed. A total of 33.0 mg was collected, a mass decrease of 3.6 mg. The combined acetonitrile washings were a cloudy, dark orange color. Neither allowing the solution to rest undisturbed for 24 h, or centrifugation for 30 min resolved the cloudiness. UV-Visible spectroscopy was performed on the diluted acetonitrile washings, producing the spectrum in Figure 5.15. The UV-Vis spectrum revealed behavior commonly observed for polypyridyl ruthenium complexes. An intense absorbance band was observed at 289 nm, typical of π - π^* transitions for bipyridine ligands. A weaker absorbance band was observed at 450 nm, consistent with MLCT transitions (d-π^*) commonly observed for ruthenium complexes.

In an attempt to identify the species in solution, two solutions were created for comparison. The first solution was created to test whether the discoloration of acetonitrile upon washing the modified carbon was due to adsorption of the precursor ruthenium complex. A 20 μM solution of [Ru(bpy)$_2$(phenNH$_2$)](PF$_6$)$_2$ in acetonitrile was created. The second solution was to test whether the discoloration was due to adsorption of diazonium decomposition products. To prepare the solution, the aryl amine of [Ru(bpy)$_2$(phenNH$_2$)](PF$_6$)$_2$ was converted to a diazonium ion and allowed to decompose under aqueous conditions. The solvent was removed under reduced pressure, and the dark orange
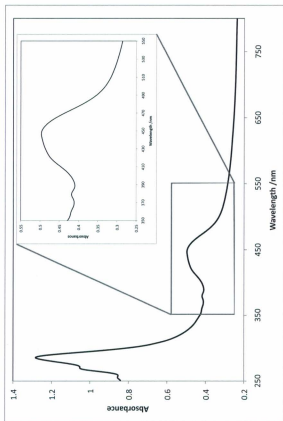
Figure 5.15: UV-Visible spectroscopy on the solution of acetonitrile washings from VulcRu(rt).
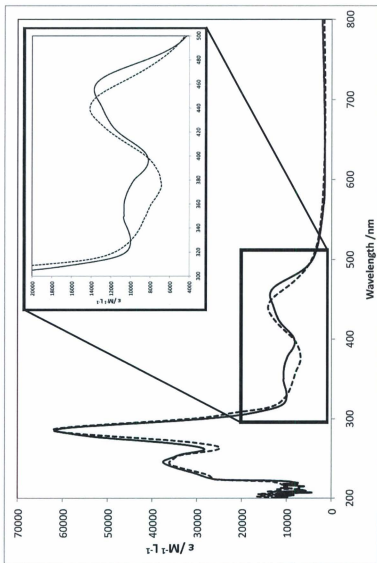
Figure 5.16: UV-Visible spectra of [Ru(bpy)$_2$(phenNH$_2$)](PF$_6$)$_2$ (20 μM solution, solid line) and [Ru(bpy)$_2$(L)](PF$_6$)$_2$ (23 μM solution, dashed line). L is the ligand resulting from the aqueous decomposition of the diazonium ion generated from [Ru(bpy)$_2$(phenNH$_2$)](PF$_6$)$_2$. Solutions prepared in acetonitrile.

residue was redissolved in H_2O. Addition of KPF_6 to the solution resulted in precipitation of a dark orange solid. The product is tentatively labelled as $[Ru(bpy)_2(phenOH)](PF_6)_2$, based on the assumption that decomposition of the diazonium converts the $phenNH_2$ ligand to phenOH. After drying, a *ca.* 23 μM solution of the decomposition product was prepared in acetonitrile. The UV-Vis spectra for both solutions are given in Figure 5.16, absorbance maxima are summarized in Table 5.8.

Table 5.8: Summary of UV-visible absorbance wavelengths (nm) and extinction coefficients (M^{-1} cm^{-1}) observed for acetonitrile solutions of several forms of $[Ru(bpy)_2(phenR)](PF_6)_2$.

Precursor Complex R = NH_2	Decomposed Aryl diazonium R = OH	VulcRu(rt) Washings[a] R = unknown
457 (13680)	439 (14100)	450 (0.495)
422 (shoulder)		422 (shoulder)
361 (10620)		
287 (61080)	286 (62200)	289 (1.23)
246 (37380)	247 (35900)	240 (0.873)

[a] concentration unknown, number in brackets is absorbance

The spectrum of the acetonitrile washings from VulcRu(rt) exhibited a larger background absorbance than the other two samples. In the non-absorbing region of 600-800 nm the acetonitrile washings showed an absorbance increase from 0.237 at 800 nm to 0.266 at 600 nm. The two polypyridyl ruthenium solutions showed an absorbance of 0.031 - 0.041 in this same region. This increased background absorbance is due to the cloudiness of the solution, which is related to the 3.6 mg decrease in mass of the modified powder upon washing.

The spectra of all three solutions exhibited similar π-π^* transitions, located at approximately 287 and 246 nm. The spectrum of $[Ru(bpy)_2(phenNH_2)](PF_6)_2$, exhibited two MLCT transitions: at 457 nm with a shoulder at approximately 422 nm, and at 361 nm. The spectrum of the complex following decomposi-

tion of the diazonium ion exhibited a single MLCT peak at 439 nm. The spectrum of the colored acetonitrile solution obtained from washing the modified carbon powder was not an exact match for either of the other two solutions. It revealed a single MLCT transition at 450 nm, with a shoulder at approximately 422 nm. The location and shape of this absorbance was very similar to that for the precursor complex. However, discoloration of the acetonitrile when washing the modified powder is obviously not due to the adsorbed $[Ru(bpy)_2(phenNH_2)](PF_6)_2$, as the second MLCT transition is not present. From differences in the UV-Vis spectra, it can also be concluded that the discoloration is also not due to adsorption of the diazonium decomposition products.

XRF spectroscopy was performed on the 33.0 mg of modified carbon powder after the acetonitrile washing. A corrected ruthenium concentration (C_{Ru}) of 1.2% was measured, identical to the value obtained before washing.

Results from XRF indicated that the concentration of ruthenium immobilized on the surface was unchanged by acetonitrile washing, although UV-Visible spectroscopy clearly revealed that some polypyridyl ruthenium was dissolved. A possible explanation comes from research concerning carbon nanotubes. It was first shown in 1998 that modification of carbon nanotubes can enhance their solubility in various organic solvents [134]. Although this is typically performed using organic oligomers or polymers, modification of the carbon surface with polypyridyl ruthenium complexes that are highly soluble in acetonitrile might be expected to produce a similar result. Carbon blacks are an amorphous form of carbon; there is a range of particle sizes. The 3.6 mg of lost mass upon washing may be due to the dissolution of very fine carbon particles with polypyridyl ruthenium immobilized on their surface. Such an occurrence would explain the cloudy nature of the washings, the larger background ab-

sorbance in UV-Vis spectroscopy and the ineffectiveness of centrifugation on the acetonitrile washings. It would also explain the lack of change in ruthenium concentration for the modified powder upon washing with acetontrile, although some polypyridyl ruthenium was obviously dissolved.

In order to obtain an approximation of the amount of ruthenium present in the VulcRu(rt) washings, two UV-vis calibration curves were created. The absorbance maxima corresponding to the most intense MLCT transition was plotted against the concentration of ruthenium for $[Ru(bpy)_2(phenNH_2)](PF_6)_2$ (457 nm) and the complex resulting from decomposed diazonium ion (439 nm). Concentrations and absorbance maxima used for calibration curve preparation are listed in Table 5.9. The absorbance values for VulcRu(rt) were modified by correction of background absorbance values. To do this, the difference in absorbance at 600 nm between VulcRu(rt) (0.266) and $[Ru(bpy)_2(phenNH_2)](PF_6)_2$ (0.031) was subtracted across the entire VulcRu(rt) spectrum. The corrected absorbance maximum for the VulcRu(rt), at 450 nm, was 0.260. Both calibration curves estimate the concentration of ruthenium in the VulcRu(rt) washings to be 1.9×10^{-5} M, or a total of 9.5×10^{-7} moles of ruthenium. Dividing this number by 3.6 mg, the amount of material removed from VulcRu(rt) by washing with acetonitrile, yields an estimated ruthenium surface coverage of 2.6×10^{-4} mol g^{-1}. The similarity of this estimation to the ruthenium surface coverage observed for VulcRu(rt) by both XRF and TGA suggests that the dissolution of polypyridyl ruthenium modified carbon particles is a feasible explanation.

Table 5.9: UV-vis absorbance data used for preparation of calibration curves. Absorbance values taken at 457 nm for $[Ru(bpy)_2(phenNH_2)](PF_6)_2$ and 439 nm for $[Ru(bpy)_2(phenOH)](PF_6)_2$.

$[Ru(bpy)_2(phenNH_2)](PF_6)_2$		$[Ru(bpy)_2(phenOH)](PF_6)_2$	
Conc. (mol L-1)	Abs	Conc. (mol L-1)	Abs.
9.9×10^{-6}	0.140	1.2×10^{-5}	0.158
2.0×10^{-5}	0.274	2.3×10^{-5}	0.311
3.0×10^{-5}	0.395	3.5×10^{-5}	0.476
3.9×10^{-5}	0.521	5.8×10^{-5}	0.785
4.9×10^{-5}	0.657	1.2×10^{-4}	1.558

5.3 Conclusions

Polypyridyl ruthenium complexes were immobilized on Vulcan XC72 using several approaches. Each approach included immobilization of a coordinating ligand on the surface. A spontaneous diazonium reaction, which has recently become popular for modification of carbon surfaces with organic molecules, was used to immobilize ruthenium complexes through a phenanthroline moiety. A benzimidazole forming reaction, in which surface bound carboxylate groups were reacted with an aryl diamine, was also used to immobilize a phenanthroline moiety. Two different coordinating polymers were synthesized in the presence of Vulcan XC72. These polymers provided bidentate coordination sites for immobilization of polypyridyl ruthenium complexes.

The quantification of ruthenium on the carbon surface was performed using XRF and TGA. Both techniques indicated ruthenium surface coverages that were approximately two orders of magnitude greater than indicated by cyclic voltammetry. Following previous results, it is unlikely that the spontaneous diazonium reaction or the benzimidazole approach managed to attain monolayer surface coverages of polypyridyl ruthenium complexes. It is therefore likely that alternate forms of ruthenium are present on the surface. Although

the form of all of the immobilized ruthenium was not conclusively revealed, sufficient evidence exists to suggest that some portion of the desired complex is immobilized on the carbon surface. This evidence includes the presence of electrochemical currents in the areas expected for modified powders, the presence of sulfur emission peaks in XRF spectra, TGA behavior, and the behavior observed using UV-vis spectroscopy when testing for adsorption.

The modified powders did not exhibit the exact electrochemical behavior expected for polypyridyl ruthenium complexes, but each of the modified samples exhibited some evidence that the desired ruthenium complexes were immobilized on the surface. Following modification with ruthenium complexes, oxidation peaks were observed in the 1.0 to 1.5 V region for carbon powders modified using the diazonium reaction and coordinating polymer approaches. These peaks can be reasonably assigned to the oxidation of Ru(II) to Ru(III). In the case of materials modified by the diazonium reaction, these oxidations were reversible. Although materials modified by the benzimidazole approach did not exhibit these ruthenium oxidation currents, they did exhibit reversible peaks in the region expected for ligand-based reductions of the respective polypyridyl ruthenium complexes. It is unclear what the cause of the poor electrochemical behvaior is. It is possible that the intimate coupling of the ruthenium complex to the surface of a highly conjugated carbon material alters the electronics of the complex.

XRF spectra acquired on powders that had been modified with $Ru(pbt)_2Cl_2$ exhibited weak emissions in the region expected for sulfur K_α emissions. In TGA, the mass loss event attributed to oxidation of the ruthenium complexes resulted in a loss that was in good agreement with the estimated mass of the ruthenium complex present. Both of these results suggest that the desired com-

plex was present on the surface.

UV-vis spectroscopy results indicated the presence of a form of polypyridyl ruthenium that did not match the spectra obtained for either the precursor ruthenium complex or the product of hydrolysis of the diazonium ion. Estimates of surface coverages made using UV-vis calibration curves indicated a ruthenium surface coverage similar to the values measured using TGA and XRF.

The agreement between XRF and TGA for quantification of ruthenium in modified powders was examined. Freestanding polybenzimidazoles were synthesized and reacted with polypyridyl ruthenium complexes. The ruthenium concentration in these polymers was examined using EA, XRF and TGA. Elemental analysis suggested the highest concentration of ruthenium in each of the three polymers examined. The ruthenium concentration was not directly measured in EA. The second highest concentration of ruthenium was consistently measured by TGA. The large gap between XRF and and the other techniques led us to use ruthenium surface coverages obtained by TGA for surface coverage comparisons.

The estimated ruthenium surface coverage obtained for the spontaneous diazonium reaction and Phillips benzimidazole reaction was 1.0×10^{-4} to 2.3×10^{-4} mol g^{-1}. Literature values for the specific surface area of Vulcan XC72 indicate this surface coverage range to be on the order of 0.5–2.5 monolayers of polypyridyl ruthenium complexes. Accounting for constriction would decrease the accessible area, indicating that enough ruthenium is present to constitute several layers of polypyridyl ruthenium. It is believed that ruthenium containing metallopolymers were likely formed on the surface of Vulcan XC72. This hypothesis was supported by cyclic voltammetry results.

5.4 Experimental

Information regarding instrumentation and chemicals can be found in Chapter 2.

5.4.1 Spontaneous Diazonium Coupling of Polypyridyl Ruthenium Complexes to Vulcan XC72

Indirect Approach. A round bottom flask was filled with 70 mL of 50% MeOH and 15 mg (0.077 mmol) of 5-amino-1,10-phenanthroline (phenNH$_2$). Once dissolved, *ca.* 150 mg of Vulcan XC72 and 7 mL of conc. HCl were added and the mixture was ultrasonicated for 15 min to disperse the carbon powder and cooled in an ice bath. A 0.58 mM solution of sodium nitrite (39.8 mg in 10 mL of H$_2$O) was then added over a 10 min period. The mixture was stirred in the ice bath for 1 hour, then the carbon powder was collected by vacuum filtration. The powder was ultrasonicated in 50% MeOH(aq) for 30 min and washed excessively with H$_2$O and CH$_3$CN. The sample was vacuum dried at 60 °C.

A dark purple solution was made by dissolving Ru(pbt)$_2$Cl$_2$ (31 mg, 52µmol) in 30 mL of 75% EtOH. A 44 mg portion of the modified carbon powder was then dispersed in this solution by ultrasonication. The suspension was refluxed for 45 h. The modified powder was then collected by vacuum filtration, washed excessively with EtOH and dried under vacuum at 60 °C. Modification was also performed using Ru(bpy)$_2$Cl$_2$ in place of Ru(pbt)$_2$Cl$_2$. Samples modified in this way are labelled VulcPhenRu(pbt)$_2$ and VulcPhenRu(bpy)$_2$.

Direct Approach. Vulcan XC72 (*ca.* 100 mg), [Ru(bpy)$_2$(phenNH$_2$)](PF$_6$)$_2$ (53 mg, 0.059 mmol) and NaNO$_2$ (40 mg, 0.58 mmol) were added to a round bottom

flask containing 10 mL of water. The flask was stirred for 10 min, then 2 mL of conc. HCl was added. The reaction mixture was stirred overnight (*ca.* 17 h), then vacuum filtered over a fine glass frit. The modified carbon powder was washed with methanol and dried under vacuum at 60 °C. The reaction was carried out both at room temperature and in an ice bath. Reactions performed in an ice bath are labelled VulcRu, those performed at room temperature are labelled VulcRu(rt). Modifications using chemically oxidized and heat treated Vulcan XC72 were performed in an ice bath and are labelled VulcOX-Ru and VulcHT-Ru, respectively.

5.4.2 Immobilization of Polypyridyl Ruthenium Complexes on Vulcan XC72 Using a Benzimidazole Linkage

In a typical synthesis, a round bottom flask was filled with 50 mL of 4 M HCl(aq) and 5,6-diamino-1,10-phenanthroline (50 mg, 0.23 mmol), producing a yellow solution. Vulcan XC72 (*ca.* 55 mg) was added to the solution and dispersed by ultrasonication. The mixture was refluxed for 23 h, then vacuum filtered. The modified carbon powder was washed with three 30 mL aliquots each of H_2O and EtOH, then dried under vacuum at 60 °C. The modified carbon was then dispersed in 60 mL of 75% EtOH(aq) by ultrasonication. A 50 mg (0.10 mmol) portion of $Ru(bpy)_2Cl_2$ (or $Ru(pbt)_2Cl_2$)was added to the suspension, which was then refluxed for 24 h. The carbon powder was collected by vacuum filtration and washed with three 30 mL aliquots of ethanol. The powder was then ultrasonicated in 30 mL of EtOH for 15 min before being collected by vacuum filtration and dried under vacuum at 60 °C. Carbon powders modified with this technique are labelled VulcBenzRu(bpy)$_2$ and VulcBenzRu(pbt)$_2$.

5.4.3 Reaction of Polypyridyl Ruthenium Complexes With Coordinating Polymers on Vulcan XC72

VulcPBPyBBIM. Modification of VulcPBPyBBIM was executed for Ru(bpy)$_2$Cl$_2$ and Ru(pbt)$_2$Cl$_2$ as follows. A round bottom flask was filled with 50 mL of 50% EtOH and 0.1 mmol of Ru(L)$_2$Cl$_2$ (L = pbt or bpy). A 150 mg portion of VulcPBPyBBIM (from Section 4.4.6) was dispersed in the solution by ultrasonication. The suspension was then refluxed with stirring for 21 h. The carbon powder was collected by vacuum filtration and rinsed with EtOH until the washings ran clear. The samples were then dried under vacuum at 60 °C. Carbon powders modified this way are abbreviated VulcPBPyBBIM-Ru(bpy)$_2$ and VulcPBPyBBIM-Ru(pbt)$_2$.

VulcPPyBBIM. The following reaction was carried out twice, using different solvents. Both 75% EtOH and dimethylformamide were used.

Approximately 50 mg of VulcPPyBBIM (from Section 4.4.6) was dispersed in a solution of Ru(bpy)$_2$Cl$_2$ (75 mg, 0.15 mmol) in 20 mL of solvent. The mixture was ultrasonicated to disperse the carbon powder, then stirred at reflux for 24 h. Upon cooling, the carbon powder was collected by vacuum filtration and rinsed with EtOH until rinsings ran clear. The modified powders were then dried under vacuum at 60 °C. The carbon powder modified this way is abbreviated VulcPPyBBIM-Ru(bpy)$_2$.

5.4.4 Reaction of Polypyridyl Ruthenium Complexes With Free-standing Coordinating Polymers

Poly([6,6'- bibenzimidazole-2,2'-diyl]-4,4'-(2,2'-bipyridine). The following procedure was used for $Ru(bpy)_2Cl_2$ and $Ru(pbt)_2Cl_2$. A 49 mg portion of dark orange colored PBPyBBIM was dispersed in a solution of the appropriate ruthenium complex (0.06 mmol) in 20 mL of 50% EtOH(aq) by ultrasonication. The suspension was refluxed for 20 h. The mixture was allowed to cool and the polymer was collected by vacuum filtration. The polymer was washed with EtOH until washings were clear. Drying under vacuum at 60 °C produced 12 mg of a red solid for the $Ru(bpy)_2Cl_2$ modified polymer, and 34 mg of a dark red solid for the $Ru(pbt)_2Cl_2$ modified polymer. Modified polymers are abbreviated PBPyBBIM-Ru(bpy)$_2$ and PBPyBBIM-Ru(pbt)$_2$.

Elemental analysis: Predicted for $[(C_{24}H_{14}N_6)_{1.49}Ru(bpy)_2]Cl_2 \cdot 4.63H_2O$: C 58.56; H 4.06; N 15.84; O 6.48; Ru 8.85; Cl 6.21. Found: C 58.62; H 4.23; N 15.68. Predicted for $[(C_{24}H_{14}N_6)_{2.67}Ru(bpy)_2]Cl_2 \cdot 16.39H_2O$: C 54.98; H 4.52; N 14.57; O 13.65; S 3.34; Ru 5.26; Cl 3.69. Found: C 54.76; H 3.93; N 15.12; S 3.38.

Poly([6,6'-bibenzimidazole-2,2'-diyl]-2,5-pyridine). The following procedure was used for $Ru(bpy)_2Cl_2$. A solution was made with 55 mg (0.11 mmol) of $Ru(bpy)_2Cl_2$ in 2 mL of 50% EtOH(aq). A 54 mg portion of rust-colored PPyB-BIM was dispersed in the solution by ultrasonication. The suspension was then heated at reflux for 23 h. The powder was collected by vacuum filtration and washed with EtOH until the rinsings ran clear. Drying under vacuum at 60 °C yielded a red solid. Modified polymer is abbreviated as PPyBBIM-Ru(bpy)$_2$.

Elemental analysis: Predicted for $[(C_{19}H_{11}N_5)_{1.46}Ru(bpy)_2]Cl_2 \cdot 5.48H_2O$: C 55.45; H 4.19; N 15.30; O 8.46; Ru 9.76; Cl; 6.84. Found: C 55.42; H 4.10; N

15.37.

A better EA data fit was obtained for all polymers following reaction with $Ru(L)_2Cl_2$ (L = bpy or pbt), compared to unmodified PPyBBIM and PBPyBBIM (Section 4.4.5).

Electrocatalytic Reduction of CO_2 by Polybenzimidazoles

6.1 Introduction

Parts of this chapter have been published in a peer-reviewed journal [140].

The immobilization of coordinating polymers on the surface of Vulcan XC72 and the subsequent addition of ruthenium to the modified material was described in Chapters 4 and 5, respectively. X-ray fluorescence spectroscopy (XRF) and X-ray photoelectron spectroscopy (XPS) confirmed the presence of ruthenium in carbon samples following exposure to $Ru(bpy)_2Cl_2$ or $Ru(pbt)_2Cl_2$. XPS and XRF also confirmed the presence of sulfur in samples that were exposed to $Ru(pbt)_2Cl_2$. The modified carbon powders were not exposed to any other source of sulfur. Therefore, the observation of sulfur confirms the presence of 2-(2-pyridyl)benzothiazole. This suggests that some portion of the ruthenium present in the modified carbon powder is likely in the desired polymer bound form, as shown in Figure 6.1.

However, although polypyridyl ruthenium complexes normally exhibit excellent electrochemical behavior, the modified carbon powders showed poor electron transfer behavior when examined with cyclic voltammetry. The expected $Ru(III)/Ru(II)$ redox peaks were present, but the magnitude was much lower than expected for the amount of ruthenium present in the sample, as measured by TGA and XRF. Moreover, poor electrochemical activity was also observed for analogous polymers that were not bound to Vulcan XC72.

Despite the unexpectedly poor electrochemical behavior, the ability of polymers to electrocatalytically reduce CO_2 was examined. In an effort to simplify the experiments, attention was focussed on polymers that were not bound to Vulcan XC72. However, a surface-bound polymer, Vulc-PBPyBBIM, was examined to ensure that the behavior of the surface bound polymers matched that of

the non-bound polymers.

A total of six polymers, depicted in Figure 6.1, were examined using cyclic voltammetry under four different conditions. The polymers, prepared as described in Chapters 4 and 5, were PPyBBIM, PPyBBIM-Ru(bpy)$_2$, PPyBBIM-Ru(pbt)$_2$, PBPyBBIM, PBPyBBIM-Ru(bpy)$_2$ and PBPyBBIM-Ru(pbt)$_2$. Each polymer was applied to a CFP electrode following the procedure described in Section 6.4.1. Each of the six samples were sequentially examined in 0.1M NEt$_4$BF$_4$ in acetonitrile under the following conditions: (i) anhydrous, N$_2$ purged, (ii) anhydrous, CO$_2$ purged, (iii) 1% H$_2$O (v/v), N$_2$ purged, and (iv) 1% H$_2$O (v/v), CO$_2$ purged. For this work, the term "dry" will be used to indicate anhydrous electrolyte solutions, and "wet" will be used to indicate electrolyte solutions containing 1% H$_2$O (v/v).

PPyBBIM　　　　　**PBPyBBIM**

M =　No metal
　　[Ru(bpy)$_2$] 2Cl
　　[Ru(pbt)$_2$] 2Cl
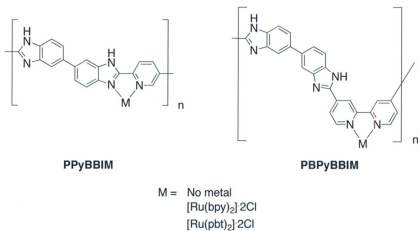
Figure 6.1: Structures of the six polymers examined for the ability to electro-catalytically reduce CO$_2$.

Following cyclic voltammetry on the samples, CO$_2$ electrolyses were performed using two techniques: constant potential electrolysis and constant cur-

rent electrolysis. New electrodes were prepared for each electrolysis. Experimental details can be found in Section 6.4.3.

6.2 Results and Discussion

6.2.1 Cyclic Voltammetry of Polymers

All cyclic voltammetry in this section was acquired using a single electrode supporting a film of each polymer. Each of the six electrodes were examined under each the four different conditions, in the order indicated in Section 6.1.

PPyBBIM Based Polymers

Cyclic voltammetry on PPyBBIM, shown in Figure 6.2, reveals several interesting features. Under anhydrous, N_2 purged conditions, the polymer exhibited no electrochemical activity until approximately -1.7 V vs. SCE, at which point the current was observed to spike.

Under anhydrous, CO_2 purged conditions, a broad, irreversible, cathodic peak was observed. Current onset for the peak was *ca.* -1.30 V, and maximum current was observed at -1.80 V. This irreversible peak was present on repeated cycling (not shown). On repeated cycling, the current onset remained static while the peak potential shifted less negative, to -1.65 V. A corresponding growth in anodic current was observed between ca. -0.5 and 0.0 V. The standard reduction potential for the one electron reduction of CO_2 is -1.90 V vs. NHE [2], indicating that this irreversible peak is not due to the simple one electron reduction of CO_2. To confirm, cyclic voltammetry was carried out under identical conditions, using a blank carbon fiber paper electrode (not shown). The peak
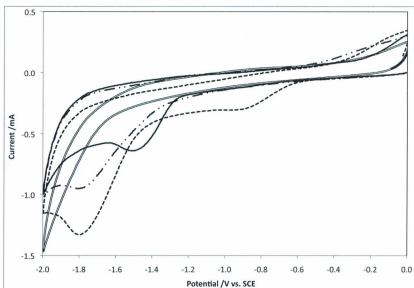
**Figure 6.2:** Cyclic voltammetry on a thin film of PPyBBIM on a strip of carbon fiber paper. Potential swept at 100 mV s^{-1} in 0.1 M NEt$_4$BF$_4$ in CH$_3$CN. Conditions employed were (i) anhydrous, N$_2$ purged (double solid line), (ii) anhydrous, CO$_2$ purged (dash-dot line), (iii) 1% H$_2$O, N$_2$ purged (dashed line), (iv) 1% H$_2$O, CO$_2$ purged (single solid line). See text for details.

in question was not observed. Therefore, the observed electrochemical activity must be caused by interactions between CO_2 and the polymer.

After allowing the electrode to air dry, cyclic voltammetry was performed under wet, N_2 purged conditions. The initial cycle exhibited an irreversible cathodic current with an onset of -0.56 V. A maximum current was reached at -0.8 V and was maintained until -1.4 V. At this point a second irreversible, cathodic peak began, with a peak potential of -1.80 V. On subsequent cycles only the second cathodic feature was observed, shown in Figure 6.3.

To ensure that the presence of H_2O wasn't the cause of the irreversible cathodic peak, a newly prepared PPyBBIM coated electrode was examined with cyclic voltammetry in wet, N_2 purged solution. The second and third cycles of this newly prepared electrode are compared to the initial two cycles of the previously used electrode in Figure 6.3. The first cycle of the new electrode was omitted due to excess H^+ presence from electrode preparation, see Section 6.4.1 for more details. The newly prepared electrode was observed to behave similarly to the PPyBBIM coated electrode in dry, N_2 purged solution. Specifically, the irreversible cathodic peaks were not observed. This confirms that the presence of H_2O is not the cause of the -1.80 V cathodic peak..

The similarity in the irreversible cathodic behavior under dry, CO_2 purged and wet, N_2 purged conditions (following cycling in wet, CO2 purged conditions) suggests the presence of a similar species in both cases. Observation of the peak in dry, N_2 purged solution suggests that CO_2 must be present. Combined with the fact that similar cathodic behavior was not observed for a freshly prepared electrode under wet, N_2 purged conditions, this indicates that CO_2 must have established a strong interaction with the polymer when cycled in dry, CO_2 purged electrolyte solution.
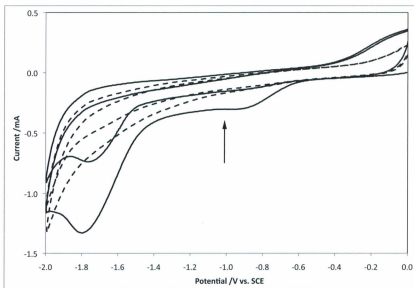
Figure 6.3: Cyclic voltammetry on a thin films of PPyBBIM on a strip of carbon fiber paper. Potential swept at 100 mV s^{-1} in 0.1 M NEt$_4$BF$_4$ in CH$_3$CN. Performed in a 1% H$_2$O, N$_2$ purged solution. The first two cycles of an electrode that was previously cycled in anhydrous, CO$_2$ purged electrolyte solution (solid line), and the second and third cycle of a newly prepared electrode (dashed line) are depicted. First cycle omitted due to large H$^+$ reduction currents, see Section 6.4.

Finally, the original PPyBBIM coated electrode was examined in wet, CO_2 purged solution. A single irreversible cathodic peak was observed with a current onset of -1.20 V and a peak potential of -1.49 V. On subsequent cycles the peak potential shifted to -1.40 V.

Inclusion of ruthenium complexes into the PPyBBIM polymer was found to result in small but important changes in the structure of the voltammograms. Cyclic voltammograms under each of the four conditions are given for PPyBBIM-Ru(bpy)$_2$ and PPyBBIM-Ru(pbt)$_2$ in Figure 6.4 and Figure 6.5, respectively. Under dry, N_2 purged conditions, PPyBBIM-Ru(bpy)$_2$ and PPyBBIM-Ru(pbt)$_2$ exhibited cathodic current increases beginning at -1.1 and -1.4 V, respectively. Based on the location of the electrochemical activity [136] and the fact that no activity was present in this area before ruthenium was introduced, it is believed that this activity is due to ligand based reductions of ruthenium complexes. Poor peak shape and reversibility was observed in this region for all ruthenium containing polymers studied.

When examined in dry, CO_2 purged solution PPyBBIM-Ru(bpy)$_2$ showed a cathodic current onset at -0.64 V. A small cathodic peak, at -0.8 V, was superimposed on a steady current increase. A weak irreversible peak was present at -1.69 V. On subsequent cycles the current growth from -0.64 V disappeared, and the irreversible peak became more pronounced. On cycling, the second peak shifted to -1.62 V, producing a voltammogram very similar to PPyBBIM. Under the same conditions, PPyBBIM-Ru(pbt)$_2$ showed a very weak cathodic current increase at -0.62 V, which gave way to a broad, irreversible peak with a peak potential of -1.76 V. On subsequent cycles the -0.62 V current growth disappeared, and the -1.76 V peak shifted to -1.60 V.

When the same electrodes were examined under wet, N_2 purged conditions,
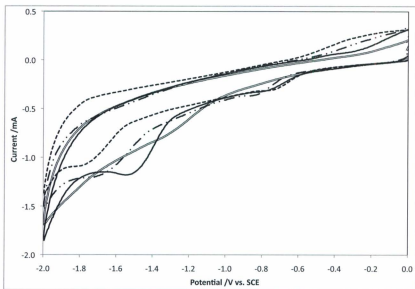
Figure 6.4: Cyclic voltammetry on a thin film of PPyBBIM-Ru(bpy)$_2$ on a strip of carbon fiber paper. Potential swept at 100 mV s^{-1} in 0.1 M NEt$_4$BF$_4$ in CH$_3$CN. Conditions employed were (i) anhydrous, N$_2$ purged (double solid line), (ii) anhydrous, CO$_2$ purged (dash-dot line), (iii) 1% H$_2$O, N$_2$ purged (dashed line), (iv) 1% H$_2$O, CO$_2$ purged (single solid line) See text for details.
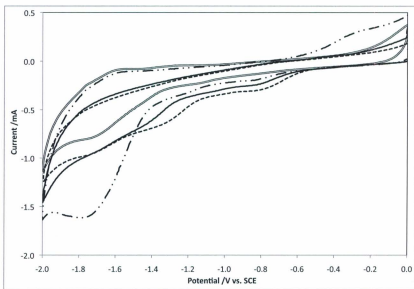
Figure 6.5: Cyclic voltammetry on a thin film of PPyBBIM-Ru(pbt)$_2$ on a strip of carbon fiber paper. Potential swept at 100 mV s^{-1} in 0.1 M NEt$_4$BF$_4$ in CH$_3$CN. Conditions employed were (i) anhydrous, N$_2$ purged (double solid line), (ii) anhydrous, CO$_2$ purged (dash-dot line), (iii) 1% H$_2$O, N$_2$ purged (dashed line), (iv) 1% H$_2$O, CO$_2$ purged (single solid line). See text for details.

both PPyBBIM-Ru(bpy)$_2$ and PPyBBIM-Ru(pbt)$_2$ exhibited a cathodic current increase at -0.47 V. The cathodic current gradually increased until the end of the negative potential sweep. The same behavior was present on subsequent cycles, but at a much smaller magnitude.

Under wet, CO$_2$ purged conditions, the electrodes again showed a cathodic current increase early in the negative potential sweep. PPyBBIM-Ru(bpy)$_2$ once again showed the increase at -0.47 V, while PPyBBIM-Ru(pbt)$_2$ showed the increase at -0.55 V. A small peak was observed at -0.77 V for PPyBBIM-Ru(bpy)$_2$, and -0.80 V for PPyBBIM-Ru(pbt)$_2$. A second, much larger peak was observed to start for PPyBBIM-Ru(bpy)$_2$ at -1.20 V, peaking at -1.52 V. On subsequent cycles this peak shifted to -1.44 V. A second peak was also observed to begin at -1.20 V for PPyBBIM-Ru(pbt)$_2$. However, on the first cycle, the peak was very broad and hard to define. On subsequent cycles, more of a peak-shape developed, with a peak potential at -1.42 V.

It is interesting that although PPyBBIM itself shows no electrochemical activity, exposure to CO$_2$ induced electrochemical activity. This suggests that the polymer and CO$_2$ come together to form an adduct. Two distinct processes are visible in the voltammograms of PPyBBIM. The onset and peak potentials are summarized in Table 6.1. The first process became visible only after electrochemical cycling in dry, CO$_2$ purged electrolyte solution. It had an onset potential of *ca.* -0.47 and a peak potential of -0.86 V. The second process was visible in both dry and wet CO$_2$ purged solutions. It had an onset potential of -1.30 V under dry conditions, and -1.20 V under wet conditions. On the first cycle the peak potential was -1.80 V under dry conditions, and -1.49 V under wet conditions. The first peak was very unstable to repeated cycling. As can be seen in Figure 6.3, it fully disappeared after a single cycle if transferred to N$_2$ purged

solution. When cycled under wet, CO_2 purged conditions, this process was not observed to totally disappear, but did significantly decrease in magnitude. The second peak was more stable to cycling.

Table 6.1: Cathodic peak onset potential and locations observed for PPyBBIM based polymers under anhydrous, CO_2 purged conditions and 1% H_2O, CO_2 purged conditions.

	Dry CO_2		Wet CO_2	
	E_{onset}	$E_p{}^a$	E_{onset}	$E_p{}^a$
PPyBBIM	-	-	-0.47	-0.86
	-1.30	-1.80 (-1.65)	-1.20	-1.49 (-1.40)
PPyBBIM-Ru(bpy)₂	-0.52	-0.83	-0.45	-0.73
	-1.40	-1.67 (-1.62)	-1.27	-1.51 (-1.39)
PPyBBIM-Ru(pbt)₂	-0.64	-0.83	-0.44	-0.80
	-1.36	-1.76 (-1.62)	-1.26	n.d. (-1.38)

n.d. - not distinguishable
[a] Values in brackets indicate E_p on the third cycle

The peak potential for the process at the more negative potential was observed to shift in a positive direction with repeated cycling. This shift in peak potential is likely due to uncompensated cell resistance, not a chemical process. The mathematics (4.2.1) and effect of uncompensated cell resistance was discussed in Chapter 4. The slanted baseline observed for the polymer coated carbon fiber paper electrodes is indicative of cell resistance. The presence of uncompensated cell resistance and the significantly larger current observed on the first cycle compared to subsequent cycles explains the observed shift in peak potential.

Incorporation of ruthenium into the polymer did not seem to interfere with the formation of an adduct. Both of the polymers containing ruthenium also exhibited two distinguishable, irreversible cathodic processes. The onset potential for the observed irreversible peaks varied by only 20-120 mV between the three samples. The peak potentials for both processes were similarly comparable.

The subtle differences between these potentials is likely due to differences in the electronic structure of the polymer upon complexation of ruthenium.

PBPyBBIM Based Polymers

Cyclic voltammetry on a PBPyBBIM modified electrode, shown in Figure 6.6, yielded similar results to the PPyBBIM modified electrode under all conditions except wet, CO_2 purged solution. As summarized in Table 6.2, two irreversible peaks were observed for the polymer once the electrode was exposed to CO_2. However, when examined under wet, CO_2 purged conditions, cyclic voltammetry revealed a significant current growth of the first irreversible cathodic peak. The irreversible cathodic current showed remarkable stability to cycling, as seen in Figure 6.7. A slight current decrease was observed between the first and second cycles. After this point, repeated cycling revealed a steady state.

Table 6.2: Cathodic peak onset potentials and locations observed for PBPyBBIM based polymers under anhydrous, CO_2 purged conditions and 1% H_2O, CO_2 purged conditions.

	Dry CO_2		Wet CO_2	
	E_{onset}	$E_p{}^a$	E_{onset}	$E_p{}^a$
PBPyBBIM	-0.60	-0.86	-0.53	-1.05
	-1.36	n.d.	-	-
PBPyBBIM-Ru(bpy)$_2$	-	-	-	-
	-1.15	-1.77	-1.15	*n.d.*
PBPyBBIM-Ru(pbt)$_2$	-	-	-0.52	-0.86
	-1.15	-1.66	-1.25	-1.62

n.d. - not distinguishable
[a]Values in brackets indicate E_p on the third cycle

The behavior following incorporation of ruthenium complexes into the polymer was dependant on the ruthenium complex employed. Cyclic voltammograms for PBPyBBIM-Ru(bpy) modified electrodes are given in Figure 6.8,
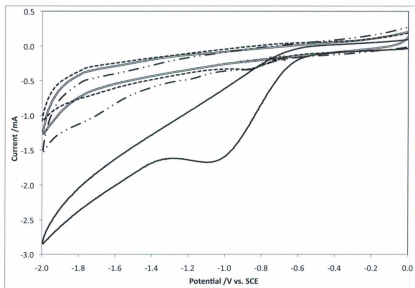
Figure 6.6: Cyclic voltammetry on a thin film of PBPyBBIM on a strip of carbon fiber paper. Potential swept at 100 mV s^{-1} in 0.1 M NEt$_4$BF$_4$ in CH$_3$CN. Conditions employed were (i) anhydrous, N$_2$ purged (double solid line), (ii) anhydrous, CO$_2$ purged (dash-dot line), (iii) 1% H$_2$O, N$_2$ purged (dashed line), (iv) 1% H$_2$O, CO$_2$ purged (single solid line). See text for details.
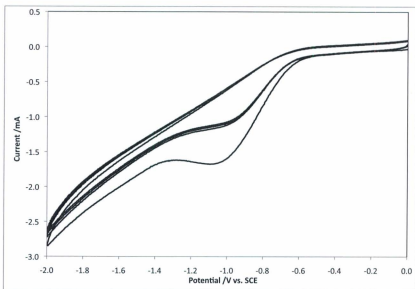
Figure 6.7: Cyclic voltammetry on a thin film of PBPyBBIM on a strip of carbon fiber paper. Four cycles are shown. Potential swept at 100 mV s^{-1} in 0.1 M NEt$_4$BF$_4$ in CH$_3$CN containing 1% H$_2$O that was purged with CO$_2$.
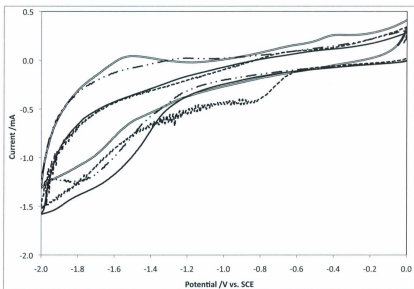
Figure 6.8: Cyclic voltammetry on a thin film of PBPyBBIM-Ru(bpy)$_2$ on a strip of carbon fiber paper. Potential swept at 100 mV s^{-1} in 0.1 M NEt$_4$BF$_4$ in CH$_3$CN. Conditions employed were (i) anhydrous, N$_2$ purged (double solid line), (ii) anhydrous, CO$_2$ purged (dash-dot line), (iii) 1% H$_2$O, N$_2$ purged (dashed line), (iv) 1% H$_2$O, CO$_2$ purged (single solid line). See text for details.
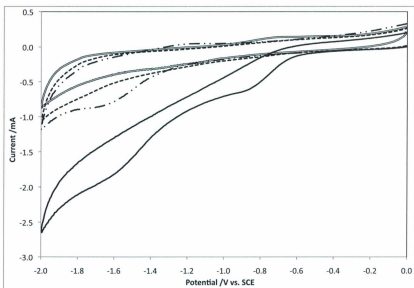
Figure 6.9: Cyclic voltammetry on a thin film of PBPyBBIM-Ru(pbt)$_2$ on a strip of carbon fiber paper. Potential swept at 100 mV s^{-1} in 0.1 M NEt$_4$BF$_4$ in CH$_3$CN. Conditions employed were (i) anhydrous, N$_2$ purged (double solid line), (ii) anhydrous, CO$_2$ purged (dash-dot line), (iii) 1% H$_2$O, N$_2$ purged (dashed line), (iv) 1% H$_2$O, CO$_2$ purged (single solid line). See text for details.

those for PBPyBBIM-Ru(pbt)$_2$ are given in Figure 6.9.

When examined under dry, N$_2$ purged conditions, PBPyBBIM-Ru(bpy)$_2$ exhibited a weak cathodic current increase between -1.5 and -1.9 V. A similarly weak anodic current was observed between -1.8 and -1.3 V. For similar reasons introduced for PPyBBIM-Ru(bpy)$_2$, this current is attributed to ligand-based reductions of ruthenium complexes.

Upon exposure to CO$_2$, PBPyBBIM-Ru(bpy)$_2$ failed to produce the first irreversible peak under dry conditions. The initial scan performed under wet, N$_2$ purged conditions possessed an irreversible cathodic current with a peak potential of -0.84 V. This peak was not observed in subsequent cycles. The second cathodic peak was observed under both wet and dry conditions, with a current onset of -1.15 V. Although difficult to distinguish due to overlap with the ligand-based reductions, the peak potential was located at approximately -1.8 V under dry conditions, and approximately -1.6 V under wet conditions.

The behavior of PBPyBBIM-Ru(pbt)$_2$ after exposure to CO$_2$ was much more similar to that of PBPyBBIM. The initial cathodic peak was not observed under dry conditions, but was observed under wet conditions. The second cathodic peak was observed in both dry and wet conditions, having a peak potential of -1.66 and -1.62 V, respectively. Under wet, CO$_2$ purged conditions, PBPyBBIM-Ru(pbt)$_2$ also exhibited the remarkably stable cathodic current spike that was observed for PBPyBBIM.

Conclusions

From the voltammograms presented in this section, it is apparent that CO$_2$ is capable of intimate interactions with both PPyBBIM and PBPyBBIM. This is

not surprising, considering that nitrogen rich solids such as amine-containing metal-organic frameworks [141], have been reported as candidates for CO_2 capture. It is very interesting to note that these interactions result in chemical species that are capable of being electrochemically reduced in two separate steps. Also note-worthy is that the presence of ruthenium was not necessary to observe the electrocatalytic reductions. It seems to be the polymer itself that is interacting with CO_2, not the transition metal complex. Taj *et al.* have previously reported on substituted polybenzimidazoles as electrocatalysts for O_2, CO_2 and H^+ [142]. The publication gives no experimental details, but states that H_2O_2, CO and H_2 were the observed products, respectively.

It is important to remember that XRF spectroscopy revealed the presence of several metals in these polymers (Chapter 5). It is unknown at this time whether these metal contaminants play a role.

The fact that a steady state curve was obtained on repeated electrochemical cycling of PBPyBBIM and PBPyBBIM-Ru(pbt)$_2$ in wet, CO_2 purged solutions suggests that the polymer is not undergoing an irreversible reaction with CO_2. Specifically, it means that transfer of electrons to the polymer-CO_2 adduct is followed by dissociation of a CO_2 derived species containing those electrons. Thus, regeneration of the polymer would allow reformation of an adduct with a new CO_2 molecule. If this were not the case, the voltammogram would be expected to show a decrease in current with repeated cycling.

The potential at which the reductive current begins in this work is similar to that reported for the pyridinium system studied by the Bocarsly group [143–146]. In their work, the Bocarsly group has reported on the electrocatalytic reduction of CO_2 using acidic, aqueous pyridine solutions. In their system, electrochemical reduction of pyridinium begins at approximately -0.5 V vs. SCE.

When the electrolyte solution is purged with CO_2, the current onset shifts to approximately -0.65 V [143]. Similarly, the peak potential shifts from approximately -0.7 to -0.85 V, and is accompanied by a peak current increase [143]. Following several mechanistic studies, the Bocarsly group has hypothesized that the electrocatalytic reduction mechanism is a series of one electron transfers to pyridinium, followed by reaction of pyridinium with CO_2 (or the appropriate intermediate) [145, 146].

Although different reaction conditions are employed, it is likely that the pyridine based polymers here follow a similar reaction mechanism as the pyridine system studied by the Bocarsly group.

Considering that electrochemical reduction of CO_2 without a catalyst requires potentials in excess of -2 V vs. SCE [2], the pyridine based polymers studied here present an intriguing electrocatalyst for CO_2 reduction. Their insolubility decreases or eliminates some of the health and environmental risks present in the pyridine system utilized by the Bocarsly group, and reduces the expense of costly ruthenium complexes [135, 147–149].

To simplify experiments, electrolysis experiments were carried out using only films of PBPyBBIM on carbon fiber paper.

6.2.2 CO_2 Electrolyses

Four CO_2 electrolyses were performed using PBPyBBIM coated electrodes following the electrochemical cell and experimental procedure described in Section 6.4.3. Potentiostatic electrolyses were performed at -1.0 V vs. SCE. The electrolysis potential was chosen to correspond to the potential at which peak current was observed for the first irreversible cathodic peak. Constant current

electrolyses were carried out with a current of -0.5 mA, the approximate peak current observed for the first irreversible cathodic peak.

Initially, a potentiostatic electrolysis of CO_2 by a PBPyBBIM coated electrode was performed in CH_3CN containing 1% H_2O and 0.1 M NEt_4BF_4. The second electrolysis followed the same procedure as the first, but used a 0.1 M $LiClO_4$ solution in place of the NEt_4BF_4 solution. The electrolyte was changed in an attempt to simplify analysis of the electrolysis solution using ^1H NMR. The third electrolysis was performed using a constant current in a 0.1 M NEt_4BF_4 solution in CH_3CN. The fourth electrolysis performed was identical to the second, utilizing an electrode with a known mass and a known amount of polymer.

Product analysis is given in a subsequent section.

Electrolysis 1: Constant Potential Using 0.1 M NEt_4BF_4 in CH_3CN

In the first electrolysis, the current was observed to decrease over the first 2 h, then steadily increase until the 20 h mark. An approximately steady current of *ca.* -0.35 mA was then observed to last until the end of the electrolysis. The electrolysis was run for a total time of 46 h and 40 min. The average current passed during the experiment, calculated by averaging the current readings, was -0.35 mA. The total charge passed, calculated by multiplying the electrolysis time (in seconds) with the average current, was 59 coulomb (C).

Two inconsistencies are present in the current-time curve for the first electrolysis (Figure 6.10). The first inconsistency is a very brief current spike at the 24 h mark. This current spike was due to the charging current upon restarting the software, explained in Section 6.4.3. The second is a prolonged current decrease between 45 and 46 h. This decrease was due to formation of a gas bubble
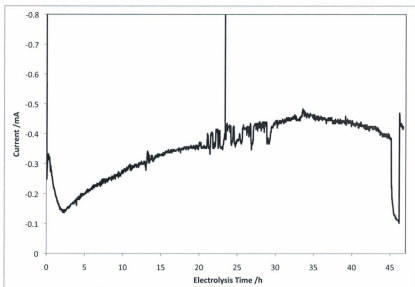
Figure 6.10: Potentiostatic CO_2 reduction electrolysis using a PBPyBBIM electrode in 0.1 M NEt_4BF_4 in CH_3CN containing 1% (v/v) H_2O (Electrolysis 1 in text). Electrolysis performed at -1.0 V vs. SCE.

at the glass frit between the working electrode compartment and counter electrode compartment. The bubble was cleared by gentle application of pressure on the counter electrode compartment with a plastic syringe. Upon removal of the bubble, the current was observed to rebound to previous levels. The electrolysis solution remained clear and colorless throughout the electrolysis. A small amount of white solid formed at the tip of the Luggin capillary, which is believed to be KCl.

Electrolysis 2: Constant Potential Using 0.1 M $LiClO_4$ in CH_3CN

The second electrolysis was run for 70 h and 50 min. The current-time curve is shown in Figure 6.11. The current was observed to fluctuate between approximately -0.4 and -0.8 mA over the entire electrolysis period, with several spikes to $ca.$ -1 mA. The short-lived current spikes at 23 and 48 h are again due to charging current upon resetting the software. The broad current depression between 39 and 42 h is due to formation of a gas bubble between the working and counter electrodes. A total charge of 185.8 C was passed. A small amount of brown solid was observed on the surface of the carbon fiber paper electrode, near where it was held by the alligator clip. A small amount of white solid was present at the tip of the Luggin capillary, and 284.5 mg of white precipitate was collected from the working electrode compartment.

A series of blank electrolyses were carried out in a 0.1 M $LiClO_4$ solution in CH_3CN containing 1% H_2O. The blank electrolyses, shown in Figure 6.12, all produced an approximately constant current of -0.2 mA over 24 h. The constant current is likely due to reduction of H^+. The presence of significantly larger currents when both PBPyBBIM and CO_2 are present confirms that the polymer is activating CO_2 for electrocatalytic reduction.
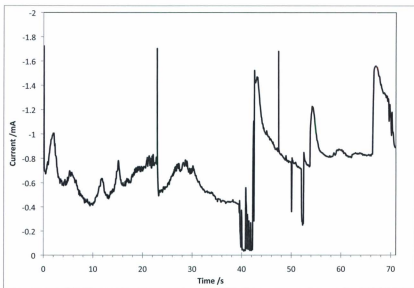
Figure 6.11: Potentiostatic CO_2 reduction electrolysis using a PBPyBBIM modified carbon fiber paper electrode in 0.1 M $LiClO_4$ in CH_3CN containing 1% (v/v) H_2O (Electrolysis 2 in text). Performed at -1.0 V vs. SCE.
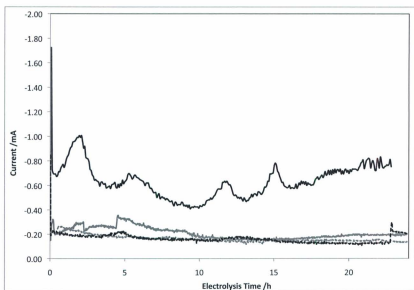
Figure 6.12: Potentiostatic CO_2 electrolysis using a PBPyBBIM electrode in CO_2 purged, 0.1 M $LiClO_4$ in CH_3CN containing 1% (v/v) H_2O (first 24 h of Electrolysis 2, solid black line). Also shown are blank electrolyses: PBPyBBIM coated electrode in N_2 purged solution (dashed black line), unmodified carbon fiber paper electrode in CO_2 purged solution (solid gray line), and unmodified carbon fiber paper electrode in N_2 purged solution (dashed gray line).

Electrolysis 3: Constant Current Using 0.1 M NEt$_4$BF$_4$ in CH$_3$CN

The third electrolysis was performed at a constant current for 73 h. The electrolysis was carried out in a 0.1 M NEt$_4$BF$_4$ in CH$_3$CN solution containing 1% H$_2$O. A constant -0.5 mA current produced an approximately constant potential of -0.7 V. A total charge of 131.8 C was passed. Over the 73 h period, the electrolysis solution changed from a clear, colorless solution to a clear, pale yellow color. A small amount of brown solid was again observed on the carbon fiber paper.

Electrolysis 4: Constant Potential Using 0.1 M NEt$_4$BF$_4$ in CH$_3$CN

A strip of carbon fiber paper (27.86 mg) was coated with a film of PBPyBBIM. After drying, the electrode mass was found to have increased to 28.32 mg, indicating a 0.46 mg loading of polymer (1.6% of total electrode mass). Following a 31.4 h potentiostatic electrolysis, in which 41.3 C of charge was passed, the electrode mass was observed to have increased by a further 6.21 mg, to 34.53 mg. Following electrolysis, the species responsible for the observed mass increase represents 18.0% of total electrode mass. The electrode was cut into pieces, and NMR, IR spectroscopy and TGA were employed to inspect the electrode for reduction products.

6.2.3 Product Identification

Commonly reported products of the electrocatalytic reduction of CO$_2$ are single carbon containing species: carbon monoxide, formic acid, formaldehyde, methanol and methane [2]. Oxalic acid is also a common product [14, 150]. More complex chemicals have also been reported. Cyanoacetic acid is known

to be produced from the reaction of the CO_2 radical anion with acetonitrile [151, 152]. More complex acids, such as glyoxylic acid, glycolic acid, tartaric acid and malic acid, have also been observed [153].

A multistep product analysis was performed. ^1H NMR was used to examine the electrolysis solutions for the common, proton containing products: formic acid, formaldehyde, and methanol. Such experiments would also be expected to identify the more complex acids. Experimental details for NMR sample preparation are given in Section 6.4.4. A commercial CO detector was employed to test the effluent gas stream for CO. The precipitate from Electrolysis 2 was analyzed by NMR and acid-base titration. The carbon fiber paper electrodes were analyzed using FT-IR with an attenuated total reflectance stand, TGA and NMR. Sample preparation for NMR is once again given in Section 6.4.4.

6.2.4 Electrolysis Solution Analysis

The ^1H NMR results for Electrolysis 1 are tabulated in Table 6.3. Integrals were calculated by setting the -CH_3 peak belonging to NEt_4^+ to 300. Setting such a large integral was necessary due to the large concentration difference between NEt_4^+ and the unknown peaks. The major peaks observed were due to NEt_4^+, H_2O and CH_3CN. Aside from the major peaks, three small peaks were observed; at 7.15, 7.80 and 7.98 ppm. A subsequent ^1H NMR spectrum acquired for a blank solution of 0.1 M NEt_4BF_4 in CH_3CN revealed that these three small peaks were due to minor impurities in the NEt_4BF_4. Both spectra are included in Appendix C.

To verify that the ^1H NMR technique used would reveal the products as

Table 6.3: Peaks observed in the ^{1}H NMR spectrum of the electrolysis solution following potentiostatic electrolysis at -1.0 V (Electrolysis 1). Electrolysis performed using a CO_2 purged solution of NEt_4BF_4 in CH_3CN containing 1% H_2O. NMR acquired using a 1:1 mixture of electrolysis solution and $CDCl_3$.

δ (ppm)	Coupling	Integral^a	Assignment
0	s	6.8	TMS
1.26	t	300	NEt_4^+ (-CH$_3$)
1.99	s	8768	CH_3CN
2.37	s	327	H_2O
3.20	q	195	NEt_4^+ (-CH$_2$-)
7.15	s	0.8	NEt_4^+ impurity^b
7.50	s	-	CDCl3
7.79	s	0.9	NEt_4^+ impurity^b
7.98	s	0.8	NEt_4^+ impurity^b

^{a} integral of 1.26 ppm peak set to 300
^{b} see text, appendix C

expected, the solution from Electrolysis 1 was spiked with each of the three chemicals of interest. Details are given in Section 6.4.4. The three spectra are given in Appendix C. Formic acid was observed to yield a singlet at 8.14 ppm. Formaldehyde produced two singlets and a series of peaks. A singlet was present at 3.33 ppm, due to methanol present in the formaldehyde solution as a stabilizer. A series of small peaks were present between 4.6 and 4.9 ppm, attributable to formaldehyde oligomers that are known to form in aqueous solutions of formaldehyde. A singlet was observed at 9.66 ppm, attributed to formaldehyde. The methanol spiked solution was observed to produce a singlet at 3.32 ppm. The ^{1}H NMR spectrum of the electrolysis solution does not contain any peaks in a comparable positions to any of the spiked solutions. This suggests that none of the three chemicals were present in the first electrolysis solution.

The second electrolysis solution was also examined with ^{1}H NMR. Upon dilu-

tion of the electrolysis solution with CDCl$_3$, a significant amount of precipitate was formed. Although this was likely only LiClO$_4$, it was decided to use D$_2$O in place of CDCl$_3$ to ensure that no product was lost as a precipitate. The NMR results are summarized in Table 6.4.

Table 6.4: Peaks observed in the ^{1}H NMR spectrum of the electrolysis solution following potentiostatic electrolysis at -1.0 V (Electrolysis 2). Electrolysis performed using a CO$_2$ purged solution of LiClO$_4$ in CH$_3$CN containing 1% H$_2$O. NMR acquired using a 1:1 mixture of electrolysis solution and D$_2$O.

δ (ppm)	Coupling	Integral[a]	Assignment
1.17	t		D$_2$O contaminant
1.99	s		CH$_3$CN
2.37	q		D$_2$O contaminant
2.81	s		Unknown
4.26	s		D$_2$O
4.34	s		Unknown

Two minor peaks were observed, due to unidentified species. In an attempt to determine the source of these peaks, ^{1}H NMR was performed on each of the three blank electrolysis solutions from Figure 6.12. A fourth blank solution was also made and examined. It was made purging a 10 mL portion of 0.1M LiClO$_4$ in CH$_3$CN with CO$_2$ for 30 min. A 1.00 mL aliquot of the purged solution was diluted with 1.00 mL of D$_2$O. ^{1}H NMR was then performed. The solutions from the initial three blank electrolyses contained both the 2.81 and 4.34 ppm peaks, but the non-electrolysed solution did not. Therefore, it seems as though the species responsible for the two unknown peaks originates from the carbon fiber paper during electrolysis, but is not a result of CO$_2$ reduction. No further effort was made to identify these peaks.

The results of ^{1}H NMR on the third electrolysis solution are presented in Table 6.5. The electrolysis solution was diluted (1:1) with CDCl$_3$ prior to NMR

acquisition. The results were found to be almost identical to those of the first electrolysis, except a new peak was observed at 9.01 ppm. This peak lies in the region of the spectrum where one would expect to see aldehydes or acids. However, it is not formaldehyde or formic acid, as they were shown to have shifts of 9.66 and 8.14 ppm.

Table 6.5: Peaks observed in the ^{1}H NMR spectrum of the electolysis solution following constant current electrolysis (Electrolysis 3). Electrolysis performed using a CO_2 purged solution of NEt_4BF_4 in CH_3CN containing 1% H_2O. NMR acquired using a 1:1 mixture of electrolysis solution and $CDCl_3$.

δ (ppm)	Coupling	Integral[a]	Assignment
0	s	8.0	TMS
1.24	t	300	NEt_4^+ (-CH_3)
1.99	s		CH_3CN
2.37	s	1046	H_2O
3.20	q	191	NEt_4^+ (-CH_2-)
7.16	s	1.3	NEt_4^+ impurity[b]
7.50	s	5.6	CDCl3
7.80	s	1.4	NEt_4^+ impurity[b]
8.00	s	1.3	NEt_4^+ impurity[b]
9.01	s	3.9	unknown

[a] integral of 1.26 ppm peak set to 300

Analysis of the ^{1}H NMR spectrum obtained for the electrolysis solution spiked with formaldehyde can provide estimates of the detection limits of the technique. To prepare the NMR solution spiked with formaldehyde, a 20 µL aliquot of 38% formaldehyde was added to 1 mL of electrolysis solution and 1 mL of $CDCl_3$. The concentration of formaldehyde in the solution was therefore 0.14 mol L^{-1}. The total formaldehyde NMR signal was distributed between the singlet due to monomeric formaldehyde (9.66 ppm) and oligomeric formaldehyde (4.6 - 4.9 ppm). The relative integration of these (1.0 and 75.9, respectively) indicates that only 1.3% of the total concentration, or 1.8×10^{-3} mol L^{-1}, was in

monomeric form.

Although the monomeric form was visible in the spectrum at this concentration, the signal strength was approximately 2.5 - 3 times the intensity of the background. This indicates that a concentration of 1.8×10^{-3} mol L^{-1} is very near the detection limit of the technique for a two proton species such as formaldehyde. Focussing on the most intense peak in the ^1H NMR spectrum of each of the three species of interest: the reduction of CO_2 to (i) formic acid requires two electrons and produces a single proton peak, (ii) formaldehyde requires four electrons and produces a two proton peak, and (iii) methanol requires six electrons and produces a three proton peak. From the electron to proton ratio between the three products, it can be seen that production of an equivalent Faradaic efficiency of any of the three products would result in ^1H NMR peaks of equivalent intensity. From this, the detection limits can be estimated as 3.6×10^{-3} mol L^{-1} for formic acid, 1.8×10^{-3} mol L^{-1} for formaldehyde (primarily present in oligimeric form, 4.6 - 4.9 ppm), and 1.2×10^{-3} mol L^{-1} for methanol.

Electrolysis 4, the smallest electrolysis performed, passed a total of 41.3 C, or 4.3×10^{-4} mol of electrons. Assuming 100% Faradaic efficiency, this would produce 2.2×10^{-4} mol of formic acid. Following a 1:2 dilution of the 30 mL electrolysis solution, the concentration can be calculated as 3.6×10^{-3} mol L^{-1}. Considering that the concentration is comparable to the predicted detection limit, the technique would be at its limit to detect any formic acid, formaldehyde or methanol produced in this electrolysis. If multiple products are produced, it is unlikely that any of the three products would be observable.

Electrolysis 2, the largest electrolysis performed, passed 185.5 C or 1.9×10^{-3} mol of electrons. Assuming 100% Faradaic efficiency, this would produce a concentration of 1.6×10^{-2} mol L^{-1} of formic acid in the NMR solution, or $ca.$ 4.5

times the detection limit. Therefore, a Faradaic yield of *ca.* 20% of any of the three chemicals of interest should be observable in the ^{1}H NMR of this solution.

Based on the NMR results it cannot be definitively stated that these three species are not products of the reduction, but they are surely not major products.

CO Analysis

A commercial CO detector was modified in an effort to obtain real-time measurements of CO(g). A Kidde brand CO detector (model KN-COPP-B-CA) was used. The detector works using a fuel cell design. The device contains two electrodes, separated by a H_2SO_4 solution. A potential difference is held between the two electrodes. When an oxidizable gas comes into contact with the anode, a current is generated. The detector is calibrated such that the magnitude of current generated is used to determine the concentration of the gas. Readings are given in ppm.

The CO detector was modified by sealing a PTFE vial over the anode of the detector. Two gas line adaptors were installed in the PTFE vial. Tygon tubing was used to connect one adaptor to the electrolysis cell, while the other was vented into a fumehood. Using such an apparatus, a constant flow of CO_2 through the electrolysis cell would carry gaseous products over the detector's anode.

The accuracy of the detector was tested using CO_2 electrolysis conditions previously reported by Hori *et al.* [6]. For the electrolysis, approximately 30 mL of 0.1 M $KHCO_3$(aq) was purged with CO_2 for 60 min. A silver wire, polished with a KimWipe until it was shiny, was used as the working electrode. A plat-

225

inum wire counter electrode and SCE reference electrode completed the cell. The cell was constantly purged with CO_2 during the electrolysis, at a rate of 3.0 mL min^{-1}. A voltage of -1.37 V was applied and the current and CO detector readings were periodically recorded.

Over a 90 min electrolysis current readings were observed to decrease from 0.29 mA to 0.24 mA, averaging 0.26 mA. The readings of the CO detector increased for the first 60 min before stabilizing around 370 ppm. The 60 min time necessary for the CO detector to stabilize is likely the time required to saturate the solution and headspace with CO.

The Faradaic efficiency of CO production can be estimated using the average current and stable CO detector readings. Equation 6.2.1 calculates the theoretical yield (n_{prod}, mol CO), for a given current (i, A) over a designated time frame (t, s). The number of electrons required for the electrochemical reaction (n_{rxn}, 2 moles of electrons per mole of CO), and the Faraday constant (F, 96485 C mol^{-1})are required. The ideal gas law converts the theoretical moles of product (n_{prod}) into theoretical volume of gas produced (V, mL) using pressure (p, 1 atmosphere), the universal gas constant (R, 82.057 mL atm K^{-1} mol^{-1}) and temperature (T, 298 K).

$$n_{prod}(\text{mol CO}) = \frac{i(A)t(s)}{n_{rxn}(\frac{\text{mol e}^-}{\text{molCO}})F(\frac{C}{\text{mol e}^-})} \qquad (6.2.1)$$

$$pV = nRT \qquad (6.2.2)$$

Using a time interval of 60 s is most convenient as it simplifies the next step. Division of the theoretical volume of CO (V) by the flow rate of gas through the

detector (electrolysis cell is being purged at a rate of 3.0 mL min^{-1}) yields the CO detector reading expected for 100% Faradaic efficiency. Dividing the observed CO detector reading (ppm) by the theoretical reading yields the estimate of the Faradaic efficiency of CO production.

The average current for the electrolysis of CO_2 using a Ag wire (0.26 mA) produces a theoretical CO detector reading of 664 ppm. A CO detector reading of 370 ppm, the value where the readings began to stabilize, indicates a Faradaic efficiency of 56%. This measurement is lower than the 81.5% efficiency reported by Hori *et al.* using this system [6]. Although the value is lower than the published yield, it indicates that the system is capable of CO detection at suitable levels, as well as at least semi-quantitative measurements of CO being produced.

Under atmospheric conditions, CO is the only gas which can be oxidized at the potentials used. In the experiments performed in this chapter, small amounts of H_2O are utilized. As a result, production of H_2 (g) is likely. Considering the style of detector used, H_2 (g) would be expected to interfere. Therefore, any reading obtained with the CO detector may be indicative of the presence of H_2.

The CO detector was attached to the electrolysis cell during Electrolysis 4, a potentiostatic electrolysis described in Section 6.2.2. In Figure 6.13, the current *vs.* time graph for the electrolysis is plotted alongside the CO detector readings. A reading of 0 ppm was observed for the first 24 h. At this point the current and CO detector readings started to increase, reaching a maximum current of -1.12 mA, and CO detector reading of 999 (instrument limit). This apparent two-stage electrolysis is discussed further in Section 6.2.4.
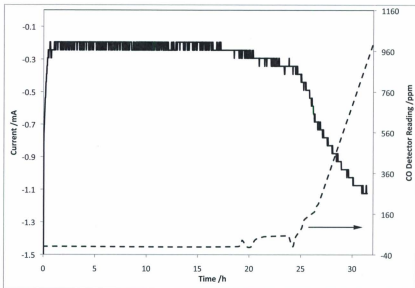
Figure 6.13: Potentiostatic CO_2 reduction electrolysis using a PBPyBBIM electrode in 0.1 M NEt_4BF_4 in CH_3CN containing 1% (v/v) H_2O (solid line, Electrolysis 4). Performed at -1.0 V vs. SCE. Secondary axis represents CO detector readings (dashed line).

Precipitate Analysis

Following the second electrolysis, 284.5 mg of white precipitate was collected from the bottom of the working electrode compartment of the electrochemical cell. The first and third electrolyses, performed using NEt_4BF_4 as an electrolyte, yielded only a small amount of white solid. In these cases the white solid was crystallized around the tip of the Luggin capillary, indicating that it is very likely KCl leaking from the SCE reference electrode. The electrolyte used in the second electrolysis, $LiClO_4$, may be involved in the precipitation, or the precipitate could have been due to the much larger charge passed in the second electrolysis. The white solid from the second electrolysis was analyzed by ^1H NMR and by acid-base titration in an attempt to identify the material.

A *ca.* 15 mg portion of the white solid was dissolved in D_2O, and ^1H NMR was performed. The solvent peak was the only peak observed. It can therefore be concluded that, as was the case for the electrolysis solution, common proton containing products were not present in the precipitate.

An acid-base titration was carried out on the precipitate to test for carboxylic acid containing products that would not show up in ^1H NMR: oxalic acid and carbonic acid. The pH of the solution was monitored using a pH meter that was calibrated as described in 6.4.5. A 200.8 mg portion of the white solid was dissolved in 50 mL of H_2O resulted in an initial pH of 4.91. Dilute HCl solution was used to acidify the solution. A titration was then carried out using a 0.0955 M NaOH solution which had been standardized against potassium hydrogen phthalate. The titration curve is shown in Figure 6.14.

Two buffer regions were observed in the titration. The first was located at a pH of approximately 2.9 and lasted *ca.* 0.4 mL, equating to 3.8×10^{-5} moles. The
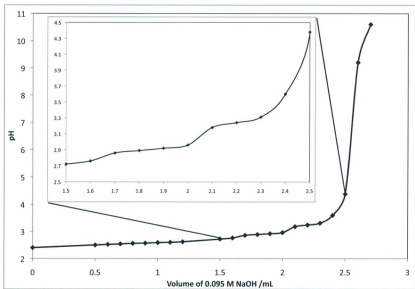
Figure 6.14: Titration curve obtained by titration of 200.8 mg of precipitate from Electrolysis 2, dissolved in 50 mL of H$_2$O, by 0.095 M NaOH (aq).

second buffering region was located at a pH of approximately 3.3 and lasted $ca.$ 0.3 mL, or 2.8×10^{-5} moles. For comparison, the pK_a value of possible carboxylic acids containing products are: (i) 3.74 for formic acid, (ii) 1.27 and 4.28 for oxalic acid, (iii) 6.35 and 10.32 for carbonic acid, (iv) 2.45 for cyanoacetic acid, (v) 3.2 for glyoxylic acid, (vi) 3.8 for glycolic acid, (vii) 3.2 and 4.85 for tartaric acid, and (viii) 3.4 and 5.2 for malic acid. Lack of a buffering effect in most of these regions indicates that it is unlikely that any of these acids are present in the white solid.

The exception is glyoxylic acid, which with a pKa of 3.2 could be responsible for the buffering observed at pH 3.3. However, ^{1}H NMR on the precipitate did not contain any peaks that could correspond to an aldehyde proton. Also, oxalic acid is an intermediate in the reaction path necessary to obtain glyoxylic acid from electrochemical reduction of CO_2 [153]. The lack of any buffering attributable to oxalic acid suggests that the observed buffering is due to a different species.

Adding the two buffer regions together results in a total of approximately 6.6×10^{-5} moles of acid. Extrapolation of this number to account for the total amount of precipitate obtained indicates that approximately 9.4×10^{-5} moles of acid are present in the 284.5 mg of white solid. A total of 185 C of charge was passed during the electrolysis, or 1.93×10^{-3} moles of electrons. Assuming a two electron reduction process to produce an acid from CO_2, the theoretical Faradaic yield of acid would be 9.3×10^{-4} moles. In this scenario, the acid indicated by titration accounts for only $ca.$ 10% of the charge passed. It seems likely that the majority of the white precipitate was therefore KCl or LiCl; present due to SCE reference electrode leakage. It is unknown which acid(s) caused the buffering observed, but the low yield compared to charge passed indicates

that, if it is a product of the electrolysis, it is a minor product. It is likely that the buffering observed here is related to the unidentified peaks that were observed in ^{1}H NMR, Table 6.4, which are believed to originate from the surface of the carbon fiber paper electrode during electrolysis.

Electrode Analysis

Following the failure to identify any reduction products in the electrolysis solution or precipitate, attention was turned to the carbon fiber paper electrode. FTIR spectroscopy, TGA and NMR were used to analyze electrodes for products. Products targeted include all those mentioned earlier, as well as carbonic acid salts and surface bound carboxylate groups. Potential mechanisms for these products will be introduced.

FTIR spectroscopy was performed on strips of carbon fiber paper using an attenuated total reflectance setup. The spectrum obtained for a thin film of PBPyBBIM on carbon fiber paper is given alongside a blank carbon fiber paper electrode in Figure 6.15. The film of PBPyBBIM on carbon fiber paper shows good agreement with the spectrum of PBPyBBIM in powder form (Figure 4.8, Chapter 4). Major absorptions that were present in the FTIR spectrum of PByB-BIM are easily distinguished here, verifying the presence of PBPyBBIM on the electrode: 1597, 1410, 800 and 702 cm^{-1}.

Following electrolysis changes were observed in the IR spectrum. Figure 6.16 compares the fingerprint region of the spectra before and after electrolysis. Some absorption bands which were previously attributed to the polymer film appear to have shifted. Most notably, the polymer absorptions at 1597 and 1410 cm^{-1}, attributed to symmetric and asymmetric bipyridine wagging in Chapter 4, were observed to pull apart from each other. The absorption originally at
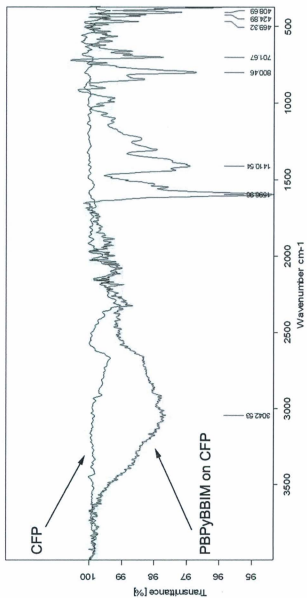
Figure 6.15: FT-IR spectrum of a thin film of PBPyBBIM deposited on a strip of CFP, compared to the spectrum obtained for an unmodified piece of CFP.
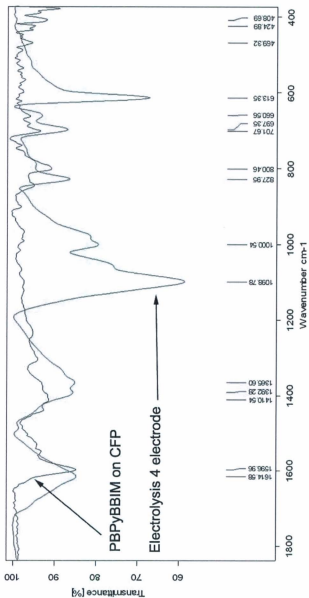
Figure 6.16: FT-IR spectrum obtained for electrode following Electrolysis 4, compared to the spectrum obtained for a thin film of PBPyBBIM on CFP.

1597 cm^{-1} shifted 17 cm^{-1} higher following electrolysis; while that at 1410 cm^{-1} shifted 18 cm^{-1} lower. Both absorption bands were also observed to broaden.

A shift in polymer absorptions would indicate chemical modification of the polymer. In this case, the modification would influence the bipyridine wagging motion. However, the IR data does not conclusively show that the polymer has been modified, as carboxylate ions are known to possess asymmetric stretching bands at *ca.* 1650-1550 cm^{-1} and symmetric stretching bands at *ca.* 1300-1420 cm^{-1} [154, 155]. Due to possible overlap of the absorption bands, it is not possible to determine whether PBPyBBIM has been chemically modified, or if the presence of a carboxylate containing species (*e.g.* carbonic acid, surface carboxylates) is responsible for the apparent shift and broadening.

Several strong absorptions appeared in the spectrum following electrolysis, while some peaks disappeared. Most obviously, very strong absorptions appeared at 1098, 1000 and 613 cm^{-1}. Absorptions that were observed between 400 and 500 cm^{-1} for the PBPyBBIM film on carbon fiber paper were no longer observed following electrolysis. Absorptions higher than 2000 cm^{-1}, not shown here, were much weaker and difficult to determine.

The dominant feature of a tetraethylammonium tetrafluoroborate IR spectrum is a strong absorption at 1084 cm^{-1} [156]. Considering the similar location, it was thought that the strong absorption at 1098 cm^{-1} observed following electrolysis may be due to the presence of tetraethylammonium. To test this, a strip of unmodified carbon fiber paper was soaked in a 0.1 M solution of NEt$_4$BF$_4$ in CH$_3$CN. After allowing the electrode to air dry, FT-IR was performed on the electrode. The IR spectrum, compared to blank carbon fiber paper, is shown in Figure 6.17. The spectrum showed an absorption at 1103 cm^{-1}, as well as a series of peaks at 1514, 1646, and 3500-3800 cm^{-1}. The absorption bands for NEt$_4$BF$_4$
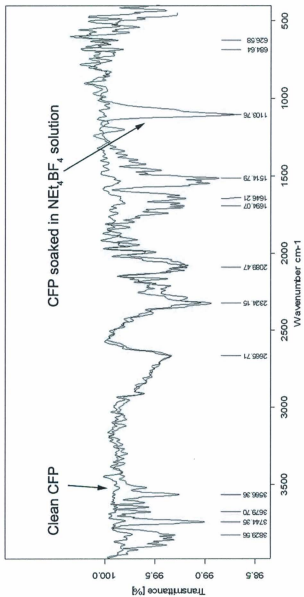
Figure 6.17: FT-IR spectrum of a strip of carbon fiber paper soaked in 0.1M NEt₄BF₄ in CH₃CN, compared to a clean strip of carbon fiber paper.

are compared with those for the electrolysis electrode in Table 6.6.

Table 6.6: Summary of peaks observed in FTIR-ATR spectrum for Electrolysis 4 electrode and a carbon fiber paper electrode with adsorbed NEt_4BF_4. Also listed are absorption bands for several oxalate salts.

Electrolysis Electrode		Absorption Bands (cm^{-1}) NEt_4BF_4	$ZnC_2O_4{}^a$	$CuC_2O_4{}^a$	$MgC_2O_4{}^a$
			498	507	502
strong	613		625		
weak	660				
medium	697				692
weak	742		741		
weak	784				
medium	827		824	824	831
medium	1000				
weak	1056				
strong	1098	1084			
medium	1365		1319	1320	1328
medium	1392		1365	1364	1373
		1514			
			1464		
medium	1614		1633	1638	1641
		1646		1640	1665
weak	2941		2925	2924	
weak	2989		2954		
weak	3398		3376		3407
		3566			
		3744			
		3829			

^{a} Major peaks, obtained from reference [156].

Although NEt_4BF_4 exhibited an absorption band near the 1100 cm^{-1} band that was observed for the electrolysis electrode, the additional peaks observed for NEt_4BF_4 could not be identified in the spectrum of the electrolysis electrode. Considering the strength of the 1100 cm^{-1} absorption, this likely indicates that NEt_4BF_4 is not present in significant amounts on the electrolysis electrode. The intensity of the 1098 cm^{-1} absorption was significantly lower for the electrode soaked in electrolyte solution than was observed for the electrolysis electrode

(99% transmittance vs. *ca.* 60% transmittance).

Inspection of the IR spectra of various tetraethylammonium salts revealed that the spectrum changes significantly with variation of the counterion (hydroxide, fluoride, chloride, acetate, perchlorate) [156]. However, a strong absorption band appears between 1000 and 1100 cm^{-1} in all samples. This fact, combined with the above information, suggests that if tetraethylammonium is present, it's counterion is likely not BF_4^-.

Considering the reaction conditions, oxalate and carbonate were identified as potential counterions. Oxalate has previously been reported as a product of electrochemical reduction of CO_2 [14, 150]. Bubbling CO_2 through a solution containing water would be expected to produce carbonate ions.

As a simple test for the presence of carbonate salts, a portion the electrolysis electrode was submersed in 1 M H_2SO_4 (aq). The electrode was observed to bubble vigorously for a short period of time, approximately 2-3 seconds, suggesting that carbonate salts are indeed present. Following acid treatment of the electrode, all IR absorption bands were observed to disappear, shown in Figure 6.18. Indicating that all material was dissolved or reacted during the acid wash.

The presence of oxalate on the electrode surface would be expected to produce absorption bands in the IR spectrum. Comparison of IR spectra for oxalate salts with various counterions once again revealed that the counterion plays a large role in the structure of the spectra [156]. Table 6.6 summarizes the major absorptions of ZnC_2O_4, CuC_2O_4 and MgC_2O_4, and compares them to those for the electrolysis electrode. Four absorption bands were consistently observed across all three model compounds: 824, 1320, 1364 and 1638 cm^{-1}. Corresponding absorption bands were observed in the spectrum for the electrolysis elec-
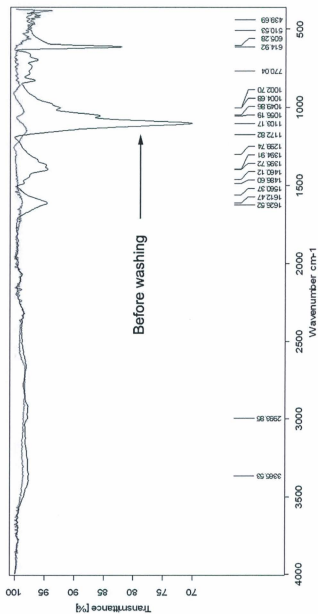
**Figure 6.18:** FT-IR spectra of a portion of the electrode from Electrolysis 4 before and after washing with 1 M H$_2$SO$_4$ (aq).

trode, suggesting that oxalate might be present. The IR spectra of the electroly-
sis electrode and ZnC_2O_4 were most comparable to each other, having a similar
location for 9 peaks. These peaks included the four mentioned earlier, as well
as 625, 741, 2925, 2954, and 3376 cm^{-1}.

Tetraethylammonium oxalate was prepared by mixing equal amounts of aque-
ous solutions of tetraethylammonium hydroxide and oxalic acid. Evaporation
of H_2O under reduced pressure resulted in a thick white sludge. When oven
dried at 90 °C a white solid was obtained. ^1H and ^{13}C NMR were performed
on the white powder using DMSO-d_6 as a solvent. The ^1H and ^{13}C NMR spec-
tra, referenced to TMS, are given in Appendix C. The ^1H NMR contained the
peaks expected for NEt_4^+: a triplet at 1.16 ppm (3.00 H)and a quartet at 3.23
ppm (2.00 H). Also present was a singlet from DMSO-d_6 at 2.51(0.07 H) and a
broad singlet at 3.60 (2.69 H), which is believed to be H_2O. The ^{13}C NMR con-
tained peaks at 7, 39, 51 and 174 ppm. The 7 and 51 ppm peaks are attributable
to NEt_4^+, the 39 ppm to DMSO-d_6, and the 174 ppm to oxalate.

A thin layer of the tetraethylammonium oxalate was applied to a strip of car-
bon fiber paper by spreading the white sludge into a thin film. The carbon
fiber paper was subsequently dried at 90 °C. FT-IR was then performed us-
ing attenuated total reflectance, producing Figure 6.19. Comparison of the IR
spectrum for tetraethylammonium oxalate on carbon fiber paper with that of
the electrode following electrolysis reveals a poor match. While the two spec-
tra share several similarities, there are numerous differences that suggest that
tetraethylammonium oxalate is not present on the electrode surface. The most
significant difference is the absence of absorptions in the electrolysis electrode
spectrum at 1560, 1300 and 770 cm^{-1}, areas where tetraethylammonium oxalate
exhibited strong absorptions.
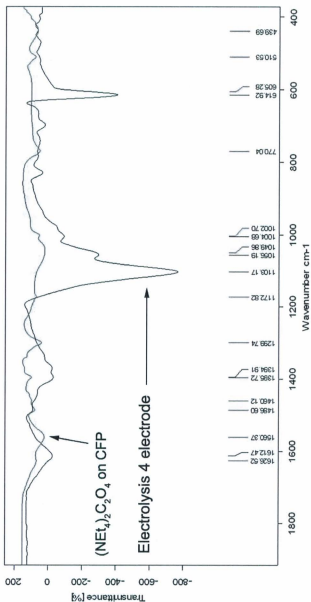
Figure 6.19: FT-IR spectrum of a thin film of tetraethylammonium oxalate on carbon fiber paper, compared to the spectrum for the electrode from Electrolysis 4. Spectra were normalized at 3600 cm⁻¹ for comparison.

241

NMR was employed in an attempt to gain additional evidence regarding the presence of carboxylate, carbonate or oxalate salts. Considering the electrolysis conditions, possible cations present in solution include NEt_4^+, H^+ and K^+ (reference electrode leakage). Considering that the electrolysis solution is 0.1 M NEt_4^+, the majority of any salts produced would be expected to contain significant amounts of NEt_4^+. If these salts exist and can be removed from the electrode, NMR would be capable of identifying their presence through identification of NEt_4^+.

A portion of the electrode from Electrolysis 3 was soaked in 2 mL of DMSO-d_6 for approximately 72 h. ^1H and ^{13}C NMR were then performed. Both spectra are included in Appendix C. The ^1H NMR spectrum contained two major peaks and two minor ones. A 2.50 ppm peak is due to DMSO. The other major peak in the spectrum was a singlet located 3.38 ppm, attributed to water [157]. Two small peaks were observed at 1.16 (1.00 H) and 3.20 ppm (0.74 H). The shift of the peaks is in the location expected for NEt_4^+, and considering the very small size of the peaks, the integration is very close to the ratio expected. However, integration shows the intensity of these peaks to be only $ca.$ 0.5% of the H_2O peak. The ^{13}C NMR spectrum contained a single set of peaks located at 39.5 ppm, due to DMSO. Although a small amount of NEt_4^+ was able to be removed from the surface, a significantly larger amount of H_2O was removed.

Thermogravimetric analysis was performed under N_2 atmosphere on (i) untreated carbon fiber paper, (ii) NEt_4BF_4 adsorbed on carbon fiber paper, (iii) a film of PBPyBBIM on carbon fiber paper and (iv) a portion of the electrode from Electrolysis 4. The thermogram of the electrode from Electrolysis 4 revealed a much different structure than the other three, possessing a number of thermal events. All thermograms and differential thermograms are given in Appendix

B, except that for the Electrolysis 4 electrode, which is given here. Peak mass loss rates are taken as the peaks observed in differential thermograms. Total mass loss percentages for each sample are given in Table 6.7.

Untreated carbon fiber paper exhibited a single mass loss event, with an onset near 550 °C and a peak rate of mass loss at 723 °C. The overall mass loss was 8.9%. The thermogram obtained for untreated carbon fiber paper is included in Appendix B. This behavior is quite similar to that observed by Toupin and Belanger for the carbon powder Vulcan XC72 [78]. When heated under N_2 atmosphere, they observed Vulcan XC72 to have a mass loss onset of *ca.* 600 °C, resulting in a 6.2% mass loss. The broad mass loss observed here can therefore be attributed to elimination of surface functional groups from the surface of the carbon fiber paper.

Table 6.7: Percent of mass lost during a thermogravimetric analysis scan from 30 °C to 1000 °C for carbon fiber paper strips.

Treatment of CFP	Total Mass Loss (%)
Pristine	8.9
72 h Soak in 0.1 M NEt_4BF_4	12.3
Coated with PBPyBBIM	18.2
Electrolysis 4 electrode	42.0

A carbon fiber paper electrode that was soaked in 0.1 M NEt_4BF_4 in CH_3CN for a 72 h period produced five mass loss events. The events occurred with peak mass loss rates at 43, 100, 449, 780 and 909 °C. The thermal events had mass losses of 0.5, 0.7, 1.5, 3.7 and 5.9%, respectively, for a total of 12.3%. Based on the low temperature of the first two events, they are likely attributable to loss of adsorbed H_2O. The presence of H_2O in this sample and not in bare carbon fiber paper is likely due to the introduction of ions to the surface, making the electrode more hydrophilic (NEt_4^+, BF_4^-). A TGA scan on solid NEt_4BF_4,

243

shown in Appendix B, showed a single mass loss event at 438 °C, resulting in 99.8% mass loss. Due to proximity, the 449 °C thermal event observed for carbon fiber paper exposed to NEt_4BF_4 can be attributed to decomposition of NEt_4BF_4. In the higher temperature region, the single broad mass loss observed for unmodified carbon fiber paper was observed to split into two distinct processes: a sharp loss of 3.7% at 780 °C and a broad loss of 5.9% centred at 909 °C. The splitting of mass loss events did not result in a significant increase in mass loss. The two mass loss events observed total 9.6%, slightly higher but comparable to the 8.9% observed for untreated carbon fiber paper. Considering the sharpness of mass loss at 780 °C, it can likely be attributed to loss of a single, specific surface functional group. It therefore seems as though NEt_4BF_4 is capable of interacting with some surface functional groups, altering the thermal stability.

TGA on a strip of carbon fiber paper coated with PBPyBBIM produced a thermogram very similar to unmodified carbon fiber paper. The dominant feature was once again a broad mass loss. The onset of the mass loss shifted lower in temperature, to approximately 475 °C. This earlier onset must be due to the presence of PBPyBBIM. The peak rate of mass loss was observed to shift to a higher temperature, to approximately 850 °C. The derivative of the thermogram reveals a small peak at 557 °C, close to the temperature at which PBPyBBIM was shown to decompose in Chapter 5 (543 °C). The total mass lost up to 1000 °C was 18.2%, indicating a polymer loading of about 9% by mass.

Examination of the electrode from Electrolysis 4 using TGA revealed 4 distinct processes. A mass loss of 5.9% was observed at 141 °C. The low temperature suggests desorption of H_2O. This assignment is supported by the presence of H_2O in the NMR spectrum following washing of the electrode with DMSO-
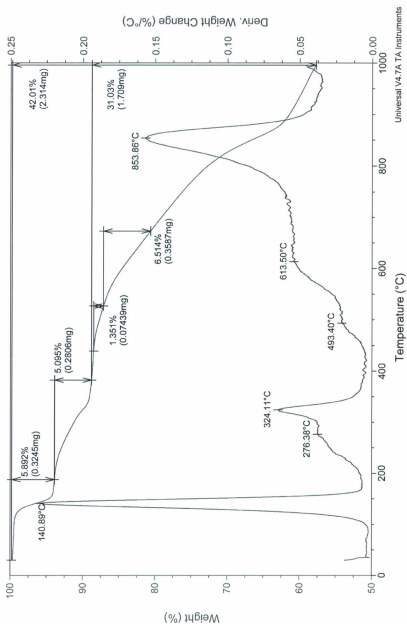
Figure 6.20: Thermogram and differential thermogram for a hi-resolution thermal scan on the electrode from Electrolysis 4 under N_2 atmosphere.

d_6. A broad mass loss begins at *ca.* 200 °C, evolving to a sharp mass loss at 324 °C. This process, which extends between 200 and 350 °C, results in a 5.1% mass loss. Following this, a broad mass loss once again begins at approximately 450 °C. The rate of mass loss increases twice, reaching a stable rate at 493 and 613 °C. A final, sharp mass loss showed a peak rate of loss at 853 °C. The three events produce 1.4, 6.5 and 23.1% mass losses, respectively. A total loss of 42.0% was observed on scanning to 1000 °C, a significant increase compared to other samples.

Although slightly lower in temperature than expected, the 493 °C event results in a mass loss very close to what is expected for decomposition of the polymer (see Section 6.2.2). The three final mass loss events were in a similar location to those observed for PBPyBBIM coated CFP, but produce a 12.8% larger mass loss (31.0% vs. 18.2%). The similarity in position of these mass loss events suggests that they're due to similar species. Recall that following electrolysis the mass of the electrode increased by 6.21 mg to 34.53 mg, an 18.0% increase. It is interesting to note that the sum of the mass lost between 200-350 °C to the additional 12.8% lost above 400 °C results in a total of 17.9%, a mass loss very close to the total mass increase following electrolysis. However, this analysis leaves H_2O unaccounted for.

Based on the large increase, and the sharpness, in mass loss around 850 °C, it is tempting to assign a portion of the mass increase of the electrode to an increase in surface carboxylates. This would necessitate the existence of counter ions, which could be NEt_4^+ or H^+. Ngo *et al.* have reported the onset of tetraethylammonium salt decomposition to occur between 264 and 439 °C, dependant on the counterion [158]. Tetraethylammonium chloride was reported to have a decomposition onset of 264 °C, close to what was observed here for

the electrolysis electrode. There is a possibility that the mass loss event between 200 and 400 °C is due to NEt_4^+ decomposition, where NEt_4^+ is strongly bound to the surface via ionic bonds to surface bound carboxylate groups. Such a scenario could explain the TGA behavior, as well as the difficulty finding traces of common CO_2 reduction products.

By washing the electrode from Electrolysis 4 with deuterated solvent, it was possible to reveal the presence of NEt_4^+ on the electrode surface. However, the strength of the NEt_4^+ peaks were very weak. It is possible that electrostatic interactions inhibited dissolution of the ion. Assuming the 140 °C mass loss event is due to desorption of H_2O, it can be estimated that *ca.* 2.04 mg (1.13 x 10^{-4} moles) of H_2O was present on the electrode surface. Similarly, if the 12.8% increase in mass loss above 400 °C is attributed to surface bound carboxylate groups, a total of *ca.* 4.42 mg (1.00 x 10^{-4} moles) of surface carboxylates can be estimated. Assuming that the 200-350 °C mass loss is due to NEt_4^+, a total of approximately 1.76 mg (1.35 x 10^{-5} moles) of NEt_4^+ can be estimated.

During the electrolysis, a total charge of 41.3 C, or 4.28 x 10^{-4} moles e$^-$, was passed. A theoretical yield of a two electron reduction product would therefore be 2.14 x 10^{-4} moles. It is interesting to note that the estimated amount of surface carboxylates (1.00 x 10^{-4} moles) is nearly 50% of this theoretical value. When combined with the fact that CO production was observed during later times in the electrolysis, it therefore appears as though carboxylation of the carbon surface is likely occurring.

If surface carboxylate groups are being grafted to the surface, they would likely need to pass through a radical intermediate. Proposed mechanisms for the reduction of CO_2 frequently begin with a single electron transfer to CO_2, producing the CO_2^{-} [2, 3, 145, 153]. In one path, this radical can then be re-

duced to either carbon monoxide or formic acid by addition of an additional electron (and two protons). In an alternate path, this radical reacts with nearby chemical species. While oxalic acid is the most common product of this type, produced by coupling of two $CO_2^{\cdot -}$ ions, higher molecular weight species have been reported [153].

Carbon surfaces have a propensity to react with radicals. This is illustrated by the fact that the most widely used carbon surface modification techniques reported in the literature rely on generation of radicals. The modification of carbon surfaces using diazonium ions, discussed in Chapter 3, relies on decomposition of diazonium ions to N_2(g) and aromatic radicals. Another example comes from Astudillo *et al.*, who have reported the use of ferrocene as a mediator for radical generation from tetrabutylammonium carboxylates [57]. Their proposed mechanism, shown in Figure 6.21, begins with the single electron oxidation of ferrocene. Subsequent single electron oxidation of an aliphatic or aromatic carboxylate by ferrocenium is followed by decomposition of the carboxylate radical to CO_2 and an aliphatic or aryl radical. The resultant radical was shown to react with carbon surfaces, forming a covalently immobilized layer on the carbon surface.

6.3 Conclusions

A series of polymers was examined with cyclic voltammetry and shown to possess interactions with CO_2. Cyclic voltammetry also revealed that one polymer in particular, PBPyBBIM, exhibited strong electrocatalytic behavior in the presence of CO_2. Potentiostatic and constant current electrolyses were carried out in CH_3CN containing a small amount of H_2O as a proton source. Working elec-
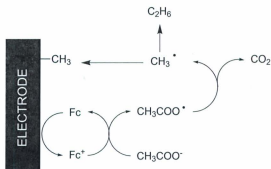
Figure 6.21: Reaction mechanism for covalent immobilization of aliphatic groups to carbon surfaces, as proposed by Astudillo *et al.* [55].

trodes consisted of PBPyBBIM deposited on a strip of carbon fiber paper. Comparison of electrolysis results with those from blank electrolyses confirmed that CO_2 was electrocatalytically reduced by PBPyBBIM.

Product analysis proved to be very difficult, owing to the complexity of the system utilized. Examination of electrolysis solutions, precipitates and electrode surfaces failed to conclusively identify any products. A CO detector suggested the production of CO does not initially occur, but begins after a period of electrolysis.

Results of FT-IR and TGA studies on electrode surfaces following electrolysis revealed composition changes of the electrode surface. While the results are not clear enough to assign the changes with absolute confidence, the most likely scenario is that reaction intermediates are reacting with the surface of the carbon fiber paper electrode.

Given that carbon surfaces are reactive towards radicals, and that reduction of CO_2 typically proceeds through a radical anion, it is feasible that carboxylation of the carbon surface is occurring here. Such a mechanism may explain the

behavior described in Section 6.2.4, where the CO detector indicated two stages to the potentiostatic electrolysis. In the first stage the CO detector indicated no production of CO. In the second stage an increase in current was accompanied by significant CO production. It is possible that CO was not detected during the first stage due to the carbon support reacting with a CO_2 radical intermediate, effectively halting the reduction path. Once the carbon surface is unable to react further, the two electron reduction to CO may become the dominant pathway. Such a description of events agrees with the statements of Taj *et al.* [142], where substituted polybenzimidazoles were reported to electrocatalytically produce CO from CO_2. It also explains the increase in mass of the carbon fiber paper electrode upon completion of electrolysis.

The difficulty in product analysis indicates the need to perform the electrolyses with a less reactive material as an electrode support, such as Pt. To accomplish this, a technique for producing stable films of PBPyBBIM on a Pt surface must first be developed. Thin films of PBPyBBIM were successfully placed on Pt disc electrodes by evaporation of very dilute, saturated solutions of PBPyBBIM in dimethylacetamide. However, PBPyBBIM films prepared this way were found to be completely removed from the electrode surface during cyclic voltammetry experiments.

6.4 Experimental

Information regarding instrumentation and chemicals can be found in Chapter 2.

6.4.1   Electrode Preparation

The polymers used in this work, shown in Figure 6.1, were found to be sparingly soluble in dimethylacetamide (DMA). Attempts at deposition of a stable thin film on glassy carbon using the dilute DMA solution were unsuccessful. The polymers were found to be much more soluble in conc. H_2SO_4. It was observed that dilution of the H_2SO_4 based solution with H_2O resulted in rapid precipitation of the polymer.

Electrodes utilized in this chapter were prepared by exploiting the low solubility of the polymers. Typical electrode preparation was carried out as follows. A saturated solution of the desired polymer in conc. H_2SO_4 was made. Solutions of PPyBBIM based polymers were pale yellow, and solutions of PBPyB-BIM based polymers were dark orange. A 1 cm wide by 3 cm long strip of carbon fiber paper was placed in a beaker and covered with approximately 0.5 mL of the polymer solution. The solution was left to soak into the carbon fiber paper overnight. In the morning, the beaker was filled with distilled H_2O and left to stand for several hours. The electrode was then rinsed with distilled H_2O, and dried at 100 °C. Typical loadings were *ca.* 0.5 mg of polymer on the CFP electrode.

"Blank" electrodes were prepared by following the same procedure, but using conc. H_2SO_4 in place of the polymer solutions.

Due to the use of H_2SO_4 in electrode preparation, the initial reductive scan on all electrodes contained a very large current due to H^+ reduction. This current was not observed on subsequent cycles. Therefore, the initial cycle for all voltammograms performed on new electrodes have been omitted.

6.4.2 Cyclic Voltammetry

Cyclic voltammetry was performed in a standard three-compartment electrochemical cell. A SCE reference electrode was connected to the working electrode compartment by a Luggin capillary. A platinum wire was used as the counter electrode. All voltammograms were collected with a scan rate of 100 mV s^{-1}. Electrolyte solutions were either 0.1 M NEt$_4$BF$_4$ or 0.1 M LiClO$_4$ in CH$_3$CN. "Dry" electrolyte solutions were prepared the day of the experiment, using anhydrous CH$_3$CN (Sigma-Aldrich, Sure/Seal^{TM} bottle). "Wet" electrolyte solutions were made with 1% H$_2$O by volume. Prior to data collection, electrolyte solutions were purged for a minimum of 30 min with N$_2$ or CO$_2$.

6.4.3 Electrolyses

Electrolyses were performed in a custom made, air-tight, three-compartment electrochemical cell. The counter electrode compartment was separated from the working electrode compartment by a fine glass frit. The reference electrode compartment was connected to the working electrode compartment using a Luggin capillary. Plastic screw-caps fitted with rubber o-rings were used to form air-tight seals around each of the three electrode casings. A gas-exhaust outlet was installed in the working electrode compartment for examination of gaseous products.

Electrolyses were carried out using a platinum wire counter electrode, an SCE reference electrode and a carbon fiber paper working electrode created as described in Section 6.4.1. For the four CO$_2$ electrolyses, the electrolyte solutions were 0.1 M NEt$_4$BF$_4$ (or LiClO$_4$) in CH$_3$CN containing 1% H$_2$O (v/v).

Electrolyte solutions were purged with CO$_2$ for a minimum of 30 min before

electrolysis. For Electrolysis 4, where exhaust gases were passed through a CO detector, the working electrode compartment was constantly purged with CO_2 using a capillary installed at the bottom of the compartment. A flow rate of 3.0 mL min^{-1} was used. To remove any residual H$^+$ from each electrode, the potential was swept from 0 to -2.0 V *vs.* SCE twice prior to each electrolysis.

Potentiostatic electrolyses were carried out at a potential of -1.0 V vs. SCE. Real-time current measurements were recorded using software written with GW-BASIC. Due to software constraints, the current monitoring software was restarted once every 24 h. Restarting the software was accompanied by resetting the applied potential. Resetting the potential results in a short lived current spike, due to charging current, once per day.

Constant current electrolyses were carried out with a constant current of -0.5 mA.

6.4.4 ^{1}H NMR Sample Preparation

Electrolysis solutions were prepared for NMR using the following procedure. A 1.00 mL aliquot of electrolysis solution was mixed with 1.00 mL of CDCl$_3$ (for NEt$_4$BF$_4$ solutions) or 1.00 mL of D$_2$O (for LiClO$_4$ solutions). After mixing well, a portion of the mixture was transferred to an NMR tube. Solutions containing CDCl$_3$ were referenced to TMS (0 ppm), those containing D$_2$O were referenced to CH$_3$CN (1.99 ppm).

A blank electrolyte solution was prepared by mixing 1.00 mL of CDCl$_3$ with 1.00 mL of fresh 0.1 M NEt$_4$BF$_4$ in CH$_3$CN containing 1% H$_2$O.

Three different 2.00 mL samples were spiked with common CO_2 reduction products as follows. A 20 μL aliquot of 90% formic acid (90.8%, J.T. Baker

Chemicals) was added to one solution. A 20 μL aliquot of aqueous formaldehyde solution (36.5-38.0%, Anachemia, contains 12-15% methanol) was added to a second solution. A 20 μL aliquot of methanol (A.C.S. grade, Sigma-Aldrich) was added to a third solution.

The white precipitate from Electrolysis 2 was prepared for NMR by dissolving *ca.* 15 mg in D_2O.

Following Electrolysis 3, a portion of the electrode was soaked in 2 mL of DMSO-d_6 for 72 h. ^1H and ^{13}C NMR were then performed on the DMSO-d_6.

6.4.5   pH Meter Calibration

A Fisher Scientific pH meter was used. The pH meter was calibrated using three commercial buffer solutions: (i) a pH 3.0 buffer solution consisting of potassium hydrogen phthalate and tartaric acid, (ii) a pH 7.21 buffer solution consisting of potassium phosphate and dipotassium phosphate, and (iii) a pH 10.0 buffer solution consisting of sodium borate and sodium carbonate. The pH of the three solutions was measured to be 3.04, 7.19 and 10.24, respectively.

6.4.6   Infrared Spectroscopy

Infrared spectroscopy was performed using a Bruker Alpha-P FT-IR equipped with an attenuated total reflectance stand using a diamond lens. The background scan was performed with an empty placeholder. Spectra were collected using 32 scans, performed from 375 cm^{-1} to 4000 cm^{-1}, with a 4 cm^{-1} resolution.

Carbon fiber paper absorbs strongly throughout the infrared region. Therefore, the OPUS software suite (Version 6.5) was used to perform a baseline cor-

rection and a 25 point smoothing operation (Savitzky-Golay algorithm) on all spectra.

6.4.7 Thermogravimetric Analysis

Thermogravimetric analysis was performed using a TA Instruments Q500 thermogravimetric analyzer and platinum sample holders. The furnace was continually purged with ultra-high purity nitrogen. After loading the sample, a 15 min equilibration period ensured complete removal of oxygen from the furnace compartment. A high resolution dynamic scan was used for all samples. This scan setting uses initial scan rate of 50 $^\circ$C min^{-1}. This scan rate automatically decreases to 1 $^\circ$C min^{-1} when a mass change is detected. The scan rate automatically speeds up when the mass stabilizes. Scans were performed from 30 to 1000 $^\circ$C.

Conclusions

7.1   Conclusions

The spontaneous diazonium grafting technique was used to modify a high surface area carbon black with 9,10-anthraquinone. The effects of modifications to the grafting procedure were followed by cyclic voltammetry. The general trends and limits observed were similar to those reported in the literature, which were acquired using different methods of analysis. It therefore appears that cyclic voltammetry may be useful in quantitative analysis carbon powders modified by the spontaneous grafting technique. This is in contrast to the electrografting of diazonium ions on carbon surfaces, in which cyclic voltammetry has been reported to be inaccurate. The maximum anthraquinone surface coverage obtained in this work was *ca.* 1.5×10^{-4} mol g^{-1}. Depending on the modification conditions, significant portions of anthraquinone were found to be non-covalently bound. It was found that quantitative removal of the physisorbed anthraquinone was not possible with common solvents such as acetonitrile and methanol, but required the use of benzene. For the first time, the electrochemistry of azo-linkages was observed following spontaneous diazonium grafting. This result, combined with the low surface coverage, suggests that the anthraquinone molecules are dispersed on the surface, and that polymerization does not occur. Cyclic voltammetry and XPS results suggest that *ca.* 10% of anthraquinone present on the surface is bound by such a linkage.

A novel method for modification of carbon surfaces was developed. Reaction of an *ortho*-diarylamine with carboxylic acid groups on the surface of carbon blacks was shown to be a feasible route for immobilization of aromatic structures to carbon surfaces. It was found that this technique could be used to perform sequential modifications or build polymers on the carbon surface. When

a chemically oxidized substrate was employed, the amount of anthraquinone immobilized on the surface by this technique was found to be comparable to those for the same carbon modified by spontaneous diazonium grafting. If the substrate was not oxidized, surface coverages were observed to decrease by *ca.* 50%. Synthesis of benzimidazole-based polymers in the presence of Vulcan XC72 was performed to produce carbon powders modified by coordination polymers.

Three approaches were examined for their ability to covalently immobilize polypyridyl ruthenium complexes on the surface of Vulcan XC72. These approaches included: (i) immobilization of a coordinating ligand on the surface using spontaneous diazonium grafting, (ii) immobilization of a coordinating ligand on the surface using the novel benzimidazole modification, and (iii) immobilization of a benzimidazole-based coordination polymer on the surface Based on several analytical techniques, each of the three modification approaches were found to result in a significant amount of ruthenium on the surface. However, it is unclear what form the ruthenium is in. Experimental evidence suggests that some of the desired polypyridyl ruthenium is present on the surface. However, based on the results obtained, the amount cannot be determined.

Examination of ruthenium containing, benzimidazole-based coordination polymers led to the discovery that the polymers themselves exhibit the ability to act as redox catalysts in the reduction of CO_2. Attempted product identification failed to identify any common CO_2 reduction products. Sufficient evidence exists to suggest that reduction products are deposited on the surface of the electrode support (carbon fiber paper).

References

[1] Centi, G.; Perathoner, S. *Catalysis Today* **2009**, *148*, 191–205.

[2] Benson, E. E.; Kubiak, C. P.; Sathrum, A. J.; Smieja, J. M. *Chem. Soc. Rev.* **2009**, *38*, 89–99.

[3] Saveant, J.-M. *Chem. Rev.* **2008**, *108*, 2348–2378.

[4] Olah, G. A.; Goeppert, A.; Surya Prakash, G. K. *J. Org. Chem.* **2009**, *74*, 487–498.

[5] Bard, A. J. *J. Am. Chem. Soc.* **2010**, *132*, 7559–7567.

[6] Hori, Y.; Wakebe, H.; Tsukamoto, T.; Koga, O. *Electrochimica Acta* **1994**, *39*, 1833–1839.

[7] Hori, Y.; Kikuchi, K.; Suzuki, S. *Chem. Lett.* **1985**, 1695–1698.

[8] Gattrel, M.; Gupta, N.; Co, A. *J. Electroanal. Chem.* **2006**, *594*, 1–19.

[9] Hernandez, R. m.; Marquez, J.; Marquez, O. P.; Choy, M.; Ovalles, C.; Garcia, J. J.; Scharifker, B. *J. Electrochem. Soc.* **1999**, *11*, 4131–4136.

[10] Yamamoto, T.; Tryk, D. A.; Hashimoto, K.; Fujishima, A.; Okawa, M. *J. Electrochem. Soc.* **2000**, *9*, 3393–3400.

[11] Hammouche, M.; Lexa, D.; Momenteau, M.; Saveant, J.-M. *J. Am. Chem. Soc.* **1991**, *113*, 8455–8466.

[12] Bhugun, I.; Lexa, D.; Saveant, J.-M. *J. Phys. Chem.* **1996**, *100*, 19981–19985.

[13] Bhugun, I.; Lexa, D.; Saveant, J.-M. *J. Am. Chem. Soc.* **1996**, *118*, 1769–1776.

[14] Angamuthu, R.; Byers, P.; Lutz, M.; Spek, A. L.; Bouwman, E. *Science* **2010**, *327*, 313–315.

[15] Chu, B. W.-K.; Yam, V. W.-W. *Langmuir* **2006**, *22*, 7437–7443.

[16] Jarzebinska, A.; Rowinski, P.; Zawisza, I.; Bilewicz, R.; Siegfried, L.; Kaden, T. *Anal. Chim. Acta* **1999**, *396*, 1–12.

[17] Bertoncello, P.; Dennany, L.; Forster, R. J.; Unwin, P. *Anal. Chem.* **2007**, *79*, 7549–7553.

[18] Taniguchi, T.; Fukasawa, Y.; Miyashita, T. *J. Phys. Chem. B* **1999**, *103*, 1920–1924.

[19] Yagi, M.; Kaneko, M. *Adv. Polym. Sci.* **2006**, *199*, 143–188.

[20] Abe, T.; Kaneko, M. *Prog. Polym. Sci.* **2003**, *28*, 1441–1488.

[21] Li, H.; Chen, J.; Han, S.; Niu, W.; Liu, X.; Xu, G. *Talanta* **2009**, *79*, 165–170.

[22] Yoshida, T.; Kamato, K.; Tsukamoto, M.; IIda, T.; Schlettwein, D.; Wohrle, D.; Kaneko, M. *J. Electroanal. Chem.* **1995**, *385*, 209–225.

[23] Walcarius, A. *Electroanalysis* **1998**, *10*, 1217–1235.

[24] Walcarius, A. *Chem. Mater.* **2001**, *13*, 3351–3372.

[25] Walcarius, A.; Mandler, D.; Cox, J. A.; Collinson, M.; Lev, O. *J. Mater. Chem.* **2005**, *15*, 3663–3689.

[26] Dvorak, O.; De Armond, M. K. *J. Phys. Chem.* **1993**, *97*, 2646–2648.

[27] Hu, C.; Yuan, S.; Hu, S. *Electrochimica Acta* **2006**, *51*, 3013–3021.

[28] Leitner, K. W.; Gollas, B.; Winter, M.; Besenhard, J. O. *Electrochim. Acta* **2004**, *50*, 199–204.

[29] Raoof, J.-B.; Ojani, R.; Kiani, A. *J. Electroanal. Chem.* **2001**, *515*, 45–51.

[30] Finklea, H. O.; Hanshew, D. D. *J. Am. Chem. Soc.* **1992**, *114*, 3173–3181.

[31] Abruna, H. D.; Denisevich, P.; Umana, M.; Meyer, T. J.; Murray, R. W. *J. Am. Chem. Soc.* **1981**, *103*, 1–5.

[32] Calvert, J. M.; Schmehl, R. H.; Sullivan, B. P.; Facci, J. S.; Meyer, T. J.; Murray, R. W. *Inorg. Chem.* **1983**, *22*, 2151–2162.

[33] Ellis, C. D.; Margerum, L. D.; Murray, R. W.; Meyer, T. J. *Inorg. Chem.* **1983**, *22*, 1283–1291.

[34] Sende, J. A. R.; Arana, C. R.; Hernandez, L.; Potts, K. T.; Keshevarz-K, M.; Abruna, H. D. *Inorg. Chem.* **1995**, *34*, 3339–3348.

[35] Collomb-Dunand-Sauthier, M.-N.; Deronzier, A.; Ziessel, R. *J. Electroanal. Chem.* **1993**, *350*, 43–55.

[36] Collomb-Dunand-Sauthier, M.-N.; Deronzier, A.; Ziessel, R. *J. Chem. Soc., Chem. Commun.* **1994**, 189–191.

[37] Chardon-Noblat, S.; Deronzier, A.; Ziessel, R.; Zsoldos, D. *J. Electroanal. Chem.* **1998**, *444*, 253–260.

[38] Chardon-Noblat, S.; Cripps, G. H.; Deronzier, A.; Field, J. S.; Gouws, S.; Haines, R. J.; Southway, F. *Organometallics* **2001**, *20*, 1668–1675.

[39] Chardon-Noblat, S.; Pellissier, A.; Cripps, G.; Deronzier, A. *J. Electroanal. Chem.* **2006**, *597*, 28–38.

[40] Moses, P. R.; Wier, L.; Murray, R. W. *Anal. Chem.* **1975**, *47*, 1882–1886.

[41] Abruna, H. D.; Meyer, T. J.; Murray, R. W. *Inorg. Chem.* **1979**, *18*, 3233–3240.

[42] Easton, E. B.; Pickup, P. G. *Electrochem. Solid-State Lett.* **2000**, *3*, 359–361.

[43] Notsu, H.; Fukazawa, T.; Tatsuma, T.; Tryk, D. A.; Fujishima, A. *Electrochem. Solid-State Lett.* **2001**, *4*, H1–H3.

[44] Balasubramanian, K.; Burghard, K. *Small* **2005**, *1*, 180–192.

[45] Wildgoose, G. G.; Banks, C. E.; Leventis, H. C.; Compton, R. G. *Microchim. Acta* **2006**, *152*, 187–214.

[46] Atoguchi, T.; Aramata, A.; Kazusaka, A.; Enyo, M. *J. Electroanal. Chem. Interfacial Chem.* **1991**, *318*, 309–320.

[47] Aga, H.; Aramata, A.; Hisaeda, Y. *J. Electroanal. Chem.* **1997**, *437*, 111–118.

[48] Belanger, D.; Pinson, J. *Chem. Soc. Rev.* **2011**, *40*, 3995–4048.

[49] Barbier, B.; Pinson, J.; Desarmot, G.; Sanchez, M. *J. Electrochem. Soc.* **1990**, *137*, 1757–1764.

[50] Deinhammer, R. S.; Ho, M.; Anderegg, J. W.; Porter, M. D. *Langmuir* **1994**, *10*, 1306–1313.

[51] Chretien, J.-M.; Ghanem, M. A.; Bartlett, P. N.; Kilburn, J. D. *Chem. Eur. J.* **2008**, *14*, 2548–2556.

[52] Ghanem, M. A.; Chretien, J.-M.; Pinczewska, A.; Kilburn, J. D.; Bartlett, P. N. *J. Mater. Chem.* **2008**, *18*, 4917–4927.

[53] Tanaka, H.; Aramata, A. *J. Electroanal. Chem.* **1997**, *437*, 29–35.

[54] Aramata, A.; Takahashi, S.; Yin, G.; Gao, Y.; Inose, Y.; Mihara, H.; Tadjeddine, A.; Zheng, W. Q.; Pluchery, O.; Bittner, A.; Yamagishi, A. *Thin Solid Films* **2003**, *424*, 239–246.

[55] Andrieux, C. P.; Gonzalez, F.; Saveant, J.-M. *J. Am. Chem. Soc.* **1997**, *119*, 4292–4300.

[56] Brooksby, P. A.; Downard, A. J.; Yu, S. S. C. *Langmuir* **2005**, *21*, 11304–11311.

[57] Astudillo, P. D.; Galano, A.; Gonzalez, F. J. *J. Electroanal. Chem.* **2007**, *610*, 137–146.

[58] Geneste, F.; Moinet, C.; Jezequel, G. *New J. Chem.* **2002**, *26*, 1539–1541.

[59] Delamar, M.; Hitmi, R.; Pinson, J.; Saveant, J. M. *J. Am. Chem. Soc.* **1992**, *114*, 5883–5884.

[60] Merson, A.; Dittrich, T.; Zidon, Y.; Rappich, J.; Shapira, Y. *Appl. Phys. Lett.* **2004**, *85*, 1075–1076.

[61] Maldonado, S.; Smith, T. J.; Williams, R. D.; Morin, S.; Barton, E.; Stevenson, K. J. *Langmuir* **2006**, *22*, 2884–2891.

[62] Bahr, J. L.; Tour, J. M. *Chem. Mater.* **2001**, *13*, 3823–3824.

[63] Bernard, M.-C.; Chausse, A.; Cabet-Deliry, E.; Chehimi, M. M.; Pinson, J.; Podvorica, F.; Vautrin-Ul, C. *Chem. Mater.* **2003**, *15*, 3450–3462.

[64] Belmont, J. A. *U.S. patent 5,554,739*, September 10, 1996.

[65] Adenier, A.; Cabet-Deliry, E.; Chausse, A.; Griveau, S.; Mercier, F.; Pinson, J.; Vautrin-Ul, C. *Chem. Mater.* **2005**, *17*, 491–501.

[66] Barriere, F.; Downard, A. J. *J. Solid State Electrochem.* **2008**, *12*, 1231–1244.

[67] Liu, Y.; McCreery, R. L. *J. Am. Chem. Soc.* **1995**, *117*, 11254–11259.

[68] Kariuki, J. K.; McDermott, M. T. *Langmuir* **2001**, *17*, 5947–5951.

[69] Allongue, P.; Delamar, M.; Desbat, B.; Fagebaume, O.; Hitmi, R.; Pinson, J.; Saveant, J.-M. *J. Am. Chem. Soc.* **1997**, *119*, 201–207.

[70] D'Amours, M.; Belanger, D. *J. Phys. Chem. B* **2003**, *107*, 4811–4817.

[71] Toupin, M.; Belanger, D. *Langmuir* **2008**, *24*, 1910–1917.

[72] Yu, S. S. C.; Tan, E. S. Q.; Jane, R. T.; Downard, A. J. *Langmuir* **2007**, *23*, 11074–11082.

[73] Brooksby, P. A.; Downard, A. J. *J. Phys. Chem. B* **2005**, *109*, 8791–8798.

[74] Pandurangappa, M.; Lawrence, N. S.; Compton, R. G. *Analyst* **2002**, *127*, 1568–1571.

[75] Kariuki, J. K.; McDermott, M. T. *Langmuir* **1999**, *15*, 6534–6540.

[76] Anariba, F.; DuVall, S. H.; McCreery, R. L. *Anal. Chem.* **2003**, *75*, 3837–3844.

[77] Brooksby, P. A.; Downard, A. J. *Langmuir* **2004**, *20*, 5038–5045.

[78] Toupin, M.; Belanger, D. *J. Phys. Chem. C* **2007**, *111*, 5394–5401.

[79] Combellas, C.; Kanoufi, F.; Pinson, J.; Podvorica, F. I. *Langmuir* **2005**, *21*, 280–286.

[80] Doppelt, P.; Hallais, G.; Pinson, J.; Podvorica, F.; Verneyre, S. *Chem. Mater.* **2007**, *19*, 4570–4575.

[81] Villenueve, C. H.; Pinson, J.; Bernard, M. C.; Allongue, P. *J. Phys. Chem. B* **1997**, *101*, 2415–2420.

[82] Saby, C.; Ortiz, B.; Champagne, G. Y.; Belanger, D. *Langmuir* **1997**, *13*, 6805–6813.

[83] Downard, A. *Langmuir* **2000**, *16*, 9680–9682.

[84] Anariba, F.; Mccreery, R. L. *J. Phys. Chem. B* **2002**, *106*, 10355–10362.

[85] Bahr, J. L.; Yang, J.; Kosynkin, D. V.; Bronikowski, M. J.; Smalley, R. E.; Tour, J. M. *J. Am. Chem. Soc.* **2001**, *123*, 6536–6542.

[86] Garret, D. J.; Lehr, J.; Miskelly, G. M.; Downard, A. *J. Am. Chem. Soc.* **2007**, *129*, 15456–15457.

[87] Adenier, A.; Barre, N.; Cabet-Deliry, E.; Chausse, A.; Griveau, S.; Mercier, F.; Pinson, J.; Vautrin-Ul, C. *Surf. Sci.* **2006**, *600*, 4801–4812.

[88] Abiman, P.; Wildgoose, G. G.; Compton, R. G. *J. Phys. Org. Chem.* **2008**, *21*, 433–439.

[89] Pognon, G.; Brousse, T.; Belanger, D. *Carbon* **2011**, *49*, 1340–1348.

[90] Marwan, J.; Addou, T.; Belanger, D. *Chem. Mater.* **2005**, *17*, 2395–2403.

[91] Jousselme, B.; Bidan, G.; Billon, M.; Goyer, C.; Kervella, Y.; Guillerez, S.; Hamad, E. A.; Goze-Bac, C.; Mevellec, J.-Y.; Lefrant, S. *J. Electroanal. Chem.* **2008**, *621*, 277–285.

[92] Boland, S.; Foster, K.; Leech, D. *Electrochim. Acta* **2009**, *54*, 1986–1991.

[93] Ricci, A.; Rolli, C.; Rothacher, S.; Baraldo, L.; Bonazzola, C.; Calvo, E. J.; Tognalli, N.; Fainstein, A. *J. Solid State Electrochem.* **2007**, *11*, 1511–1520.

[94] Yesildag, A.; Ekinci, D. *Electrochim. Acta* **2010**, *55*, 7000–7009.

[95] *IUPAC GoldBook*, http://goldbook.iupac.org (accessed Dec. 12, 2011).

[96] Goertzen, S. L.; Theriault, K. D.; Oickle, A. M.; Tarasuk, A. C.; Andreas, H. A. *Carbon* **2010**, *48*, 1252–1261.

[97] Oickle, A. M.; Goertzen, S. L.; Hopper, K. R.; Abdalla, Y. O.; Andreas, H. A. *Carbon* **2010**, *48*, 3313–3322.

[98] *CCCBDB Computational Chemistry Comparison and Benchmark Database*, http://cccbdb.nist.gov (accessed Oct. 26, 2011).

[99] *Solver*, FrontlineSolvers, http://www.solver.com (accessed Nov. 25, 201).

[100] Cameron, C. G. Ph.D. thesis, Memorial University of Newfoundland, 2000.

[101] Barbieri, O.; Hahn, M.; Herzog, A.; Kotz, R. *Carbon* **2005**, *43*, 1303–1310.

[102] Smith, R. D. L.; Pickup, P. G. *Electrochimica Acta* **2009**, *54*, 2305–2311.

[103] Wildgoose, G. G.; Lawrence, N. S.; Leventis, H. C.; Jiang, L.; Jones, T. G. J.; Compton, R. G. *J. Mater. Chem.* **2005**, *15*, 953–959.

[104] Branton, S.; Belanger, D. *Electrochimica Acta* **2008**, *53*, 6961–6967.

[105] Hurley, B. L.; McCreery, R. L. *J. Electrochem. Soc.* **2004**, *5*, B252.

[106] Buttry, D. A.; Peng, J. C. M.; Donnet, J.-B.; Rebouillat, S. *Carbon* **1999**, *37*, 1929–1940.

[107] Zollinger, H. *Acc. Chem. Res.* **1973**, *6*, 335–341.

[108] Kornblum, N. *Org. Synth.* **1941**, *21*, 30.

[109] Robison, M. M.; Robison, B. L. *Org. Synth.* **1956**, *36*, 94.

[110] Kornblum, N.; Kelley, A. E.; Cooper, G. D. *J. Am. Chem. Soc.* **1952**, *74*, 3074–3076.

[111] Tamam, I.; Kraack, H.; Ocko, B. M.; Pershan, P. S.; Ofer, E.; Deutsch, M. *J. Phys. Chem. C* **2007**, *111*, 2573–2579.

[112] Smith, R. D. L.; Pickup, P. G. *Electrochem. Commun.* **2009**, *11*, 10–13.

[113] Neuse, E. W. *Adv. Polym. Sci.* **1982**, *47*, 1–42.

[114] Wright, J. B. *Chem. Rev.* **1951**, *48*, 397–541.

[115] Arnold Jr., F. E.; Arnold, F. E. *Adv. Polym. Sci.* **1994**, *117*, 257–295.

[116] Hein, D. W.; Alheim, R. J.; Leavitt, J. J. *J. Am. Chem. Soc.* **1957**, *79*, 427–429.

[117] Osaheni, J. A.; Jenekhe, S. A. *Chem. Mater.* **1992**, *4*, 1282–1290.

[118] Osaheni, J. A.; Jenekhe, S. A. *Macromolecules* **1995**, *28*, 1172–1179.

[119] Rong-huan, H.; Bao-ying, S.; Jing-shuai, Y.; Quan-tong, C. *Chem. Res. Chinese Universities* **2009**, *25*, 585–589.

[120] Lin, S.; Yang, L. *Tetrahedron Lett.* **2005**, *46*, 4315–4319.

[121] Gogoi, P.; Konwar, D. *Tetrahedron Lett.* **2006**, *47*, 79–82.

[122] Chan, W. K. *Coord. Chem. Rev.* **2007**, *251*, 2104–2118.

[123] Cameron, C. G.; Pickup, P. G. *Chem. Commun.* **1997**, *3*, 303–304.

[124] Bard, A. J.; Faulkner, L. R. *Electrochemical Methods: Fundamentals and Applications*; John Wiley Sons, Inc., 2001.

[125] Gritsan, N. P.; Klimenko, L. S.; Leonenko, Z. V.; Mainagashev, I. Y.; Mamtyuk, V. I.; Vetchinov, V. P. *Tetrahedron* **1996**, *51*, 3061–3076.

[126] Bruice, P. Y. *Organic Chemistry*, Fourth Edition ed.; Pearson Education, Inc., 2004.

[127] Noel, V.; Randriamahazaka, H.; Chevrot, C. *J. Electroanal. Chem.* **2003**, *558*, 41–48.

[128] *Encyclopedia of Electrochemistry of the Elements*; Bard, A. J., Ed.; Marcel Dekker, Inc., 1984; Vol. XV.

[129] Regisser, F.; Lavoie, M.-A.; Champagne, G. Y.; Belanger, D. *J. Electroanal. Chem.* **1996**, *415*, 47–54.

[130] Langley, L. A.; Villanueva, D. E.; Fairbrother, D. H. *Chem. Mater.* **2006**, *18*, 169–178.

[131] *NIST X-ray Photoelectron Spectroscopy Database, Version 3.5*, http://srdata.nist.gov/xps/Default.aspx (accessed Oct. 17, 2011).

[132] Liang, Z.; Jiang, X.; Xu, H.; Chen, D.; Yin, J. *Macromol. Chem. Phys.* **2009**, *210*, 1632–1639.

[133] Cameron, C. G.; Pickup, P. G. *J. Am. Chem. Soc.* **1999**, *121*, 11773–11779.

[134] Chen, J.; Hamon, M. A.; Hu, H.; Chen, Y.; Rao, A. M.; Eklund, P. C.; Haddon, R. C. *Science* **1998**, *282*, 95–98.

[135] Begum, A.; Pickup, P. G. *Electrochem. Commun.* **2007**, *9*, 2525–2528.

[136] Lever, A. B. P. *Inorg. Chem.* **1990**, *29*, 1271–1285.

[137] Abruna, H. D.; Meyer, T. J.; Murray, R. W. *Inorg. Chem.* **1979**, *18*, 3233–3240.

[138] Gohier, A.; Nekelson, F.; Helezen, M.; Jegou, P.; Deniau, G.; Palacin, S.; Maybe-L'Hermite, M. *J. Mater. Chem.* **2011**, *21*, 4615–4622.

[139] Mesnage, A.; Magied, M.; Simon, P.; Herlin-Boime, N.; Jegou, P.; Deniau, G.; Palacin, S. *J. Mater. Sci.* **2011**, *46*, 6332–6338.

[140] Smith, R. D. L.; Pickup, P. G. *Electrochem. Commun.* **2010**, *12*, 1749–1751.

[141] Vaidhyanathan, R.; Iremonger, S. S.; Shimizu, G. K. H.; Boyd, P. G.; Alavi, S.; Woo, T. K. *Science* **2010**, *330*, 650–653.

[142] Taj, S.; Sankarapapavinasam, S.; Ahmed, M. F. *J. Appl. Polym. Sci.* **2000**, *77*, 112–115.

[143] Seshadri, G.; Lin, C.; Bocarsly, A. B. *J. Electroanal. Chem.* **1994**, *372*, 145–150.

[144] Barton, E. E.; Rampulla, D. M.; Bocarsly, A. B. *J. Am. Chem. Soc.* **2008**, *130*, 6342–6344.

[145] Cole, E. B.; Lakkaraju, P. S.; Rampulla, D. M.; Morris, A. J.; Abelev, E.; Bocarsly, A. B. *J. Am. Chem. Soc.* **2010**, *132*, 11539–11551.

[146] Morris, A. J.; McGibbon, R. T.; Bocarsly, A. B. *Chem. Sus. Chem.* **2011**, *4*, 191–196.

[147] Bolinger, C. M.; Sullivan, B. P.; Conrad, D.; Gilbert, J. A.; Story, N.; Meyer, T. J. *Chem. Commun.* **1985**, 796–797.

[148] Ishida, H.; Fujiki, K.; Ohba, T.; Ohkubo, K.; Tanaka, K.; Terada, T.; Tanaka, T. *Dalton Trans.* **1990**, 2155–2160.

[149] Nagao, H.; Mizukawa, T.; Tanaka, K. *Inorg. Chem.* **1994**, *33*, 3415–3420.

[150] Ali, M. M.; Sato, H.; Mizukawa, T.; Haga, M.; Tanaka, K. *Chem. Commun.* **1998**, 249–250.

[151] Batanero, B.; Barba, F.; Sanchez-Sanchez, C. M.; Aldaz, A. *J. Org. Chem.* **2004**, *69*, 2423–2426.

[152] Scialdone, O.; Sabatino, M. A.; Galia, A.; Filardo, G.; Silvestri, G. *J. Electroanal. Chem.* **2008**, *614*, 175–178.

[153] Eggins, B. R.; Robertson, P. K. J.; Murphy, E. P.; Woods, E.; Irvine, J. T. S. *J. Photochem. Photobiol. A: Chem.* **1998**, *118*, 31–40.

[154] Silverstein, R. M.; Webster, F. X.; Kiemle, D. J. *Spectroscopic Identification of Organic Compounds*, Seventh Edition ed.; John Wiley Sons, Inc., 2005.

[155] Crews, P.; Rodriguez, J.; Jaspars, M. *Organic Structure Analysis*; Oxford University Press, 1998.

[156] *Spectral Database for Organic Compounds*, http://riodb01.ibase.aist.go.jp (accessed July 26, 2011).

[157] Gottlieb, H. E.; Kotlyar, V.; Nudelman, A. *J. Org. Chem.* **1997**, *62*, 7512–7515.

[158] Ngo, H. L.; LeCompte, K.; Hargens, L.; McEwen, A. *Thermochimica Acta* **2000**, *357-358*, 97–102.
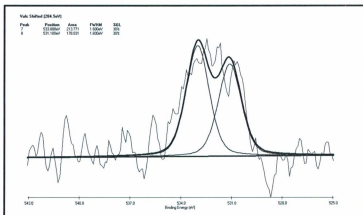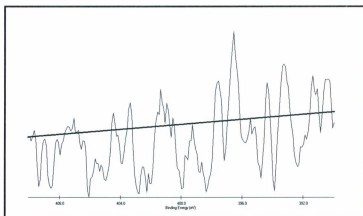
XPS Spectra

Figure A.1: Curve-fitted XPS spectra for N 1s (top) and O 1s (bottom) regions of Vulcan XC72.
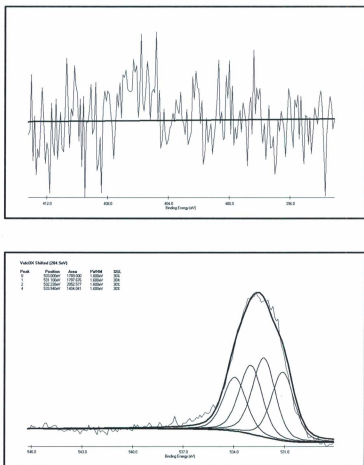
Figure A.2: Curve-fitted XPS spectra for N 1s (top) and O 1s (bottom) regions of chemically oxidized Vulcan XC72 (VulcOX).
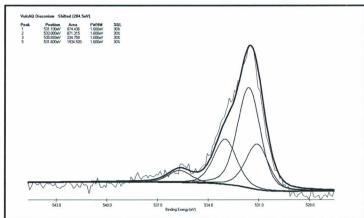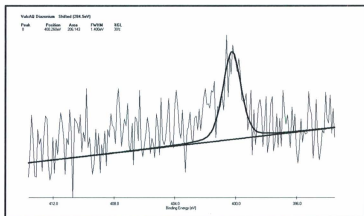
Figure A.3: Curve-fitted XPS spectra for N 1s (top) and O 1s (bottom) regions of Vulcan XC72 modified by the spontaneous diazonium with Fast Red AL salt.
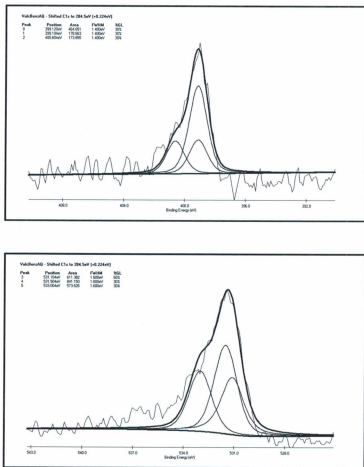
Figure A.4: Curve-fitted XPS spectra for N 1s (top) and O 1s (bottom) regions of Vulc-DAAQ(HCl).
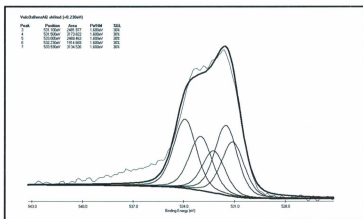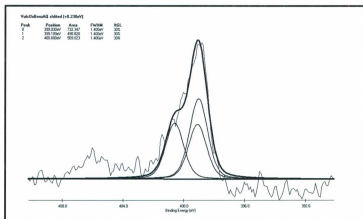
Figure A.5: Curve-fitted XPS spectra for N 1s (top) and O 1s (bottom) regions of VulcOX-DAAQ(HCl)
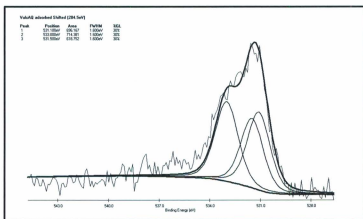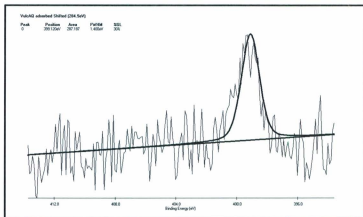
Figure A.6: Curve-fitted XPS spectra for N 1s (top) and O 1s (bottom) regions of 1-amino-9,10-anthraquinone adsorbed on the surface of Vulcan XC72.
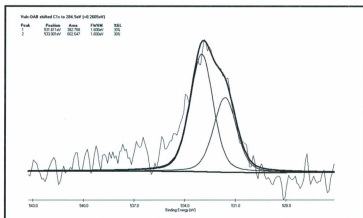
Figure A.7: Curve-fitted XPS spectra for O 1s region of Vulc-DAAB.
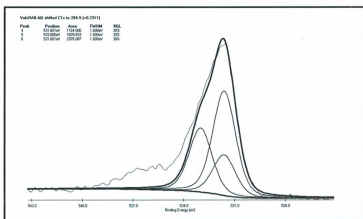
Figure A.8: Curve-fitted XPS spectra for O 1s region of Vulc-DAB-AQ.
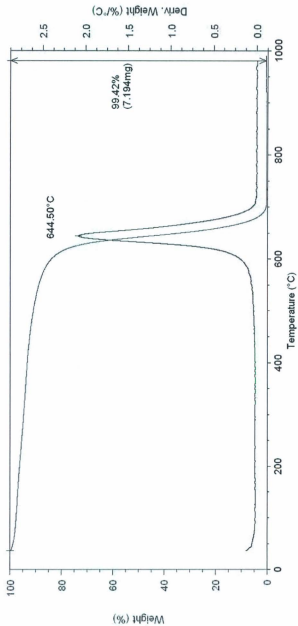
TGA Thermograms

Figure B.1: Thermogram obtained on chemically oxidized Vulcan XC72 (VulcOX) under air atmosphere.

281
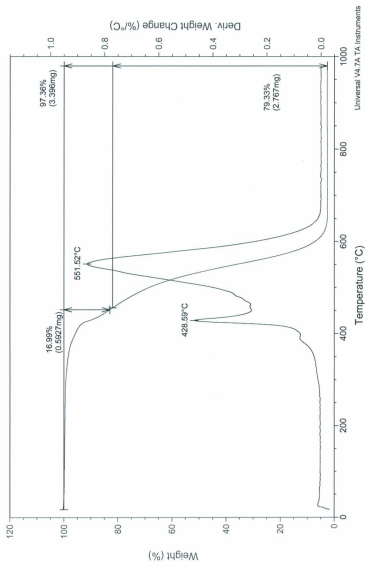
Figure B.2: Thermogram obtained from a dynamic, high-resolution TGA scan on 3.49 mg of VulcPhenRu(pbt)$_2$. TGA performed under air atmosphere.
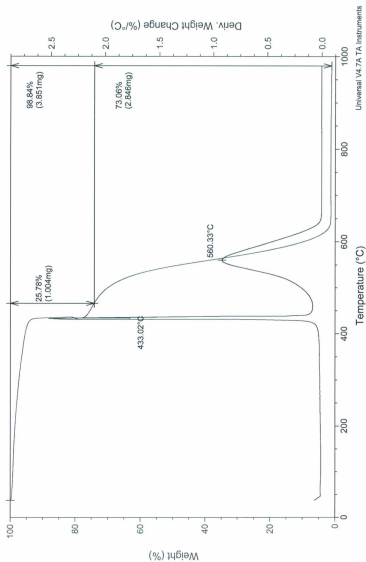
Figure B.3: Thermogram obtained from a dynamic, high-resolution TGA scan on 3.89 mg of VulcBenzRu(pbt)$_2$. TGA performed under air atmosphere.
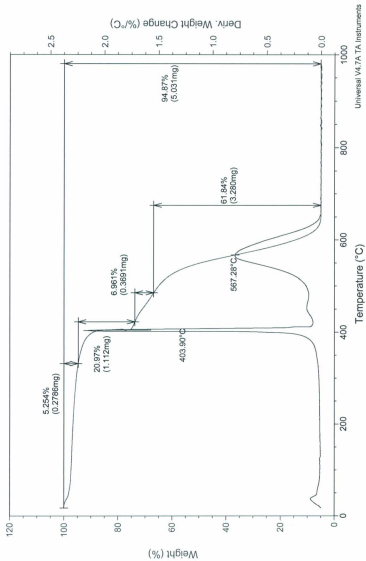
Figure B.4: Thermogram obtained from a dynamic, high-resolution TGA scan on 5.30 mg of VulcPPyBBIM-Ru(bpy)₂. TGA performed under air atmosphere.
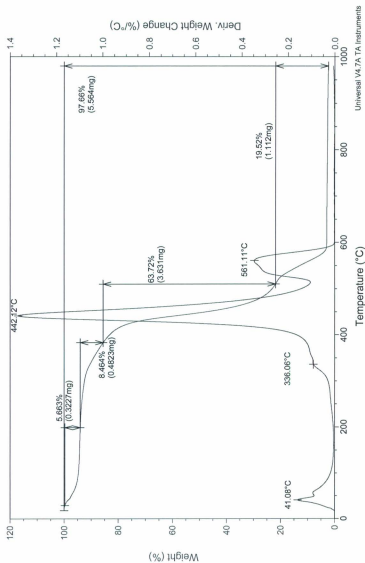
Figure B.5: Thermogram obtained from a dynamic, high-resolution TGA scan on 5.70 mg of VulcPBPyBBIM-Ru(pbt)$_2$. TGA performed under air atmosphere.
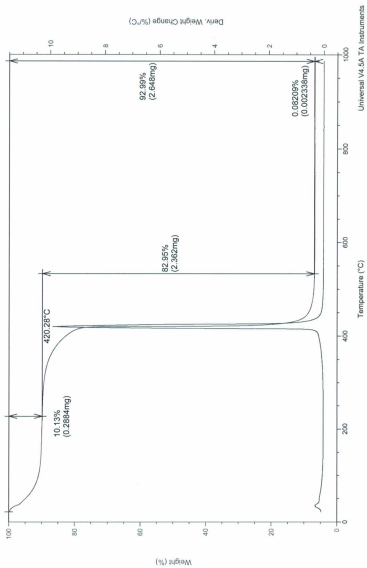
Figure B.6: Thermogram obtained from a dynamic, high-resolution TGA scan on 2.89 mg of PBPyBBIM-Ru(pbt)$_2$. TGA performed under air atmosphere.
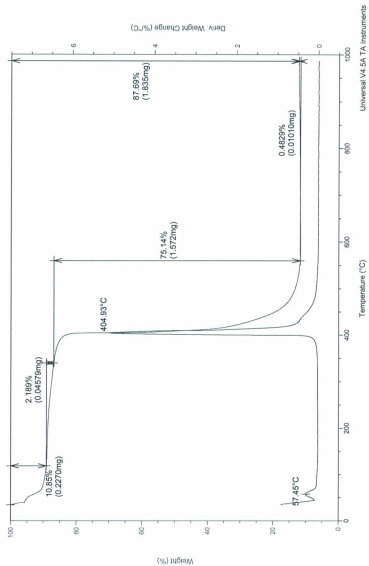
Figure B.7: Thermogram obtained from a dynamic, high-resolution TGA scan on 2.09 mg of PPyBBIM-Ru(pbt)$_2$. TGA performed under air atmosphere.
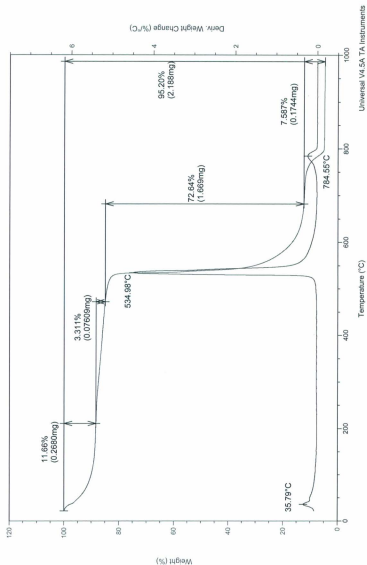
Figure B.8: Thermogram obtained from a dynamic, high-resolution TGA scan on 2.30 mg of PPyBBIM. TGA performed under air atmosphere.
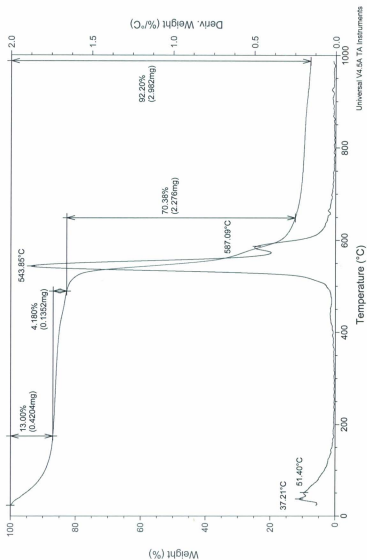
Figure B.9: Thermogram obtained from a dynamic, high-resolution TGA scan on 3.23 mg of PBPyBBIM. TGA performed under air atmosphere.
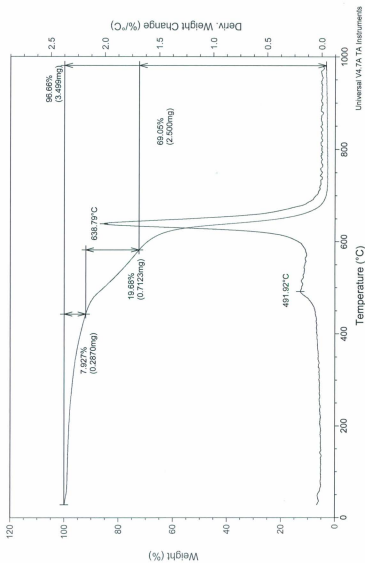
Figure B.10: Thermogram obtained from a dynamic, high-resolution TGA scan on 3.62 mg of VulcPPyBBIM. TGA performed under air atmosphere.
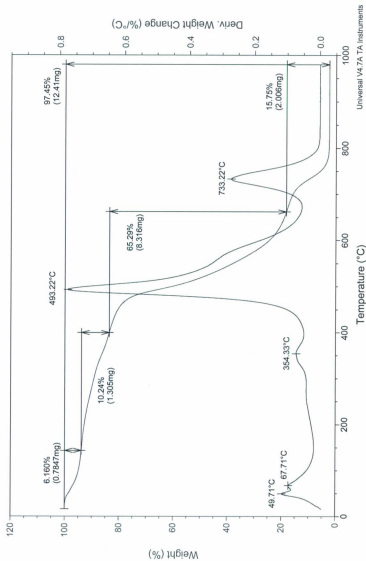
Figure B.11: Thermogram obtained from a dynamic, high-resolution TGA scan on 12.74 mg of VulcPBPyBBIM. TGA performed under air atmosphere.
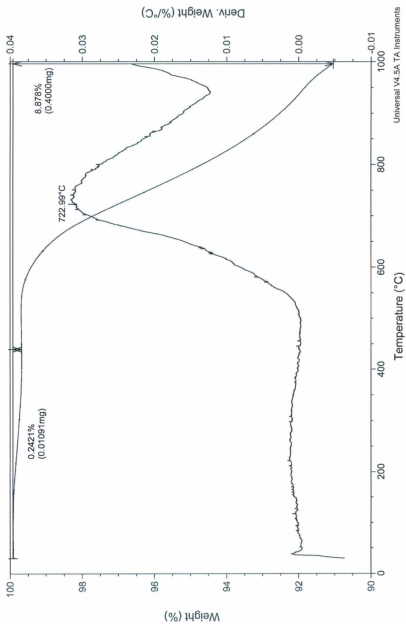
Figure B.12: Thermogram and differential thermogram obtained on an unmodified piece of carbon fiber paper under N_2 atmosphere.

292
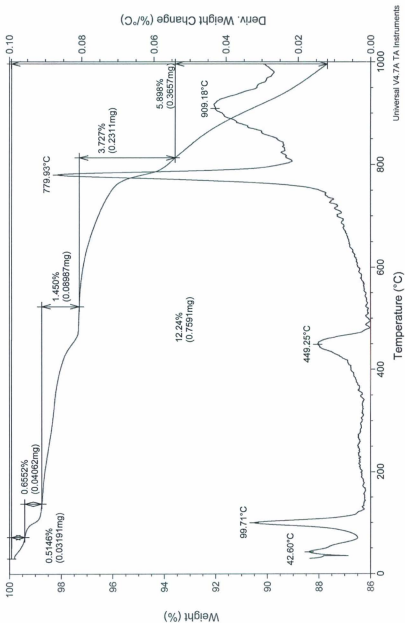
Figure B.13: Thermogram and differential thermogram obtained, under N_2 atmosphere, on a strip of carbon fiber paper that was soaked in 0.1 M NEt_4BF_4 in CH_3CN.
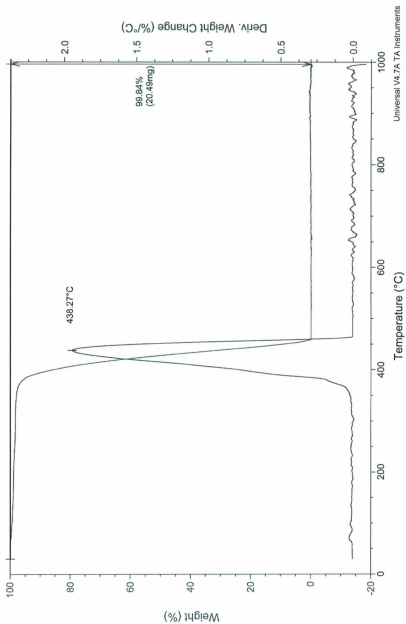
Figure B.14: Thermogram and differential thermogram obtained on NEt$_4$BF$_4$ under N$_2$ atmosphere.
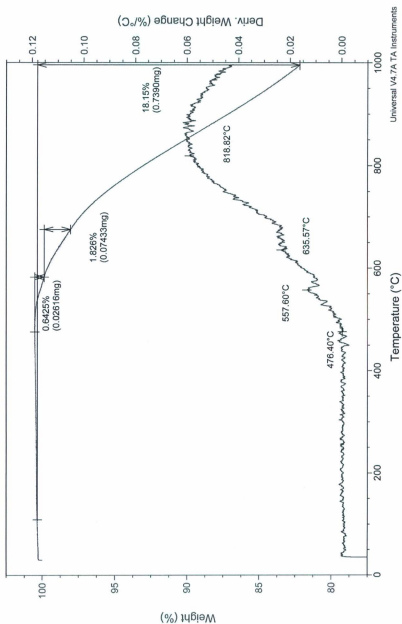
Figure B.15: Thermogram and differential thermogram obtained, under N_2 atmosphere, on a thin film of PBPyBBIM deposited on a piece of carbon fiber.

295
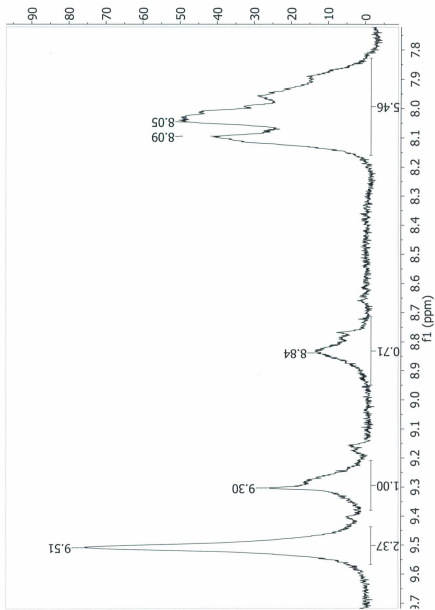
NMR Spectra

Figure C.1: ^{1}H NMR spectrum for PPyBBIM dissolved in D_2SO_4.
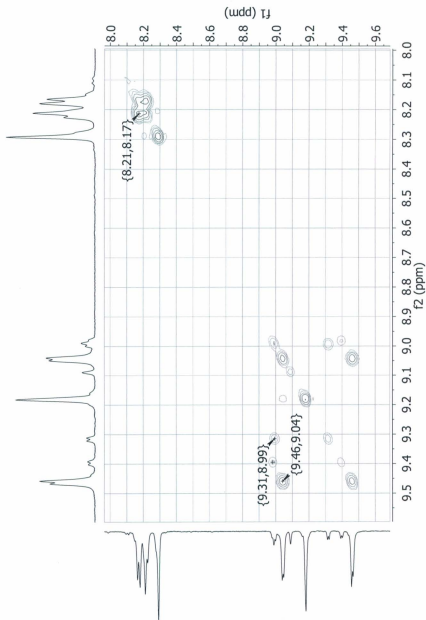
Figure C.2: Homonuclear correlation spectroscopy (600 MHz, ^{1}H-^{1}H) obtained for PBPyBBIM dissolved in D_2SO_4. Spectrum was acquired at 80 °C to enhance spectral resolution.
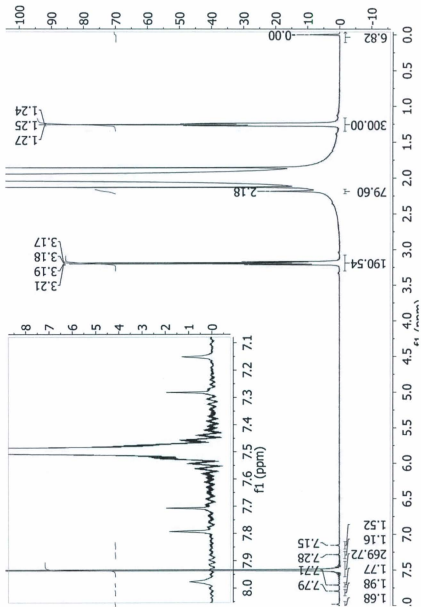
Figure C.3: ^{1}H NMR on a 1:1 mixture of CDCl$_3$ and 0.1M NEt$_4$BF$_4$ in CH$_3$CN containing 1% H$_2$O (Blank). Results discussed in Section 6.2.4.
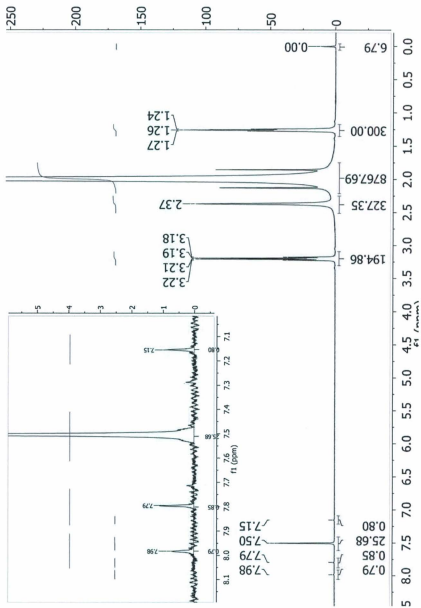
Figure C.4: ^{1}H NMR on electrolysis solution from Electrolysis 1. Sample was prepared by preparing a 1:1 mixture of the electrolysis and CDCl$_3$. Results discussed in Section 6.2.4.
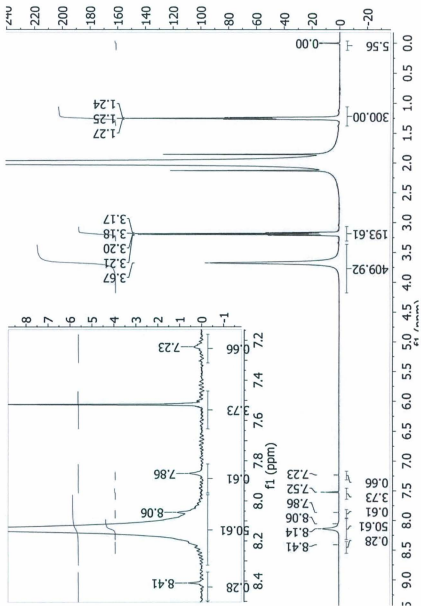
Figure C.5: ^{1}H NMR on electrolysis solution (Electrolysis 1) spiked with formic acid. Solution preparation described in Section 6.4.4, results discussed in Section 6.2.4
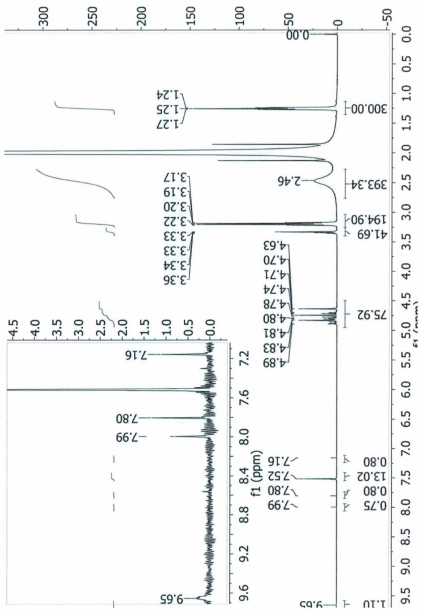
Figure C.6: ^{1}H NMR on electrolysis solution (Electrolysis 1) spiked with formalin solution. Solution preparation described in Section 6.4.4, results discussed in Section 6.2.4
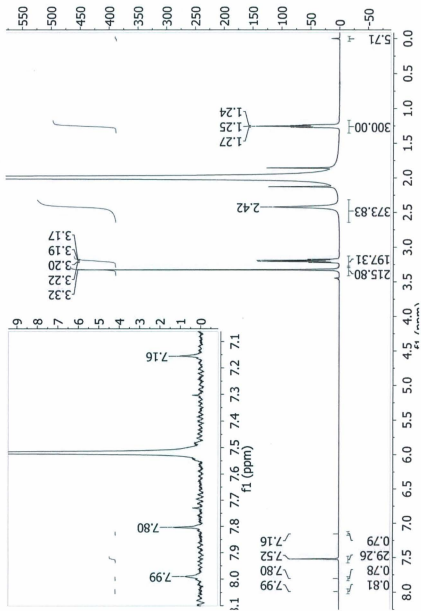
Figure C.7: ^{1}H NMR on methanol spiked electrolysis solution (Electrolysis 1). Solution preparation described in Section 6.4.4, results discussed in Section 6.2.4
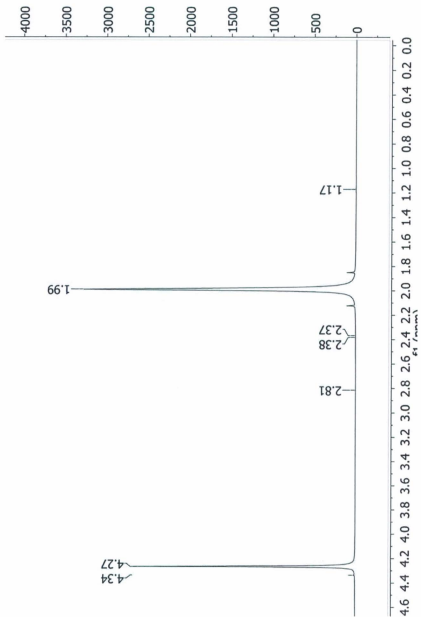
Figure C.8: ^{1}H NMR on electrolysis solution from Electrolysis 2. Sample preparation described in Section 6.4.4. Results discussed in Section 6.2.4.
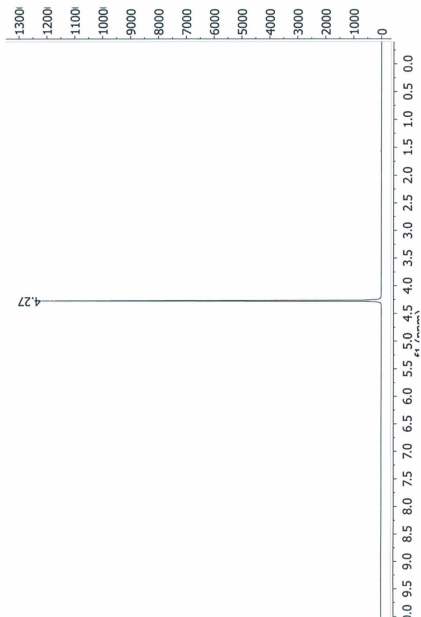
Figure C.9: ^{1}H NMR on a solution of the precipitate from Electrolysis 2, dissolved in D_2O. Results discussed in Section 6.2.4
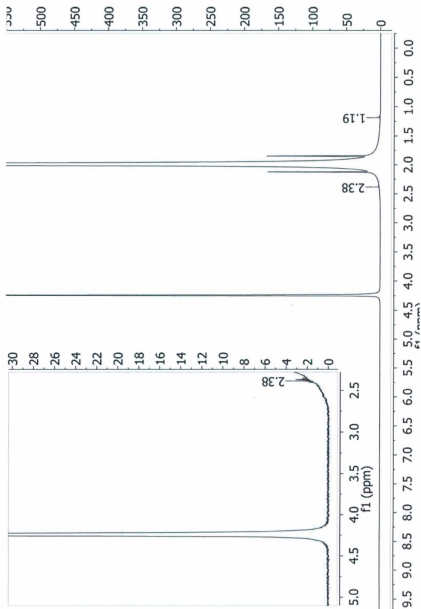
Figure C.10: ^{1}H NMR on 1:1 mixture of D_2O and 0.1 M $LiClO_4$ in CH_3CN containing 1% H_2O. Electrolyte solution was purged with CO_2 for 60 min before mixing. Results discussed in Section 6.2.4.
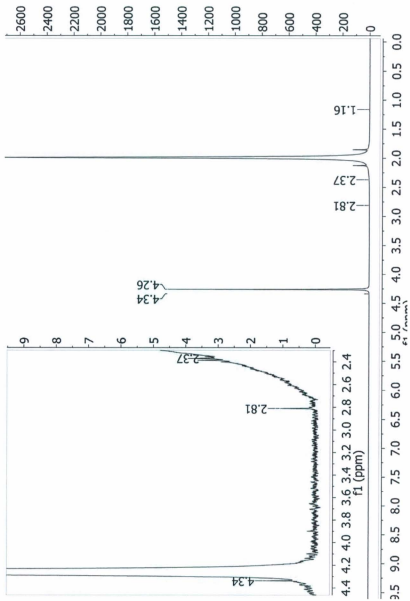
Figure C.11: ^1H NMR on 1:1 mixture of D_2O and blank electrolysis solution. Electrolysis was performed for a period of 24 h using an unmodified carbon fiber paper as the working electrode. Electrolyte solution was purged with CO_2 before electrolysis. Results discussed in Section 6.2.4.
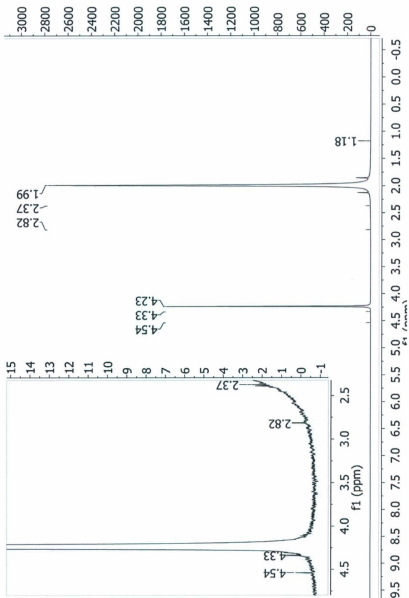
Figure C.12: ^{1}H NMR on 1:1 mixture of D_2O and blank electrolysis solution. Electrolysis was performed for a period of 24 h using an unmodified carbon fiber paper as the working electrode. Electrolyte solution was purged with N_2 before electrolysis. Results discussed in Section 6.2.4.
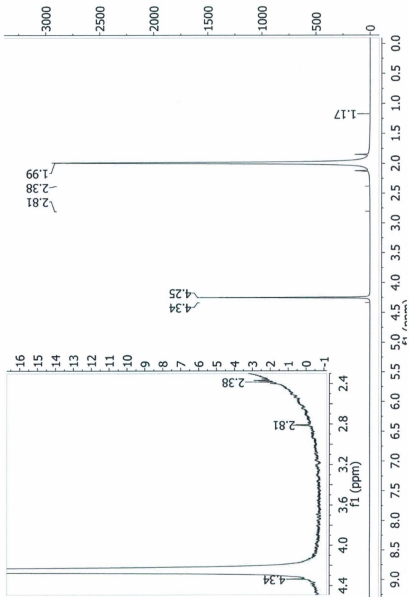
Figure C.13: ^{1}H NMR on 1:1 mixture of D_2O and blank electrolysis solution. Electrolysis was performed for a period of 24 h using a carbon fiber paper with a PBPyBBIM film as the working electrode. Electrolyte solution was purged with N_2 before electrolysis. Results discussed in Section 6.2.4.
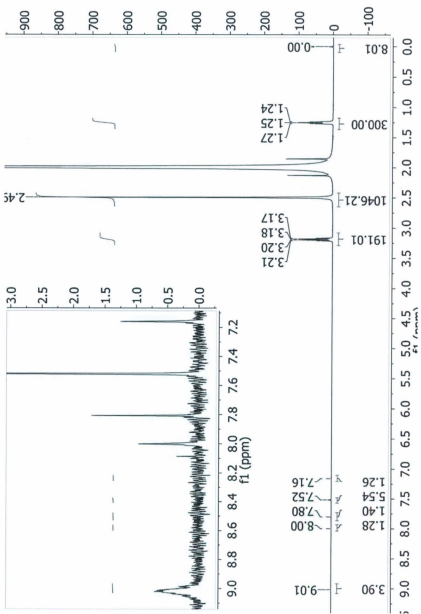
Figure C.14: ^{1}H NMR on electrolysis solution from Electrolysis 3. Sample preparation described in Section 6.4.4. Results discussed in Section 6.2.4.
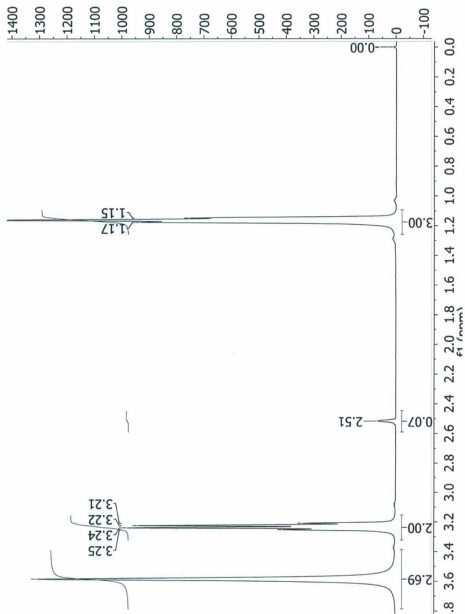
Figure C.15: ^{1}H NMR on tetraethylammonium oxalate, acquired in DMSO-d$_6$.
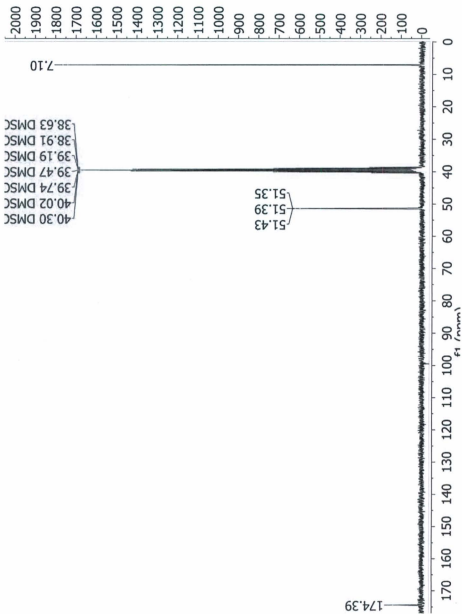
Figure C.16: ^{13}C NMR on tetraethylammonium oxalate, acquired in DMSO-d$_6$.
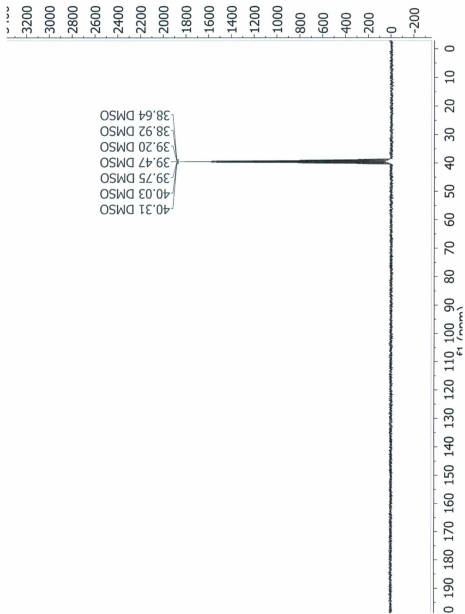
Figure C.17: Electrode from Electrolysis 3 was soaked in DMSO-d$_6$ for *ca.* 72 h. ^{13}C NMR was then performed on the DMSO-d$_6$ solution.
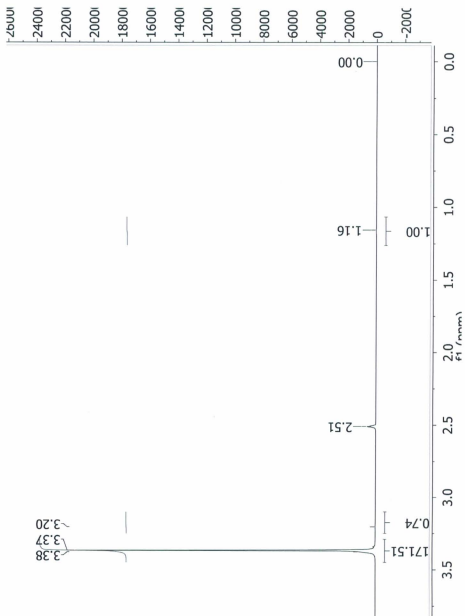
Figure C.18: Electrode from Electrolysis 3 was soaked in DMSO-d_6 for *ca.* 72 h. ^{1}H NMR was then performed on the DMSO-d_6 solution.

# Cyclic Voltammograms
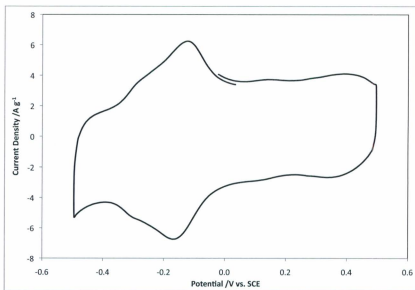
**Figure D.1:** Cyclic voltammogram obtained for VulcOX-PDA. Voltammogram collected at 100 mV s^{-1} in 1M H$_2$SO$_4$(aq)
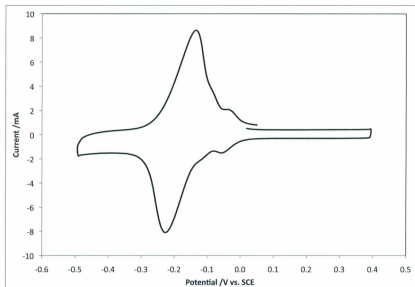
Figure D.2: Cyclic voltammogram obtained for 1,2-diaminoanthraquinone adsorbed on the surface of Vulcan XC72. Voltammogram collected at 100 mV s^{-1} in 1M H$_2$SO$_4$(aq)
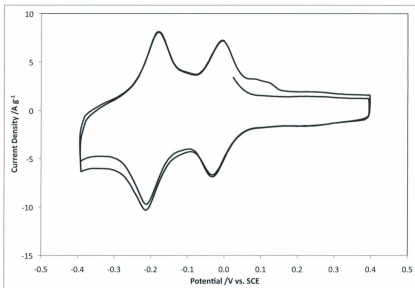
Figure D.3: Cyclic voltammogram obtained for VulcDAAQ(HCl) following re-
fluxing in 1 M NaOH(aq). Voltammogram collected at 100 mV s^{-1}
in 1M H$_2$SO$_4$(aq)
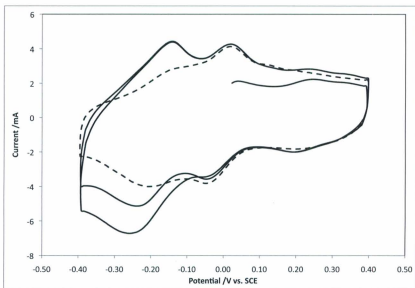
Figure D.4: Cyclic voltammogram obtained for VulcOX-DAAQ(HCl) before (solid line) and after (dashed line) 3 hours of electrochemical cycling. Cyclic voltammetry performed in 1.0 M H_2SO_4 at 100 mV s^{-1}.